CZECH TECHNICAL UNIVERSITY IN PRAGUE
FACULTY OF ELECTRICAL ENGINEERING
DEPARTMENT OF ELECTROMAGNETIC FIELD

Habilitation Thesis

Source Concept Based Analysis and Synthesis of Small Radiating Structures

Miloslav Čapek

Prague, September 2015

Author's Declaration

I declare that, except where explicit reference is made to the contribution of others, this dissertation is the result of my own work. I certify that, to the best of my knowledge, my work does not infringe upon anyone's copyright nor violate any proprietary rights and that any ideas, techniques, quotations, or any other material from the work of other people included in my thesis, published or otherwise, are fully acknowledged in accordance with the standard referencing practices.

Author

in Prague, 12. 9. 2015

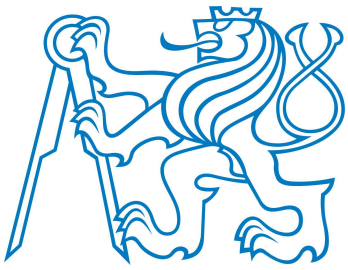

Preface

This thesis is conceived as a brief discourse covering a major part of the author's career and his achievements. It is not intended as a comprehensive guide covering all aspects of antenna design for that is a task that could never be done. Instead, the intent is to communicate a general line of reasoning, together with an outline of what has been and should be done both in the near and distant future.

It is recommended that the reader consult the main text, together with the papers and manuscripts attached in Appendix A. For the reader's convenience, all works enclosed in this thesis are denoted by an extra asterisk, e.g., [0∗]. The list of all attached publications can be found immediately following the Bibliography and at the end of the thesis.

The core of the habilitation thesis deals with the intricate problem of electromagnetic stored energy, its evaluation and interpretation. This challenging and unsolved problem is closely related to the physical meaning of radiated energy. The evaluation of these quantities is crucial for the determination of the quality factor and the investigation of the intrinsic bandwidth. Consequently, this thesis significantly extends the work on the small antenna theory described in the dissertation thesis. The original aspects of the thesis are discussed in Section 1.5.

The (fifteen) papers, relevant for the development of the thesis, are found in Appendix A. For a complete understanding of the topic, three important papers [1∗], [2∗], and [3∗], which recapitulate the introductory topics of source concept, are attached despite their being present in the dissertation thesis [4].

Acknowledgement

It is my pleasure and privilege to offer my sincere thanks to Pavel Hazdra and Lukáš Jelinek, my colleagues and friends, who have significantly influenced this early stage of my scientific career. I wish our cooperation to continue.

I am grateful to have had the opportunity to engage in many fruitful discussions with Lukas Jelinek, Guy Vandenbosch, Mats Gustafsson and Lars Jonsson who always pose stimulating questions leading to surprising findings. Likewise, the scientific visits in KU Leuven are highly appreciated as they gave me a chance to see these issues in a broader context.

I would like to express my thanks to the past and present heads of the Department of Electromagnetic Field, namely Miloš Mazánek and Pavel Pechač, who have been able to attract and assemble a great team of individuals and have created an amicable working environment. I can only hope that this situation will continue for many years to come.

I am also indebted to many colleagues, notably Pavel Hamouz, Jan Eichler, Ota Jícha, Filip Kozák, Viktor Adler, Vašek Kabourek, Ivana Hrebiková, Zdeněk Hradecký, Martin Mudroch, Zbyněk Škvor, Milan Příhoda, Petr Černý amongst others, and grateful for our numerous (and often quite "tasty") discussions. It should be noted that many of these discussions would never have been possible without the great enthusiasm of Zdeněk Hradecký who truly united our department not only as a collective team of professional co-workers, but, mostly, as a group of friends.

Last, but certainly not least, I am grateful to my family and to Eva for their eternal encouragement and without whom this thesis would never have seen the light of day.

Contents

List of Figures

Chapter 1

Introduction

Nowadays, wireless communication is inherently interconnected with our everyday lives. It has become simply indispensable. Today, the number of potential communication channels are immense and there is no end in sight. According to a CISCO prediction [11], more than half of all IP addresses in 2017 will be associated with wireless devices. Since wireless devices need to be ubiquitous, they should also be small and efficient. To give but one example, we can refer to modern smartphones and built-in electrically small antennas.

Antennas are irreplaceable constituents of wireless communication systems and they are being forced to deliver more and more requirements, namely high efficiency, reasonable antenna gain, and maximum bandwidth, or, alternatively, big data throughput for many mobile services often operating simultaneously [12]. However, all these improvements come at the expense of diminished available volume where the radiator can be placed.

Unfortunately, the electrical size of the radiator and its performance characteristics are in strict opposition [13], thus an optimal trade-off needs to be found on a case-by-case basis. To make matters more complicated, modern design dictates that devices should not have any visible protuberances, which bring with it a whole new class of problems, as antennas must operate in the vicinity of complex background media. This is true not only for cellular phones, but also for RFID tags [14], GPS devices [15], modern automotive radars, or antennas in medicine [16].

It means that the design of "optimal" radiators and scatterers has become a crucial task as current antenna systems may soon become deficient. This, of course, happens periodically throughout the advancement of antenna systems, but beyond such a turbulent development, some fundamental questions remain frustratingly unanswered, notwithstanding the constant and determined effort of researchers. Regarding the small (sub-wavelength) antennas theory, the most prominent ones can be summarized as follows:

- Which geometrical shape of the radiator and which material distribution are optimal in terms of a selected trade-off between crucial parameters?

- Where should the radiator be fed for optimal performance and how should the matching circuit be designed?

Although these questions are mutually intertwined, they can be addressed one by one and all these issues can be grasped by the so-called Source Concept. However, before

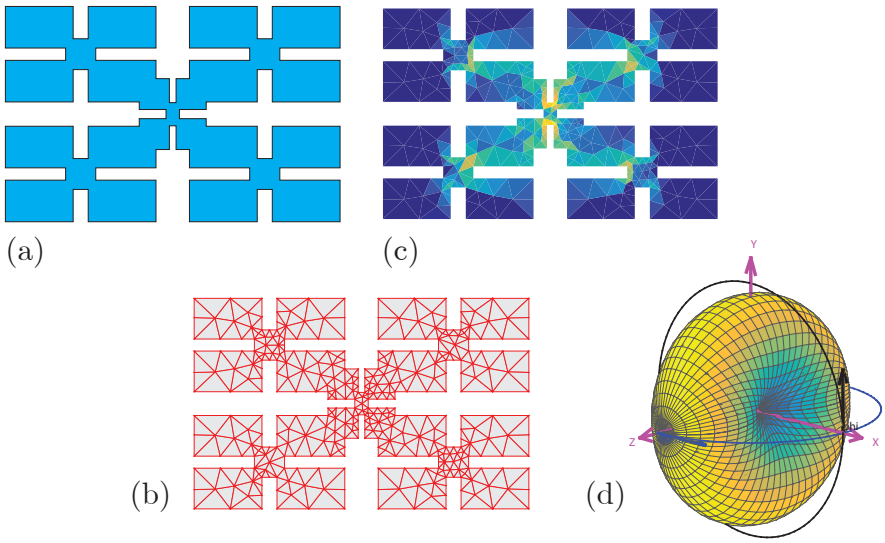

Figure 1.1: Analysis of a fractal shape of the second iteration generated by the iterated function system [5]. The subfigures depict: the shape of the original geometry (a), discretization of the original problem (b), absolute value of the normalized modal current density in the first natural resonance (c), and corresponding radiation pattern (d).

the Source Concept can be appropriately introduced, the antenna analysis and synthesis should be differentiated.

1.1 Antenna analysis and synthesis

The design of an (electrically small) antenna generally consists of an analysis and a synthesis [8].

Antenna analysis, typically, first specifies the geometry, including the material distribution and the used boundary conditions, and then determines the unknown current or, alternatively, the electromagnetic field, see Fig. 1.1. While classical antennas are usually fed from an external source, e.g., by a coaxial probe or micro-strip line, scattering obstacles such as RFID chips are fed by an incident electromagnetic wave. All these feeding scenarios can then be incorporated into the boundary conditions representing the sources. Another option takes into account an antenna analyzed without any feeding. Such a scenario is the subject of an eigen-decomposition which covers a dazzling array of possible applications. As soon as the currents are known, the electromagnetic field quantities and the desired antenna characteristics can be evaluated in a straightforward fashion.

Since the shape of the antenna is determined at the beginning of the analysis, the designer must have previous experience with similar antennas as it usually takes many attempts to find an adequate structure to fulfill all the requirements from the impedance and radiation point of view [17]. The design of an antenna is, thus, an iterative process, requiring vast amounts of antenna parameter evaluations. This procedure is time-consuming, making the above iterative design process prohibitively slow.

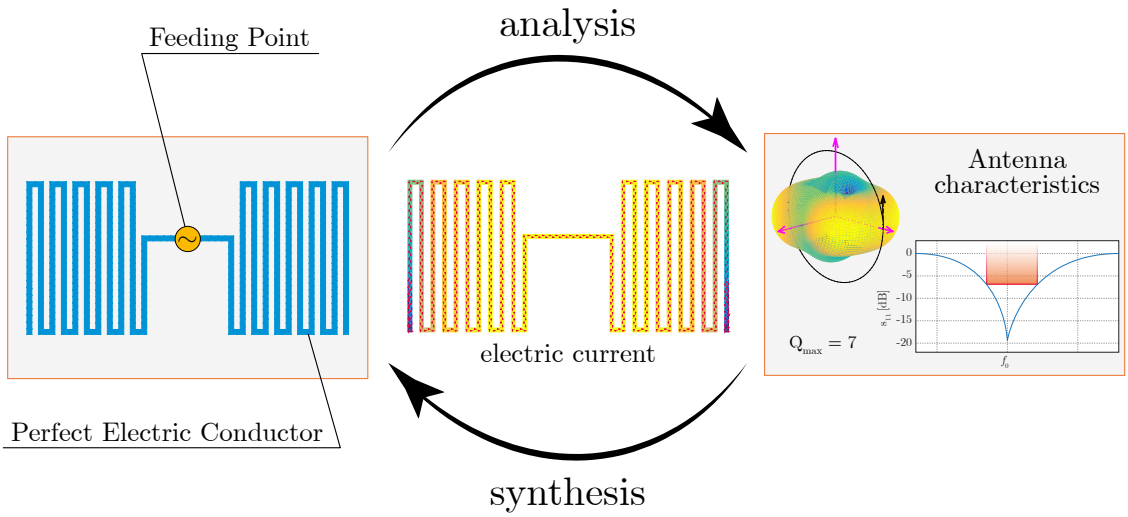

Figure 1.2: A comparison of antenna analysis and synthesis. Antenna analysis is performed by a transition from the left to the right part of the figure, antenna synthesis ideally follows the steps from the right to the left part. The key instrument for both the analysis and the synthesis is the current (in the middle). The electrical size of the original dipole antenna operating in its first resonance has been reduced from $ka = \pi/2$ to $ka = 0.4$ where k is the wavenumber and a is the smallest sphere circumscribing the antenna. The compact size of the meandered dipole is overbought by a relatively high quality factor and high radiation losses.

The earliest idea of the synthesis lies in the determination of the best shape, from an infinite number of options, based entirely on the initial requirements and limitations including the space allocated for the antenna, desired operating frequency, position and form of the feeding and, crucially, the required trade-off between parameters in view, see Fig 1.2. Antenna analysis has been mastered, thanks to modern analytical and numerical methods [18, 19], however, antenna synthesis involves two challenging tasks. The first task is to find which radiator's geometry is the most suitable for the given purpose, and the second is to reveal the best excitation for this shape. These two steps are closely interconnected through the fundamental laws of classical electrodynamics: the Maxwell equations [20].

Research on antenna synthesis, focusing primarily on the linear arrays [21], was pioneered by Schelkunoff and Friis in the late 1940s. Analytical studies of antenna array synthesis were continued by Elliot [8], among others. The possibilities in the antenna synthesis have been significantly extended by heuristic optimization algorithms which appeared in the 1980s [22]. Although powerful and effective, these optimization techniques only iteratively execute the tasks of the antenna analysis and, thus, they cannot be considered as the final stage of antenna synthesis. However these algorithms find the optimum is far better than brute-force advances of the past.

The antenna synthesis presents an, as yet, unsolved problem. One of the major issues is the infinite, in principle, degrees of freedom in the possible shapes of the antenna body to comply with the particular criteria as an antenna can take the form of almost any shape. Thus, the antenna synthesis poses a serious problem.

1.2 Seeking for the optimal antenna: fundamental bounds

Analyzing and synthesizing an antenna are, in all cases, extremely difficult processes in terms of the demands placed on a radiator whose parameters extend to the limits of fundamental physics. This is often the case for small antennas where we strive for electrically small dimensions of the radiating device in comparison with its operating frequency. Unfortunately, the electrically small, or sub-wavelength [23], antennas are inherently connected with a narrow frequency bandwidth and small radiation efficiency [24] due to the great amount of stored electromagnetic energy they accumulate.

Knowledge of the fundamental bounds helps to explain the principal limitations that cannot be overlooked and makes it easy to say how far a particular antenna design is from its optimum, or, what the optimal trade-off between the required parameters is. Determining the fundamental bounds is a challenging task, as can be demonstrated with an example of quality factor Q and its bounds. The limits of quality factor Q were first studied by Chu and Wheeler in the 1940s, but they were only able to address canonical cases. Chu investigated the fundamental bounds of a spherical shell by isolating the circuit in which each part described the electromagnetic behavior of one spherical mode [25]. He was unable to calculate the energy stored inside the sphere (since spherical harmonics are not complete there). Wheeler's work is more practically oriented. He described electrically small antennas as capacitors and inductors, and carefully investigated their operational limits [26]. Both Chu and Wheeler transferred the complicated electromagnetic problem into a circuit problem and while their ingenious techniques are presently considered as classics, they are also quite restrictive. Consequently, their successors tried to handle the problem directly in the realm of the electromagnetic field. Collin and Rothschild [27] were able to calculate the fundamental bounds of spherical antennas by utilizing electric and magnetic field components directly. Subsequently, in the 1990s, Hansen and Collin [28] followed this approach and extended the fundamental bounds for the energy stored inside the sphere. In recent years, the problem of the spherical shell has been reconsidered by several groups [29, 30] and reformulated for other canonical bodies (cylinder, spheroid) until finally being solved for electrical currents generating spherical harmonics [31].

The paragraph above briefly recapitulated more than seventy years of solving one particular problem, though it has been attacked by many prominent researchers and is not completely resolved since the influence of the material coating is still extensively studied [32, 33]. Moreover, even if the fundamental bounds of quality factor Q were to be found, they would only approximately reflect the potential bandwidth of the antenna.

Relatively great progress has been made in the estimation of available antenna gain G or, more specifically, in evaluation of the ratio of gain to quality factor G/Q, especially in the approach via static polarizability which seems to be very promising [34]. Broadly speaking, polarizability expresses the ability of a given structure to separate the positive and negative charge. Static polarizability is, then, the static limit of the polarizability function, which depends on frequency and which can be obtained by utilizing the optical theorem [35], together with an equality between the spectral integral of the extinction cross-section and the product of polarizability dyadics. Static polarizabilities are analytically known for several canonical bodies [36] and can be easily computed numerically.

The most problematic characteristic of small antennas is radiation efficiency. Consid-

ering real (lossy) metallization, its upper bounds are completely unknown and far beyond present-day knowledge [13].

Small antenna systems are rarely composed of more than one radiator. However, antenna arrays offer appealing options that cannot be reached in the case of a single radiator. Hot topics in this area are the limits of superdirectivity [37], and the design of superbackscattering arrays [38], although analyzing these systems is even more complicated as not only the shape of the individual radiators has to be taken into account, but the interactions between all components as well.

1.3 Source Concept: What is it really?

Any device whose physical behavior is governed by the laws of electromagnetism – a device made of conductors, connected to feeding and matching circuits, coated by dielectrics or magnetic materials – can be entirely replaced by an equivalent current. This operation can be done thanks to the equivalence principle and the induction theorem [39], powerful concepts which, in principle, say that any region with a known electromagnetic field ($\boldsymbol{\mathcal{E}}$ and $\boldsymbol{\mathcal{H}}$) can be replaced by sources ($\boldsymbol{\mathcal{J}}$ and $\boldsymbol{\mathcal{M}}$) which produce the same field outside. The equivalent current is electric or magnetic (or a combination of both) and flows in the planar surfaces (surface current) or in the volume (volumetric current). It is noteworthy that, compared to field quantities, currents all always bounded and are often direct outputs from electromagnetic simulators. These virtues suggest using the current as the only quantity to represent the radiating system completely. The paradigm seeking to achieve this objective is thenceforth called the Source Concept.

The following idea helps to imagine the additional insight provided by the Source Concept. The small antennas are traditionally delimited as radiating structures whereon the electromagnetic wave travels with a smaller phase velocity than light in free space [24]. Although this is valid characterization, the Source Concept offers a more instructive point of view: to enable the current to resonate in a region significantly smaller than the equivalent resonant length, the current needs to be distorted as can be seen in the electrically small meandered dipole antenna in Fig. 1.2. Once we find the geometry, we realize that efficiency decreases, stored energy and the corresponding quality factor increases, and the gain approaches the gain of a short dipole antenna. All these phenomena can easily be explained thanks to the Source Concept by analyzing the resulting current directly. We will see, and this is generally true for any small antenna, that the parts with the out-of-phased current are often placed close together, thus prohibiting effective radiation. Many similar observations are mentioned later.

If we rely only on the current, we, surprisingly, reveal numerous instrumental tools which originate in diverse scientific disciplines and are helpful in the further development of the Source Concept, see Fig. 1.3. These fantastic possibilities are exploited by the enhanced demands on scientists in the field, the primary reasons being the complexity of the underlying mathematical and physical machinery and the multidisciplinary character of the research.

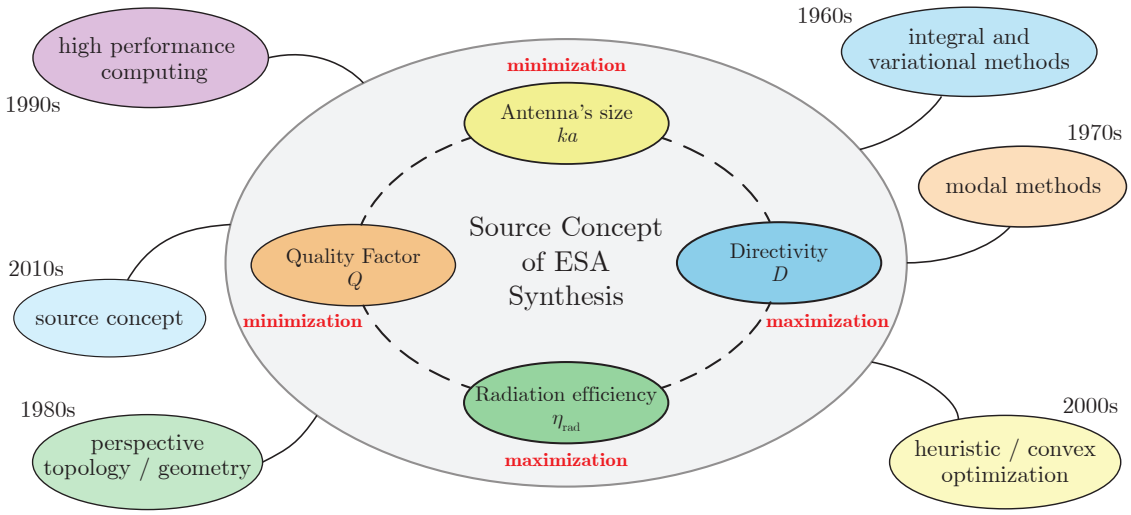

Figure 1.3: Schematic depiction of the Source Concept, its objectives and major components. The primary objective of the Source Concept is to link the important antenna characteristics (in the large gray oval) to the electromagnetic current. This was made possible thanks to many methods from various branches. The depicted small antenna parameters commonly need to be maximized/minimized as indicated by the red labels.

1.4 Organization and scope of the habilitation thesis

The thesis is divided into several chapters, covering all major aspects of the Source Concept and focusing on the highly exposed field of electrically small radiators. The achievements of the author and his colleagues will be briefed together with related contributions of other researchers. The thesis is meant to be a short integrating text, referring mainly to the attached papers.

With one exception in Chapter 3, only frequency domain techniques are used hereinafter. The reasons for this decision may be summarized as follows: these techniques are extremely effective for electrically small (narrow-band) antennas; characteristic modes decomposition, introduced in Chapter 2, is defined in its present form only for the time-harmonic current; and, last but not least, all important small antenna characteristics are defined for an antenna in its stationary state. For the sake of simplicity, the influence of the materials is wittingly left aside and only the radiators made of the perfect electric conductor (PEC) of finite extent operating in a vacuum are assumed. If the losses are considered, the current calculated for a structure made of the PEC is transferred to a structure made of the lossy media.

In Chapter 2, the potential ways how to obtain the source quantities are recalled. Attention is paid to modal methods and an artificial current, which both form the basis of further developments of the Source Concept. The current is utilized in Chapter 3 to calculate important antenna characteristics, many of them by novel methods. A simple analysis is probed in Chapter 4 and extends towards the antenna synthesis by employing the modal decomposition together with advanced post-processing. Chapter 5 is devoted to the practical implementation of the Source Concept. The thesis is concluded in Chapter 6.

1.5 Novelty in the habilitation thesis

It may be of interest how the habilitation thesis relates to the dissertation thesis [4] and, more specifically, what novelty is achieved. In this section, all technical details are left aside and only the original aspects are discussed.

This thesis partly results from the dissertation thesis[1] which established several important principles. These fundamental principles, namely the source definition of the impedance quality factor [2∗], and the interconnection of the characteristic modes and the evaluation of modal quantities [1∗], [3∗], led to a deeper, enduring interest in the physical meaning of the quality factor and its true functional dependence to the fractional bandwidth. The main contribution of the habilitation thesis, thus, lies in understanding and resolving the radiation energy extraction and the consequent evaluation of stored electromagnetic energy, one of the final hurdles of classical electrodynamics.

More specifically, the new paper [40∗] deals with the essential topic of the disputed proportionality between the quality factor and the intrinsic bandwidth, and finally proves that there is, in fact, no exact functional dependence between these quantities. The short contribution [41∗] assembles all state-of-the-art concepts of stored energy and, moreover, refutes an existing theory based on erroneous hypotheses. The paper [31∗] analytically solves, for the first time, the impedance quality factor for dominant spherical modes, pointing out that there are actually no practical lower bounds. Six other attached papers (not included in the dissertation thesis), mainly covering the ambitious topic of antenna synthesis via modal currents [42∗] and artificial currents [43∗], [44∗], are included.

The three recent papers, already published at the e-print archive arXiv.org, are devoted to the current topic of stored energies and the characteristic modes. One of these papers analyses the numerical stability of the characteristic mode decomposition with the analytical functional underlying the decomposition being derived there within [45∗], another paper compares different definitions of radiation energy [46∗], and, finally, the last paper [47∗] introduces the novel technique of how to evaluate stored electromagnetic energy. All these works have already been widely discussed at prestigious conferences [48–52].

Much work has also been done in the area of source concept implementation. The Antenna Toolbox for Matlab (AToM) represents the first existent attempt on how to implement it [53] with many powerful features already being exhibited.

[1] Both the diploma thesis and the dissertation thesis can be found on the author's webpage, `capek.elmag.org`. Many of the cited papers (if not included in the Appendix A) can be found on `arxiv.org`, `ieeexplore.ieee.org`, or `researchgate.net`.

Chapter 2

Determining the electromagnetic current

This chapter describes how we may potentially obtain the current distribution that fully represents the electromagnetic behavior of the structure. As has already been said, the electric and magnetic currents are the only physical quantities which enter the Source Concept, hence they deserve our full attention. After a short introduction to field integral equations in Section 2.1, the rest of the chapter deals with the characteristic modes decomposition.

2.1 Solution of Electric Field Integral Equation

The electromagnetic quantities will solely be represented by their frequency domain substitutes, the phasors [54]. The vector wave equation, expressed from Maxwell's equations, is transformed into the Electric Field Integral Equation (EFIE, [55]) in a straightforward manner. Mathematically, the EFIE is a Fredholm integral of the first kind [56] with the convolution kernel and singularities in the source region [57]. The singularities emerge from the Green function theory [58] used, and one has to be cautious about their evaluation. The classical treatment involves barycentric transformation [59] and integration by parts in a simplex coordinate system [60]. The analytical results for the self-terms can be incorporated into the numerical solution.

The EFIE's counterpart is the Magnetic Field Integral Equation (MFIE, [55]), which can be used to stabilize the numerical solution, especially if the PEC cavities are present [61]. The ultimate approach is the Combined Field Integral Equation (CFIE, [55]) which combines the EFIE and the MFIE. Since this thesis focuses only on the radiating structures, closed (non-radiating) cavities are not dealt with, and only the EFIE is further elaborated.

In case the current is unknown, the closed form solution of the EFIE is practically impossible. However, the current can be found numerically by the method of moments (MoM) which has been established in electromagnetism by Harrington [62]. The MoM procedure covers three main steps: discretization of a given shape [63] for which the current is sought, selection and pre-calculation of the basis and testing functions [64], and finally the evaluation of the potential and singular integrals [61]. The assembled impedance

matrix is an algebraic representation of the EFIE integro-differential operator. The types of numerical errors which have been accumulated into the algebraic solution are described in [61]. If the basis and the testing functions are the same, the moment solution has properties of the Ritz-Galerkin method [65, 66], i.e., the resulting matrix is symmetric and numerical errors accumulated during the matrix inversion are minimized in a variational sense since they are orthogonal to the chosen subspace of the Hilbert space [67].

Essentially, the impedance matrix, which completely represents the radiator, can be inverted or decomposed. Decomposition can be done by the singular expansion method [68], or by characteristic modes decomposition. The singular expansion method is a formulation of an eigen-value problem [69] which produces a basis of complex eigen-currents and eigen-numbers that reflect the exponential damping of each mode. Far better properties are possessed by the characteristic modes, which are later discussed in detail. Aside from the decomposition of the impedance matrix, the most common approach is to use inversion. If the inverted matrix is multiplied by a column vector representing the excitation, the unknown current is obtained [62]. It does not matter if the current is a product of inversion or decomposition, it can be the subject of post-processing which is described in the following chapter.

2.2 Characteristic modes decomposition

The impedance matrix carries more information than any of its particular (MoM) current solutions. The only exception would be a complete basis of modal currents [70], which could reconstruct any particular current without the necessity of an additional impedance matrix inversion. In order to obtain these modal currents, it has been proved that a natural choice for radiation problems lies in the decomposition into the characteristic modes (CM). The primary reason being that only a few characteristic currents are necessary to compose the total current. The ingenious idea of the CM, thus, provides an excellent transition from the impedance matrix to the Source Concept. The rest of the section is devoted to the explanation of the CM decomposition and its consequences.

The CM decomposition has been introduced by Garbacz [71] and then reformulated by Harrington and Mautz [72]. They also describe important computational aspects of the CM decomposition [73]. The full potential of the CM, however, has remained, more or less, unrecognized for 40 years. The capabilities of the CM were revisited in 2007 [74] and, since then, interest in the CM has dramatically increased. The recent boom of CM theory is reflected by the number of prominent publications in Fig. 2.1 with notable milestones depicted in Fig. 2.2.

The complete transition from EFIE to CM is recapitulated in [1∗] and [75] and includes several examples. An evaluation of the basis and testing functions is depicted in [1∗], in which the singularity treatment is studied as well. That said, only CM fundamentals are emphasized here.

Let us consider a symmetric (non-hermitian) impedance matrix $\mathbf{Z} = \mathbf{R} + \mathrm{j}\mathbf{X}$, in which $\mathbf{R}$ and $\mathbf{X}$ are the resistance and the reactance matrix, respectively. The characteristic modes decomposition is a generalized eigen-value problem [69] defined as follows [72]:

$$\mathbf{X}\mathbf{J}_n = \lambda_n \mathbf{R}\mathbf{J}_n. \tag{2.1}$$

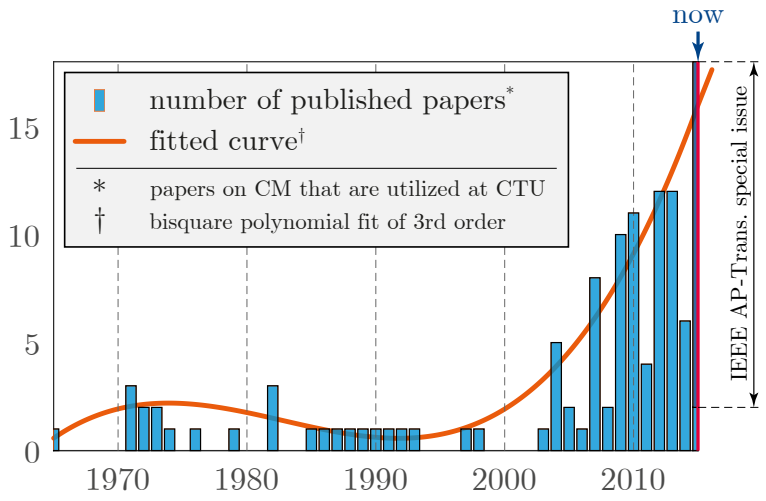

Figure 2.1: A histogram depicting a number of papers involving CM development at CTU (not all papers are listed). It can be seen that following humble beginnings in the 1980s and 1990s, there has been a boom in CM since 2000. Important milestones of CM development are graphically depicted in Fig. 2.2.

The resulting characteristic currents $\mathbf{J}_n$ are normalized according to (7)–(9) of [76], which means that they are orthonormal with respect to modal far-fields. The physical meaning of the CM is summarized in Harrington and Mautz's original papers [72, 77], as well as in a review paper [74]. An illustrative example of the first five modes on a planar inverted-F antenna (PIFA) is depicted in Fig. 2.3.

Important problem which has yet to be completely solved is the tracking of CM. Many persistent issues were analyzed, addressed and finally solved in [75], including the fact that modes can suddenly appear or disappear, depending on their modal significance. The remaining problems are subjects of ongoing research [78–80], so the ultimate tracking technique is far from being implemented.

Similar to other generalized eigen-value problems, CM decomposition is ill-posed, and no pre-conditioner actually exists since the ill-posedness of CM is the true feature of radiating modes. This fact has been elucidated in [45∗], including another persistent problem, the presumed existence of a differential mode.

It should be noted there are essentially two ways how to perform the CM decomposition: the QZ algorithm (commonly known as the generalized Schur decomposition, [81]) and Implicitly Restarted Arnoldi Method [81]. By utilizing the QZ algorithm, we obtain the complete basis, i.e., N modes for the impedance matrix of size $N \times N$. This approach is suitable for any subsequent superposition since (ideally) we know the whole basis. Utilizing the Arnoldi method, we always get $M \leq N$ (mostly only $M \ll N$) modes, in which M has been set by the user. It may seem that the QZ algorithm is far better, though unfortunately the answer is not so clear, since the asymptotic complexity of QZ is $\propto \mathcal{O}\left(N^3\right)$, while the complexity of the Arnoldi method is only $\propto \mathcal{O}\left(N^2\right)$. Other aspects can be found in [82], whereas the direct implications of the QZ utilization are studied in [75] and [45∗].

To verify CM capabilities, the fractal antenna has been studied by CM in [83]. The initial shape has been found by employing the cavity model [84] so that the minimum

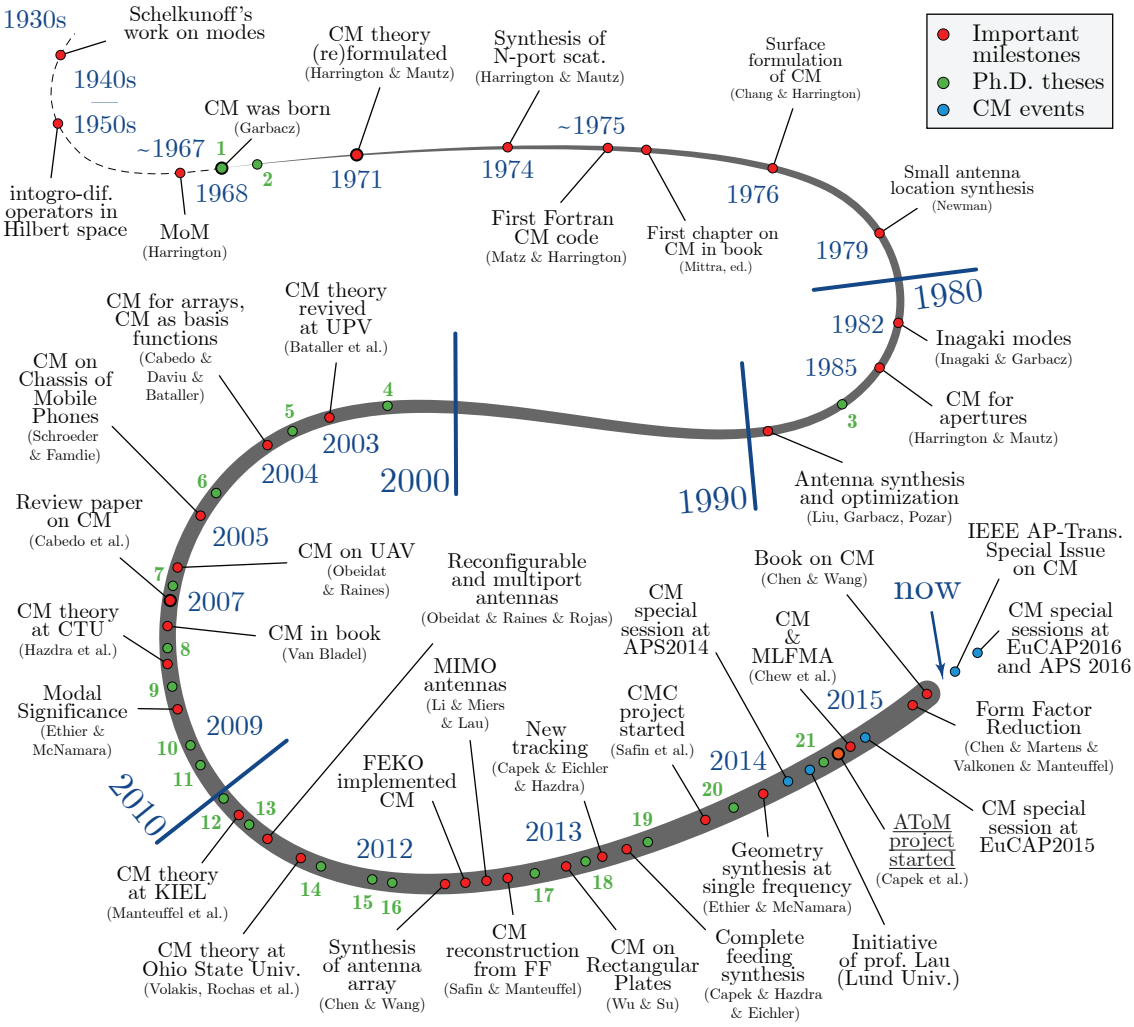

1 (Garbacz, 1968)
2 (Turpin, 1969)
3 (Liu, 1986)
4 (Strohschein, 2002)
5 (Bekers, 2004)
6 (Surittikul, 2006)
7 (Cabedo Fabres, 2007)
8 (Famdie, 2007)
9 (Antonino Daviu, 2008)
10 (Hazdra, 2009)
11 (Sonkki, 2009)
12 (Obeidat, 2010)
13 (Lawrence, 2010)
14 (Adams, 2011)
15 (Raines, 2011)
16 (Strojny, 2011)
17 (Ethier, 2012)
18 (Alroughani, 2013)
19 (Hamad, 2013)
20 (Capek, 2014)
21 (Eichler, 2014)

Figure 2.2: A summary of the development of the characteristic modes theory. Attention should be drawn to the boom at the beginning of the 2010s. The first special session on CM was held at APS in 2014, then, at EuCAP 2015 and another is to take place at EuCAP 2016 and APS 2016 as well. The first book specializing in CM theory was published in 2015, the first commercial software, FEKO, implemented CM in 2012, and another company, CST, is about to implement it in 2016.

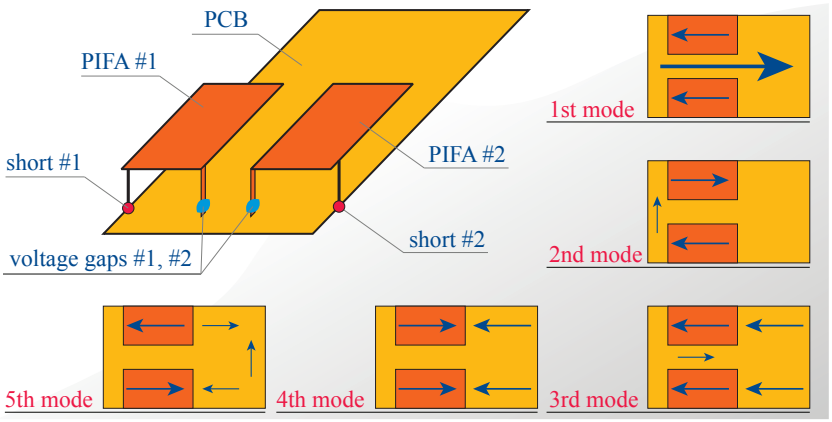

Figure 2.3: A schematic depiction of the first five characteristic modes of PIFA. Two active radiators are fed by voltage gaps and induce the current on the ground plane. The antenna is capable of a dual-band/dual-polarization operation [6∗]. A more sophisticated version of PIFA is often mounted in cellular phones.

resonant frequency has been reached. To verify the underlying procedures, the antenna sample has been manufactured and measured. The full potential of CM has been utilized in [85∗] to design a dual-band antenna with orthogonal polarizations fed by a dual L-probe [86]. Proper positioning of the L-probe has been estimated by CM analysis and refined by a commercial full-wave simulator CST-MWS [87].

CM is, without a doubt, a state-of-the-art technique which perfectly fits into the domain of the Source Concept and provides deep physical insight and understanding of the antenna operation. Its influence can be further enlarged in several ways. Incorporation of the periodical boundary condition [61] may extend our present understanding of the periodical structures, antenna arrays and fractal antennas. The true breakthrough would be the adaptation of the existent fast numerical methods, such as the Multilevel Fast Multipole Algorithm (MLFMA, [88]) for calculating the CM [82].

2.3 Artificial current

The artificial current is referred in this thesis as such a current that has been defined a priori regardless of its analyticity or fulfillment of the boundary and the radiation conditions [89]. The absence of physical limitations enables higher degrees of freedom in comparison to the set of the currents satisfying the vector wave equation. Although the introduction of the artificial current is not completely rigorous, to the point that the equivalent current is often used [39], it pertinently describes its role within the Source Concepts as an arbitrary complex-valued function of compact support in $\mathbb{R}^3$.

In the frame of the Source Concept, the artificial current can be utilized in many ways. Its key role resides in analytical proofs and other operations that cannot be, in principle, done numerically. This approach is actually well-known in classical antenna theory. For example, the radiation resistance of the Hertzian dipole is calculated by considering the current-carrying filament of the constant current. Exactly the same approach can be repeated for a thin-wire half-wavelength dipole fed in the middle for which radiated power

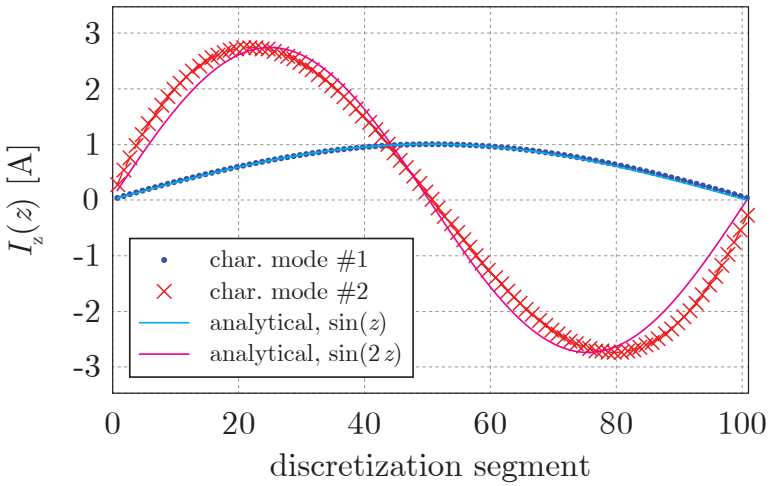

Figure 2.4: A comparison of the first two characteristic modes at resonance and their analytical substitutes for a thin-wire dipole discretized into 101 equidistant segments. The difference between an exact solution (markers) and an analytical substitution (solid lines) is negligible for the first resonance (blue), but is more meaningful for higher resonances (red). All curves are normalized with respect to the radiated power and to the unitary amplitude of the first modal current.

can be calculated analytically if the sinusoidal (artificial) current distribution is considered [90] with the result being obtained in a closed-form. This is far from possible for realistic current distribution, whose behavior is analytically unknown, yet very similar to the sine function [90], see Fig. 2.4.

The analytically prescribed artificial current can be used for benchmarking the numerical techniques. It can also be utilized wherever the impedance matrix inversion or the decomposition cannot be carried out or is superfluous. A good example is the geometrical optimization of the double U-notched loop antenna performed in [91]. The loop antenna is analyzed only in its first resonance, in which a good approximation of the current distribution can be found analytically. Much numerical effort is saved by skipping the full-wave MoM/CM solution, and this extra time is then invested into the solution of the real problem – the determination of the optimal shape of the antenna. Similar to the loop antenna, the papers [44∗] and [43∗] employ an artificial current to investigate the quality factor Q of the dipole arrangements efficiently. The amount of computational time is reduced and the additional insight is reached.

The artificial current arises from structural decomposition [2∗], a promising technique detailed in the following chapters, or from convex optimization [92], a sub-field of mathematical optimization [93]. The artificial current can be helpful in semi-analytical methods, often imitating the modal current. It can be imposed into the numerical model by substituting analytical values into the discretization scheme. Note, once again, the example of the spherical shell from Section 1.2. Its CM decomposition [71] results in spherical harmonics [94], a set of orthogonal functions which forms a natural basis of spherical geometry. The symmetry makes the spherical shell the only body of finite extend with analytically known CM. This unique feature can be used for the verification of meshing schemes or the stability of the eigen-decomposition.

Chapter 3

Analysis based on the Source Concept

If we already have the current, we can utilize it to collect important antenna characteristics. Novel advanced techniques showing how to gather this information are mentioned within this chapter which focuses primarily on the parameters depicted in Fig. 1.3. The topic is dealt with in detail in the attached papers, thereby, only the key achievements are remarked upon here.

3.1 Quality factor Q

The focal point of the small antenna analysis is the evaluation of quality factor Q which reflects the bandwidth potential of the radiator [13]. As can immediately be seen from Fig. 3.1, the problem of the quality factor is immensely complex, covering circuit theory, system theory and electrodynamics.

How complex is the problem of the quality factor Q in electromagnetics is gradually revealed as all problems associated with it start with its definition. The introduction of the quality factor was motivated by its presumptive relation to the fractional bandwidth (FBW) which is, however, neither known nor proven to exist. Traditionally, two various hypotheses are recognized. As far as the first one is concerned, the quality factor is based on the stored electromagnetic energy and reads

$$Q \equiv \frac{\omega W_{\mathrm{sto}}}{P_{\mathrm{d}}}, \tag{3.1}$$

where ω is angular frequency, W_{sto} is stored electromagnetic energy, and $P_{\mathrm{d}} = P_{\mathrm{rad}} + P_{\mathrm{lost}}$ is dissipated power which aggregates the radiated power P_{rad} and the losses P_{lost}. As for the second hypothesis, it makes use of the frequency sensitivity of the input impedance and reads

$$Q_Z \equiv \frac{\omega}{2P_{\mathrm{rad}}} \left| \frac{\partial Z_{\mathrm{in}}}{\partial \omega} \right|, \tag{3.2}$$

in which Z_{in} is the input impedance and the current flowing through the input port is normalized to 1 A.

Stored energy is a mysterious quantity – while its definition is well-known for the stationary field, the radiation which is produced by the non-stationary field complicates

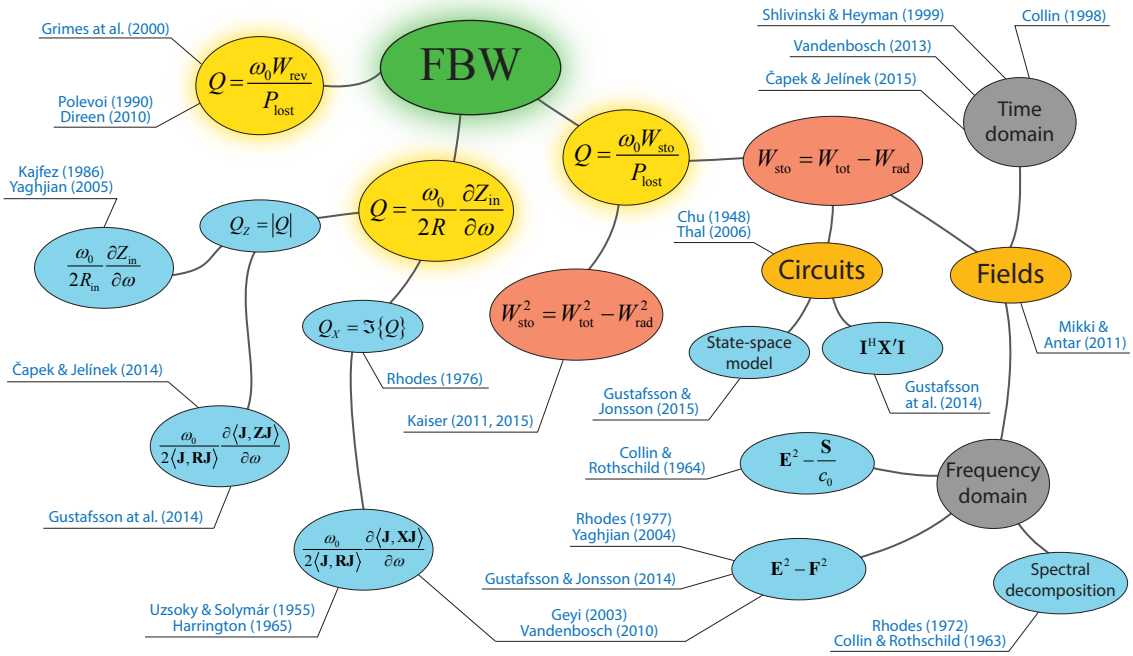

Figure 3.1: A relationship between quality factor Q and the fractional bandwidth (FBW) depicted as a mindmap. The quantity of primary importance is the FBW (green bubble). The realm of the quality factor evaluation consists of thee various definitions (yellow bubbles). The leading concepts are depicted by the blue bubbles.

any attempt for an explicit and general definition. The formidable challenge here is to subtract the radiation energy correctly (remembering the infiniteness of the radiation energy within the time-harmonic operational state) which, unfortunately, often leads to non-physical features like coordinate dependence, gauge variance of the negativeness of the resultant stored energy prescription [46∗]. Contemporary approaches on how to do this are summarized in [46∗], including a comparative study of radiation extraction for the case of a dominant TE_{10} spherical mode. The history of stored energy evaluation is recapitulated in the introduction of [47∗].

The pivotal concept of Vandenbosch [95] interposed the long period, when the same ideas of stored energy evaluation were recycled again and again, and introduced a new technique of radiation energy subtraction by challenging the problem in an entirely new way. The resulting expressions of stored electromagnetic energy are fully compatible with the Source Concept which were verified in [44∗] in the arrangement of two closely spaced thin-wire dipoles with in-phased and out-of-phased artificial current distributions, settings which resemble the first two characteristic modes. A good agreement between quality factor Q from [95], Q_Z from [96] and Q_X from [97] has been observed. Despite the fact that the artificial current has been used, a minima of quality factor Q, which depends on the separation distance d between the dipoles, has been found and verified numerically in FEKO [98]. Interestingly, the minimum is prescribed by a transcendent equation in the form of $\tan(kd) = kd$, where k is the wave number. The same approach, focusing on the effects of the shape variations on the minimization of the natural resonance, has been

repeated for a loop antenna. By combining the CM, together with an artificial current distributed on a parametrized curve of loop topology, the overall size of the radiator has been reduced without any significant deterioration of its radiating performance. It has also been demonstrated in [99∗] that the elaborate derivation made in [95] can be simplified by utilizing the electromagnetic potentials [100] leading to the same subtraction scheme in a much more straightforward manner.

It was not until 2012 when Gustafsson et al. [101] found an example where Vandenbosch's expressions yield a negative value of stored energy. Subsequently, it has been recognized that the problem is primarily posed by electrically large radiators with uniform current density. Such a current is clearly unphysical[1] and, thus, it is no wonder that this phenomena cannot be tested in any other way than by the substitution of an artificial current directly into Vandenbosch's relations. These findings have rendered these expressions as incomplete, even though they are still extremely useful in many practical cases.

An attempt has recently been made to utilize Foster's theorem [54] to deliver expressions for stored energy compatible with the Source Concept. This work has been commented on in [41∗] for the reason that it contains an erroneous derivation under the mistaken premise that Foster's theorem is valid for antennas [102]. The comment [41∗] also explicitly demonstrates which relations hold between the formulations of Vandenbosch [95], Gustafsson and Jonsson [30], Capek, Jelinek et al. [2∗], Yagjian and Best [96], and Geyi [103] and, in particular, the way how the coordinate dependence of [96] and [30] is annihilated if the approach from [2∗] is applied. The reply to the comment [41∗] is available on arXiv [104].

A completely new paradigm to evaluate stored electromagnetic energy is postulated in [47∗], utilizing a time-domain integration of the radiation energy in the far-field. The stored energy within this paradigm is considered to be the rest of the mass residing in the near-field of the antenna. Two separate runs of the method are required to distil the radiation energy and to avoid infiniteness. The principle of the method is that the ill-defined stored energy is transformed by an antenna to the radiation which can be easily integrated in the far-field. This technique exhibits all necessitated properties, thereby representing the most advanced evaluation scheme of stored energy.

Tracing back the origin of (3.2) is even harder than in the case of (3.1). The widely used quality factor Q_Z, see Fig. 3.1, has been established for antennas by Yaghjian and Best [96], utilizing the same definition already known in the circuit theory [105]. A tremendous benefit of Q_Z lies in its direct measurability via explicit dependence on the input impedance. This quality has been exploited in [43∗] which reconsiders the problem of out-of-phased closely space dipoles from [44∗]. The original arrangement from [44∗] is replaced by a dipole over an infinite ground plane by the method of images [106], then the analytical formula for input impedance [107] is substituted into (3.2) and computed.

The transformation of quality factor Q_Z into the Source Concept has been performed in [2∗] in which the complex power balance [100], together with the electromagnetic potentials, has been employed. Quality factor Q_Z is then transformed into an integral bilinear form of current. As compared to Vandenbosch, one additional term occurs. This energy term contains a frequency derivation which cripples the attractive properties of the

[1] The expressions should still be able to accept any thinkable current and yield non-negative results.

Source Concept definition of Q_Z since it prevents the usage of modal methods or of convex optimization [2∗].

Despite now having the Source Concept of quality factor Q_Z, one insistent question, which has been addressed in [31∗], remains to be answered: Are the fundamental bounds of quality factors Q and Q_Z the same? The fundamental bounds of the spherical shell, which have been analytically worked out following the procedure from [2∗] and represented by the dominant spherical modes TE_{10} and TM_{10}, have been inspected. Considering the standalone modes, the Q_Z formulation yields similar bounds as classical quality factor Q [31∗]. Evaluating a linear combination of the TE_{10} and TM_{10} modes, however, quality factor Q_Z can be zeroed practically for any ka, where a is the radius of the spherical shell [31∗]. Note that this surprising result is in direct conflict with the statement of quality factor in the IEEE Standard Definitions concerning Terms for Antennas [108].

The long-believed notion that the quality factor of an antenna has exact functional dependence to its FBW, a quantity of paramount importance, has been recently refuted. A series of counterexamples [109, 110] culminated in [40∗], proving the non-existence of general functional dependence between quality factor Q and FBW. Fortunately, this embarrassment is only formal under the important case of small antennas which are characterized by a high quality factor ($Q \gg 2$) for which the relationship to the FBW is near to be exact. Nevertheless, the disproof has far-reaching consequences, since the exact functional dependence between the quality factor is often taken for granted.

3.2 Evaluation of radiation efficiency

Radiation efficiency significantly affects the power budget of the radio link. It also enters into (3.1) and (3.2) as an additional term affecting the quality factor. The explanation for the radiation losses lies in joule heating caused by the electric current passing through the finite conducting material [100].

Radiation efficiency decreases when the antenna becomes small or highly irregular (when a current of high amplitude is induced) or if the material is too lossy. When a good conductor (such as copper or gold) is used, the only explanation for substantial radiation losses is the geometry of the radiating body. Hence, the evaluation of radiation efficiency is critical for a precise investigation of highly irregular, often electrically small, shapes for which radiation losses predominate over the radiated power.

Analytical studies of radiation losses are rare and focus solely on a dipole arrangement [111]. The conventional numerical approach utilizes a proper modification of boundary conditions, respecting as it does the Impedance Boundary Condition (IBC, [112]). This approach is, however, encumbered with several restrictions including the modification of the MoM formulation for perfectly conducting surfaces.

Numerical models that can evaluate radiation efficiency directly from a surface current without any modifications are scarce [113], though one possible approach has been derived in [1∗] where the thin-sheet approximation [113] is utilized, together with the key assumption that the current distribution on the PEC surface is almost the same as in the case of an extremely good conductor. This assumption has been verified against the conventional IBC. The exponentially decaying current wave propagates though the half-space area, filled by the lossy conductor. It is imposed that the cross-section integral of the vol-

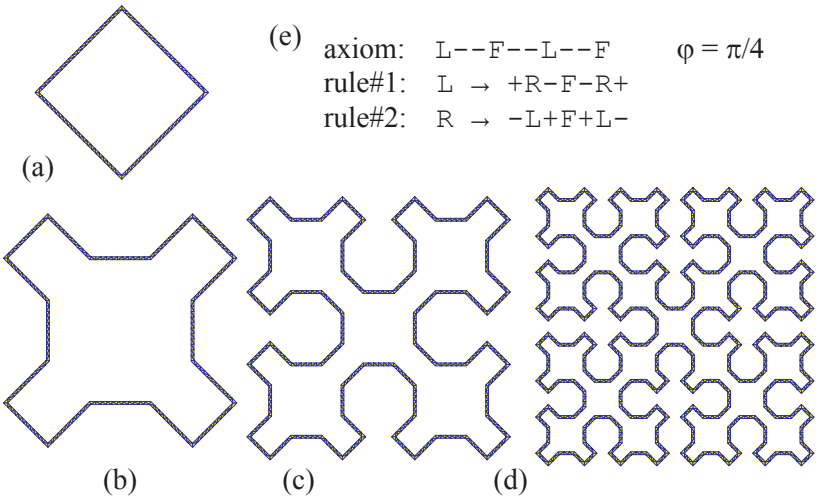

Figure 3.2: An example of the Lindenmayer system [5], (a) Sierpinski cross fractal curve of the first (b), the second (c), and the third (d) iteration. The initial shape and grammar are depicted in subfigures (a) and (e), respectively.

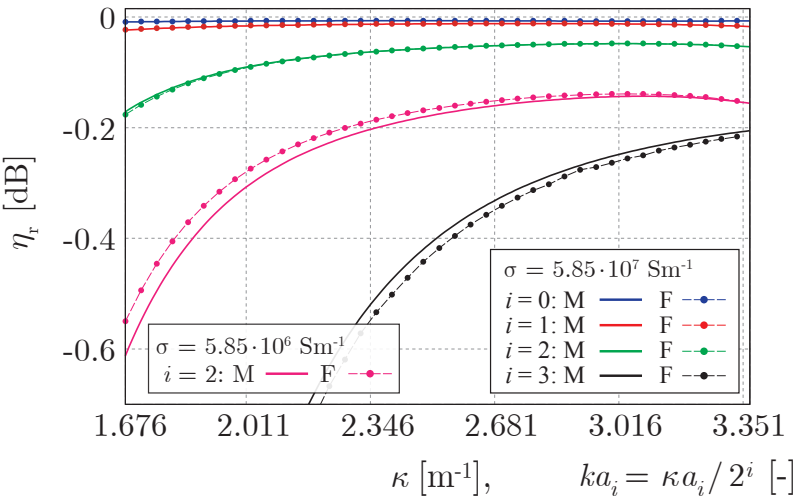

Figure 3.3: The total radiation efficiency of the Sierpinski cross fractal curve of various iterations (see Fig. 3.2) excited by one delta gap, M — Matlab [7] implementation of the novel technique [1∗], F — FEKO implementation of the IBC. It is observed that losses grow with higher iteration i. The variable a is the radius of the sphere circumscribing the antenna.

umetric current has the same magnitude as the original surface current. For all realistic scenarios (reasonable high conductivity and metallization) the results of the novel method were in excellent agreement with the IBC, see, as an example, the Sierpinski cross fractal curve in Fig. 3.2, and the results in Fig. 3.3. Furthermore, no MoM modifications nor any specification of the feeding are required which opens new possibilities when calculating radiation losses during the post-processing stage on demand.

3.3 Analysis of modal currents

We have seen in Section 2.1 that modal analysis is a powerful technique. In this section, its elegance will be incorporated into the expressions for quality factor Q and radiation efficiency. Notably, newly introduced concepts of modal quality factor and modal radiation efficiency broaden the scope of the Source Concept. But, before we can do this, several important conditions, discussed at the beginning of [1∗] and [3∗], must be met.

Previous attempts to substitute modal currents into the evaluation of quality factor Q are generalized in [1∗]. A rigorous superposition formula is derived containing modal stored energies and the so-called beta matrix which couples all modal quantities with the external world represented here by the feeding. The superposition formula is, for the first time, exact and is not dependent on any particular expressions for stored energy, i.e., any formula for stored energy can be properly substituted (if it meets the necessary conditions).

Analogous to the modal quality factor, the concept of modal radiation efficiency has been proposed in [1∗], including the superposition formula also based on the beta matrix. Thanks to this work, it has been explained why the efficiency of two closely out-of-phased dipoles is too low.

The modal radiation phenomena of the microstrip patch antennas were studied in [42∗] using the motif from [85∗] and another pre-fractal shape. The influence of the iteration number and the height above the ground plane has been investigated. In general, it has been observed that the quality factor decreases for higher distances from the ground plane and for a smaller number of iterations. Quantification of these phenomena reaps the profit from the derived integral bilinear forms of the current [2∗].

Chapter 4

Source Concept and antenna synthesis

Having full control over the currents and all related antenna characteristics, we can now do much more than the cut-and-try analysis.

All techniques mentioned above solely concern antenna analysis. But what about antenna synthesis? It is necessary to admit that a complete synthesis is, still, unreachable. Nevertheless, many ingenious techniques have recently been adopted to approach the synthesis as closely as possible. Single- and multi-objective optimization algorithms have proved themselves to be essential tools, in particular the convex optimization [93, 114] and heuristic optimization [10, 115] techniques which can be advantageously combined with the physical machinery introduced in the previous chapters.

Based on the initial assignment, synthesis problems can be divided into three levels of rapidly increasing difficulty:

1. the geometry of the individual radiators is given (see Section 4.1)
   - feeding is unknown,
   - in case of more radiators, their relative position is unknown,
2. the initial geometry or topology is given, typically as a low-dimensional optimization problem (see Section 4.2)
   - feeding can be unknown,
   - topology can be restricted,
   - geometry constraints are given,
3. only the feasible area is limited, the desired antenna parameters are given (see section 4.3)
   - solvable under certain circumstances, the result is an artificial current. It is not known how this current can be supported by a properly fed PEC structure.

The lower level is always a subset of the higher level and all of these levels of synthesis are examined in the following short sections.

4.1 Fixed Radiator Geometry

This section represents the first real step towards antenna synthesis. Since the shape of a radiator remains fixed during the whole procedure and the feeding is the only unknown, CM decomposition is an excellent option to provide an ultimate solution.

The methods presented in [1∗] and [3∗] make it possible to perform the feeding synthesis or, in other words, to find the optimal location, amplitude and phase of the feeding ports so that the minimum quality factor, maximum radiation efficiency, maximum antenna gain, or their preferred combination, is found. The procedure involves the pre-calculation of modal energies and modal lost powers including the off-diagonal terms which represent the non-zero near-field interaction of the characteristic fields whose existence must be taken into account properly inside the summation formulas. The possibilities of the feeding synthesis based on modal quantities are demonstrated in the result sections of [1∗] and [3∗].

How complex the design of the feeding network can be is demonstrated in [116]. The radiator is formed only by a rectangular plate, but, thanks to the sophisticated 8-port feeding system which has been designed with the aid of the CM decomposition, the antenna offers many concurrently operational states enabling multiple-input multiple-output (MIMO) wireless communication. The related work [117] investigates and evaluates the influence of antenna impedance loading on the characteristic modes. The effect of the losses in the matching components and the load elements are properly taken into account here. Combining radiation losses from Section 3.2 and losses in the matching network presents a subject of ongoing research.

4.2 Initial geometry is given

Compared to the previous section, a more involved problem occurs when we have only the initial shape which needs to be appropriately modified to meet the prescribed criteria (usually high efficiency, given resonant frequency, low quality factor, defined radiation pattern).

One technique which perfectly fits this section is structural decomposition. The initial structure is usually divided into several parts according to their functionality. These parts are then analyzed separately and the coupling is described by the cross-terms. Any part can be a further subject of geometry optimization. The motivation of the structural decomposition is to answer the question how the selected part contributes to the overall characteristics as shown in the example of an electrically small loop in Fig. 4.1.

The potential of the structural decomposition has been revealed in [2∗]. The loop antenna is decomposed into the CM, next the mode with the best radiating behavior is isolated, and then the structure is split into well-radiated parts and the parts predominantly storing the energy. The shape is optimized so that the current maxima are on the well-radiated straight parts, while the minima are on the poorly-radiated meanders which are capable of reducing electrical size. The amount of magnetic energy stored in the meanders is minimized thanks to the negligible current density. On the other hand, the stored electric energy is remarkably high. It is, however, compensated by the magnetic energy of the whole loop. Additional degrees of freedom are the dimensions of the meanders that can be modified to get better efficiency and quality factor. A remarkable question of this

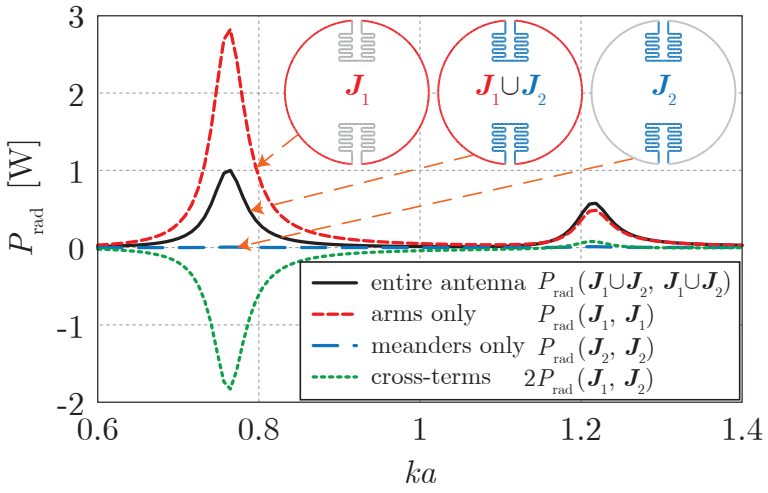

Figure 4.1: Structural decomposition of the optimized double U-notched antenna [2∗]. An artificial current that imitates the first CM is utilized and the radiated power is calculated by the integral bilinear form. The results are normalized with respect to the maximum radiated power of the entire structure. It can be seen that the power radiated by only the arms (red) is almost three times higher than the power radiated by the entire structure. The reason is not due to the meanders (blue), but to the significant contribution of the cross-terms which is negative.

particular example is the theoretical existence of the optimal ratio between the electrical length of the radiating (straight) and the non-radiating (meandered) parts. This ratio significantly affects the trade-off between electrical size and potential bandwidth. Structural decomposition is closely related to the sub-structural modes [118, 119] as they represent the CM associated with only a part of the whole antenna body. It is only a question of time as to when these two techniques will be intermingled.

Nowadays, thanks especially to powerful computers and efficient optimization algorithms, we can start to think of the geometry optimization. The most widely used techniques first divide the optimized space into small segments, then fill these segments by the PEC material [22] and calculate the current by the MoM. The whole procedure is controlled by the heuristic optimization (often a genetic algorithm or one of the swarm approaches). Since the first attempts were undertaken with small square segments [120] resembling pixels, the technique became known as pixelling, see Fig. 4.2. Other authors call the technique topology optimization [121] or shape optimization [122], but the working principle is always the same. One of the first published works combining shape optimization and CM is [123]. Notwithstanding recent attempts, the second level of the synthesis, discussed in this section, is still in its infancy.

The shape optimization has been done in [83] preserving the same topology for all particle swarm optimization agents, see Fig. 4.3. The similarity has been achieved by utilizing the iterated function system [5]. To reduce the computational time of the full-wave MoM, the cavity model has been employed in Comsol Multiphysics [124]. The data post-processing and the particle swarm optimizer run in Matlab. It has been demonstrated in the examples of the fractal shapes that by applying this technique the electrical size of the radiator can be significantly reduced. Moreover, the fractal shapes embody several

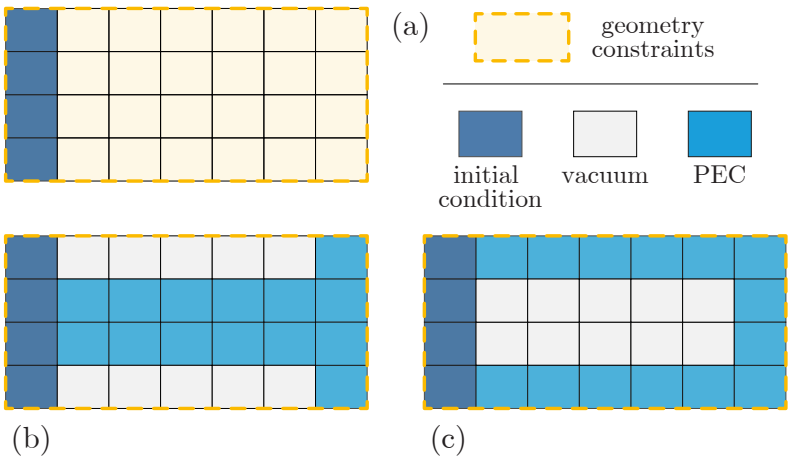

Figure 4.2: Geometry optimization with given constraints. The rectangular plate delimited by the dashed orange line represents a feasible region for optimization (a). The region is discretized into "pixels" with the dark blue pixels representing the additional boundary condition. At the beginning, the impedance matrix is calculated for the entire region which is supposed to be continuously filled by the PEC. The resulting impedance matrix is then pruned by a heuristic algorithm. Two different solutions are depicted in (b) and (c), the first one resembles a dipole, the second one a loop.

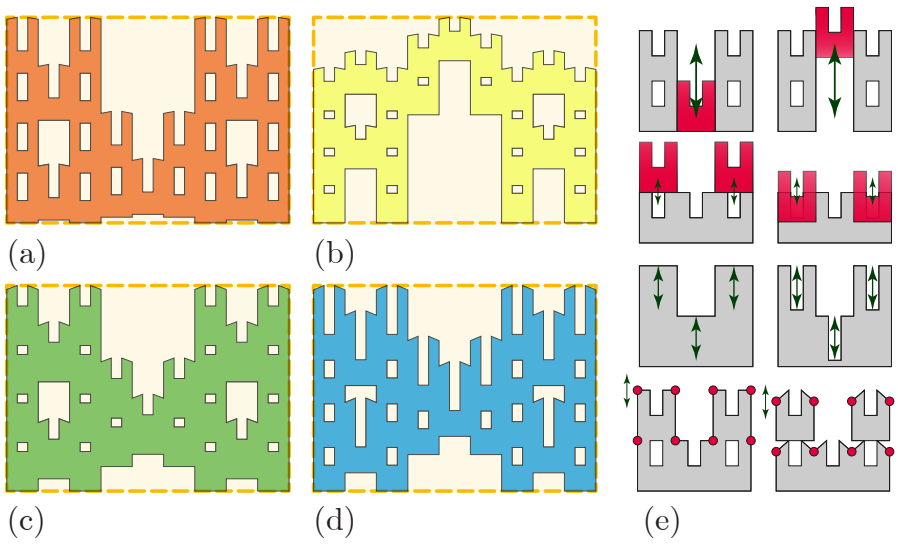

Figure 4.3: Geometry optimization of the IFS fractal of the 2nd iteration. The width and the height of the antenna is fixed (as shown by the dashed orange line). Only four IFS parameters are optimized which ensure that the same topology and the qualitative behavior is preserved. All optimization agents are axially symmetric with respect to the vertical axis, contain same patterns and have a dominant resonance along the horizontal axis, see (a)–(d). Thanks to the optimization of only four IFS parameters, the dimension of the variable space is significantly reduced. The right column (e) represents all available transformations in their min–max extremes.

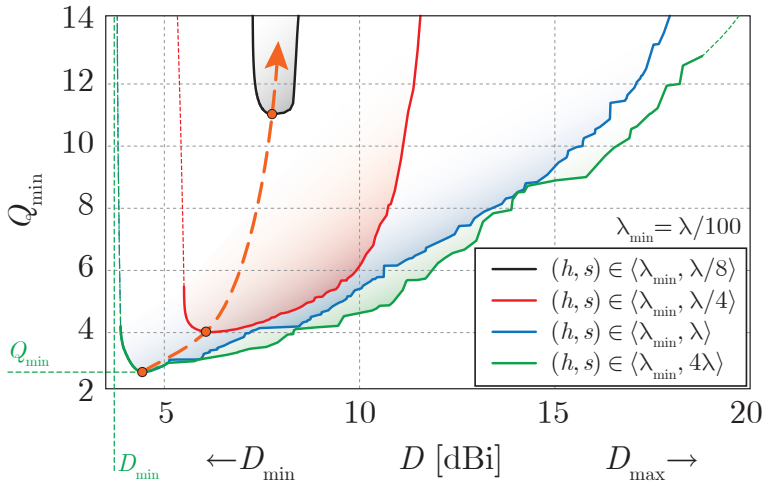

Figure 4.4: The Pareto fronts for two dipoles separated by distance s and placed at height h above the perfectly conducting infinity ground plane. Restricting the interval of the available h and s leads to a significant shift of the Pareto front (from the green line to the black line). Notice the problem always has the minimum value of quality factor Q, whereas the behavior of the directivity is more intricate and the theory of antenna arrays [8] is necessary for its correct interpretation. All curves were obtained via an in-house multi-objective optimizer powered by a hybrid of the particle swarm optimization [9] and the self-organizing migrating algorithm [10] with an adaptively pruned external archive and epsilon dominance metric.

unique features. For example, certain high-ordered modes are able to mimic the antenna array. Their behavior is noteworthy when the number of iterations increases as resonant frequency decreases at the expense of stored energy and radiation losses rapidly increase.

The geometry optimization can also be understood from an alternative perspective. Consider for a moment the example of an antenna array for which the best performance is sought. While the shape of the individual radiators is given, their adjustment is unknown. If unsolvable analytically [8], this certainly poses an interesting optimization problem. From a certain point of view it is a problem of the structural decomposition. However, the individual parts have a constant shape and, in addition, they are galvanically isolated. A practical example of a small dipole array which makes use of multi-objective optimization is depicted in Fig. 4.4.

4.3 Geometry is completely unspecified

So far, there is only one numerical method which fits into this category: convex optimization. Convex optimization [93] is unable to find the best geometry directly, so, instead, it finds an artificial current which minimizes the prescribed functional [92]. Since the resulting current is artificial, it does not fulfill the boundary conditions and there is no known procedure as to how to extract the equivalent PEC shape from this current. Notwithstanding these limitations, convex optimization is helpful since it establishes the fundamental bounds. With the particular shape optimized (for example by the pixelling), we can check how far its performance is from the optimum [92].

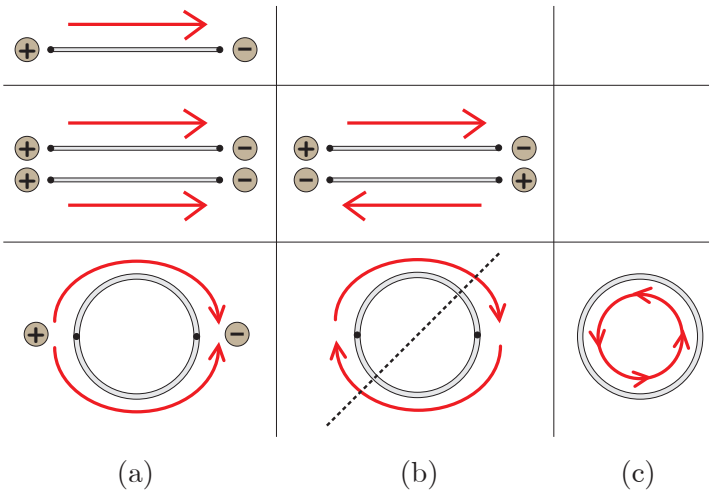

Figure 4.5: A comparative study of different topologies at their first natural resonance: a dipole, two dipoles placed in parallel, and a loop.

Much can be done in the investigation of various topologies. One example, underpinned by numerical results in [2∗] and [45∗] is depicted in Fig. 4.5. Focusing only on the first natural resonance, the single dipole offers only one possible configuration of the modal current, while two dipoles have two possible configurations, i.e., an in-phased and out-of-phased mode. The study of a loop is more intricate. It has only one resonating mode, as can be seen by the bottom line in Fig. 4.5a, since the hypothetical out-of-phased mode violates the continuity equation. However, to complete the modal basis, the static mode must exist. Interesting test cases can be deduced from these conclusions, see [2∗].

It could be objected that the examples listed in this chapter could only be understood as an automated analysis, not as a synthesis. This stricture is essentially correct. However, the automation of the design has been done in a way that significantly reduces the effort exerted to find the optimal antenna. From this perspective, this chapter covers, at least partly, synthesis and analysis.

Admittedly, the major part of the theory that covers antenna synthesis has not yet been fully explored, and any progress is highly appreciated. It may also be true that complete synthesis remains inaccessible, mainly because of the non-invertible transition from the geometry to the electromagnetic currents, see Fig. 1.2.

Chapter 5

Source Concept Implementation

A great deal of effort has been spent not only on coping with analytical expressions, but also in mastering them in a numerical way. This short chapter is intended as an implementation report. Without exception, all codes have been written in Matlab and its toolboxes.

5.1 In-house codes

Almost all numerical results presented in this thesis have been obtained via an in-house numerical package TCMapp whose implementation is described in [76]. The package is based on the EFIE which is discretized by RWG basis functions [64] distributed over a triangular mesh grid generated in FEKO, distMesh [125], or an in-house mesher. The CM are found by the QZ algorithm from the LAPACK package [126]. Tasks are sliced in the frequency domain and parallelized via the Parallel Computing Toolbox [127]. Advanced eigen-mode tracking [75] is improved by an adaptive frequency solver which independently determines the frequency points for which the CM solution is found. The post-processing part from Chapter 3 is completely implemented, including partial support of the GPU computing. The feeding synthesis can be done via external scripts. In order to deal with the optimization tasks, the particle swarm optimization [9] and the self-organizing migrating algorithm [10] have been coded, including the multi-objective hybrids. A tool for generating the iterated function system fractals has been implemented, including an interactive GUI in Matlab. The TCMapp, as a whole, exceeds 30 thousands of code lines in Matlab.

Many particular problems had to be resolved during the numerical implementation. To give but one example, the influence of different meshing schemes and their impact of the precision of the results have been studied in [128∗]. Considering the individual mesh cell, the numerical error is minimized for an equilateral triangle (which, however, cannot be used everywhere), but the global optimal density function of the mesh grid and its impact was unknown. The study [128∗] recommends certain meshing schemes to improve the performance of the CM decomposition. To confirm these conclusions, the same study should be independently repeated for cases of structures with a known CM basis. The only possible shape is a spherical shell.

In addition to scientific purposes, the TCMapp package has been utilized in education

Figure 5.1: Logo of the AToM project, further information can be found at `antennatoolbox.com`.

(both at Czech Technical University and at international level). Over time, however, the tool has became obsolete. It suffered from many imperfections, particularly because it was coded "in haste" and only for scientific purposes. The used paradigm of functional programming is inefficient and difficult to maintain with several parts that needed to be updated according to the latest findings. Consequently, the AToM project came into being.

5.2 Antenna Toolbox for Matlab (AToM)

The last five years have allowed the capabilities of the Source Concept to be recognized and software tools associated with its implementation have begun to appear, including, in particular, the emergence of the CM tools documented in Fig. 2.2.

To support this common effort and to accelerate the development of the in-house tool TCMapp, a new project was submitted, in conjunction with a commercial partner, MECAS-ESI, and colleagues from the Brno University of Technology, to the Technology Agency of the Czech Republic. Fortunately, it has been receiving funding since July, 2014. The project has two central purposes: to transfer existing know-how into commercial software and to establish a tool to assist in the future development of the Source Concept and related scientific activities.

An important part of the project is called the Antenna Toolbox for Matlab (AToM) whose logo can be seen in Fig. 5.1. The AToM package is derived from the TCMapp, but all its routines will be completely rewritten and generalized. The AToM package aggregates all present scientific know-how of the Source Concept and it will remain in the ownership of Czech Technical University and Brno university of technology. Due to a lack of space, a detailed specification of the AToM is not mentioned here, but all information can be found at the website of the project (see Fig. 5.1). The author of this thesis hopes that the AToM project augurs the prime of the Source Concept and paves the way for its everyday use.

Chapter 6

Conclusion

This thesis discussed the advent of the Source Concept and its potential to become a leading design procedure for electrically small antennas. Beyond the scope of small antennas, antenna arrays, such as superbackscattering arrays, frequency selective surfaces, or MIMO antennas can be studied from new perspectives. By closely investigating ultra-wideband antennas, we can take advantage of the novel time domain method to evaluate stored electromagnetic energy. The feeding synthesis can be applied to beam steering arrays or to MIMO devices.

The important incremental tasks can speed up the development of the Source Concept, especially in connecting pixelling and convex optimization, the implementation of discrete particle swarm optimization and genetic algorithms, improvement of the tracking algorithm (by combining a heuristic approach, far-field correlation and Pearson's correlation formula), the acceleration of the adaptive frequency solver for CM decomposition, or the incorporation of the MLFMA and Arnoldi algorithm.

Specific and highly ambitious tasks include CM preconditioning, the analytical evaluation of the characteristic mode of an important canonical example of a half-wavelength dipole at its first resonance, a deeper understanding of the characteristic modes and underlying algebra, further research in fractal geometry (which also requires significant progress in mathematics, especially in fractal calculus) and the study of the influence of the non-integer Hausdorff dimension.

Looking far into the feature, the main goals are clear: a mastery of structural decomposition could open a direct path to antenna synthesis. In the meantime, the role of geometry for radiation processes should be examined since we are far from having a complete understanding of this mechanism. It may be that, one day, radiation losses will be flung aside by high-frequency compatible superconductors with critical temperatures high enough to operate at outdoor temperatures. Then the role of fractal geometry may become crucial as radiators would not be limited by radiation losses. The resolution of these persistent problems would represent great progress in the fields of antenna theory and classical electromagnetism. Whether these breakthroughs see the light of day is certainly not assured.

To conclude, the Source Concept represents a promising framework providing a unified theory of the evaluation, decomposition and manipulation of electromagnetic currents in ways as yet imagined. It is a mixture of powerful techniques, both analytical and

numerical, together with the idea that an electromagnetic current can be substituted into any expression relevant to small antenna design. Although the Source Concept turned out to be instructive for small antennas, it is thoroughly applicable for radiators of any electrical size and shape. The Source Concept, fueled by recent progress in numerical techniques and increasing computational performance, is now in the spotlight of the entire antenna community. While its capabilities are not in question, the final stage of antenna synthesis, the "Holy Grail" of antenna theory, is far from being reached and a great deal of tremendous, but hopefully exciting, steps certainly need to be taken in the future.

Bibliography

[1] M. Capek, P. Hazdra, and J. Eichler, "A method for the evaluation of radiation Q based on modal approach," *IEEE Trans. Antennas Propag.*, vol. 60, no. 10, pp. 4556–4567, Oct. 2012;.

[2] M. Capek, L. Jelinek, P. Hazdra, and J. Eichler, "The measurable Q factor and observable energies of radiating structures," *IEEE Trans. Antennas Propag.*, vol. 62, no. 1, pp. 311–318, Jan. 2014.

[3] M. Capek, J. Eichler, and P. Hazdra, "Evaluation of radiation efficiency from characteristic currents," *IET Microw. Antennas Propag.*, vol. 9, no. 1, pp. 10–15, Jan. 2015.

[4] M. Capek, "Modal analysis and optimization of radiating planar structures," Ph.D. dissertation, CTU in Prague, 2014.

[5] K. J. Falconer, *Fractal Geometry – Mathematical Foundations and Applications*. John Wiley, 2003.

[6] P. Hamouz, P. Hazdra, M. Capek, J. Eichler, A. Diallo, F. Ferrero, and C. Luxey, "Polarization diversity in umts mobile phones analyzed with characteristic modes," Tech. Rep., 2014. [Online]. Available: http://www.antennatoolbox.com/pdf/studijni-opory/atom/Polarization_diversity_analysis.pdf

[7] The MathWorks. (2015) The Matlab. [Online]. Available: www.mathworks.com

[8] R. Elliot, *Antenna Theory and Design*. IEEE Press, 2003.

[9] J. Kennedy and R. C. Eberhart, *Swarm Intelligence*. Academic Press, 2001.

[10] G. C. Onwubolu and B. V. Babu, *New Optimization Techniques in Engineering*. Springer, 2004.

[11] CISCO. (2014) The zettabyte era: Trends and analysis. [Online]. Available: www.cisco.com/c/en/us/solutions/collateral/service-provider/visual-networking-index-vni/VNI_Hyperconnectivity_WP.pdf

[12] D. A. Sánchez-Hernández, Ed., *Multiband Integrated Antennas for 4G Terminals*. Artech House, 2008.

[13] J. L. Volakis, C. Chen, and K. Fujimoto, *Small Antennas: Miniaturization Techniques & Applications*. McGraw-Hill, 2010.

[14] J.-M. Laheurte, C. Ripoll, D. Paret, and C. Loussert, *UHF RFID Technologies for Identification and Traceability.* Wiley–ISTE, 2014.

[15] B. R. Rao, W. Kunysz, R. L. Fante, and D. McDonald, *GPS/GNSS Antennas.* Artech House, 2012.

[16] F. Gross, Ed., *Frontiers in Antennas: Next Generation Design & Engineering.* McGraw-Hill Professional, 2011.

[17] C. A. Balanis, *Modern Antenna Handbook.* John Wiley, 2008.

[18] R. Garg, *Analytical and Computational Methods in Electromagnetics.* Artech House, 2008.

[19] J.-M. Jin, *Theory and Computation of Electromagnetic Fields.* John Wiley, 2010.

[20] J. C. Maxwell, *A Treatise on Electricity and Magnetism.* Clarendon Press, 1873, vol. 2.

[21] S. A. Schelkunoff and H. T. Friis, *Antennas: Theory and Practice.* John Wiley, 1952.

[22] Y. Rahmat-Samii and E. Michielssen, Eds., *Electromagnetic Optimization by Genetic Algorithm.* John Wiley, 1999.

[23] R. C. Hansen, *Electrically Small, Superdirective, and Superconductive Antennas.* John Wiley, 2006.

[24] K. Fujimoto and H. Morishita, *Modern Small Antennas.* Cambridge University Press, 2013.

[25] L. J. Chu, "Physical limitations of omni-directional antennas," *J. Appl. Phys.*, vol. 19, pp. 1163–1175, 1948.

[26] H. A. Wheeler, "Fundamental limitations of small antennas," *Proc. of IRE*, vol. 35, no. 12, pp. 1479–1484, 1947.

[27] R. E. Collin and S. Rothschild, "Evaluation of antenna Q," *IEEE Trans. Antennas Propag.*, vol. 12, no. 1, pp. 23–27, Jan. 1964.

[28] R. C. Hansen and R. E. Collin, "A new Chu formula for Q," *IEEE Antennas Propag. Magazine*, vol. 51, no. 5, pp. 38–41, Oct. 2009.

[29] G. A. E. Vandenbosch, "Simple procedure to derive lower bounds for radiation Q of electrically small devices of arbitrary topology," *IEEE Trans. Antennas Propag.*, vol. 59, no. 6, pp. 2217–2225, June 2011.

[30] M. Gustafsson and B. L. G. Jonsson, "Stored electromagnetic energy and antenna Q," *Prog. Electromagn. Res.*, vol. 150, pp. 13–27, 2014.

[31] L. Jelinek, M. Capek, P. Hazdra, and J. Eichler, "An analytical evaluation of the quality factor Q_Z for dominant spherical modes," *IET Microw. Antennas Propag.*, vol. 9, no. 10, pp. 1096–1103, 2015.

[32] O. S. Kim and O. Breinbjerg, "Reaching the Chu lower bound on Q with magnetic dipole antennas using a magnetic-coated PEC core," *IEEE Trans. Antennas Propag.*, vol. 59, no. 8, pp. 2799–2805, Aug. 2011.

[33] O. S. Kim, "Electric dipole antennas with magnetic-coated PEC cores: Reaching the Chu lower bound on Q," *IEEE Trans. Antennas Propag.*, vol. 60, no. 3, pp. 1616–1619, March 2012.

[34] M. Gustafsson, C. Sohl, and G. Kristensson, "Physical limitations on antennas of arbitrary shape," *Proc. of Royal Soc. A*, vol. 463, pp. 2589–2607, 2007.

[35] R. G. Newton, *Scattering Theory of Waves and Particles*. Dover, 1982.

[36] R. E. Collin, *Field Theory of Guided Waves*. John Wiley - IEEE Press, 1990.

[37] E. E. Altshuler, T. H. O'Donnell, A. D. Yaghjian, and S. R. Best, "A monopole superdirective array," *IEEE Trans. Antennas Propag.*, vol. 2005, no. 8, pp. 2653–2661, Aug. 53.

[38] I. Liberal, I. Ederra, R. Gonzalo, and R. W. Ziolkowski, "Superbackscattering antenna arrays," *IEEE Trans. Antennas Propag.*, vol. 63, no. 5, pp. 2011–2021, May 2015.

[39] F. R. Morgenthaler, *The Power and Beauty of Electromagnetic Fields*. Wiley-IEEE Press, 2011.

[40] M. Capek, L. Jelinek, and P. Hazdra, "On the functional relation between quality factor and fractional bandwidth," *IEEE Trans. Antennas Propag.*, vol. 63, no. 6, pp. 2787–2790, June 2015.

[41] M. Capek and L. Jelinek, "Comments on 'On Stored Energies and Radiation Q'," *IEEE Trans. Antennas Propag.*, 2015.

[42] J. Eichler, P. Hazdra, M. Capek, and M. Mazanek, "Modal resonant frequencies and radiation quality factors of microstrip antennas," *International J. of Antenas and Propag.*, vol. 2012, pp. 1–9, 2012.

[43] P. Hazdra, M. Capek, J. Eichler, and M. Mazanek, "The radiation Q-factor of a horizontal $\lambda/2$ dipole above ground plane," *IEEE Antennas Wireless Propag. Lett.*, vol. 13, pp. 1073–1075, 2014.

[44] P. Hazdra, M. Capek, and J. Eichler, "Radiation Q-factors of thin-wire dipole arrangements," *IEEE Antennas Wireless Propag. Lett.*, vol. 10, pp. 556–560, 2011.

[45] M. Capek, P. Hazdra, and M. Masek, "On some theoretical and numerical aspects of characteristic mode decomposition," 2015. [Online]. Available: http://arxiv.org/abs/1509.02825

[46] M. Capek and L. Jelinek, "Various interpretations of the stored and the radiated energy density," 2015. [Online]. Available: http://arxiv.org/abs/1503.06752

[47] M. Capek, L. Jelinek, and G. A. E. Vandenbosch, "Stored electromagnetic energy and quality factor of radiating structures," 2015. [Online]. Available: http://arxiv.org/abs/1403.0572

[48] M. Capek and L. Jelinek, "The relation between fractional bandwidth and q factor," in *IEEE International Symposium on Antennas and Propagation and USNC-URSI Radio Science Meeting*, Vancouver, BC, Canada, July 2015.

[49] ——, "On the properties of stored electromagnetic energy," in *Proceedings of PIERS 2015 in Prague*, Prague, Czech Republic, July 2015.

[50] L. Jelinek and M. Capek, "On the stored and radiated energy density," in *Proceedings of the 9th European Conference on Antennas and Propagation (EUCAP)*, Lisbon, Portugal, July 2015.

[51] M. Capek, L. Jelinek, G. A. E. Vandenbosch, and P. Hazdra, "Time domain scheme for stored energy evaluation," in *IEEE International Symposium on Antennas and Propagation and USNC-URSI Radio Science Meeting*, Vancouver, BC, Canada, July 2015.

[52] ——, "A novel scheme for stored energy evaluation," in *Proceedings of the 9th European Conference on Antennas and Propagation (EUCAP)*, Lisbon, Portugal, April 2015.

[53] M. Capek, P. Hazdra, M. Mazanek, Z. Raida, and J. Rymus, "The antenna toolbox for matlab (atom)," in *Proceedings of the 9th European Conference on Antennas and Propagation (EUCAP)*, Lisbon, Portugal, July 2015.

[54] R. F. Harrington, *Time-Harmonic Electromagnetic Fields*, 2nd ed. John Wiley – IEEE Press, 2001.

[55] J. L. Volakis and K. Sertel, *Integral Equation Methods for Electromagnetics*. Scitech Publishing Inc., 212.

[56] P. M. Morse and H. Feshbach, *Methods of Theoretical Physics*. McGraw-Hill, 1953.

[57] J. G. Van Bladel, *Singular Electromagnetic Fields and Sources*. John Wiley - IEEE Press, 1991.

[58] D. G. Duffy, *Green's Functions with Applications*, 1st ed. Chapman and Hall/CRC, 2001.

[59] W. C. Gibson, *The Method of Moments in Electromagnetics*, 1st ed. Chapman and Hall/CRC, 2007.

[60] P. Arcioni, M. Bressan, and L. Perregrini, "On the evaluation of the double surface integrals arising in the application of the boundary integral method to 3-D problems," *IEEE Trans. Microwave Theory Tech.*, vol. 44, no. 3, pp. 436–438, March 1997.

[61] A. F. Peterson, S. L. Ray, and R. Mittra, *Computational Methods for Electromagnetics*. John Wiley – IEEE Press, 1998.

[62] R. F. Harrington, *Field Computation by Moment Methods*. John Wiley – IEEE Press, 1993.

[63] J. A. De Loera, J. Rambau, and F. Santos, *Triangulations – Structures for Algorithms and Applications*. Springer, 2010.

[64] S. M. Rao, D. R. Wilton, and A. W. Glisson, "Electromagnetic scattering by surfaces of arbitrary shape," *IEEE Trans. Antennas Propag.*, vol. 30, no. 3, pp. 409–418, May 1982.

[65] M. N. O. Sadiku, *Numerical Techniques in Electromagnetics with Matlab*, 3rd ed. CRC Press, 2009.

[66] H. Sagan, *Boundary and Eigenvalue Problems in Mathematical Physics*. Dover, 1989.

[67] J. R. Mautz, "Variational aspects of the reaction in the method of moments," *IEEE Trans. Antennas Propag.*, vol. 42, no. 12, pp. 1631–1638, Dec. 1994.

[68] C. Baum, "The singularity expansion method: Background and developments," *IEEE Antennas Propag. Society Newsletter*, vol. 28, no. 4, pp. 14–23, Aug. 1986.

[69] J. H. Wilkinson, *The Algebraic Eigenvalue Problem*. Oxford University Press, 1988.

[70] P. Hazdra and P. Hamouz, "On the modal superposition lying under the MoM matrix equations," *Radioengineering*, vol. 17, no. 3, pp. 42–46, Sept. 2008.

[71] R. J. Garbacz, "A generalized expansion for radiated and scattered fields," Ph.D. dissertation, The Ohio State Univ., 1968.

[72] R. F. Harrington and J. R. Mautz, "Theory of characteristic modes for conducting bodies," *IEEE Trans. Antennas Propag.*, vol. 19, no. 5, pp. 622–628, Sept. 1971.

[73] ——, "Computation of characteristic modes for conducting bodies," *IEEE Trans. Antennas Propag.*, vol. 19, no. 5, pp. 629–639, Sept. 1971.

[74] M. Cabedo-Fabres, E. Antonino-Daviu, A. Valero-Nogueira, and M. F. Bataller, "The theory of characteristic modes revisited: A contribution to the design of antennas for modern applications," *IEEE Antennas Propag. Magazine*, vol. 49, no. 5, pp. 52–68, Oct. 2007.

[75] M. Capek, P. Hazdra, P. Hamouz, and J. Eichler, "A method for tracking characteristic numbers and vectors," *Progress In Electromagnetics Research B*, vol. 33, pp. 115–134, 2011.

[76] M. Capek, P. Hamouz, P. Hazdra, and J. Eichler, "Implementation of the theory of characteristic modes in Matlab," *IEEE Antennas Propag. Magazine*, vol. 55, no. 2, pp. 176–189, April 2013.

[77] R. F. Harrington, J. R. Mautz, and Y. Chang, "Characteristic modes for dielectric and magnetic bodies," *IEEE Trans. Antennas Propag.*, vol. 20, no. 2, pp. 194–198, March 1972.

[78] B. D. Raines and R. G. Rojas, "Wideband characteristic mode tracking," *IEEE Trans. Antennas Propag.*, vol. 60, no. 7, pp. 3537–3541, July 2012.

[79] D. J. Ludick, U. Jakobus, and M. Vogel, "A tracking algorithm for the eigenvectors calculated with characteristic mode analysis," in *Proceedings of the 8th European Conference on Antennas and Propagation (EUCAP)*, 2014, pp. 629–632.

[80] Z. Miers and B. K. Lau, "Wide band characteristic mode tracking utilizing far-field patterns," *IEEE Antennas Wireless Propag. Lett.*, vol. 14, pp. 1658–1661, 2015.

[81] G. W. Stewart, *Matrix Algorithms, Volume II: Eigensystems.* SIAM, 2001.

[82] Q. I. Dai, J. W. Wu, L. L. Meng, W. C. Chew, and W. E. I. Sha, "Multilevel fast multipole algorithm for characteristic mode analysis," Dec. 2014. [Online]. Available: http://arxiv.org/abs/1412.1756v2

[83] M. Capek, P. Hazdra, J. Eichler, and M. Mazanek, "Software tools for efficient generation, modelling and optimisation of fractal radiating structures," *IET Microw. Antennas Propag.*, vol. 5, no. 8, pp. 1002–1007, 2011.

[84] R. Garg, P. Bhartia, I. Bahl, and A. Ittipiboon, *Mictrostrip Antenna Design Handbook.* Artech House, 2001.

[85] J. Eichler, P. Hazdra, M. Capek, T. Korinek, and P. Hamouz, "Design of a dual-band orthogonally polarized L-probe-fed fractal patch antenna using modal methods," *IEEE Antennas Wireless Propag. Lett.*, vol. 10, pp. 1389–1392, 2011.

[86] C. Mak, K. Luk, K.-F. Lee, and Y. Chow, "Experimental study of a microstrip patch antenna with an L-shaped probe," *IEEE Trans. Antennas Propag.*, vol. 48, no. 5, pp. 777–783, May 2000.

[87] CST Computer Simulation Technology. (2014) CST MWS. [Online]. Available: http://www.cst.com/

[88] O. Ergul and L. Gurel, *The Multilevel Fast Multipole Algorithm (MLFMA) for Solving Large-Scale Computational Electromagnetics Problems.* Wiley - IEEE Press, 2014.

[89] E. J. Rothwell and M. J. Cloud, *Electromagnetics.* CRC Press, 2001.

[90] C.-H. Papas, *Theory of Electromagnetic Wave Propagation.* Dover, 1965.

[91] V. Zavada, "Energetic functional of U-notched loop antenna," Master's thesis, CTU in Prague, 2014, (in Czech).

[92] M. Gustafsson and S. Nordebo, "Optimal antenna currents for Q, superdirectivity, and radiation patterns using convex optimization," *IEEE Trans. Antennas Propag.*, vol. 61, no. 3, pp. 1109–1118, March 2013.

[93] S. Boyd and L. Vandenberghe, *Convex Optimization*. Cambridge University Press, 2004.

[94] N. N. Lebedev, *Special Functions & Their Applications*. Dover, 1972.

[95] G. A. E. Vandenbosch, "Reactive energies, impedance, and Q factor of radiating structures," *IEEE Trans. Antennas Propag.*, vol. 58, no. 4, pp. 1112–1127, Apr. 2010.

[96] A. D. Yaghjian and S. R. Best, "Impedance, bandwidth and Q of antennas," *IEEE Trans. Antennas Propag.*, vol. 53, no. 4, pp. 1298–1324, April 2005.

[97] D. R. Rhodes, "Observable stored energies of electromagnetic systems," *J. Franklin Inst.*, vol. 302, no. 3, pp. 225–237, 1976.

[98] EM Software & Systems-S.A. FEKO. [Online]. Available: www.feko.info

[99] P. Hazdra, M. Capek, and J. Eichler, "Comments to 'Reactive Energies, Impedance, and Q Factor of Radiating Structures' by G. Vandenbosch," *IEEE Trans. Antennas Propag.*, vol. 61, no. 12, pp. 6266–6267, Dec. 2013.

[100] J. D. Jackson, *Classical Electrodynamics*, 3rd ed. John Wiley, 1998.

[101] M. Gustafsson, M. Cismasu, and B. L. G. Jonsson, "Physical bounds and optimal currents on antennas," *IEEE Trans. Antennas Propag.*, vol. 60, no. 6, pp. 2672–2681, June 2012.

[102] S. R. Best, "The Foster reactance theorem and quality factor for antennas," *IEEE Antennas Wireless Propag. Lett.*, vol. 3, no. 1, pp. 306–309, Dec. 2004.

[103] W. Geyi, "On stored energies and radiation Q," *IEEE Trans. Antennas Propag.*, vol. 63, no. 2, pp. 636–645, Feb. 2015.

[104] ——, "Reply to Comments on 'Stored energies and radiation Q'," 2015. [Online]. Available: http://arxiv.org/abs/1509.07252

[105] D. Kajfez and W. P. Wheless, "Invariant definitions of the unloaded Q factor," *IEEE Antennas Propag. Magazine*, vol. 34, no. 7, pp. 840–841, 1986.

[106] J. G. Van Bladel, *Electromagnetic Fields*, 2nd ed. John Wiley – IEEE Press, 2007.

[107] J. D. Kraus and R. J. Marhefka, *Antennas for all applications*. McGraw-Hill, 2002.

[108] *Standard Definitions of Terms for Antennas 145 – 1993*, IEEE Antennas and Propagation Society Std.

[109] M. Gustafsson and S. Nordebo, "Bandwidth, Q factor and resonance models of antennas," *Progress In Electromagnetics Research*, vol. 62, pp. 1–20, 2006.

[110] M. Gustafsson and B. L. G. Jonsson, "Antenna Q and stored energy expressed in the fields, currents, and input impedance," *IEEE Trans. Antennas Propag.*, vol. 63, no. 1, pp. 240–249, Jan. 2015.

[111] P. Hansen, "The radiation efficiency of a dipole antenna located above an imperfectly conducting ground," *IEEE Trans. Antennas Propag.*, vol. 20, no. 6, pp. 766–770, Nov. 1972.

[112] Z. G. Qian, W. C. Chew, and R. Suaya, "Generalized impedance boundary condition for conductor modeling in surface integral equation," *IEEE Trans. Microwave Theory Tech.*, vol. 55, no. 11, pp. 2354–2364, 2007.

[113] A. Karlsson, "Approximate boundary conditions for thin structures," *IEEE Trans. Antennas Propag.*, vol. 57, no. 1, pp. 144–148, Jan. 2009.

[114] J. Nocedal and S. Wright, *Numerical Optimization.* Springer, 2006.

[115] K. Deb, *Multi-Objective Optimization using Evolutionary Algorithms.* John Wiley, 2001.

[116] R. Martens and D. Manteuffel, "Systematic design method of a mobile multiple antenna system using the theory of characteristic modes," *IET Microw. Antennas Propag.*, vol. 8, no. 12, pp. 887–893, Sept. 2014.

[117] E. Safin and D. Manteuffel, "Manipulation of characteristic wave modes by impedance loading," *IEEE Trans. Antennas Propag.*, vol. 63, no. 4, pp. 1756–1764, April 2015.

[118] J. L. T. Ethier and D. McNamara, "Sub-structure characteristic mode concept for antenna shape synthesis," *Electronics Letters*, vol. 48, no. 9, pp. 471–472, April 2012.

[119] J. Ethier, "Antenna shape synthesis using characteristic mode concepts," Ph.D. dissertation, University of Ottawa, 2012.

[120] Y. Rahmat-Samii, J. M. Kovitz, and H. Rajagopalan, "Nature-inspired optimization techniques in communication antenna design," *Proc. of IEEE*, vol. 100, no. 7, pp. 2132–2144, July 2012.

[121] E. Hassan, D. Noreland, R. Augustine, E. Wadbro, and M. Berggren, "Topology optimization of planar antennas for wideband near-field coupling," *IEEE Trans. Antennas Propag.*, vol. 63, no. 9, pp. 4208–4213, Sept. 2015.

[122] B. Yang and J. J. Adams, "Systematic shape optimization of symmetric mimo antennas using characteristic modes," *IEEE Trans. Antennas Propag.*, 2015.

[123] J. L. T. Ethier and D. A. McNamara, "Antenna shape synthesis without prior specification of the feedpoint locations," *IEEE Trans. Antennas Propag.*, vol. PP, no. 99, p. 1, MM 2014.

[124] COMSOL Multiphysics. [Online]. Available: www.comsol.com

[125] P.-O. Persson, "Mesh generation for implicit geometries," Ph.D. dissertation, MIT, 2006.

[126] E. Anderson, et al., *LAPACK Users' Guide.* Society for Industrial and Applied Mathematics (SIAM), 1999.

[127] The MathWorks, *Parallel Computing Toolbox*, 2012.

[128] J. Eichler, P. Hazdra, and M. Capek, "Aspects of mesh generation for characteristic mode analysis," *IEEE Antennas Propag. Magazine*, vol. 56, no. 6, pp. 172–183, June 2014.

Chapter 7

Appendix A – Selected author's publications

The following appendix contains the full texts of the works cited in this thesis and belonging to the habilitant.

I M. Capek, P. Hazdra, and J. Eichler, "A method for the evaluation of radiation Q based on modal approach," *IEEE Trans. Antennas Propag.*, vol. 60, no. 10, pp. 4556–4567, Oct. 2012. [1∗]

II M. Capek, L. Jelinek, P. Hazdra, and J. Eichler, "The measurable Q factor and observable energies of radiating structures," *IEEE Trans. Antennas Propag.*, vol. 62, no. 1, pp. 311–318, Jan. 2014. [2∗]

III M. Capek, J. Eichler, and P. Hazdra, "Evaluation of radiation efficiency from characteristic currents," *IET Microw. Antennas Propag.*, vol. 9, no. 1, pp. 10–15, Jan. 2015. [3∗]

IV M. Capek, L. Jelinek, and G. A. E. Vandenbosch, "Stored Electromagnetic Energy and Quality Factor of Radiating Structures,", 2015, submitted, arXiv: 1403.0572. [47∗]

V M. Capek and L. Jelinek, "Various interpretations of the stored and the radiated energy density," 2015, submitted, arXiv: 1503.06752. [46∗]

VI M. Capek, L. Jelinek, and P. Hazdra, "On the functional relation between quality factor and fractional bandwidth," *IEEE Trans. Antennas Propag.*, vol. 63, no. 6, pp. 2787–2790, June 2015. [40∗]

VII L. Jelinek, M. Capek, P. Hazdra, and J. Eichler, "An analytical evaluation of the quality factor Q_Z for dominant spherical modes," *IET Microw. Antennas Propag.*, vol. 9, no. 10, pp. 1096–1103, 2015. [31∗]

VIII M. Capek and L. Jelinek, "Comments on 'On Stored Energies and Radiation Q'," *IEEE Trans. Antennas Propag.*, vol. 63, 2015. [41∗]

IX P. Hazdra, M. Capek, J. Eichler, and M. Mazanek, "The radiation Q-factor of a horizontal $\lambda/2$ dipole above ground plane," *IEEE Antennas Wireless Propag. Lett.*, vol. 13, pp. 1073–1075, 2014. [43∗]

X J. Eichler, P. Hazdra, and M. Capek, "Aspects of mesh generation for characteristic mode analysis," *IEEE Antennas Propag. Magazine*, vol. 56, no. 6, pp. 172–183, June 2014. [128∗]

XI P. Hazdra, M. Capek, and J. Eichler, "Comments to 'Reactive Energies, Impedance, and Q Factor of Radiating Structures' by G. Vandenbosch," *IEEE Trans. Antennas Propag.*, vol. 61, no. 12, pp. 6266–6267, Dec. 2013. [99∗]

XII J. Eichler, P. Hazdra, M. Capek, and M. Mazanek, "Modal resonant frequencies and radiation quality factors of microstrip antennas," *International J. of Antenas and Propag.*, vol. 2012, pp. 1–9, 2012. [42∗]

XIII J. Eichler, P. Hazdra, M. Capek, T. Korinek, and P. Hamouz, "Design of a dual-band orthogonally polarized l-probe-fed fractal patch antenna using modal methods," *IEEE Antennas Wireless Propag. Lett.*, vol. 10, pp. 1389–1392, 2011. [85∗]

XIV P. Hazdra, M. Capek, and J. Eichler, "Radiation Q-factors of thin-wire dipole arrangements," *IEEE Antennas Wireless Propag. Lett.*, vol. 10, pp. 556–560, 2011. [44∗]

XV M. Capek, P. Hazdra, and M. Masek, "On some theoretical and numerical aspects of characteristic mode decomposition," 2015, submitted, arXiv: 1509.02825. [45∗]

I

M. Capek, P. Hazdra, and J. Eichler, "A method for the evaluation of radiation Q based on modal approach," *IEEE Trans. Antennas Propag.*, vol. 60, no. 10, pp. 4556–4567, Oct. 2012. [1∗]

A Method for the Evaluation of Radiation Q Based on Modal Approach

Miloslav Capek, *Student Member, IEEE*, Pavel Hazdra, *Member, IEEE*, and Jan Eichler, *Student Member, IEEE*

***Abstract*—A new formula for the evaluation of the modal radiation Q factor is derived. The total Q of selected structures is to be calculated from the set of eigenmodes with associated eigen-energies and eigen-powers. Thanks to the analytical expression of these quantities, the procedure is highly accurate, respecting arbitrary current densities flowing along the radiating device. The electric field integral equation, Delaunay triangulation, method of moments, Rao-Wilton-Glisson basis function and the theory of characteristic modes constitute the underlying theoretical background. In terms of the modal radiation Q, all necessary relations are presented and the essential points of implementation are discussed. Calculation of the modal energies and Q factors enable us to study the effect of the radiating shape separately to the feeding. This approach can be very helpful in antenna design. A few examples are given, including a thin-strip dipole, two coupled dipoles a bowtie antenna and an electrically small meander folded dipole. Results are compared with prior estimates and some observations are discussed. Good agreement is observed for different methods.**

***Index Terms*—Antenna theory, eigenvalues and eigenfunctions, electromagnetic theory, Q factor.**

I. Introduction

THE radiation Q factor has long been discussed as one of the most significant and interesting parameter of the radiating system, especially in the field of the electrically small antenna (ESA) theory [1]. Each radiating shape has a minimum possible Q which is related to the maximum possible bandwidth potential [2].

There are many methods for estimating Q approximately (chronologically Wheeler [3], Chu [4], Harrington [5], Collin and Rotschild [6], McLean [7], Geyi [8]). Earlier work [3]–[7] do not consider actual current distribution, so they have to deal only with bounds related to dimensions of the enclosing sphere. The first attempt to include source distribution (current/charge) was presented by Geyi [8], but these energies are still quasistatic. Different approach taking the actual shape into account (based on static polarizability), was presented by Gustafsson *et al.* [9].

For effective ESA design as well as for the rigorous study of radiating structures, it is appropriate to use the calculation method based directly on the sources (currents), respecting their topology. These requirements have been fulfilled by G. Vandenbosch [10]. The derived expressions are rigorous, widely usable and easy to implement. They have been verified and successfully tested for simple examples in [11].

We extend this theory for modal analysis purposes, based on the theory of characteristic modes (TCM) [12] and then utilize them for the investigation of radiation Q for some canonical antennas. This approach allows us to study the behaviour of the shape of the radiating structure and its feeding separately. This means that the modal quantities have only to be calculated once and then the effect of the feeding port on superposition is studied through the coupling matrix, later denoted as $\boldsymbol{\beta}$. In addition, understanding the behaviour of modal energies assists in effective ESA design as will be shown in the case of optimization of the meander folded dipole.

The main objective of this paper is to derive the expression for the summation of modal energies and powers in order to obtain total Q. The comparison between the final expressions (24), (25) and some estimations of Q are given in Section V. All algorithms were coded in Matlab R2011a and employed in our in-house antenna tool. The described method could be used for arbitrary (triangularized) surface antennas with air dielectric.

II. The Radiation Q-Factor

The radiation Q factor is usually defined for antennas as [1]

$$Q = \frac{2\omega_0 \max\{W_e, W_m\}}{P_r}, \tag{1}$$

where W_e and W_m are the time averaged stored electric and magnetic energies and P_r is radiated power. The (1) assumes that the antenna is tuned to the resonance at angular frequency ω_0 by an ideal lossless reactive element so that the input impedance is pure real, [6]. Moreover, it is known that Q is inversely proportional to the antenna (fractional) bandwidth and for the constant $\mathrm{VSWR} < s$

$$\mathrm{FBW} \approx \left(\frac{s-1}{\sqrt{s}}\right)\frac{1}{Q}, \tag{2}$$

where the Q factor in (2) is assumed to be much greater than one.

The following expressions for W_e, W_m and P_r are analytically derived in [10] and generalized to a suitable form for the sake of the proposed method (note that the indexes u and v will be associated with the mode indexes in subsequent sections)

$$W_e^{u,v} = \frac{1}{16\pi\omega_0^2\epsilon_0}\left(I_{We}^{u,v} - I_{Wr}^{u,v}\right) \tag{3}$$

Manuscript received August 17, 2011; revised March 21, 2012; accepted May 11, 2012. Date of publication July 10, 2012; date of current version October 02, 2012. This work was supported by the Grant Agency of the Czech Technical University in Prague, under Grants SGS12/142/OHK3/2T/13 and COST IC0803 (RFCSET).

The authors are with the Department of Electromagnetic Field, Faculty of Electrical Engineering, Czech Technical University in Prague, Technicka 2, 16627, Prague, Czech Republic (e-mail: miloslav.capek@fel.cvut.cz).

Color versions of one or more of the figures in this paper are available online at http://ieeexplore.ieee.org.

Digital Object Identifier 10.1109/TAP.2012.2207329

and

$$W_m^{u,v} = \frac{1}{16\pi\omega_0^2\epsilon_0}\left(I_{Wm}^{u,v} - I_{Wr}^{u,v}\right) \tag{4}$$

where

$$I_{We}^{u,v} = \int_{\Omega_1}\int_{\Omega_2} q_u(\mathbf{r_1})q_v^*(\mathbf{r_2})\frac{\cos(k_0 r_{21})}{r_{21}}\mathrm{d}\Omega_1\mathrm{d}\Omega_2, \tag{5}$$

$$I_{Wm}^{u,v} = k_0^2\int_{\Omega_1}\int_{\Omega_2}\left(\mathbf{J}_u(\mathbf{r_1})\cdot\mathbf{J}_v^*(\mathbf{r_2})\right)\frac{\cos(k_0 r_{21})}{r_{21}}\mathrm{d}\Omega_1\mathrm{d}\Omega_2, \tag{6}$$

$$I_{Wr}^{u,v} = \frac{k_0}{2}\int_{\Omega_1}\int_{\Omega_2}\Big[k_0^2\left(\mathbf{J}_u(\mathbf{r_1})\cdot\mathbf{J}_v^*(\mathbf{r_2})\right) - q_u(\mathbf{r_1})q_v^*(\mathbf{r_2})\Big]\sin(k_0 r_{21})\mathrm{d}\Omega_1\mathrm{d}\Omega_2. \tag{7}$$

Finally, the radiated power is determined as

$$P_r^{u,v} = \frac{1}{8\pi\omega_0\epsilon_0}\int_{\Omega_1}\int_{\Omega_2}\Big[k_0^2\left(\mathbf{J}_u(\mathbf{r_1})\cdot\mathbf{J}_v^*(\mathbf{r_2})\right) - q_u(\mathbf{r_1})q_v^*(\mathbf{r_2})\Big]\frac{\sin(k_0 r_{21})}{r_{21}}\mathrm{d}\Omega_1\mathrm{d}\Omega_2. \tag{8}$$

$W_e^{u,v}$, $W_m^{u,v}$ and $P_r^{u,v}$ define the energies and the total radiated power based on uth source (J_u or q_u) on domain Ω_1 and vth source (J_v or q_v) on domain Ω_2. In the $\mathcal{R}^3$ Euclidean space, the distance r_{21} is 2-norm distance $r_{21} = |\mathbf{r}_2 - \mathbf{r}_1|$.

Note that for wavelength λ_0 the angular wavenumber $k_0 = 2\pi/\lambda_0$ and the charge density is defined as $q_u = \nabla\cdot J_u$. In most studied cases the domains Ω_1 and Ω_2 are equal ($\Omega = \Omega_1 = \Omega_2$), for $\Omega_1 \neq \Omega_2$ see [11].

III. Modal Q Formulation

In order to obtain modal Q's, we have to introduce a proper modal method to obtain eigenmodes and eigenvalues. This method is, in our case, the Theory of Characteristic Modes.

Eigenmodes $\mathbf{j}_u$ and eigenvalues λ_u are physically vivid and valuable characteristics of electromagnetic operators such as the electric field integral equation (EFIE) [13], [14]. In the following text, spectral eigen-decomposition of the EFIE complex impedance matrix is performed in the frequency domain. The next section briefly summarizes the mathematical formulation of the EFIE as well as the TCM since it is crucial to know all the properties of relevant variables.

A. The Electric Field Integral Equation

The EFIE can be formulated by employing a boundary condition for the tangential incident ($\mathbf{E}^i$) and a scattered electric field on the perfect electric conductor (PEC)

$$\left[L(\mathbf{J}) - \mathbf{E}^i\right]_{\tan} = 0. \tag{9}$$

The operator $L(\mathbf{J})$ is defined as

$$L(\mathbf{J}) = \mathrm{j}\omega\mathbf{A}(\mathbf{J}) + \nabla\phi(\mathbf{J}), \tag{10}$$

where $\mathbf{A}(\mathbf{J})$ and $\phi(\mathbf{J})$ are vector and scalar potentials respectively [15]. Physically, $-L(\mathbf{J})$ gives the scattered electric field intensity. Therefore, L has the characteristics of impedance

$$Z(\mathbf{J}) = [L(\mathbf{J})]_{\tan}. \tag{11}$$

The solution of (11) can be treated directly

$$\mathbf{J}_{MoM} = \mathbf{Z}^{-1}\mathbf{E}^i \tag{12}$$

as usually employed in the method of moments (MoM) [17] or by the superposition of the characteristic currents [12], [18]. This knowledge is important for our later expectations.[1]

In both cases, the impedance matrix and the (unknown) surface induced current density have to be expanded by appropriate basis functions (the most suitable are the well-known RWG basis functions $\mathbf{f}_s$ [19]); Galerkin's method is used.

The Q factor based on total current density from MoM has already been successfully calculated in [10] and [11] (MoM in Matlab with a thin-wire reduced kernel). However, to the knowledge of the authors, modal Q factors and stored energies have never been rigorously computed.

B. Theory of Characteristic Modes

The TCM evaluates the total surface current density as a sum of characteristic (eigen-) currents. They depend only on the shape and frequency, not on excitation. Details can be found in [12] and [20].

The impedance matrix $\mathbf{Z} = \mathbf{R} + \mathrm{j}\mathbf{X}$ is complex and symmetric (but not Hermitian), its parts $\mathbf{R}$ and $\mathbf{X}$ are real and symmetric. After a little manipulation we get the associated Euler's equation (a generalized eigenvalue problem)

$$\mathbf{X}\mathbf{j} = \lambda\mathbf{R}\mathbf{j}. \tag{13}$$

A solution of (13) may easily be obtained using the `eig` routine in Matlab [21]. The square impedance matrix $\mathbf{Z}$ of order U (the number of inner edges) produces U eigen-pairs $(\lambda_u, \mathbf{j}_u)$. Each eigenvector $\mathbf{j}_u$ together with the RWG functions forms the vector modal current density

$$\mathbf{J}(\mathbf{r}) = \sum_{u=1}^{U} j_u\mathbf{f}_u(\mathbf{r}), \tag{14}$$

where the basis functions $\mathbf{f}_u$ are defined in [19].

The total current density can be expressed as a linear combination of these modal currents

$$\mathbf{J}_{tot} = \sum_{u=1}^{U}\alpha_u\mathbf{J}_u = \sum_{u=1}^{U}\frac{\langle\mathbf{j}_u, \mathbf{E}^i\rangle}{1+\mathrm{j}\lambda_u}\mathbf{J}_u. \tag{15}$$

The expansion coefficient α_u is obviously the modal amplitude. The result of $\langle\mathbf{j}_u, \mathbf{E}^i\rangle = \mathbf{j}_u^T\mathbf{E}^i$ is a scalar value called the modal excitation factor [20]. Remember that the $\mathbf{E}^i$ and $\mathbf{J}_{tot}$ have the same meaning in both MoM and TCM. Without the loss of generality, we consider only real feeding of $\mathbf{E}^i$ for the rest of the paper. It should be pointed out, that the sum (15) is in fact incomplete. There is certain portion of evanescent imaginary cur-

[1]To get more insight on the relationship between the direct MoM and the TCM see [16].

rent arising from the voltage-gap [22], contributing to the stored energies. This is reason why there are slight discrepancies between Q_M and Q_{Jtot} as will be seen later. Such residual current could be obtained as

$$\mathbf{J}_{res} = \mathbf{J}_{MoM} - \mathbf{J}_{tot} = \mathbf{Z}^{-1}\mathbf{E}^i - \sum_{u=1}^{U} \frac{\langle \mathbf{j}_u, \mathbf{E}^i \rangle}{1 + \mathrm{j}\lambda_u} \mathbf{J}_u \tag{16}$$

and its contribution included. Since its effect is not crucial, it is omitted here, however this issue is currently under study.

Thanks to the linearity of the divergence operator, the total charge density $q = \nabla \cdot \mathbf{J}$ is

$$q(\mathbf{r}) = \sum_{u=1}^{U} j_u \nabla \cdot \mathbf{f}_u(\mathbf{r}), \tag{17}$$

and

$$\nabla \cdot \mathbf{f}_u(\mathbf{r}) = \begin{cases} \frac{l_u}{A_u^{\pm}} & \mathbf{r} \text{ in } \Omega_u^{\pm} \\ 0 & \text{otherwise} \end{cases} \tag{18}$$

On the basis of (15)–(17) we have

$$\mathbf{q}_{tot} = \sum_{u=1}^{U} \alpha_u \mathbf{q}_u = \sum_{u=1}^{U} \frac{\langle \mathbf{j}_u, \mathbf{E}^i \rangle}{1 + \mathrm{j}\lambda_u} \mathbf{q}_u. \tag{19}$$

The modal decomposition (`eig` function) is time-consuming but can be parallelized.[2] Even thought the TCM forms the orthogonal set of modes, the eigencurrents are of yet indetermined amplitudes. This problem is handled by normalization to unit radiated power for each frequency of interest [12]

$$\langle \mathbf{J}_u^*, \mathbf{R}\mathbf{J}_u \rangle = 1 \text{ W} = P_r^{u,u}. \tag{20}$$

C. Calculation of Modal Energies

Let us consider only (the first) two modes ($M = 2, u \in \{1, 2\}$) for simplicity and write out the current summation

$$\mathbf{J}_{tot} = \sum_{1,2} \alpha_u \mathbf{J}_u = \alpha_1 \mathbf{J}_1 + \alpha_2 \mathbf{J}_2. \tag{21}$$

The total charge density is obtained in the same way. Because variables $\mathbf{f}_s, \mathbf{j}_u$ and $\mathbf{q}_u$ are real, both modal currents and charge densities are real. However, the coefficients $\alpha_u = \langle \mathbf{j}_u, \mathbf{E}^i \rangle / 1 + \mathrm{j}\lambda_u$ are still complex and thus both the total current and charge densities are complex-valued.

If we take a look at (5)–(8), only parts $\mathbf{J}_u(d) \cdot \mathbf{J}_v^*(d)$ and $q_u(d) q_v^*(d)$ have to be worked out at a given frequency f_0 and on a triangularized shape Ω (or just a selected triangle T). Using (21)

$$\begin{aligned} \mathbf{J}_u(d) \cdot \mathbf{J}_v^*(d) &= \mathbf{J}_{tot}(d) \cdot \mathbf{J}_{tot}^*(d) \\ &= (\alpha_1 \mathbf{J}_1(d) + \alpha_2 \mathbf{J}_2(d)) (\alpha_1^* \mathbf{J}_1(d) + \alpha_2^* \mathbf{J}_2(d)) \\ &= \underbrace{\alpha_1 \alpha_1^* \mathbf{J}_1 \cdot \mathbf{J}_1}_{\sim \text{INT11}} + \underbrace{(\alpha_1^* \alpha_2 + \alpha_1 \alpha_2^*) \mathbf{J}_1 \cdot \mathbf{J}_2}_{\sim \text{INT12, INT21}} \\ &\quad + \underbrace{\alpha_2 \alpha_2^* \mathbf{J}_2 \cdot \mathbf{J}_2}_{\sim \text{INT22}} \end{aligned} \tag{22}$$

[2]This has been done via the Matlab Distributed Computing toolbox gaining a speed-up of about 9 for 12 nodes.

and analogously for the $q_u(d) q_v^*(d)$ part. Parts INT11/INT22 and INT12/INT21 are recognized as self and mutual interactions respectively. All discussed integrals may be divided in M^2 subintegrals (22) with corresponding modes u, v as the input data. For clarity, the "summation matrix" is introduced for electric/magnetic energy

$$\mathbf{W}_{e/m}^{M=2} = \begin{bmatrix} W_{e/m}^{11} & W_{e/m}^{12} \\ W_{e/m}^{21} & W_{e/m}^{22} \end{bmatrix} \sim \begin{bmatrix} \text{INT11} & \text{INT12} \\ \text{INT21} & \text{INT22} \end{bmatrix} \tag{23}$$

The above procedure can be generalized to any number of modes (for proof see the Appendix). The total number of M modes form the energy matrices $W_{e/m}$ of $M \times M$ size. Then the radiation Q is expressed by a novel relation

$$Q_M = 2\omega_0 \frac{\max \left\{ \sum_u^M \sum_v^M \beta_{u,v} W_e^{u,v}, \sum_u^M \sum_v^M \beta_{u,v} W_m^{u,v} \right\}}{\sum_u^M \sum_v^M \beta_{u,v} P_r^{u,v}}, \tag{24}$$

where the coupling matrix β is written as

$$\beta_{u,v} = \frac{\langle \mathbf{j}_u, \mathbf{E}^i \rangle \langle \mathbf{j}_v, \mathbf{E}^i \rangle (1 + \lambda_u \lambda_v)}{(1 + \lambda_u^2)(1 + \lambda_v^2)}. \tag{25}$$

Using the Hadamard product $(A \circ B)_{u,v} = (A)_{u,v}(B)_{u,v}$ [23]

$$Q_M = 2\omega_0 \frac{\max \left\{ \sum_{u,v} (\boldsymbol{\beta} \circ \mathbf{W}_e)_{uv}, \sum_{u,v} (\boldsymbol{\beta} \circ \mathbf{W}_m)_{uv} \right\}}{\sum_{u,v} (\boldsymbol{\beta} \circ \mathbf{P}_r)_{uv}}. \tag{26}$$

Modal energies $W_e^{u,v}$ and $W_m^{u,v}$ respect (3) and (4) with input current and charge densities (14) and (17) respectively. $\mathbf{W}_{e/m}$ and $\boldsymbol{\beta}$ are in matrix form (23). At a given frequency, eigenvectors $\mathbf{j}_{u,v}$, eigenvalues $\lambda_{u,v}$ and stored modal energies $W_{e/m}^{u,v}$ are known. Therefore, the total Q_M factor can be tuned by just a single parameter—the actual feeding $\mathbf{E}^i$. In Section V we will verify that (24) is close to the total Q and is suitable for use in antenna design[3]. Both modal (3), (4) and total (23) energies give important additional information about the radiating structure. It is worth noting that the total Q factor can only be calculated from the modal stored energies and powers—direct superposition of modal Q factors is impossible.

IV. Software Implementation

The EFIE core is based on the RWG elements [24]. Thus, proper discretization has to be employed. The Matlab PDE toolbox usually creates mesh of poor quality (particularly for complex shapes like fractals), better results are obtained by the Comsol Multiphysics mesh generator. In order to control meshing, the authors work on an in-house mesh generator that employs the `distmesh` code from MIT [25]. In this paper we assume that the analysed geometry Ω is properly triangularized into T triangles with U inner edges. Note that the quality and number of triangles are crucial for the resulting convergence of the solution.

[3]For $M \to \infty$, the Q_∞ in (24) is simply equal to total Q. In practice, however, it is sufficient to sum only finite (low) numbers of modes $M \approx 5$.

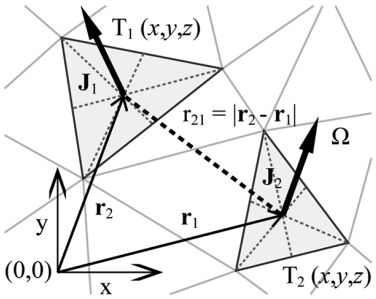

Fig. 1. Distance between non-overlapping current elements.

MoM solutions of thin-strip structures are usually assumed to be fed by the delta-gap [15]. Some planar structures are fed by the incident plane wave—usually only the x- or y-component $\mathbf{E}^i = [E_x, E_y, E_z]$ is used, [24]. The respective eigenproblem is solved in Matlab and all modes are sorted (tracked) and represented in terms of the characteristic angles [26]

$$\delta_u = 180 - \arctan(\lambda_u). \tag{27}$$

The characteristic angles are continuous through the values of 90-270, resonance of the uth mode occurs when $\delta_u = 180$. An illustrating example is shown in Section V.

A. Numerical Evaluation of $W_{e,m}$ and P_r—Distant Elements

The key expressions (5)–(8) consist of double surface integrals over a given planar structure Ω. In our case, Ω is discretized using the Delaunay triangulation, Fig. 1. Hence the integration is now performed via the compact set of triangles T.

The modal current matrices $\mathbf{J}_{u/v}$ are calculated from eigenvectors and the RWG basis function via (14). The order of $\mathbf{j}_{u/v}$ is $1 \times U$, but the order of the modal current $\mathbf{J}_{u/v}$ is $3 \times T$. Similarly, the modal charge distributions are calculated from (17) and each matrix $\mathbf{q}_{u/v}$ is of order $1 \times T$. Thus, one current vector $[J_x, J_y, J_z]$ and charge density q are assigned to each triangle. These values are considered constant throughout the triangle area and are assumed to be located at the centre of the triangles [27]. It will be shown later that this centroid approximation is accurate enough. However, it could fail e.g. for patch antennas at very small heights above the ground plane.

B. Numerical Evaluation of $W_{e,m}$—Overlapping Elements

As one can see, there are singularities in (5) and (6) for overlapping triangles ($T_1 = T_2$). The so-called self-coupling term [28] plays a major role in Q factor calculation and therefore it should be treated carefully. We are looking for a fast and sufficiently accurate solution to the following problem:

$$I_1(T_1 = T_2) = \int_{T_1}\int_{T_2} \frac{\cos(k_0 r_{21})}{r_{21}} \mathrm{d}t_1 \mathrm{d}t_2, \tag{28}$$

where $r_{21} = \sqrt{(x_2 - x_1)^2 + (y_2 - y_1)^2 + (z_2 - z_1)^2}$. The (28) is expanded in a Maclaurin series and since $k_0 R_{21} \to 0$ (R_{21} is the longest side of the triangle T_1) is satisfied, one can only use its first term. Then the cosine function $\cos(k_0 r_{21})$ from (28) reduces to the static singular part $1/r_{21}$. There is still a problem with the triangular region of integration.

TABLE I
CONVERGENCE OF THE SELECTED MODES, RECT. PLATE 30 × 20 cm

	1st mode				2nd mode	
edges	P_r [W]	Q_1	e_1 [%]	t [s]	Q_2	e_2 [%]
42	1.0041	0.738	87.23	0.015	–	–
180	1.0007	0.804	95.04	0.016	0.666	77.99
412	1.0002	0.814	96.25	0.031	0.789	92.39
926	0.9999	0.853	100.83	0.125	0.830	97.19
1691	0.9998	0.854	100.95	0.390	0.825	96.60
4704	0.9997	0.846	100	2.621	0.854	100

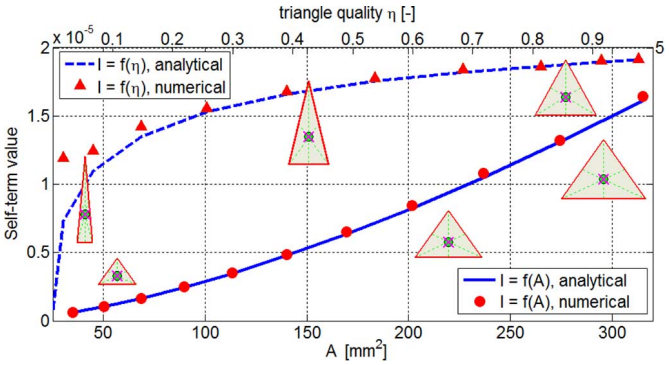

Fig. 2. Self-term values depending on the quality and area of the triangle.

The above issue was solved e.g. in [28] and the result was simplified in accordance with [29]

$$I_2 = -\frac{4}{3}A^2 \left(\frac{\ln\left(1 - \frac{2|\mathbf{h}_{12}|}{O}\right)}{|\mathbf{h}_{12}|} + \frac{\ln\left(1 - \frac{2|\mathbf{h}_{13}|}{O}\right)}{|\mathbf{h}_{13}|} + \frac{\ln\left(1 - \frac{2|\mathbf{h}_{23}|}{O}\right)}{|\mathbf{h}_{23}|} \right), \tag{29}$$

where $|\mathbf{h}_{12/13/23}|$ denote the length of the edges of the triangle and O is its perimeter. The computational cost of evaluating (29) is mainly determined by the $\ln$ functions (see fifth column in Table I).

Fig. 2 shows the behaviour of (29) while varying the triangle area and the triangle quality which is defined as

$$\eta = \frac{4\sqrt{3}A}{|\mathbf{P}_1 - \mathbf{P}_2|^2 + |\mathbf{P}_1 - \mathbf{P}_3|^2 + |\mathbf{P}_2 - \mathbf{P}_3|^2}. \tag{30}$$

The coefficient η is between 0 (three points on a line) and 1 (equilateral triangle). When varying the triangle area, quality is fixed (at value $\eta = 0.98$, solid line at Fig. 2) and when varying the triangle quality, area is fixed (dashed line at Fig. 2).

Finally note that the term $\sin(k_0 r_{21})/r_{21}$ in (8) is not singular and changes negligible within the triangle

$$\lim_{r_{21}\to 0} \frac{\sin(k_0 r_{21})}{r_{21}} = k_0 \lim_{k_0 r_{21}\to 0} \frac{\sin(k_0 r_{21})}{k_0 r_{21}} = k_0 \tag{31}$$

C. Convergence Analysis

It is very important that the algorithm is convergent with an increasing number of RWG basis functions (the parameter U). To verify this assumption, we consider a 30 × 20 cm rectangular plate in free space. This plate is discretized with a different number of triangles and analyzed using the TCM solver. Then,

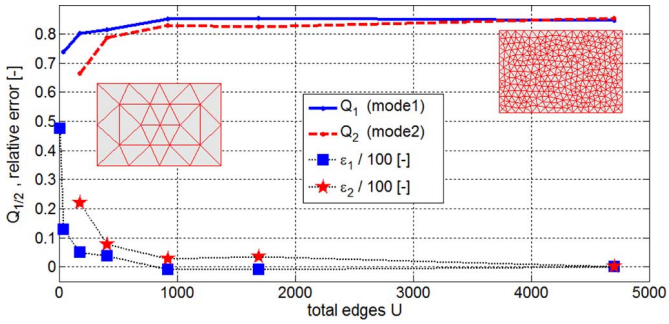

Fig. 3. Algorithm convergence, rect. plate 30 × 20 cm.

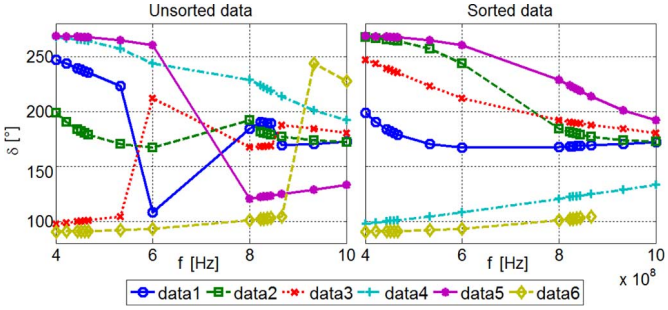

Fig. 4. The original data from the TCM (left) and the sorted ones (right), rec. plate 30 × 20 cm (634 triangles, 926 edges).

modal radiated power and Q factors are calculated for the 1st and 2nd modes, see Table I.

In terms of convergence, (8) is very interesting since from (20) it is observed that the modal radiated power should be equal to one (in case of 1st mode $u = v = 1$). Table I confirms that the modal radiated power P_r is very close to 1 W.

It can therefore be assumed that the numerical integration of radiated power (8) as well as the stored energies (3) and (4) are performed correctly. Singularity treatment can be illustrated at Fig. 3, which shows the convergence of modal Q factors for the 1st and 2nd modes of the rectangular plate. Note, that the inaccurate Q results for low values of U (typically fewer than 150 edges) are caused by a poorly conditioned TCM task. In the case of 42 edges the resonant frequency of the second mode was not found.

Given that energies $W_e^{u,v}$ and $W_m^{u,v}$ are very small (ranging in the order of $10^{-7} \div 10^{-9}$ relative to the unit radiated power), we can conclude that the convergence is sufficient.

Run-time complexity: The complexity of the TCM solution for F frequency samples is $\mathcal{O}(FU^3)$. Considering just one mode at a single frequency, the modal energy computation has a quadratic time complexity $\mathcal{O}(T^2)$ (see the 5th column in Table I). Finally, the complexity of (24) is $\mathcal{O}(Q_M) \propto \mathcal{O}(M^2T^2)$. Because it is sufficient to calculate only half of all the energies $W_e^{u,v}$ and $W_m^{u,v}$ (see Appendix), the time-complexity is $\mathcal{O}(Q_M) \propto \mathcal{O}((M^2/2)T^2)$. And since in practice $M \ll U$, the total calculation time is strongly dominated by the eigen-decomposition, see Section V-D2. Fortunately, in the frequency domain both (13) and (24) can be parallelized (at most F nodes may be employed).

D. Tracking of Eigenvalues and Eigenvectors

The spectral decomposition of the moment impedance matrix $\mathbf{Z}$ doesn't always produce well ordered eigenmodes (see Fig. 4 left). This issue is particularly caused by finite numerical accuracy and slight asymmetry of the frequency-dependent matrix (although the MoM code is based on the Galerkin testing procedure, the Z-matrix is not purely symmetrical). At specific frequencies, the decomposition issue might be ill-posed and non-uniquely defined as well.

Proper manipulation and tracking of the modes is the key to preventing physically different current distributions along the frequency samples. Many matrix preconditioners could be used but the resulting modes still need tracking. There are many issues that have to be considered and therefore a specific heuristic method was coded and implemented. Detailed description is beyond the scope of this paper although further information can be found in [30].

Another problem is caused by slight asymmetry of the TCM solution (currents are not ideally orthogonal to each other) and the fact that the current $\mathbf{J_{u/v}}$ can be computed with random sign. To explain this matter, we extend (13) to a formally correct form $C\mathbf{Xj} = C\lambda\mathbf{Rj}$. While the magnitude of the constant C can be removed by normalization to unit radiated power $\widehat{\mathbf{j}} = \mathbf{j}/\sqrt{\langle \mathbf{j}, \mathbf{Rj} \rangle}$, the sign of C remains unchanged.[4]

Fig. 4 shows that the frequency samples aren't spaced equidistantly. This is because that an adaptable frequency solver (AFS) is used in our tool. The AFS starts with an initial set of samples (specified by the user) and then dynamically adds additional samples to the locations with large changes in eigenvalues. This technique significantly saves computational time and helps the tracking of modes.

V. Application: Numerical Results

In this section we demonstrate our efforts on some selected problems. To validate the above mentioned approach, several Q estimates are compared.

The radiation Q factor may be estimated from the input impedance $\mathbf{Z}$ variation around the resonant frequency f_0 [2]

$$Q_Z = \omega_0 \frac{\left|\frac{\partial Z(\omega)}{\partial \omega}\right|}{2R(\omega_0)}. \tag{32}$$

The above equation could be converted to the modal form Q_{Zu}. Let us expand both the numerator and the denominator by current $|I|^2/2$ and suppose that Ω is PEC

$$\begin{aligned} Q_Z &= \omega_0 \frac{\left|\frac{\partial R(\omega)}{\partial \omega} + \mathrm{j}\frac{\partial X(\omega)}{\partial \omega}\right| \frac{|I|^2}{2}}{2R(\omega)\frac{|I|^2}{2}} \\ &= \frac{\omega_0 \left|\frac{\partial (P_r)}{\partial \omega} + \mathrm{j}\frac{\partial (2\omega(W_m - W_e))}{\partial \omega}\right|}{2P_r} \end{aligned} \tag{33}$$

Since from (20) $P_r = 1$ W, implying that $\partial(P_r)/\partial\omega = 0$, then

$$Q_{Zu} = \frac{\omega_0}{2} \left| \frac{\partial \left(2\omega \left(W_m^u(\omega) - W_e^u(\omega)\right)\right)}{\partial \omega} \right| \tag{34}$$

[4]This causes problems on adjacent frequencies. For example the current orientation at frequency F is $\{J_u, J_v\} \sim \{+,+\}$ and at freq. $F+1$ is $\{J_u, J_v\} \sim \{+,-\}$. Then, due to the slight non-orthogonality, the results at F and $F+1$ are significantly different.

TABLE II
COMPARISON OF ALL DEFINED Q THAT CONSIDER FEEDING

	Q_Z	Q_{MoM}	Q_{Jtot}	Q_M
Equation	(32)	(11)	(15)	(37)
Source	Z_{in}	$\mathbf{J}_{MoM}, \mathbf{q}_{MoM}$	$\mathbf{J}_{tot}, \mathbf{q}_{tot}$	$\boldsymbol{\beta}$, $\mathbf{W}_{e/m}$
Reference	[2]	[10]	×	×
Based on solver	MoM	MoM	TCM	TCM
Comp. speed	+++	++	+	+++
Information	+	++	++	+++

TABLE III
COMPARISON OF MODAL APPROACHES TO CALCULATION OF Q

	Q_n	$Q_{u,v}$	$\mathbf{W}_{e/m}$
Equation	(35)	(1)	(3), (4)
Source	λ_n	$\mathbf{W}_{e/m}$	$\mathbf{J}_u, \mathbf{q}_u$
Reference	[31]	×	[10]
Based on solver	TCM	TCM	×
Comp. speed	++	+++	+
Information	+	+++	++

The second modal-approach relation is based on the Rayleigh quotient formula for eigenvalue λ_n, [31]

$$Q_n = \frac{\omega_0}{2}\left|\frac{\partial\lambda_n(\omega)}{\partial\omega}\right|, \tag{35}$$

where $\partial\lambda_n/\partial\omega$ is the slope of the nth eigenvalue. Expressions (34) and (35) are equal, provided that

$$2\omega\left(W_m^u(\omega) - W_e^u(\omega)\right) = \lambda_u(\omega). \tag{36}$$

It can be proven that at resonance $Q_n = Q_{Zu}$. The above derived (24) can be formally simplified by using the Frobenius product, [23]. Because the Frobenius product is an inner product of the vector space, we use the same notation as in (15) or (20)

$$Q_M = 2\omega_0 \frac{\max\left\{\langle\boldsymbol{\beta}, \mathbf{W}_e\rangle, \langle\boldsymbol{\beta}, \mathbf{W}_m\rangle\right\}}{\langle\boldsymbol{\beta}, \mathbf{P}_r\rangle}. \tag{37}$$

It has to be noted that (37) is the total Q factor calculated from M selected modes. However, if we consider only one mode u (without any feeding, $\beta_u = 1$), the corresponding Q factor will be referred to as the Q_u factor.

In many cases it isn't necessary to consider the whole matrix $\boldsymbol{\beta}$ because only the diagonal terms $u = v$ are relevant (the others are typically in the order of 10^{-20}, see Section V-B). We denote the diagonal terms as β_u.

Finally, for the comparison of Q_M, we introduce two more radiation factors Q_{MoM} and Q_{Jtot}. Both are also calculated using (3)–(8). The input current distribution $\mathbf{J}_{MoM}$ of factor Q_{MoM} is obtained directly from MoM, the total current $\mathbf{J}_{tot}$ of factor Q_{Jtot} is calculated by (15). See Table II and Table III for comparison of all defined radiation factors.

All the following examples are chosen in order to clarify the presented results. At first, we verify the modal method (RWG, TCM), then we calculate (32)–(37) and compare them with each other.

A. The Thin-Strip Dipole

The first antenna is a dipole in a free space. The length $2L$ is 300 mm and the width d is 2 mm. The dipole was discretized into 432 triangles (534 inner edges) and fed by a voltage gap [15]. This structure is analyzed over a large frequency band (including the small antenna regime).

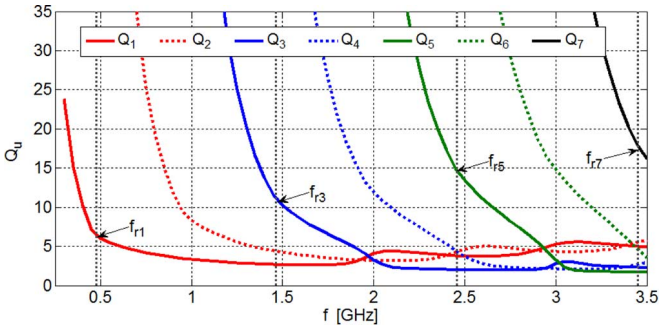

Fig. 5. The first seven modal Q_u factors of the 300 × 2 mm dipole.

TABLE IV
MODAL Q FACTORS IN RESONANCE AND THE β_u FACTORS FOR DIPOLE

u	f_r [MHz]	Q_n	Q_{Zu}	Q_u	$\beta_{u(1/2)}$	$\beta_{u(1/4)}$
1	475.9	6.78	6.20	6.62	93.29	50.03
2	969.0	9.15	8.28	8.93	$8 \cdot 10^{-23}$	95.31
3	1463.7	11.16	10.02	11.09	84.72	40.04
4	1959.3	12.93	11.53	13.00	$3 \cdot 10^{-24}$	0.20
5	2455.5	14.52	12.88	14.91	78.76	44.50
6	2952.4	16.00	14.09	16.43	$2 \cdot 10^{-22}$	76.44
7	3449.9	22.11	19.41	19.37	70.26	33.23

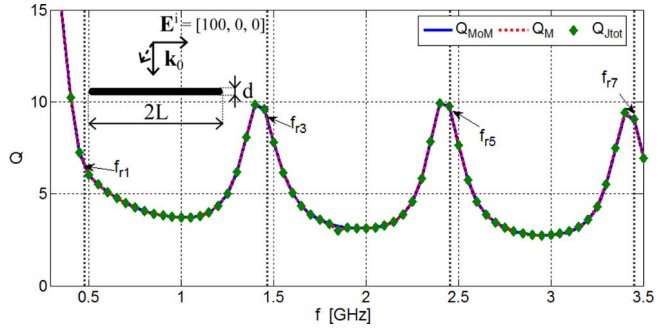

Fig. 6. Q_{MoM}, Q_M and Q_{Jtot} for the dipole 300 × 2 mm fed by an incident plane wave.

Let us look first at the modal Q_u factors that form the total Q_M. The first seven modal Q_u factors ($u \in \{1, \ldots, 7\}$) are depicted at Fig. 5. It is worth mentioning that all modes cyclically intertwine with each other in the lower right corner of Fig. 5. Table IV shows all modal Q factors compared numerically at the resonant frequency of each mode. Modal Q approximations (34), (35) and the exact Q_u factor agree quite well.

Further analysis assumes that the dipole is being excited. We consider an incident plane wave as well as two different feed edge positions.

At first, the total Q_M with incident plane wave feeding is shown at Fig. 6. The incident wave is polarized in the x-direction ($\mathbf{E}^i = [100, 0, 0]$). In this case, the agreement of Q_{MoM}, Q_M and Q_{Jtot} is excellent.

1) Central Feeding: The dipole is fed by a voltage gap ($E^i = 100$ V) located at the middle edge. The modal factors Q_u are not changed as they describe the intrinsic behaviour of the radiator. Due to symmetry, only odd modes are excited (see column $\beta_{u(1/2)}$ in Table IV).

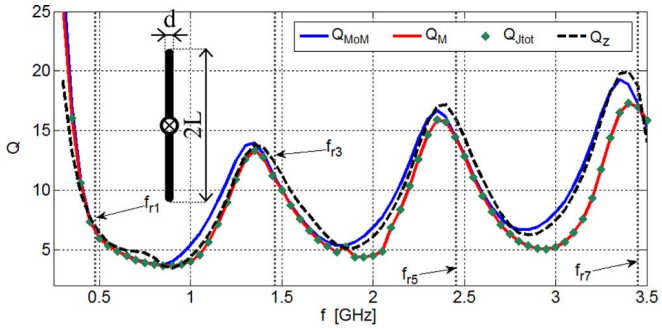

Fig. 7. Q_{MoM}, Q_M, Q_{Jtot} and Q_Z of the dipole 300 × 2 mm, feeding is placed in the middle of the dipole.

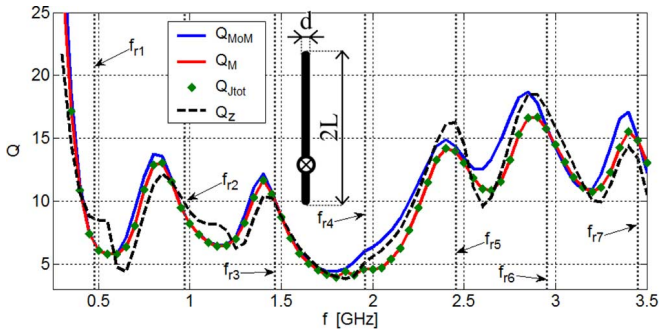

Fig. 8. Q_{MoM}, Q_M, Q_{Jtot} and Q_Z of the dipole 300 × 2 mm, feeding is placed at one quarter of the dipole length.

This explains why total Q factors at Fig. 7 are affected only by odd modal Q_u factors (see solid lines at Fig. 5). Comparison between Fig. 6 and Fig. 7 shows that the voltage gap case converges relatively poorly because of issues mentioned at Section III-B.

The total Q factor is an oscillating function with an absolute minimum of $f/f_{r1} \doteq 1.76$, see Fig. 7. It can be seen, that the agreement of the Q_{MoM} with the Q_Z approximations (directly derived from impedance matrix $\mathbf{Z}$) is quite good. Slight differences between Q_M and Q_{Jtot} at higher frequencies are also (except for the voltage gap issue) addressed by the fact that Q_M is calculated only for the first few modes M, which may no longer be effective at higher frequencies.

2) Feeding at 1/4 of the Dipole Length: Now the dipole is fed at the 1/4 of its length, more modes can be now excited and accordingly, the coefficients β_u changed significantly (see column $\beta_{u(1/4)}$ in Table IV). Hence the total Q factors at Fig. 8 are notably different as well—compare to Fig. 7. With the exception of the fourth mode (which cannot be excited), all modes somehow contribute to the total Q_M.

This example shows how the modal approach is effective and illuminating. The eigenproblem is calculated only once, after that we consider only the arrangement of the excitation.

B. The Mutually Coupled Dipoles—In-Phase Currents

The second example studies the Q factor of two side-by-side coupled dipoles. Both are 100 mm long and 1 mm wide, spaced by the distance d and fed in the middle of the antenna(s) with the same amplitude and phase ($E^i = 100$ V, $\mathbf{J}_1 = \mathbf{J}_2$). Dipoles

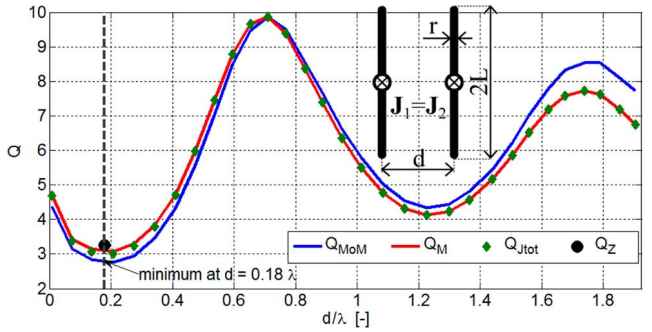

Fig. 9. Q_{MoM}, Q_M, Q_{Jtot} and Q_Z for in-phase fed dipoles of distance d.

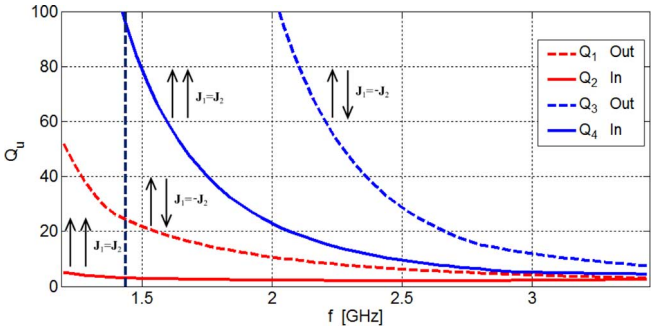

Fig. 10. The first four modal Q_u factors (two dipoles of distance $d = 0.18\lambda$).

TABLE V
MODAL Q FACTORS IN RESONANCE FOR TWO COUPLED THIN-STRIP DIPOLES OF DISTANCE $d = 0.18\lambda$ (MINIMAL TOTAL Q)

u	f_r [MHz]	Q_n	Q_{Zu}	Q_u
1	1386.5	31.40	27.21	26.74
2	1437.2	3.39	3.12	**3.01**
3	2816.3	15.52	13.98	15.17
4	2980.2	5.72	5.07	5.09

were discretized into 576 triangles (718 inner edges). This scenario is equivalent to a single horizontal dipole lying $d/2$ above a perfect magnetic infinite plane (PMC).

The total Q_M factor was calculated as a function of distance d. Comparison with other total Q factors is depicted at Fig. 9. Again, the total Q_M is an oscillating function with an absolute minimum of $d = 0.18\lambda$. While the case of out-of-phase currents was analytically verified in [11] ($d(\min(Q)) = 0.716\lambda$), for in-phase currents a similar study is more complicated.

Nevertheless, this behaviour can be easily explained by the TCM. Resonant frequencies and modal quality factors are displayed in Table V, Fig. 10 shows the first four modal Q_u factors ($u \in \{1, 2, 3, 4\}$); current orientation is schematically depicted as well. Table V shows that the in-phase modes have significantly lower Q_u than the out-of-phase modes.

Obviously, the total in-phase current is formed by the dominant in-phase mode at a given frequency (which is the frequency of the second mode with $f_{r2} = 1437.2$ MHz and $Q_u = 3.01$). Let us consider summation of four modes at frequency $f = f_{r2}$ and for distance $d = 0.18\lambda$. Then we obtain the values in Table VI. For Q_M calculation at this point, we can omit all coefficients and energies of an order less than 10^{-10}. In this case that is all except the second mode ($u = v = 2$), see Table VI).

TABLE VI
SUMMATION DATA AT RESONANCE FOR 2ND MODE ($f_{r2} = 1437.2$ MHz, IN-PHASE CURRENT) OF TWO COUPLED THIN-STRIP DIPOLES WITH DISTANCE $d = 0.18\lambda$ (MINIMAL TOTAL Q)

u	$\beta_{u,u}$ [-]	λ_u [-]	$2\omega(W_m^u - W_e^u)$	Q_u
1	$7 \cdot 10^{-24}$	1.72	1.94	24.42
2	**156**	**0.01**	**0.04**	**3.01**
3	$5 \cdot 10^{-29}$	-759.38	-680.53	902.10
4	$2 \cdot 10^{-27}$	-80.54	-72.64	95.48

Also all products of $\beta_{u,v} W_{e/m}^{u,v}$ for $u \neq v$ are negligible. As a result, only the second mode contributes to the total Q

$$Q_M = 2\omega_0 \frac{\max\left\{\beta_2 W_e^{2,2}, \beta_2 W_m^{2,2}\right\}}{\beta_2 P_r^{2,2}}. \tag{38}$$

Since $P_r^{2,2} \doteq 1$, we simplify (38) by extracting β_2

$$\begin{aligned} Q_M &= 2(2\pi f_{r2}) \max\left\{W_e^{2,2}, W_m^{2,2}\right\} \\ &= 4\pi 1.437 \cdot 10^9 \max\{1.642 \cdot 10^{-10}, 1.663 \cdot 10^{-10}\} \\ &= 3.01 \end{aligned}$$

It is seen that the minimal $Q_M = 3.01$ is directly equal to the modal Q_u of the second mode.

Note that the above described behaviour is also valid for the folded dipole with sufficient conductor coupling and a separation distance of $d \ll 0.05\lambda$.

C. The Bowtie Antenna

The next antenna under study is a bowtie in a free space. Its length L is 100 mm, width d is 60 mm and gap width t is 4 mm, see Fig. 13. The structure is discretized into 309 triangles with 436 inner edges (these values are doubled in the case of an infinite ground plane as described later). Two feeding scenarios have been considered—incident plane waves with polarizations $\mathbf{E}_1^i = [100, 0, 0]$ and $\mathbf{E}_2^i = [100, 100, 0]$.

The first step is the modal analysis of the bowtie without a ground plane. Characteristic angles are shown at Fig. 11 (solid lines), Fig. 12 depicts schematically the main current paths of these modes. For clarity we show only the first five modes, but in fact we analyze the first ten significant modes at a given frequency range. Nonetheless the results may be inaccurate at the end of the frequency spectrum (about $3.5 \div 4$ GHz).

Polarization of the incident plane wave dramatically affects the total sum for Q—Fig. 13. Total Q factors are the same for both polarizations up to a frequency of about 2.3 GHz. For higher frequencies, results start to strongly depend on the excitation of modes 2–10.

An interesting study is presented at Fig. 14, only $\mathbf{E}_1^i$ polarization is assumed. All the first ten modes are divided into four groups (see Fig. 14 left), while each group contains similar modes (regarding current distributions). Fig. 14 shows the effects on the total Q_M depending on which groups are summed up. It is clearly seen that the inductive (non-radiating, group D at Fig. 14 left) modes significantly affect the behaviour of the antenna (compare sum $A + B + C$ and $A + B + C + D$ at Fig. 14 right).

Then the bowtie is placed above an infinite ground plane at a height of h. Changes in eigen-angles are depicted at

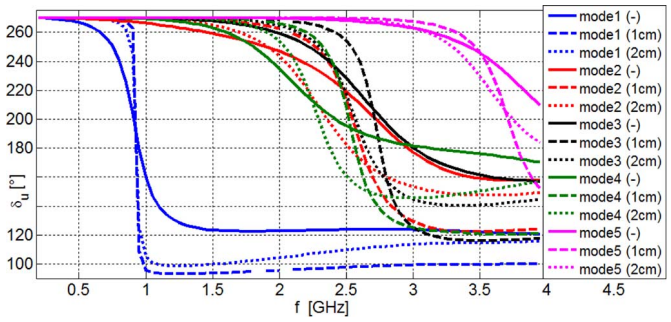

Fig. 11. The first five modes represented by the eigen-angles δ_u as a function of frequency, the bowtie antenna (solid line: no ground plane; dashed lines: infinite ground planes of height 1 cm and 2 cm, respectively).

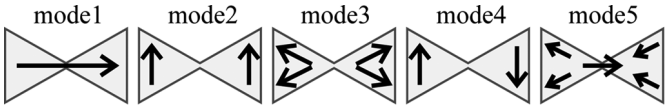

Fig. 12. Schematic depiction of the first five modes of the bowtie antenna.

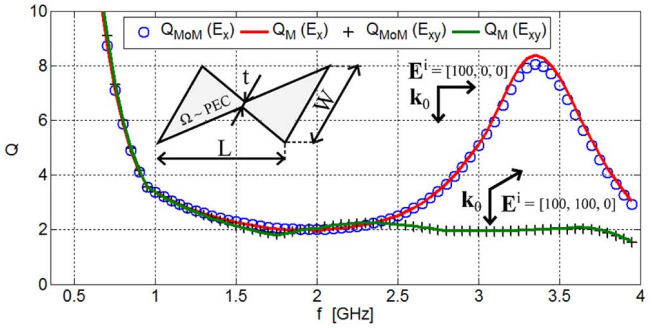

Fig. 13. Q_{MoM} and Q_M of the bowtie (two incident plane wave polarizations are considered).

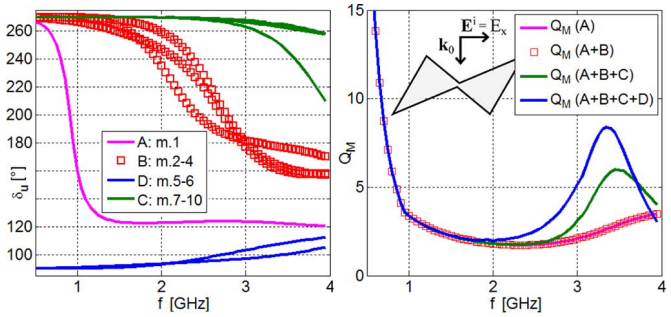

Fig. 14. The first ten modes of bowtie with associated four scenarios of Q_M factors (E_x polarization).

Fig. 11. With increasing height above the ground, the slope of eigen-angles decrease. Because of a minimum (and more or less constant) resonant frequency, only the dominant mode TM_{01} (without any feeding) will be studied. Using the image theory [15], the radiator in the $x - y$ plane placed h above the infinite electric ground plane is modeled as two bowties separated by the distance $2h$, see Fig. 15. In the TCM analyzer, proper out-of-phase mode is selected and analysed.

The modal factors Q_u and Q_n of the first mode are depicted at Fig. 16. These were obtained at resonance ($\delta_u = 0$) as a func-

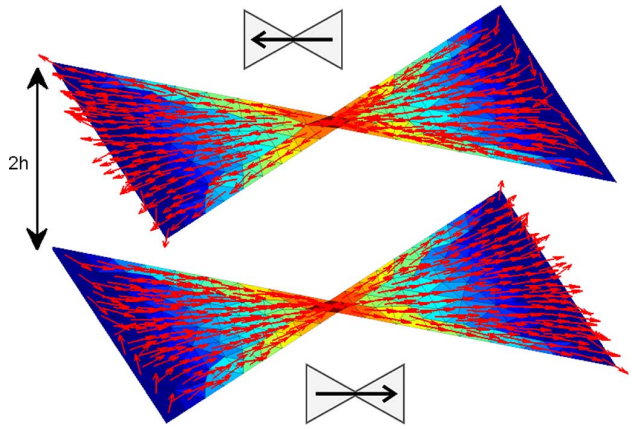

Fig. 15. Bowtie above infinite ground plane $h = 5$ mm, dominant mode TM_{01} shown.

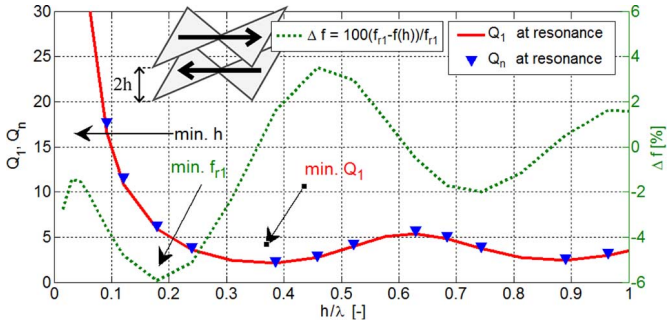

Fig. 16. The modal radiation Q_u and the resonant frequency for dominant mode of bowtie antenna as a function of height h.

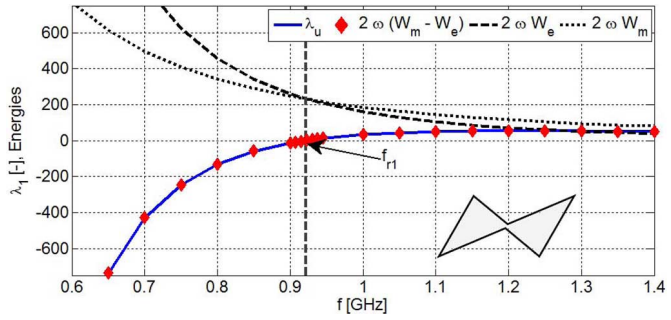

Fig. 17. The eigenvalues, electric and magnetic stored energies of the first mode at height 5 mm, bowtie.

tion of height h. For larger values of h the Q_u factor becomes smaller. The second curve at Fig. 16 (green dashed line) represents changes in the resonance frequency of the first mode, calculated as

$$\Delta f_{\%} = 100\frac{f_{r1}(\infty) - f_{r1}(h)}{f_{r1}(\infty)} \tag{39}$$

and displayed in [\%]. This allows us to locate zones with minimum values of h and Q_u and to find a compromise between them for a specific application. For comparison, the reactive energies of the 1st mode for height $h = 5$ mm ($f_{1r} = 927$ MHz) are plotted at Fig. 17. It is obvious that resonance occurs when the stored energies are equal and so the eigenvalue $\lambda_1 = 0$, (36).

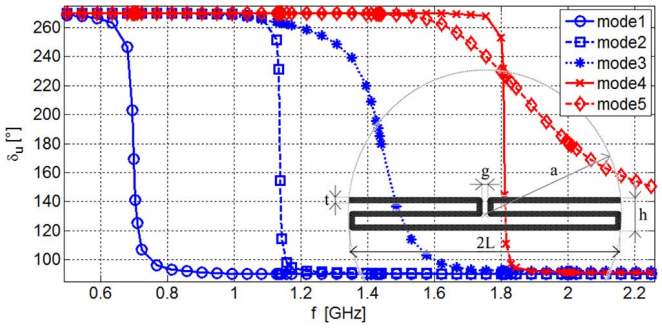

Fig. 18. The first five characteristic angles of meander folded dipole.

TABLE VII
MODAL Q FACTORS IN RESONANCE FOR MEANDER FOLDED DIPOLE (THE FIRST FIVE MODES ARE CONSIDERED)

u	f_r [MHz]	ka	Q_n	Q_u
1	697.8	0.736	43.34	43.54
2	1136.5	1.199	196.67	195.83
3	1442.2	1.521	13.76	13.82
4	1809.2	1.908	357.40	355.52
5	2005.1	2.115	3.45	3.41

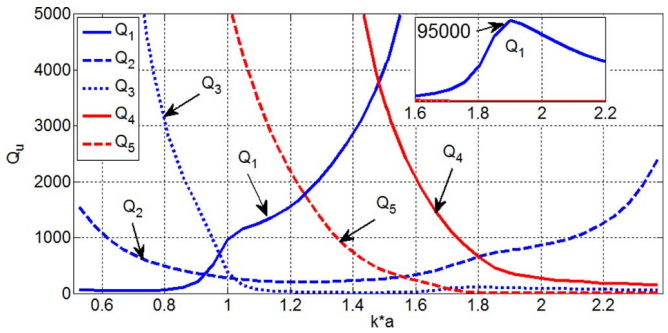

Fig. 19. The modal Q_u of the first five modes of meander folded dipole.

D. The Meander Folded Dipole

The last example is an electrically small meander folded dipole. Length $2L$ is 100 mm, overall width h is 12 mm (so enclosing a sphere of radius $a = \sqrt{L^2 + (h/2)^2} = 50.35$ mm), the width of strip t is 2 mm and the gap width g is also 2 mm. The dipole is discretized into 736 triangles with 929 inner edges. All the outer corners are bent with radius 1 mm and refined—see the lower right corner of Fig. 18. The frequency range for analysis is chosen from 0.5 GHz ($ka = 0.527$) to 2.25 GHz ($ka = 2.373$).

Modal analysis is performed with an adaptable frequency solver. The initial frequency step is set to 50 MHz (36 samples) with two additional iterations (60 samples are obtained at the end of calculation). Eigen-numbers are successfully sorted and converted to the eigenangles, see Fig. 18. There are five modes that are dominant in the selected frequency range.

The modal radiation factors Q_n (only at resonance) and Q_u were calculated for each mode, see Table VII and Fig. 19. The difference between Q_n and Q_u is caused primarily by numerical evaluation of derivation in (35), so the calculation of Q_n gets more inaccurate with higher values of Q. Also in this case the AFS solver is very useful. Note that the first mode is purely inductive at mid-range frequencies, thus the Q_1 rises very fast

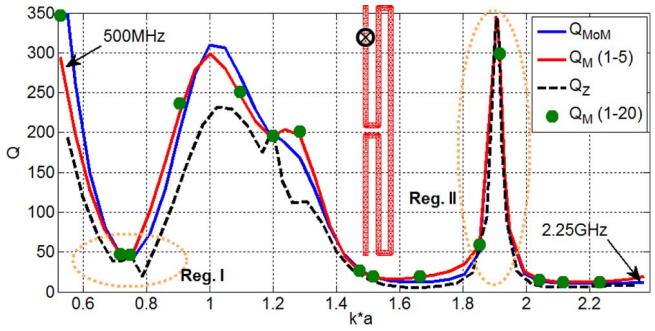

Fig. 20. Q_{MoM}, Q_M and Q_Z of meander folded dipole.

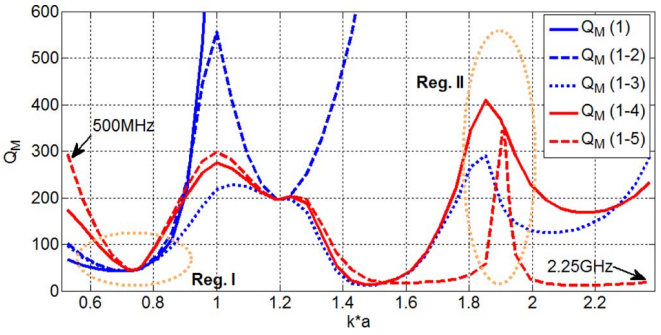

Fig. 21. Total Q_M calculation based on various number of modes (numbers in the legend characterize what modes have been summarized).

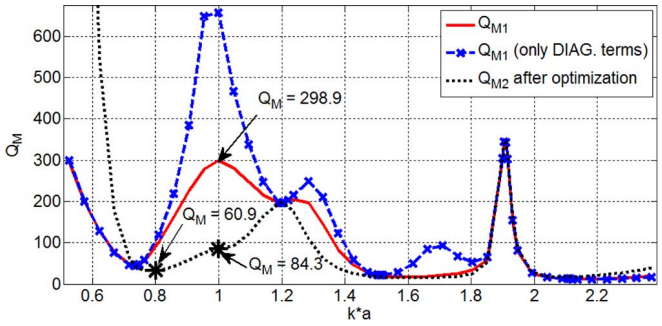

Fig. 22. Comparison between full Q_M and Q_M based only on diagonal terms in matrix $\boldsymbol{\beta}$, minimalized Q_M is displayed as an asterisk.

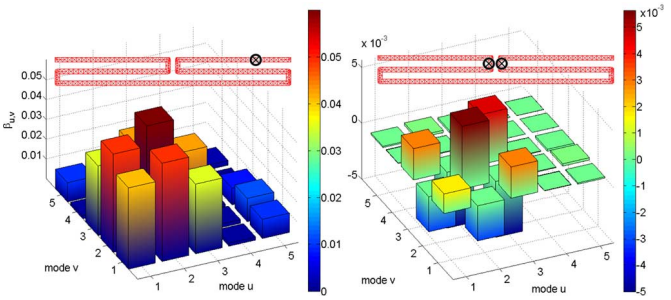

Fig. 23. $\boldsymbol{\beta}$ matrix for two feeding scenarios: the original feeding ($Q_M = 298.9$ at $ka = 1$) and the optimized feeding ($Q_M = 84.3$ at the same ka), first five modes are considered.

(reaching a value of 95000). A detailed description of the modal currents is beyond the scope of this paper.

1) Total Q_M Calculation: To obtain the total Q (both Q_M, Q_Z and Q_{MoM}), feeding has to be incorporated. For this purpose a voltage gap generator ($E^i = 100$ V) was placed at the inner edge of no. 39, highlighted at Fig. 20. Then the total Q factors are calculated and are shown at Fig. 20. Some observations are listed as follows.

- The course of Q_M is smooth and more or less equal with Q_{MoM}. On the other hand, Q_Z doesn't match very well, especially in locations distant from the modal (natural) resonances, [2].
- Q_M (1–5) for the first five modes is close to Q_M (1–20) for the first 20 modes (Q_M (1–20) is considered only at some frequencies to keep the figure readable).
- The fact that Q_M (1–5) is very close to Q_{MoM} is very interesting from the engineering point of view-no matter where the feeding is located, the summation of the first five modes is sufficient enough to obtain accurate Q_M in the "low ka" region.

One minimum of total Q is located in the small antenna regime (for $ka = 0.736$, that is the resonant frequency of the first mode). Then the total Q rises to a value of about 350. As will be shown later, total Q can be effectively reduced in relatively broadband regions.

From Fig. 21 is also obvious that the total Q_M for a growing number of modes ($M = 1, \ldots, M = 5$) is increasingly better matched with Q_{MoM}. In fact, the Q_M factor is perfectly adjusted at natural resonances because there is only one significant entry of the $\boldsymbol{\beta}$ matrix (for example it is β_2 for $ka = 1.2$ at Fig. 21).

Including all β entries (not only the diagonal ones) is generally necessary for correct calculation. Compare the red solid line at Fig. 22 (which shows full summation where all members are used) with blue dashed lines (which consider only the diagonal terms of the $\boldsymbol{\beta}$ matrix). For simple structures (like a dipole), it is usually sufficient to use the self coupling diagonal terms, but generally energies produced by eigencurrents seem to be non orthogonal (unlike radiated powers).

2) Total Q_M Minimization: The following subsection draws out some benefits of the proposed method. We choose $ka = 1$ with $Q_M = 298.9$, see Figs. 20–22. Using optimization we now try to minimize the Q_M factor in the neighborhood of the selected point $ka = 1$ (which is the boundary value of ESA).

A significant advantage is that the TCM solution and ergo the modal energies $\mathbf{W}_e$ and $\mathbf{W}_m$ are computed only once. All single-calculated operations (eigensolution (13), 60 freq. samples, time: 229 s; tracking [30], 20 modes, time: 10 s; and modal energies calculation (3), (4), 5 modes, time: 62 s) took totally[5] 301 s. Our in-house Particle Swarm Optimization algorithm [32] is utilized to find optimal feeding scenarios—we consider two (voltage) gaps with independent magnitudes $E^i_{1/2} \in (0, 100)$V that may be located at any inner edges.

Equations (25) and (37) form the so-called fitness function (f.f.) which was evaluated for 50 agents and 300 iterations. Optimization takes a total of 1741 seconds which is only 0.116 second per f.f. call.

The original and the optimized feeding points are depicted at Fig. 23, together with the $\boldsymbol{\beta}$ matrices before and after optimization. Note here that the modal energies as well as the radi-

[5]All calculations presented in this paper were performed at computer with i7-X980 3.33 GHz processor, 24 GB RAM and SDD disc. As mentioned above, some processes were parallelized (with 8 threads).

ated power matrices are the same in both cases. The resulting impressed gap magnitudes are identical 80 V. The total Q_M is significantly decreased to the value $Q_M = 84.3$ at $ka = 1$. The optimized Q_M is shown at Fig. 22 as a black dashed line with an asterisk mark at the studied value of ka.

VI. Conclusion

Rigorous expressions for electric and magnetic stored energies are utilized for the evaluation of the radiation Q factor based on the superposition of the characteristic mode currents. It is demonstrated that the newly derived coupling matrix $\beta_{u,v}$ (that includes the frequency and the feeding effects) determines the total radiation factor Q_M. This matrix may be viewed as a connection between the intrinsic behaviour of the antenna (described by the set of characteristic currents) and the external world, represented by feeding.

The presented algorithm is implemented and verified for several examples. An up-to-date tracker is applied for sorting the modal data obtained from paralleled eigen-decomposition. Good agreement between the proposed summation technique and conventional methods is observed. All the examples clearly illustrate that the novel expressions together with the robust modal method can be used for the investigation of the modal and total Q factors.

The method stated above can be used for effective design of multiband and broadband ESAs. It also provides a deep physical insight into the studied structures. The commonly used Q_Z factor gives a nice estimation of the radiation Q, but it only answers the question "what is the overall Q?" In turn, the Q_M approach is much more general since answers also on important question "what might the overall Q be?" The presented concept opens novel possibilities for lowering the Q by using multipoint feeds and the design of MIMO antennas. The presented method has been successfully employed in the optimization loop as well. Further work is aimed to study complex planar geometries and detailed analysis of the exact relationship between (modal) radiation factors and maximum bandwidth.

Appendix
Sum of Modal Energies

Consider (23) with M modes expressed as a double sum

$$W_{e/m}^{M} = \sum_{u=1}^{M}\sum_{v=1}^{M} \alpha_u \alpha_v^* W_{e/m}^{u,v}(\mathbf{J}_u, \mathbf{J}_v, q_u, q_v) \tag{40}$$

where modal energies $W_{e/m}^{u,v}(\ldots)$ are calculated by (3), (4). In the following, the arguments of energies $W_{e/m}^{u,v}$ are omitted. The (40) may be divided into two parts

- $u = v$
  The term $\alpha_u \alpha_v^*$ is real and equal (see (15)) to

$$\alpha_u \alpha_v^* = \frac{\langle \mathbf{j}_u, \mathbf{E}^i \rangle^2}{1 + \lambda_u^2}. \tag{41}$$

  If we expand the product (41) by $(1 + \lambda_u^2)$, then

$$W_{e/m}(u,u) = \sum_{u=1}^{M} \frac{\langle \mathbf{j}_u, \mathbf{E}^i \rangle^2 \left(1 + \lambda_u^2\right)}{\left(1 + \lambda_u^2\right)^2} W_{e/m}^{u,u}. \tag{42}$$

- $u \neq v$
  Since $\Re\{\alpha_u \alpha_v^*\} = \Re\{\alpha_u^* \alpha_v\}$, $\Im\{\alpha_u \alpha_v^*\} = -\Im\{\alpha_u^* \alpha_v\}$ and $W_{e/m}^{u,v} = W_{e/m}^{v,u}$ we can sum two terms at a time

$$W_{e/m}(u,v) + W_{e/m}(v,u) = \left(\alpha_u \alpha_v^* + \alpha_u^* \alpha_v\right) W_{e/m}^{u,v} \tag{43}$$

  and from (15) after several manipulations

$$W_{e/m}(u,v) + W_{e/m}(v,u) = \frac{2\langle \mathbf{j}_u, \mathbf{E}^i \rangle \langle \mathbf{j}_v, \mathbf{E}^i \rangle (1 + \lambda_u \lambda_v)}{\left(1 + \lambda_u^2\right)\left(1 + \lambda_v^2\right)} W_{e/m}^{u,v}. \tag{44}$$

Using (42) and (44)

$$W_{e/m}^{M} = \sum_{u=1}^{M}\sum_{v=1}^{M} \frac{\langle \mathbf{j}_u, \mathbf{E}^i \rangle \langle \mathbf{j}_v, \mathbf{E}^i \rangle (1 + \lambda_u \lambda_v)}{\left(1 + \lambda_u^2\right)\left(1 + \lambda_v^2\right)} W_{e/m}^{u,v}. \tag{45}$$

Acknowledgment

The authors would like to thank N. Bell, P. Hamouz, Dr. V. Sobotikova and Dr. J. Kral for their comments. The authors are also grateful for fruitful discussion with Prof. G. Vandenbosch. Also, we would like to thank three anonymous reviewers who suggested valuable improvements to the paper.

References

[1] J. L. Volakis, Ch.-Ch. Chen, and K. Fujimoto, "Survey of small antenna theory," in *Small Antennas: Miniaturization Techniques & Applications*, 1st ed. New York: McGraw-Hill, 2010, ch. 2, pp. 3–100.
[2] A. D. Yaghjian and S. R. Best, "Impedance, bandwidth and Q of antennas," *IEEE Trans. Antennas Propag.*, vol. 53, no. 4, pp. 1298–1324, Apr. 2005.
[3] H. A. Wheeler, "Fundamental limitations of small antennas," in *Proc. IRE*, Dec. 1947, vol. 35, pp. 1479–1484.
[4] L. J. Chu, "Physical limitations of omni-directional antennas," *J. Appl. Phys.*, vol. 19, pp. 1163–1175, Dec. 1948.
[5] R. F. Harrington, "Effect of antenna size on gain, bandwidth, and efficiency," *J. Res. Nat. Bur. Standards*, vol. 64D, pp. 1–12, Jan.–Feb. 1960.
[6] R. E. Collin and S. Rotchild, "Evaluation od antenna Q," *IEEE Trans. Antennas Propag.*, vol. 12, pp. 23–27, Jan. 1964.
[7] J. S. McLean, "A re-examination of the fundamental limits on the radiation q of electrically small antennas," *IEEE Trans. Antennas Propag.*, vol. 44, pp. 672–675, May 1996.
[8] Y. Geyi, "A method for the evaluation of small antenna Q," *IEEE Trans. Antennas Propag.*, vol. 51, pp. 2124–2129, Aug. 2003.
[9] M. Gustafsson, C. Sohl, and G. Kristensson, "Physical limitations on antennas of arbitrary shape," in *Proc. Royal Society A: Mathematical, Physical and Engineering Sciences*, 2007, vol. 463, no. 2086, pp. 2589–2607.
[10] G. A. E. Vandenbosch, "Reactive energies, impedance, and Q factor of radiating structures," *IEEE Trans. Antennas Propag.*, vol. 58, no. 4, pp. 1112–1127, Apr. 2010.
[11] P. Hazdra, M. Capek, and J. Eichler, "Radiation Q-factors of thin-wire dipole arrangements," *IEEE Antennas Wireless Propag. Lett.*, vol. 10, pp. 556–560, May 2011.
[12] R. F. Harrington and J. R. Mautz, "Theory of characteristic modes for conducting bodies," *IEEE Trans. Antennas Propag.*, vol. 19, no. 5, pp. 622–628, Sept. 1971.
[13] R. F. Harrington, *Field Computation by Moment Methods*. New York: John Wiley—IEEE Press, 1993.
[14] K. F. Warnick, *Numerical Analysis for Electromagnetic Integral Equations*. Norwood, MA: Artech House, 2008.
[15] C. A. Balanis, *Advanced Engineering Electromagnetics*. New York: Wiley, 1989.
[16] P. Hazdra and P. Hamouz, "On the modal superposition lying under the MoM matrix equations," *Radioengineering*, vol. 17, no. 3, pp. 42–46, Sep. 2008.
[17] W. C. Gibson, *The Method of Moments in Electromagnetics*, 1st ed. London, U.K.: Chapman & Hall, 2008.
[18] R. F. Harrington and J. R. Mautz, "Computation of characteristic modes for conducting bodies," *IEEE Trans. Antennas Propag.*, vol. 19, no. 5, pp. 629–639, Sept. 1971.

[19] S. M. Rao, D. R. Wilton, and A. W. Glisson, "Electromagnetic scattering by surfaces of arbitrary shape," *IEEE Trans. Antennas Propag.*, vol. 30, no. 3, pp. 409–418, May 1982.
[20] M. Cabedo-Fabres *et al.*, "The theory of characteristic modes revisited: A contribution to the design of antennas for modern applications," *IEEE Antennas Propag. Mag.*, vol. 49, no. 5, pp. 52–68, Oct. 2007.
[21] E. Anderson *et al., LAPACK Users' Guide*. Philadelphia, PA: Society for Industrial and Applied Mathematics (SIAM), 1999.
[22] M. Cabedo-Fabres, "Systematic Design of Antennas Using the Theory of Characteristic Modes," Ph.D. dissertation, UPV, Spain, Feb. 2007.
[23] R. A. Horn and C. R. Johnson, *Topics in Matrix Analysis*. Cambridge, U.K.: Cambridge Univ. Press, 1994.
[24] S. N. Makarov, *Antenna and EM Modeling with Matlab*, 1st ed. New York: John Wiley, 2002.
[25] P.-O. Persson, "Mesh Generation for Implicit Geometries," PhD. Thesis, MIT, , 2005.
[26] E. H. Newman, "Small antenna location synthesis using characteristic modes," *IEEE Trans. Antennas Propag.*, vol. 27, no. 4, pp. 530–531, July 1979.
[27] J. F. Shaeffer, MOM3D Method of Moments Code Theory Manual Denmar, Marietta, Georgia, Contract NAS1-18603, Rep. 189594, Mar. 1992.
[28] T. F. Eibert and V. Hansen, "On the calculation of potential integrals for linear source distributions on triangular domains," *IEEE Trans. Antennas Propag.*, vol. 43, no. 12, pp. 1499–1502, Dec. 1995.
[29] P. Arcioni, M. Bressan, and L. Perregrini, "On the evaluation of the double surface integrals arising in the application of the boundary integral method to 3-D problems," *IEEE Trans. Microwave Theory Tech.*, vol. 45, no. 3, pp. 436–439, Mar. 1997.
[30] M. Capek, P. Hazdra, P. Hamouz, and J. Eichler, "A method for tracking characteristic numbers and vectors," *Progr. Electromagn. Res. B*, vol. 33, pp. 115–134, 2011.
[31] R. F. Harrington and J. R. Mautz, "Control of radar scattering by reactive loading," *IEEE Trans. Antennas Propag.*, vol. 20, no. 4, pp. 446–454, Jul. 1972.
[32] M. Capek, P. Hazdra, P. Hamouz, and M. Mazanek, "Software tools for efficient generation, modeling and optimisation of fractal radiating structures," *IET Microw., Antennas Propag.*, vol. 5, no. 8, pp. 1002–1007, Jun. 2011.

Miloslav Capek (S'09) received the M.Sc. degree in electrical engineering from the Czech Technical University, Prague, Czech Republic, in 2009, where he is currently working towards the Ph.D. degree.

His research interests are in the area of electrically small antennas, numerical techniques, fractal geometry and optimalization.

Pavel Hazdra (M'03) received the M.S. and Ph.D. degrees in electrical engineering from the Czech Technical University in Prague, in 2003 and 2009, respectively.

He is a Research and Teaching Assistant with the Department of Electromagnetic Field, CTU-FEE. His research interests are in the area of electromagnetic theory, computational electromagnetics, fractal geometry, planar antennas and special prime-feed antennas.

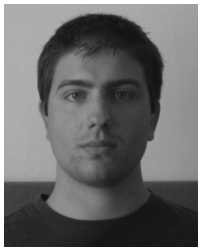

Jan Eichler (S'10) received the B.Sc. and M.Sc. degrees in electrical engineering from the Czech Technical University in Prague, in 2008 and 2010, respectively, where he is currently working towards the Ph.D. degree.

His research interests include multiband antennas, their simulation (full-wave or modal), fractal motifs and the quality factor of an antenna.

II

M. Capek, L. Jelinek, P. Hazdra, and J. Eichler, "The measurable Q factor and observable energies of radiating structures," *IEEE Trans. Antennas Propag.*, vol. 62, no. 1, pp. 311–318, Jan. 2014. [2∗]

The Measurable Q Factor and Observable Energies of Radiating Structures

Miloslav Capek, *Student Member, IEEE*, Lukas Jelinek, Pavel Hazdra, *Member, IEEE*, and Jan Eichler, *Student Member, IEEE*

***Abstract*—New expressions are derived to calculate the Q factor of a radiating device. The resulting relations link Q based on the frequency change of the input impedance at the input port (Q_X, Q_Z) with expressions based solely on the current distribution on an radiating device. The question of which energies of a radiating system are observable is reviewed, and then the proposed Q factor as defined in this paper is physical. The derivation is based on potential theory rather than fields. This approach hence automatically eliminates all divergent integrals associated with electromagnetic energies in infinite space. The new formulas allow us to study the radiation Q factor for antennas without feeding (through e.g., characteristic modes) as well as fed by an arbitrary number of ports. The new technique can easily be implemented in any numerical software dealing with current densities. To present the merits of proposed technique, three canonical antennas are studied. Numerical examples show excellent agreement between the measurable Q_Z derived from input impedance and the new expressions.**

***Index Terms*—Antenna theory, electromagnetic theory, Poynting theorem, Q factor.**

I. Introduction

THE radiation Q factor is recognized as one of the most significant parameters of the radiating system and its evaluation for antennas has long been discussed in the literature, see e.g., [1] and references therein. The most recent approaches by Vandenbosch [2] and Gustafsson [3] use the actual distribution of the sources of radiation (currents) from which the electromagnetic energies and radiated power are evaluated. It has recently been shown [4] that Q as defined in [2] (i.e., with the "radiated energy" included) may deliver nonphysical negative values. Hence, the question of which energies should be included as stored in the Q factor is still unsolved.

Rhodes [5] poses exactly this question and develops formulas for the observable energies, i.e., energies which are measurable and thus physical. He defines the observable energy as that part of the total energy that has a measurable effect upon the input impedance and hence upon the frequency bandwidth. His results are interesting from the theoretical point of view, but since electric and magnetic fields in all the space are involved, they are not practical for numerical calculations.

It is known that the total energy of a radiating system in the frequency domain is infinite. This is true for the total energy evaluated from electromagnetic fields (which are stored in an infinite volume) [5], [6]. Rhodes [7] showed that for observable energies the infinities in the integrals cancel in a special way, leaving a finite residue. Vandenbosch [2] was able to analytically subtract the far-field energy from the total energy, isolating the residue and developing expressions for modified vacuum energies based on the currents at the radiating device, and he used them for evaluating Q.

This paper is inspired by [2], [3], [5] and [6], but the line of reasoning is different. It is recognized here for the first time that the only useful and reasonable Q factors of a radiator are the measurable ones, based on frequency changes of the input reactance Q_X, or more generally input impedance Q_Z, see [8]. The proposed development connects sources of radiation (surface currents flowing on an antenna) and the "external world", represented by the frequency behavior of the input impedance at the input port through the complex Poynting theorem. The necessary frequency derivatives on the source side are performed analytically at the level of electromagnetic potentials [9], which are advantageously utilized instead of field quantities [10], [11]. Consequently, there are no infinite integrals present in the derivations. Similarly to previous works, we assume electric currents flowing in free space.

The main result is the expression for Q_Z in terms of different electromagnetic quantities, linked to the current and charge on the antenna through three energy functionals arising from the complex Poynting theorem and its frequency differentation. In this way, a generalized impedance theorem for antennas is established, assuming not only frequency changes of Green's function, as in [2] or [3], but also frequency changes of the current itself. As we show later in the paper, this gives a new additional term: the energy associated to reconfiguration of the current.

A huge advantage over Q_Z as defined by Yaghjian and Best [8] is the possibility of using new expressions for modal currents (i.e., currents computed for a structure without any feeding, see also [12], [13]). It is also possible to examine only a part of the structure of interest and to determine how much this part of the antenna affects the overall Q. In contrast with the quality factors derived in [2] and [3], the Q_Z proposed here is a measurable quantity and hence of interest for the design of arbitrary antennas with respect to their bandwidth.

The paper is organized as follows. In Section II, the measurable Q is derived in terms of the electric currents flowing on the

Manuscript received May 09, 2013; revised October 04, 2013; accepted October 15, 2013. Date of publication October 28, 2013; date of current version December 31, 2013. This work was supported in part by the Grant Agency of the Czech Technical University in Prague under Grant SGS12/142/OHK3/2T/13 and in part by the Grant Agency of the Czech Republic under project 13-09086S.

The authors are with the Department of Electromagnetic Field, Faculty of Electrical Engineering, Czech Technical University in Prague, Technicka 2, 16627, Prague, Czech Republic (e-mail: miloslav.capek@fel.cvut.cz).

Color versions of one or more of the figures in this paper are available online at http://ieeexplore.ieee.org.

Digital Object Identifier 10.1109/TAP.2013.2287519

antenna. Section III discusses differences between previous attempts to calculate radiation Q and the newly derived formulas. Section IV presents numerical examples to verify the proposed theory on three representative antennas: a dipole, a loop and, a small double U-notched loop antenna. The consequences and applications are discussed, and selected results are compared with FEKO [14] and CST [15] software.

II. Measurable Q-Factor in Terms of Field Sources

The purpose of the following derivations is to connect the measurable quality factor with the sources of the field. We will not *a priori* rely on the classic expression $Q = \omega W/P$ as the defining relation with W being the total reactive energy and P the radiated power. Rather, we start with quality factor Q_Z, which originates from the behavior of the RLC circuit [16] and which has been shown to be useful also for estimating antenna performance regarding its impedance bandwidth [8]:

$$Q_Z = \frac{\omega}{2R_{\mathrm{in}}}\left|\frac{\partial Z_{\mathrm{in}}}{\partial \omega}\right| = |Q_R + \jmath Q_X| \tag{1}$$

where

$$Q_R + \jmath Q_X = \frac{\omega}{2R_{\mathrm{in}}}\frac{\partial(R_{\mathrm{in}} + \jmath X_{\mathrm{in}})}{\partial \omega} \tag{2}$$

$\jmath = \sqrt{-1}$ and $Z_{\mathrm{in}} = R_{\mathrm{in}} + \jmath X_{\mathrm{in}}$ is the input impedance of the antenna. In (2) and in the rest of the paper, time harmonic fields [17] with angular frequency ω and the convention $\boldsymbol{\mathcal{F}}(t) = \sqrt{2}\Re\{\mathbf{F}(\omega)\mathrm{e}^{\jmath\omega t}\}$ are assumed.

In order to link (2) with the field sources and their energies, the power definition of the impedance is used

$$P_{\mathrm{in}} = (R_{\mathrm{in}} + \jmath X_{\mathrm{in}})|I_0|^2 \tag{3}$$

where P_{in} is the complex power [9], and I_0 is the input current on the antenna's port. For the same situation, Poynting's theorem [9] allows us to write

$$P_{\mathrm{in}} = -\int_{\Omega} \mathbf{E}\cdot\mathbf{J}^*\,\mathrm{d}\mathbf{r} = \jmath\omega\int_{\Omega}(\mathbf{A}\cdot\mathbf{J}^* - \varphi\rho^*)\,\mathrm{d}\mathbf{r} \tag{4}$$

where $\mathbf{E}$ is the electric field intensity, $\mathbf{J}$ is the current density, and ρ is the charge density inside Ω region, respectively, $\mathbf{A}$ and φ are the vector and scalar potential, respectively, and $*$ denotes complex conjugation. In the last step, the electromagnetic potentials [9] have been used, see the Appendix A. Furthermore, using radiation integrals for $\mathbf{A}, \varphi$ in the Lorentz gauge and charge conservation, (4) can be rewritten as [9]

$$P_{\mathrm{in}} = (P_{\mathrm{m}} - P_{\mathrm{e}}) + \jmath\omega(W_{\mathrm{m}} - W_{\mathrm{e}}) \tag{5}$$

where

$$W_{\mathrm{m}} - \jmath\frac{P_{\mathrm{m}}}{\omega} = k^2\mathcal{L}(\mathbf{J},\mathbf{J}), \tag{6a}$$

$$W_{\mathrm{e}} - \jmath\frac{P_{\mathrm{e}}}{\omega} = \mathcal{L}(\nabla\cdot\mathbf{J}\nabla\cdot\mathbf{J}) \tag{6b}$$

and where, in order to ease the notation, the following energy functional

$$\mathcal{L}(\mathbf{U},\mathbf{V}) = \frac{1}{4\pi\epsilon\omega^2}\int_{\Omega'}\int_{\Omega}\mathbf{U}(\mathbf{r})\cdot\mathbf{V}^*(\mathbf{r}')\frac{\mathrm{e}^{-\jmath kR}}{R}\,\mathrm{d}\mathbf{r}\,\mathrm{d}\mathbf{r}' \tag{7}$$

has been defined. In (7), $R = \|\mathbf{r}-\mathbf{r}'\|$ is the Euclidean distance, $k = \omega/c_0$ is the wavenumber and c_0 is the speed of light. The integration in principle runs over the entire space, but assuming sources of finite extent, the integrals are always finite. Within the chosen naming convention in (5), (6a), (6b), the quantity W_{m} is usually related to magnetic energy, while W_{e} is usually related to electric energy. This association is not unique, however, under the assumption of a linear, passive and lossless antenna, $P_{\mathrm{m}} - P_{\mathrm{e}}$ is the power radiated by the antenna and $\omega(W_{\mathrm{m}} - W_{\mathrm{e}})$ is the net reactive power. Assuming now input current $I_0 = 1\,\mathrm{A}$, substituting (3), (5) into (2), and comparing with (6a) and (6b), it is straightforward to arrive at[1] (8) in which[2]

$$W_{\mathrm{rad}} - \jmath\frac{P_{\mathrm{rad}}}{\omega} = -\jmath k(k^2\mathcal{L}_{\mathrm{rad}}(\mathbf{J},\mathbf{J}) - \mathcal{L}_{\mathrm{rad}}(\nabla\cdot\mathbf{J},\nabla\cdot\mathbf{J})) \tag{9a}$$

$$W_{\omega} - \jmath\frac{P_{\omega}}{\omega} = k^2\mathcal{L}_{\omega}(\mathbf{J},\mathbf{J}) - \mathcal{L}_{\omega}(\nabla\cdot\mathbf{J},\nabla\cdot\mathbf{J}) \tag{9b}$$

and where two more energy functionals are defined as

$$\mathcal{L}_{\mathrm{rad}}(\mathbf{U},\mathbf{V}) = \frac{1}{4\pi\epsilon\omega^2}\int_{\Omega'}\int_{\Omega}\mathbf{U}(\mathbf{r})\cdot\mathbf{V}^*(\mathbf{r}')\,\mathrm{e}^{-\jmath kR}\,\mathrm{d}\mathbf{r}\,\mathrm{d}\mathbf{r}' \tag{10a}$$

$$\mathcal{L}_{\omega}(\mathbf{U},\mathbf{V}) = \frac{1}{4\pi\epsilon\omega^2}\int_{\Omega'}\int_{\Omega}\omega\frac{\partial\mathbf{U}(\mathbf{r})\cdot\mathbf{V}^*(\mathbf{r}')}{\partial\omega}\frac{\mathrm{e}^{-\jmath kR}}{R}\,\mathrm{d}\mathbf{r}\,\mathrm{d}\mathbf{r}' \tag{10b}$$

for details see the Appendix B. In (8) (shown at the bottom of the page), (9a), and (9b) the quantity $W_{\mathrm{rad}} - \jmath P_{\mathrm{rad}}/\omega$ can be attributed to the energy associated with radiation [2], [5],

[1]The upper index (n) in the following expressions denotes the number of included P-terms and W-terms.

[2]Please note that the term denoted as P_{rad}, is not radiated power.

$$Q_R^{(4)} + \jmath Q_X^{(4)} = \frac{\omega}{2(P_{\mathrm{m}} - P_{\mathrm{e}})}\frac{\partial((P_{\mathrm{m}} - P_{\mathrm{e}}) + \jmath\omega\,(W_{\mathrm{m}} - W_{\mathrm{e}}))}{\partial\omega} = \frac{(P_{\mathrm{m}} + P_{\mathrm{e}} + P_{\mathrm{rad}} + P_{\omega}) + \jmath\omega(W_{\mathrm{m}} + W_{\mathrm{e}} + W_{\mathrm{rad}} + W_{\omega})}{2(P_{\mathrm{m}} - P_{\mathrm{e}})} \tag{8}$$

while the term $W_\omega - \jmath P_\omega/\omega$ should be interpreted as the energy needed for the current (charge) reconfiguration during a frequency change.

Neglecting the W_ω and P_ω terms in (8) results in

$$Q_R^{(3)} + \jmath Q_X^{(3)} = \frac{(P_\mathrm{m} + P_\mathrm{e} + P_\mathrm{rad}) + \jmath\omega(W_\mathrm{m} + W_\mathrm{e} + W_\mathrm{rad})}{2(P_\mathrm{m} - P_\mathrm{e})} \quad (11)$$

which is just the radiation quality factor derived in [2], [3].

By omitting also the terms associated with radiation (which are usually small in comparison with the reactive power), one obtains

$$Q_R^{(2)} + \jmath Q_X^{(2)} = \frac{(P_\mathrm{m} + P_\mathrm{e}) + \jmath\omega(W_\mathrm{m} + W_\mathrm{e})}{2(P_\mathrm{m} - P_\mathrm{e})}. \quad (12)$$

Note that $Q_X^{(2)}$ is the classical definition of the radiation quality factor [18].

III. Discussion

This section presents some important remarks:

- The derivation of the general result (8) required only measurable quantities as radiated power $(P_\mathrm{m} - P_\mathrm{e})$ and net reactive power $\omega(W_\mathrm{m} - W_\mathrm{e})$. This is in contrast to the approach in [2], [3], which required the ambiguous separation of the net reactive power into an electric part and a magnetic part.
- The structure of the developed quality factor is compatible with the primary definition $Q = \omega W/P$, indirectly validating (1) in [8]. It is now clearly seen how the change of input impedance is transferred into different forms of energy terms arising from various ω derivatives of (3).
- The $Q_Z^{(4)}$ expressed in (8) holds for any angular frequency ω and represents an untuned Q factor that has the strict physical meaning only in the self-resonances of the antenna Ω. One can, however, compensate the nonzero reactive energy $W_\mathrm{m} - W_\mathrm{e}$ of the antenna at each frequency by an additional energy W_add that is mostly concentrated in a adjacent tuning region[3] Ω_add, containing currents $\mathbf{J}_\mathrm{add}$, so that the antenna system $\Omega_0 = \Omega \cup \Omega_\mathrm{add}$ is tuned to the resonance at ω_0. Considering now that the tuning region is lossless and nonradiative, there is $Q_R^{(4)}(\mathrm{tuned}) = Q_R^{(4)}$. Furthermore, it is possible to calculate the $Q_X^{(4)}(\mathrm{tuned})$ according to (8)

$$Q_X^{(4)}(\mathrm{tuned}) = \frac{\omega_0(W_\mathrm{m} + W_\mathrm{e} + W_\mathrm{rad} + W_\omega + W_\mathrm{add})}{2(P_\mathrm{m} - P_\mathrm{e})} \quad (13)$$

  substituting $\mathbf{J}_0 = \mathbf{J} + \mathbf{J}_\mathrm{add}$ into the related functionals (7), (10a) and (10b). At this point it is important to note, that W_add is a function not only of $\mathbf{J}_\mathrm{add}$ but of $\mathbf{J}$ as well. This results from the fact that W-terms are bilinear forms and thus W_add consists of self-terms $(\mathbf{J}_\mathrm{add}, \mathbf{J}_\mathrm{add})$ as well as cross-terms $(\mathbf{J}, \mathbf{J}_\mathrm{add})$ and its permutation.
- In order to get an additional insight, imagine that the compensation is made by a serial lumped reactance $X_\mathrm{add} = -X_\mathrm{in}$. Using the circuit concept one obtains $Q_X(\mathrm{tuned}) \propto \partial(X_\mathrm{add} + X_\mathrm{in})/\partial\omega_0$. On the contrary, the field concept leads to $Q_X(\mathrm{tuned}) \propto \partial\,\omega_0(W_\mathrm{m}(\mathbf{J}_0) - W_\mathrm{e}(\mathbf{J}_0))/\partial\omega_0$.
  Generally, these two $Q_X(\mathrm{tuned})$ will differ, since the circuit concept neglects all the cross-terms mentioned in the previous point. In other words, $X_0 \neq X_\mathrm{in} + X_\mathrm{add}$, where X_0 is the measured input reactance of the antenna system (including the tuning region). However, considering the compensation made by ideal lumped elements, the energy cross-terms will become negligible in comparison to the self-terms due to the field localization at the lumped circuits. In such cases we can approximately write $W_\mathrm{add} \approx L_\mathrm{add} \Leftrightarrow W_\mathrm{m} < W_\mathrm{e}$ in the case of added serial inductor, and $W_\mathrm{add} \approx 1/\omega_0^2 C_\mathrm{add} \Leftrightarrow W_\mathrm{m} > W_\mathrm{e}$ in the case of added serial capacitor.
- On the basis of the previous discussion, the classical concept of tuned Q can be adopted into the proposed definition. Considering that the energies W_m and W_e are positively semi-definite, we obtain from (13)

$$Q_X^{(4)}(\mathrm{tuned}) = \frac{2\omega_0 \max\{W_\mathrm{m}, W_\mathrm{e}\} + \omega_0(W_\mathrm{rad} + W_\omega)}{2(P_\mathrm{m} - P_\mathrm{e})} \quad (14)$$

  or neglecting the W_rad and W_ω

$$Q_X^{(2)}(\mathrm{tuned}) = \frac{\omega_0 \max\{W_\mathrm{m}, W_\mathrm{e}\}}{(P_\mathrm{m} - P_\mathrm{e})} \quad (15)$$

  which is the classical definition of tuned Q, [18], [2].
- The only difference between (8) and the quality factor derived in [2], [3] is the presence of W_ω, P_ω terms. However, in practice, they are not observable in Q_Z, at least for the particular antennas studied in the next section. Furthermore, the terms $W_\omega, P_\omega, W_\mathrm{rad}, P_\mathrm{rad}$ cannot be strictly separated from each other, as their (internal) energy exchange cannot be detected at the port.
- Only W_ω, P_ω terms require current normalization (i.e., specification of the input current I_0). Dropping them (which fortunately has a very small effect on the measurable Q_Z factor) thus allows the calculation of the Q_Z factor of the arbitrary current distribution (for example modal currents) without referring to a particular feeding network.
- By analogy with [2] and [13], the derived expressions for the quality factor are easy to implement in any method of moment (MoM) [19] code as a post processing routine. The only complication is the existence of $\cos(kR)/R$ terms in the energy functionals (7), (10a), (10b). These singularities are, however, removable and integrable analytically [20], [13].

IV. Numerical Results

In this section we will show numerical results for three canonical antennas, discuss the most important features of the Q factor defined by (8), and compare it with other available definitions. To this point, the expressions given in Section II were implemented in our in-house MoM solver [21] based on RWG basis

[3]The same consideration as in [8], Fig. 2 is made for the field concept.

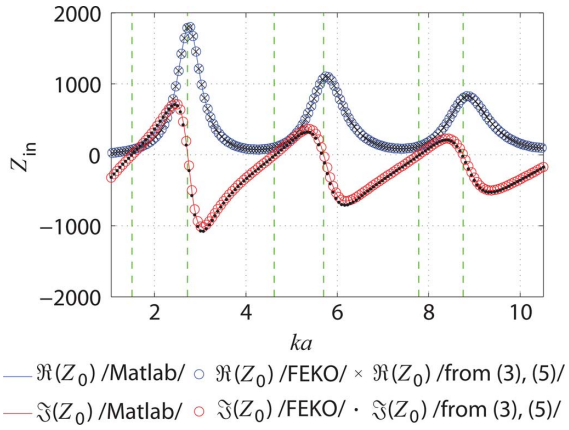

Fig. 1. Real and imaginary parts of the input impedance of a thin-strip dipole simulated in Matlab RWG-MoM and in FEKO software. The "Matlab" and "FEKO" parts are directly calculated as a ratio of voltage and current at the feeding port, while the part denoted as "from (3) and (5)" comes from the direct integration of current distribution on the antenna. The green dashed lines mark resonances and antiresonances.

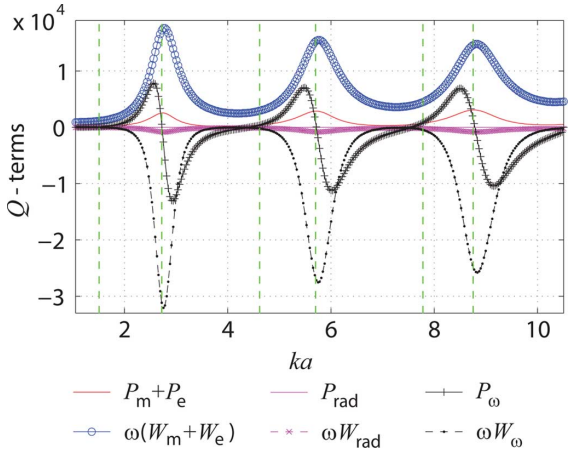

Fig. 2. Frequency dependence of terms composing the nominator of (8) for the thin-strip dipole of Fig. 1.

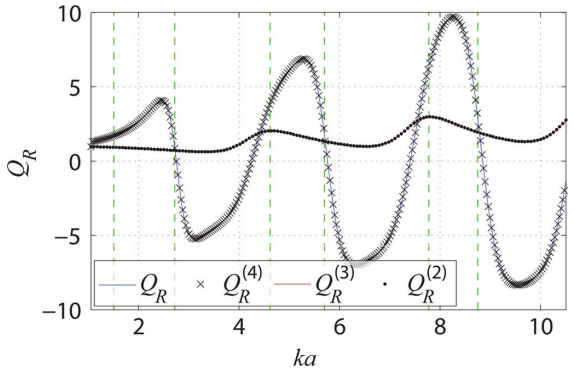

Fig. 3. Comparison of the radiation Q_R factors of the thin-strip dipole of Fig. 1. The green dashed lines mark resonances and antiresonances, see Fig. 1.

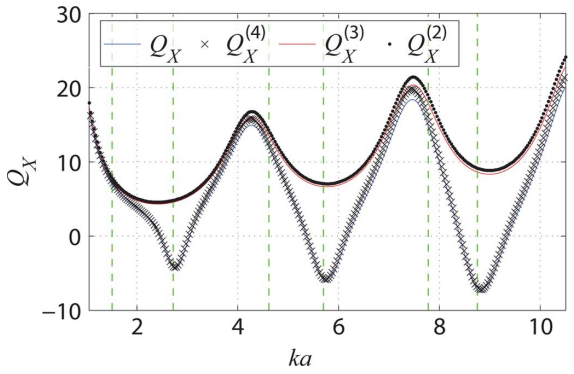

Fig. 4. Comparison of the radiation Q_X factors of the thin-strip dipole of Fig. 1. The green dashed lines mark resonances and antiresonances, see Fig. 1.

functions [22] in Matlab [23]. Thanks to implementation on a GPU card [24], all the calculations are extremely fast (about 0.01 s for one frequency sample and 200 RWG functions). Note that in order to keep the discussion as general as possible, a dimensionless quantity ka is used instead of frequency, with a being the smallest radius of a sphere circumscribing all the sources.

A. A Thin-Strip Dipole

The first example deals with a dipole radiating in free space. The dipole is made of an infinitesimally thin perfectly conducting strip with length $2L$ and width $w = 2L/250$. The dipole is discretized into 201 triangles and is fed by a delta gap [?] in its center (the voltage corresponds to the input current $I_0 = 1$ A). The real and imaginary parts of the input impedance are shown in Fig. 1. For comparison, the dipole was also simulated in FEKO software. Note, that almost exact correspondence in Fig. 1 validates the correct implementation of the MoM and the integration routines, and furthermore, it demonstrates the equality between (3) and (5). Good correspondence between the results justifies the use of our Matlab RWG-MoM code in the rest of the paper.

We now turn to a brief discussion of the terms composing the nominator of (8). The most relevant terms are depicted in Fig. 2. The first observation is that $P_{\rm rad}$ can be safely neglected. Its small value is caused by almost exact cancellation of the real parts of otherwise important terms $k^2\mathcal{L}_{\rm rad}(\mathbf{J},\mathbf{J}), \mathcal{L}_{\rm rad}(\nabla\cdot\mathbf{J},\nabla\cdot\mathbf{J})$, see (9a). The same is approximately valid also for the $W_{\rm rad}$ term, though there the cancellation is not as perfect. There should thus be no important difference between the quality factor defined by (11) and by (12). The second observation relates to $W_\omega - \jmath P_\omega/\omega$. The absolute value of this quantity evidently reaches its maximum at antiresonances and its minimum in the vicinity of resonances. This is coherent with the interpretation as reconfiguration energy, mentioned in Section II: stable eigenmodes exist in the vicinity of resonances, while the change from one eigenmode to another peaks at antiresonances.

In order to check the discussion above, the radiation quality factors given by (2), (8), (11) and (12) are depicted in Figs. 3–5. A central difference has been used to calculate (2). Note that the correspondence between (2) and (8) verifies the numerical implementation, since the expressions are analytically equal. As expected, the quality factors given by (11) and (12) are mostly alike at all frequencies. By contrast, the biggest difference between the $Q_R^{(4)}, Q_X^{(4)}$ factors given by (8) and $Q_R^{(3)}, Q_X^{(3)}$ and

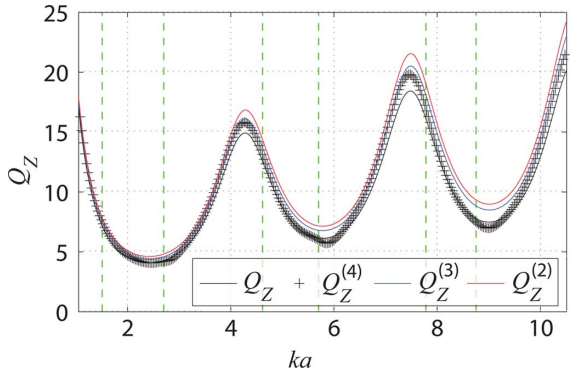

Fig. 5. Comparison of the radiation Q_Z factors of the thin-strip dipole of Fig. 1. The green dashed lines mark resonances and antiresonances, see Fig. 1.

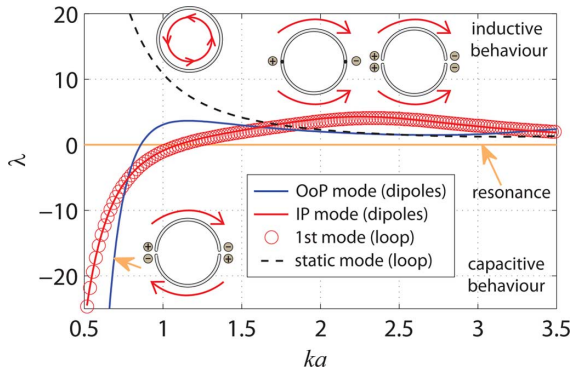

Fig. 6. Eigennumbers of two dipoles and the loop, IP stands for in-phase mode, OoP stands for out-of-phase mode.

$Q_R^{(2)}, Q_X^{(2)}$ appears at antiresonances, which is due to the presence of W_ω, P_ω terms. On the other hand, in the case of resonances the reconfiguration energy is small and all the depicted quality factors are very similar. Observing the differences in the Q_R, Q_X factors, it is however quite remarkable that in the case of Q_Z the W_ω, P_ω terms play almost no role.

B. Modal Solution of a Loop, and an Analogy With Two Dipoles

The second example reveals other benefits of the new technique: the utilization of modal methods. The former Q_Z definition cannot be used in these cases. From the previous example we know that the W_ω term is important for calculating Q_R and Q_X but it can be omitted in calculating Q_Z. Thus, current normalization is not necessary, and no port needs to be specified.

In this example, two basic radiators, a loop and two closely spaced semicircular dipoles that occupy the same volume as the loop does, were decomposed to the characteristic modes, [12], [13]. The radius of the loop is R, and the length of the dipoles is πR. An infinitesimally thin perfectly conducting strip of width $R/12$ is considered both for the loop and the dipoles. The dipoles are separated by a gap of width $R/16$.

The two dipole scenario consists of two possible modes around the first resonant frequency: the in-phase mode (IP) and the out-of-phase mode (OoP), see Fig. 6. The solution of the loop at the same frequency consists of the static (inductive)

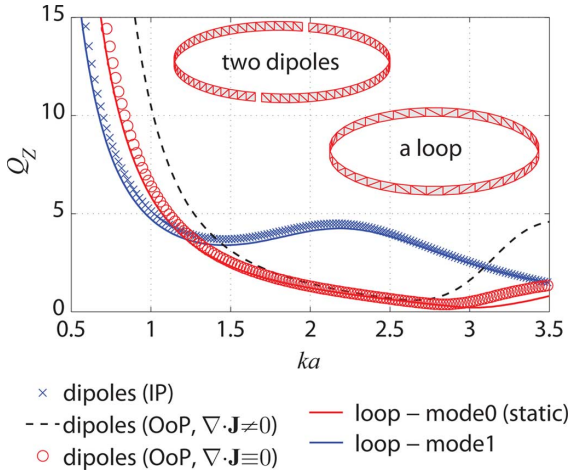

Fig. 7. Equivalence of two topologically different structures—the loop and two closely spaced circular dipoles, IP stands for the in-phase mode, OoP stands for the out-of-phase mode.

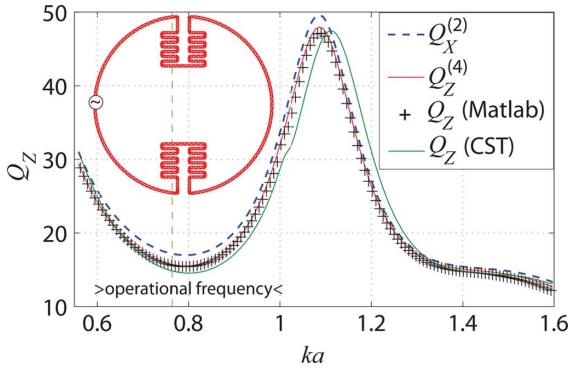

Fig. 8. Comparison of the Q_Z factors from Matlab RWG-MoM (both definition (1) and definition (8) definitions are shown) and CST-MWS [definition (1)]. The antenna operates around the vertical dashed green line.

mode and the first mode, as depicted in Fig. 6. The eigennumbers λ determine the modal behavior, mode is capacitive for $\lambda < 0$, inductive for $\lambda > 0$, and is in resonance for $\lambda = 0$. The eigennumbers for the loop and the dipoles are shown in Fig. 6. The Q_Z factors defined by (8) were calculated from the modal currents. Thanks to the freedom in the current definition, we also calculated the case of OoP dipoles with the charge completely eliminated (setting $\nabla \cdot \mathbf{J} \equiv 0$). As depicted in Fig. 7, the Q_Z of the static mode of the loop looks like the Q_Z of the out-of-phase mode of semicircular dipoles with all charge terms eliminated, see the red line and the red circular marks in Fig. 7. Similarly, the first mode of the loop has the same Q_Z factor as the in-phase mode of the dipoles (no modification is needed in this case because the charge distribution is the same for both cases). Note that the static mode is always excited (irrespective of feed position). Thus, the static mode increases the total Q at all frequencies [13].

C. Small U-Notched Loop Antenna

The electrically small U-notched loop antenna was designed in CST-MWS [15]. The radius of the antenna is R, the width of the infinitesimally thin strip is $R/36$, and PEC is considered, see Fig. 8. To make the antenna electrically smaller, the parts

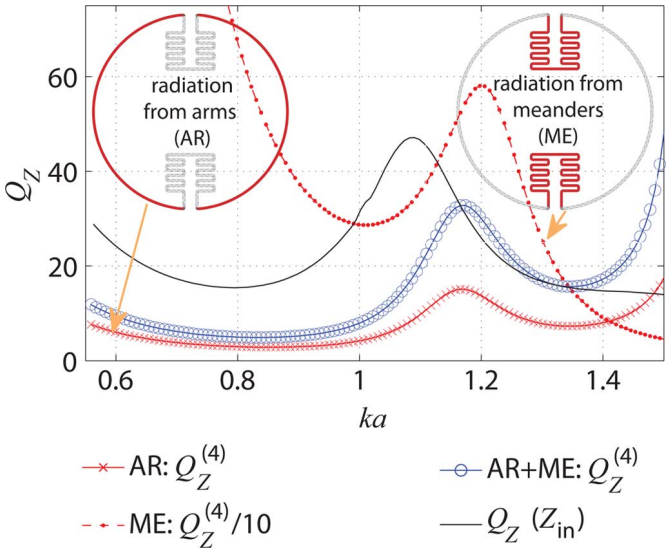

Fig. 9. Study of the particular Q that corresponds to the selected radiating parts of the U-notched loop antenna. AR stands for radiating from the arms, ME stands for radiating from the meanders. The overall Q_Z (solid black line) is added as a reference.

with negligible current density are meandered. The same structure was simulated in Matlab RWG-MoM and decomposed into characteristic modes.

We can estimate the overall Q_Z factor of the fabricated antenna approximately from the -3 dB fractional bandwidth ($\text{FBW}_{-3\,\text{dB}}$) as [8]

$$Q_Z \approx \frac{\sqrt{2}}{2}\frac{1}{\text{FBW}_{-3\,\text{dB}}}. \tag{16}$$

Relation (16) holds for $Q \gg 1$. In the case of the manufactured U-notched antenna, the Q factor (16) is equal to 14.8. For the same procedure in CST-MWS we obtained $Q = 15.5$. From differentiation of Z_{in} in CST-MWS we obtained $Q_Z = 14.8$, and from integrating the current distribution in Matlab we obtained $Q_Z^{(4)} = 15.6$, see Fig. 8. The moderate difference between CST and Matlab in Fig. 8 can be attributed to numerical issues.

The last discussed feature of the proposed definition is calculating the radiation Q_Z factor for a selected part of a radiating device only. While the arms of the antenna radiate well, the meanders accumulate a great deal of net reactive power because of the out-of-phase currents. Thus, we try to calculate the Q_Z of these two parts separately. To do so, the total current distribution $\mathbf{J}$ is separated as

$$\mathbf{J}_1(\mathbf{r}) = \mathbf{J}(\mathbf{r})\delta_1(\mathbf{r}) \tag{17a}$$

$$\mathbf{J}_2(\mathbf{r}) = \mathbf{J}(\mathbf{r})\delta_2(\mathbf{r}) \tag{17b}$$

where $\delta_1(\mathbf{r}) = 1$ for all $\mathbf{r}$ where $|\mathbf{r}| > 35R/36$ and $\delta_1(\mathbf{r}) = 0$ otherwise, $\delta_2 = 1 - \delta_1$. The results are depicted in Fig. 9. While the particular Q that corresponds to the arms of the antenna is very low, the Q factor corresponding to the meanders is extremely high (note that the corresponding values of Q_Z are divided by 10 in Fig. 9).

If we sum up the energetic terms corresponding to the separated arms ($\mathbf{J}_1$) and meanders ($\mathbf{J}_2$) and calculate Q_Z, we do not get the overall Q_Z of whole structure ($\mathbf{J}$), Fig. 9. This was expected, and the reason lies in the fact that the operators (7), (10a) and (10b) are not linear for $\mathbf{J} = \mathbf{J}_1 + \mathbf{J}_2$ and thus all possible interactions of the separated parts are omitted. However, these interactions can be calculated by substituting $\mathcal{L}(\mathbf{J}_1, \mathbf{J}_2)$, $\mathcal{L}(\nabla \cdot \mathbf{J}_1, \nabla \cdot \mathbf{J}_2)$ and similarly for (10a), (10b) into the Q_Z calculation.

V. Conclusion

A new formulation of the radiation Q factor is derived in terms of field sources instead of fields. The utilization of the complex Poynting theorem and potential theory had two main effects: a) interpretation and justification of the questionable concept of separating electric and magnetic energy in nonstationary fields is not required, b) integrations over the entire space are not present.

It is well known as the reactance theorem that the total energy of a passive electromagnetic system is proportional to the change of input impedance with frequency. The same derivation is analytically performed on the source side of the complex Poynting theorem, resulting in energetic expressions of a different nature, compactly expressed as functionals of the current. They form the observable quantities which can be measured through the input impedance—and this is the only concept that can be physically tested and thus is of practical interest. Moreover it is shown that the formulas are also valid for modal currents, where no feeding is present.

A novel energy term, related to the current reshaping, is shown to be the cause of negative values of measured Q_X in the antiresonances. Interestingly, this reconfiguration energy is almost not transferred into Q_Z.

The examples, presented here have verified the new expressions and have illustrated some benefits of the method. The proposed concept is easy to implement and offers new challenges in small antenna and MIMO antenna design, especially in conjunction with modal decomposition and optimization.

Appendix A
Complex Power in Terms of Potentials

The purpose of this Appendix is to derive the relation

$$-\int_\Omega \mathbf{E}\cdot\mathbf{J}^*\,\mathrm{d}\mathbf{r} = \jmath\omega\int_\Omega (\mathbf{A}\cdot\mathbf{J}^* - \varphi\rho^*)\,\mathrm{d}\mathbf{r} \tag{18}$$

which has been used in (4). The equality (18) is most easily derived by direct substitution of the defining relation of electromagnetic potentials [9]

$$\mathbf{E} = -\nabla\varphi - \jmath\omega\mathbf{A} \tag{19}$$

into the LHS of (18). This leads to

$$-\int_\Omega \mathbf{E}\cdot\mathbf{J}^*\,\mathrm{d}\mathbf{r} = \jmath\omega\int_\Omega \mathbf{A}\cdot\mathbf{J}^*\,\mathrm{d}\mathbf{r} + \int_\Omega \nabla\varphi\cdot\mathbf{J}^*\,\mathrm{d}\mathbf{r}. \tag{20}$$

The relation (20) can be further rewritten with the use of vector identity

$$\nabla\varphi\cdot\mathbf{J}^* = \nabla\cdot(\mathbf{J}^*\varphi) - \varphi\nabla\cdot\mathbf{J}^* \tag{21}$$

continuity equation

$$\nabla \cdot \mathbf{J} = -\jmath\omega\rho \tag{22}$$

and Gauss theorem into

$$-\int_{\Omega} \mathbf{E}\cdot\mathbf{J}^*\mathrm{d}\mathbf{r} = \jmath\omega\int_{\Omega}(\mathbf{A}\cdot\mathbf{J}^* - \varphi\rho^*)\mathrm{d}\mathbf{r} + \int_{\partial\Omega}\varphi\mathbf{J}^*\cdot\mathrm{d}\mathbf{S}. \tag{23}$$

Now, using the fact that the current component normal to the surface $\partial\Omega$ is zero, the last term in (23) identically vanishes and we arrive at (18).

Appendix B
Derivation of Relation (8)

The first step of the derivation is the use of the radiation integrals for vector and scalar potentials in homogenous, isotropic and open region [9]

$$\mathbf{A}(\mathbf{r}) = \frac{\mu}{4\pi}\int_{\Omega'}\mathbf{J}(\mathbf{r}')\frac{\mathrm{e}^{-\jmath kR}}{R}\,\mathrm{d}\mathbf{r}' \tag{24}$$

and

$$\varphi(\mathbf{r}) = \frac{1}{4\pi\epsilon}\int_{\Omega'}\rho(\mathbf{r}')\frac{\mathrm{e}^{-\jmath kR}}{R}\,\mathrm{d}\mathbf{r}' \tag{25}$$

together with (22) and (7) to obtain

$$\int_{\Omega}(\mathbf{A}\cdot\mathbf{J}^* - \varphi\rho^*)\,\mathrm{d}\mathbf{r} = k^2\mathcal{L}(\mathbf{J},\mathbf{J}) - \mathcal{L}(\nabla\cdot\mathbf{J},\nabla\cdot\mathbf{J}). \tag{26}$$

The next step consists of substituing (4) into (3) and afterwards to (2) and evaluating various ω derivatives. In particular, there is

$$\begin{aligned}\frac{\partial k^2\mathcal{L}(\mathbf{J},\mathbf{J})}{\partial\omega} &= \frac{\partial\dfrac{\mu}{4\pi}\displaystyle\int_{\Omega'}\int_{\Omega}\mathbf{J}(\mathbf{r})\cdot\mathbf{J}^*(\mathbf{r}')\frac{\mathrm{e}^{-\jmath kR}}{R}\,\mathrm{d}\mathbf{r}\,\mathrm{d}\mathbf{r}'}{\partial\omega}\\ &= \frac{k^2}{\omega}(\mathcal{L}_\omega(\mathbf{J},\mathbf{J}) - \jmath k\mathcal{L}_{\mathrm{rad}}(\mathbf{J},\mathbf{J}))\end{aligned} \tag{27}$$

and

$$\begin{aligned}\frac{\partial\mathcal{L}(\nabla\cdot\mathbf{J},\nabla\cdot\mathbf{J})}{\partial\omega} &= \frac{\partial\dfrac{1}{4\pi\epsilon\omega^2}\displaystyle\int_{\Omega'}\int_{\Omega}\nabla\cdot\mathbf{J}(\mathbf{r})\nabla\cdot\mathbf{J}^*(\mathbf{r}')\frac{\mathrm{e}^{-\jmath kR}}{R}\,\mathrm{d}\mathbf{r}\,\mathrm{d}\mathbf{r}'}{\partial\omega}\\ &= -\frac{1}{\omega}(2\mathcal{L}(\nabla\cdot\mathbf{J},\nabla\cdot\mathbf{J}) - \mathcal{L}_\omega(\nabla\cdot\mathbf{J},\nabla\cdot\mathbf{J})\\ &\quad + \jmath k\mathcal{L}_{\mathrm{rad}}(\nabla\cdot\mathbf{J},\nabla\cdot\mathbf{J})).\end{aligned} \tag{28}$$

It is important to remember that although the input current is normalized ($I_0 = 1$ A), the current density $\mathbf{J}$ is still a function of angular frequency.

Putting all together and using the abbreviations (6a), (6b), (9a), and (9b) we immediately arrive at (8).

Acknowledgment

The authors would like to thank Prof. Guy A. E. Vandenbosch for fruitful discussions, as well as the three anonymous reviewers whose remarks improved the clarity of the paper.

References

[1] J. L. Volakis, C.-C. Chen, and K. Fujimoto, *Survey of Small Antenna Theory*, ser. Small Antennas: Miniaturization Techniques & Applications, 1st ed. New York, NY, USA: McGraw-Hill, 2010.

[2] G. A. E. Vandenbosch, "Reactive energies, impedance, and Q factor of radiating structures," *IEEE Trans. Antennas Propag.*, vol. 58, no. 4, pp. 1112–1127, Apr. 2010.

[3] M. Gustafsson and B. L. G. Jonsson, Stored Electromagnetic Energy and Antenna Q [Online]. Available: http://adsabs.harvard.edu/abs/2012arXiv1211.5521G, eprint arXiv: 1211.5521.

[4] M. Gustafsson, M. Cismasu, and B. L. G. Jonsson, "Physical bounds and optimal currents on antennas," *IEEE Trans. Antennas Propag.*, vol. 60, no. 6, pp. 2672–2681, Jun. 2012.

[5] D. R. Rhodes, "Observable stored energies of electromagnetic systems," *J. Franklin Inst.*, vol. 302, no. 3, pp. 225–237, 1976.

[6] D. R. Rhodes, "A reactance theorem," in *Proc. Roy. Soc. Lond. A*, Feb. 1977, vol. 353, pp. 1–10.

[7] D. R. Rhodes, "On the stored energy of planar apertures," *IEEE Trans. Antennas Propag.*, vol. 14, no. 6, pp. 676–684, Nov. 1966.

[8] A. D. Yaghjian and S. R. Best, "Impedance, bandwidth and Q of antennas," *IEEE Trans. Antennas Propag.*, vol. 53, no. 4, pp. 1298–1324, Apr. 2005.

[9] J. D. Jackson, *Classical Electrodynamics*, 3rd ed. Hoboken, NJ, USA: Wiley, 1998.

[10] C. J. Carpenter, "Electromagnetic energy and power in terms of charges and potentials instead of fields," *Proc. IEE A*, vol. 136, no. 2, pp. 55–65, Mar. 1989.

[11] P. Hazdra, M. Capek, and J. Eichler, "Comments to "reactive energies, impedance, and Q factor of radiating structures" by G. Vandenbosch," *IEEE Trans. Antennas Propag.,* to be published.

[12] R. F. Harrington and J. R. Mautz, "Theory of characteristic modes for conducting bodies," *IEEE Trans. Antennas Propag.*, vol. AP-19, no. 5, pp. 622–628, Sep. 1971.

[13] M. Capek, P. Hazdra, and J. Eichler, "A method for the evaluation of radiation Q based on modal approach," *IEEE Trans. Antennas Propag.*, vol. 60, no. 10, pp. 4556–4567, Oct. 2012.

[14] FEKO, EM Software & Systems-S.A [Online]. Available: http://www.feko.info [Online]. Available:

[15] CST Computer Simulation Technology [Online]. Available: http://www.cst.com [Online]. Available:

[16] M. Gustafsson and S. Nordebo, "Bandwidth, Q factor and resonance models of antennas," *PIER*, vol. 62, pp. 1–20, 2006.

[17] R. F. Harrington, *Time-Harmonic Electromagnetic Fields*, 2nd ed. : John Wiley—IEEE Press, 2001.

[18] R. E. Collin and S. Rotchild, "Evaluation of antenna Q," *IEEE Trans. Antennas Propag.*, vol. AP-12, no. 1, pp. 23–27, Jan. 1964.

[19] R. F. Harrington, *Field Computation by Moment Methods*. : John Wiley—IEEE Press, 1993.

[20] P. Arcioni, M. Bressan, and L. Perregrini, "On the evaluation of the double surface integrals arising in the application of the boundary integral method to 3-D problems," *IEEE Trans. Microw. Theory Tech.*, vol. 44, no. 3, pp. 436–438, Mar. 1997.

[21] M. Capek, P. Hamouz, P. Hazdra, and J. Eichler, "Implementation of the theory of characteristic modes in Matlab," *IEEE Antennas Propag. Mag.*, vol. 55, no. 2, pp. 176–189, Apr. 2013.

[22] S. M. Rao, D. R. Wilton, and A. W. Glisson, "Electromagnetic scattering by surfaces of arbitrary shape," *IEEE Trans. Antennas Propag.*, vol. AP-30, no. 3, pp. 409–418, May 1982.

[23] The MathWorks, The Matlab [Online]. Available: http://www.mathworks.com [Online]. Available:

[24] M. Capek, P. Hazdra, J. Eichler, P. Hamouz, and M. Mazanek, "Acceleration techniques in Matlab for EM community," presented at the 7th Eur. Conf. Antennas and Propagation (EUCAP), Gothenburg, Sweden, Apr. 2013.

Miloslav Capek (S'09) received the M.Sc. degree in electrical engineering from the Czech Technical University, Prague, Czech Republic, in 2009, where he is currently pursuing Ph.D. degree in electromagnetic fields.

His research interests are in the area of electromagnetic theory, electrically small antennas, numerical techniques, fractal geometry and optimization.

Lukas Jelinek received the Ph.D. degree from the Czech Technical University (CTU), Prague, Czech Republic, in 2006.

Currently, he is a researcher with the Department of Electromagnetic Fields, Faculty of Electrical Engineering, CTU. His main fields of interest include wave propagation in complex media, general field theory, and numerical techniques. His recent research interest is focused on metamaterials, specifically on resonant ring systems.

Pavel Hazdra (M'03) received the M.S. and Ph.D. degrees in electrical engineering from the Faculty of Electrical Engineering (FEE), Czech Technical University (CTU), Prague, Czech Republic, in 2003 and 2009, respectively.

He is a research and teaching assistant with the Department of Electromagnetic Field, FEE, CTU. His research interests are in the area of electromagnetic theory, computational electromagnetics, fractal geometry, planar antennas, and special prime-feed antennas.

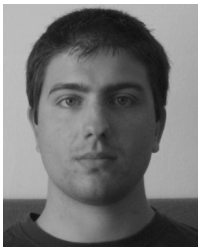

Jan Eichler (S'10) received the B.Sc. and M.Sc. degrees in electrical engineering from the Czech Technical University, Prague, Czech Republic, in 2008 and 2010, respectively, where he is currently pursuing the Ph.D. degree.

His research interests include modal methods for antenna design and connecting them with full-wave methods. He is also interested in developing and simulating active antennas.

III

M. Capek, J. Eichler, and P. Hazdra, "Evaluation of radiation efficiency from characteristic currents," *IET Microw. Antennas Propag.*, vol. 9, no. 1, pp. 10–15, Jan. 2015. [3]

www.ietdl.org

Published in IET Microwaves, Antennas & Propagation
Received on 29th August 2013
Revised on 3rd May 2014
Accepted on 3rd July 2014
doi: 10.1049/iet-map.2013.0473

ISSN 1751-8725

Evaluating radiation efficiency from characteristic currents

Miloslav Capek, Jan Eichler, Pavel Hazdra

Department of Electromagnetic Field, Faculty of Electrical Engineering, Czech Technical University in Prague, Technicka 2, 16627, Prague, Czech Republic
E-mail: miloslav.capek@fel.cvut.cz

Abstract: This study describes an effective technique for calculating modal radiation efficiency calculation based on decomposition into characteristic modes. The key assumption is that the current distribution on the perfect electric conductor is almost the same as in the case of a very good conductor, for example, metals such as copper, aluminium and silver. This assumption is verified against the conventional technique, the impedance boundary condition (IBC). The proposed approach does not require any modification of the formulation of method of moments for perfectly conducting surfaces, which is assumed for the modal decomposition. Modal efficiencies provide an additional insight that is useful especially for the design of small antennas. Taking the feeding into account, the modal losses can be summed up to obtain the total efficiency. The technique works perfectly for common metals, is fully comparable with the IBC, and can easily be incorporated into any present-day in-house solver. A numerical analysis of three antennas is presented to demonstrate the merits of the approach. Radiation efficiency of coupled dipoles, an electrically small meandered dipole, and PIFA were investigated by the presented method. The results are in perfect agreement with the reference commercial package.

1 Introduction

Antenna radiation efficiency [1] is a very important parameter, especially if the electrical dimensions are small [2]. A common approach for computing the radiation efficiency of an antenna is to take a lossy material into account in the numerical simulation. This approach is general and accurate, but it does not provide much physical insight into the lossy antenna operation.

In the proposed approach, the current density evaluated on a perfect electric conductor (PEC) is assumed to be approximately the same as for a lossy metal of infinite thickness. It will be shown that this assumption works perfectly for common metals such as copper and aluminium. Moreover, the radiation efficiency can be evaluated very quickly in a post-processing step, once the currents on PEC are evaluated by the method of moments (MoM) solver.

A more precise evaluation is based on the surface impedance boundary condition (IBC) [3, 4]. However, time-consuming recalculation of the MoM matrix is needed whenever the conductivity σ or the thickness t of the metal is changed.

To gain a better physical picture of the operation of a lossy antenna, the theory of characteristic modes (TCM) [5–7] is adopted for calculating individual modal efficiencies. This theory enables to calculate a set of so-called characteristic currents by decomposition of the MoM impedance matrix. These currents are orthogonal (with respect to the radiated power), and may be summed to form the total current flowing on an antenna if the feeding is connected. Thus TCM makes it possible to study the antenna geometry without the specific feeding, and to understand its operation through modal superposition of various quantities based on the surface current density [8, 9]. Remark that very simple calculation of the (modal) radiation efficiency has already been treated in [10] where the skin effect was not taken into account and no summation of the modal losses was presented.

This paper develops a fast and physically illustrative procedure for approximating the radiation losses for characteristic modes particularly on RWG [11] meshes, but the technique is not limited to any discretisation scheme.

2 Calculating the radiation efficiency from surface currents

Expressions for calculating the radiation efficiency will be derived in this section. The input of the procedure is an antenna consisting of an infinitesimally thin PEC. Next, suppose that the antenna is discretised using the RWG basis functions and the current density is computed by the MoM [12].

Begin with the definition of the radiation efficiency [1]

$$\eta = \frac{P^{\mathrm{R}}}{P^{\mathrm{R}} + P^{\mathrm{L}}} \tag{1}$$

where P^{R} is the radiated power and P^{L} is the power loss. If no losses are present (i.e. a PEC antenna in a lossless dielectric), P^{R} is equal to the power received by the antenna from the feed

port. It is therefore needed to compute P^{L} if there were losses in the metal. The procedure is as follows.

Suppose a PEC surface on which the surface current density $\boldsymbol{J}^{\mathrm{surf}}$ is computed by the MoM. Next, the skin-effect will be taken into account by introducing the equivalent volume current density

$$\boldsymbol{J}^{\mathrm{eq}}(z) = \boldsymbol{J}_0^{\mathrm{eq}}\, \mathrm{e}^{-(1+j)\gamma z} \tag{2}$$

where z is the distance from the metal surface, and the attenuation constant [13] for a highly conductive material is

$$\gamma = \sqrt{\frac{\omega\mu\sigma}{2}} \tag{3}$$

where μ is the permeability and ω is the angular frequency. Now, it is assumed that the current flowing on the perfectly conducting body has the same shape as if small losses are introduced

$$\left|\int_0^t \boldsymbol{J}^{\mathrm{eq}}(z)\mathrm{d}z\right| = \left|\boldsymbol{J}^{\mathrm{surf}}\right| \tag{4}$$

and also that the metallisation thickness t is high enough to neglect the reflection from the other side of the metal body. From (2) and (4) one obtains

$$\left|\boldsymbol{J}_0^{\mathrm{eq}}\right| = \frac{\sqrt{2}\gamma\left|\boldsymbol{J}^{\mathrm{surf}}\right|}{\left|1-\mathrm{e}^{-(1+j)\gamma t}\right|} \tag{5}$$

Considering now a triangulated surface and constant current $\boldsymbol{J}_n^{\mathrm{surf}}$ on each triangle n, the power loss can be expressed as [13]

$$\begin{aligned} P^{\mathrm{L}} &= \int_\Omega \boldsymbol{E}\cdot\boldsymbol{J}^*\mathrm{d}V \simeq \sum_n \int_\Omega \frac{\left|\boldsymbol{J}_n^{\mathrm{eq}}\right|^2}{\sigma}\mathrm{d}V \\ &= F(\omega,\sigma,t)\sum_n A_n\left|\boldsymbol{J}_n^{\mathrm{surf}}\right|^2 \end{aligned} \tag{6}$$

where * denotes the complex conjugation, A_n is the area of triangle n, $\Omega = \bigcup_n A_n$ is the PEC surface, and

$$F(\omega,\sigma,t) = \frac{\gamma}{\sigma}\frac{(1-\mathrm{e}^{-2\gamma t})}{\left|1-\mathrm{e}^{-(1+j)\gamma t}\right|^2} \tag{7}$$

3 Modal radiation efficiency

The radiation efficiency of a certain characteristic current will be defined in this section. Then a summation formula for these modal radiation efficiencies is obtained. The physical background of how particular modes contribute to the overall radiation efficiency can be thus explored. Since it is enough to include only the first few modes [14] for an electrically small antenna, this knowledge can help the designer to modify the antenna geometry to suppress certain modes and increase the overall radiation efficiency of the antenna. The second goal is to derive a fast formula for computing and optimising the radiation efficiency. Recall that for a certain structure at a given frequency, the impedance matrix does not need to be recalculated and the total radiation efficiency is controlled only through the position of the feeding port that affects the expanding coefficients.

3.1 Theory of characteristic modes

The principles of the TCM which are important for defining the modal radiation efficiency are briefly presented here. A detailed description of TCM and its derivation can be found in [5] and a recent revision in [7].

The theory is based on eigen-decomposition of the electric field integral equation operator [15] $\mathcal{Z}(\boldsymbol{J}) = \mathcal{R}(\boldsymbol{J}) + j\mathcal{X}(\boldsymbol{J})$ on a PEC surface, according to the generalised eigenvalue problem

$$\mathcal{X}\boldsymbol{J}_u = \lambda_u\mathcal{R}\boldsymbol{J}_u \tag{8}$$

where λ_u is the uth characteristic number (eigenvalue) and $\boldsymbol{J}_u$ is the characteristic vector or current [5]. All modal current densities are normalised [5] at every frequency to radiate the power $P_u^{\mathrm{R}} = 1\mathrm{W}$

$$\langle \boldsymbol{J}_u, \mathcal{R}\boldsymbol{J}_u\rangle = 1 = P_u^{\mathrm{R}} \tag{9}$$

where the symmetrical product was used. Note here, that the symmetrical product of $\boldsymbol{a}$, $\boldsymbol{b}$ is defined as $\langle \boldsymbol{a}, \boldsymbol{b}\rangle = \int_\Omega \boldsymbol{a}\cdot\boldsymbol{b}\,\mathrm{d}\Omega$, and the dot product is defined in the usual way as $\boldsymbol{a}\cdot\boldsymbol{b} = \sum a_i b_i$ was used. Thus the modes satisfy the orthogonality relations

$$\langle \boldsymbol{J}_u, \mathcal{R}\boldsymbol{J}_v\rangle = \delta_{uv} \tag{10}$$

$$\langle \boldsymbol{J}_u, \mathcal{X}\boldsymbol{J}_v\rangle = \lambda_u\delta_{uv} \tag{11}$$

$$\langle \boldsymbol{J}_u, \mathcal{Z}\boldsymbol{J}_v\rangle = (1+\lambda_u)\delta_{uv} \tag{12}$$

where δ_{uv} is the Kronecker delta function, ${}^3\delta_{uv} = 0$ for $u \neq v$ and $\delta_{uv} = 1$ for $u = v$. The total current on the antenna surface can be found by summation as [5]

$$\boldsymbol{J} = \sum_u \alpha_u\boldsymbol{J}_u \tag{13}$$

For an impressed field $\boldsymbol{E}^{\mathrm{i}}$, representing the excitation, the expanding coefficients α_u are [5]

$$\alpha_u = \frac{\langle \boldsymbol{J}_u, \boldsymbol{E}^{\mathrm{i}}\rangle}{1+j\lambda_u} \tag{14}$$

3.2 Deriving the modal radiation efficiency

Considering surface current density $\boldsymbol{J}^{\mathrm{surf}}$ expressed as a superposition of the characteristic modes according to (13), $\left|\boldsymbol{J}_n^{\mathrm{surf}}\right|^2$ reads

$$\begin{aligned} \left|\boldsymbol{J}_n^{\mathrm{surf}}\right|^2 &= \sum_u \alpha_u\boldsymbol{J}_{nu}^{\mathrm{surf}}\cdot\sum_v \alpha_v^*(\boldsymbol{J}_{nv}^{\mathrm{surf}})^* \\ &= \sum_u\sum_v \beta_{uv}\boldsymbol{J}_{nu}^{\mathrm{surf}}\cdot(\boldsymbol{J}_{nv}^{\mathrm{surf}})^* \end{aligned} \tag{15}$$

The coupling $\boldsymbol{\beta} = [\beta_{uv}]$ matrix is defined in [8] as

$$\beta_{uv} = \Re\{\alpha_u\alpha_v^*\} = \frac{\langle \boldsymbol{J}_u, \boldsymbol{E}^i\rangle\langle \boldsymbol{J}_v, \boldsymbol{E}^i\rangle(1+\lambda_u\lambda_v)}{(1+\lambda_u^2)(1+\lambda_v^2)} \tag{16}$$

The modal power loss is

$$P_{uv}^{\mathrm{L}} = F(\omega, \sigma, t) \sum_{n} A_n \boldsymbol{J}_{nu}^{\mathrm{surf}} \cdot \boldsymbol{J}_{nv}^{\mathrm{surf}} \tag{17}$$

Note that the characteristic currents are real by definition [5], so the complex conjugation rising from (15) can be omitted. Since the modal radiated power is normalised to 1 W, the modal radiation efficiency of mode u is expressed as

$$\eta_u = \frac{1}{1 + P_{uu}^{\mathrm{L}}} \tag{18}$$

The total power loss may now be expressed as a superposition of the modal radiation losses

$$P^{\mathrm{L}} = \sum_{u} \sum_{v} \beta_{uv} P_{uv}^{\mathrm{L}} = \langle \boldsymbol{\beta}, \boldsymbol{P}^{\mathrm{L}} \rangle \tag{19}$$

Using the orthogonal property of characteristic modes (9) and (1), the radiation efficiency is finally written as

$$\eta = \frac{\sum_{u} \beta_{uu}}{\sum_{u} \beta_{uu} + \sum_{u} \sum_{v} \beta_{uv} P_{uv}^{\mathrm{L}}} = \frac{\mathrm{Tr}(\boldsymbol{\beta})}{\mathrm{Tr}(\boldsymbol{\beta}) + \langle \boldsymbol{\beta}, \boldsymbol{P}^{\mathrm{L}} \rangle} \tag{20}$$

4 Numerical results

To verify the presented derivation is valid and that the approximations that have been made are reasonable, three test structures were chosen. The test structures are a meandered strip dipole (Fig. 1), a coupled active and parasitic dipole (Fig. 2) and a PIFA antenna [16] over a finite ground plane (Fig. 3). Note that these cases were computed in a wide frequency range and are of various types (electrically small, planar, strips, highly resonant structures, with and without a finite ground plane).

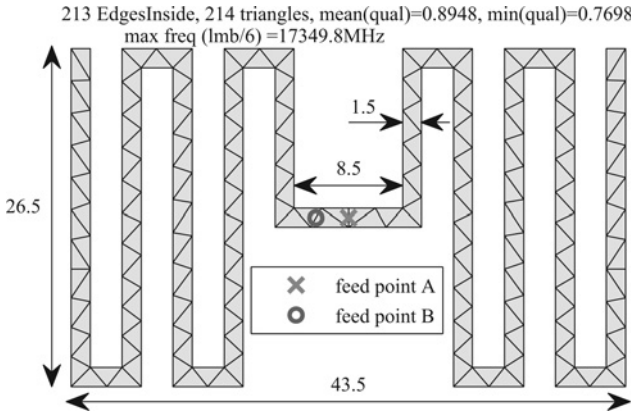

Fig. 1 *Triangular mesh of the meandered dipole with various feeding points, dimensions are in (mm)*

The 'qual' means the quality of triangles ('mean' is the average quality and 'min' is the quality of the worst triangle), and 'max freq' (lmb/6) is related to the highest frequency that can be safely calculated under the condition that the edges length is <λ/6

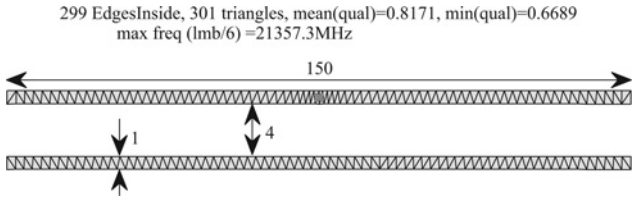

Fig. 2 *Triangular mesh of coupled dipoles. Feeding point is at the top dipole, marked by the green cross. Dimensions are in (mm)*

The 'qual' means the quality of triangles ('mean' is the average quality and 'min' is the quality of the worst triangle), and 'max freq' (lmb/6) is related to the highest frequency that can be safely calculated under the condition that the edges length is <λ/6

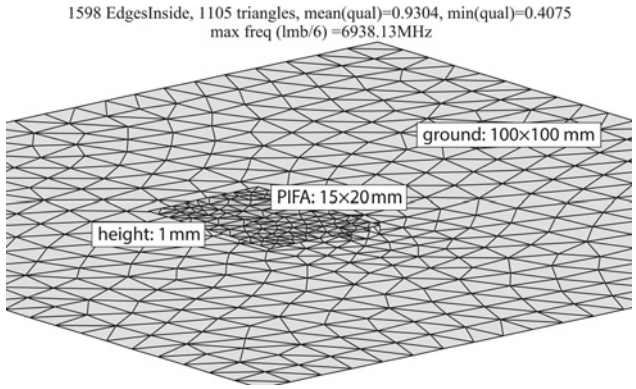

Fig. 3 *Detailed view of the triangular mesh of the PIFA*

The 'qual' means the quality of triangles ('mean' is the average quality and 'min' is the quality of the worst triangle), and 'max freq' (lmb/6) is related to the highest frequency that can be safely calculated under the condition that the edges length is <λ/6

4.1 Effect of changes in current distribution between the lossy case and the lossless case

In Section 2, it has been assumed that the current distribution on an antenna made of thin metal (with $\sigma > 10^5$ S/m) and on an antenna made of PEC is approximately the same. The validity of this important assumption will be numerically verified in this section.

The centre-fed meandered dipole, Fig. 1, feed point A, was modelled in FEKO [17] and the current density as well as the area of the triangular elements was exported in ASCII format. The data for $\sigma = \{5.85 \times 10^7, 5.85 \times 10^6, 5.85 \times 10^5\}$ S/m and for PEC were imported into the Matlab [18] routine, and the total radiation efficiency was computed according to (6) and (1), see Fig. 4 for a comparison.

The differences between the radiation efficiency computed from the currents on a PEC antenna and on a lossy antenna are generally very small. The same procedure was repeated for each of the test structures and for all combinations of $\sigma = \{5.85 \times 10^7,\ 5.85 \times 10^6,\ 5.85 \times 10^5\}$ S/m and $t = \{18, 50\}$ μm, that is, 18 different cases. The results were qualitatively similar to Fig. 4. It should be mentioned that the radiation efficiency minimum computed from the PEC currents was slightly shifted upwards in frequency (25 MHz shift at 8 GHz for a meandered dipole, $\sigma = 5.85 \times 10^5$ S/m, $t = 50$ μm), Fig. 4. However, this 0.3 % frequency shift for low-conductivity metals can be neglected for practical purposes. Thus it is concluded that the assumptions of Section 2 hold very well for all tested combinations.

doi: 10.1049/iet-map.2013.0473

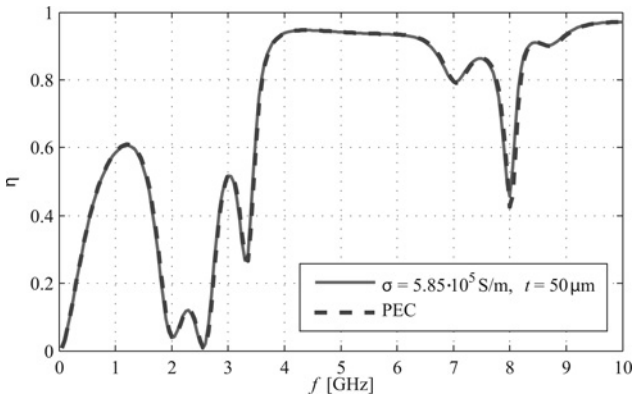

Fig. 4 *Computation of radiation efficiency from currents on PEC and a lossy surface*

4.2 MoM solution using an in-house software tool

In this section, the results using a commercial software package will be compared with the in-house MoM tool [9]. The tool is based on [19], and only considers perfectly conducting metal bodies. The power loss is computed according to (6). In FEKO, the structure is modelled as infinitesimally thin, but t and σ are defined for a material model based on the IBC [20] that is used in the simulation. Figs. 5–7 show that these two approaches give very similar

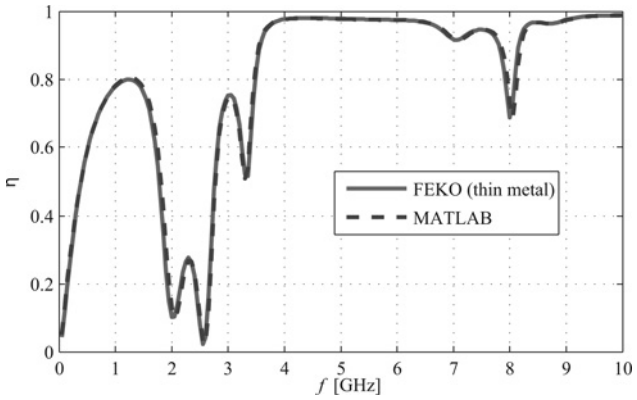

Fig. 5 *Radiation efficiency computed by FEKO and by MATLAB*
Meandered dipole, $\sigma = 5.85 \times 10^6$ S/m, $t = 50$ μm

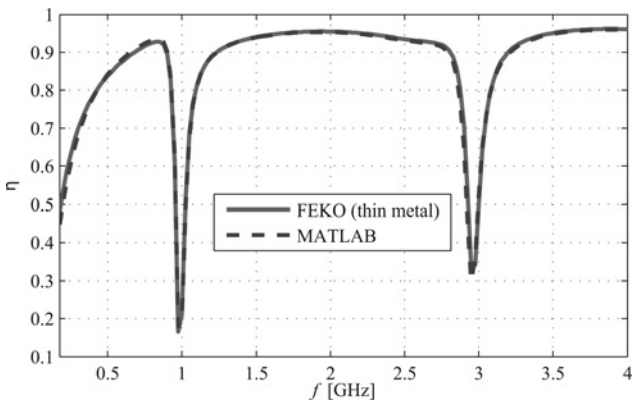

Fig. 6 *Radiation efficiency computed by FEKO and by MATLAB*
Coupled dipoles, $\sigma = 5.85 \times 10^6$ S/m, $t = 18$ μm

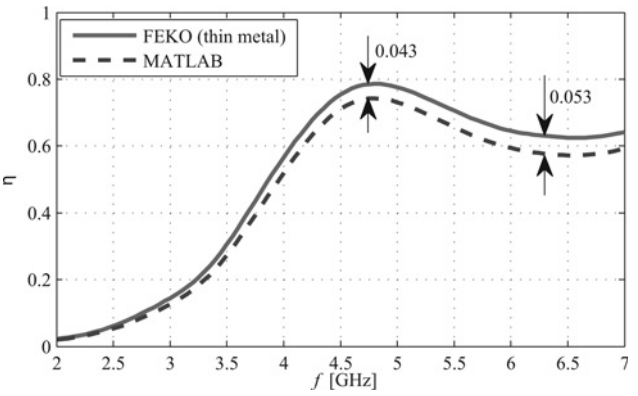

Fig. 7 *Radiation efficiency computed by FEKO and by MATLAB*
PIFA, $\sigma = 5.85 \times 10^5$ S/m, $t = 50$ μm

results. The biggest difference for PIFA and low σ is plotted in Fig. 7. Thus it is seen that FEKO (MoM + IBC) and MATLAB code (MoM on PEC + (6)) give very comparable results.

4.3 Modal radiation efficiency

Features of modal radiation efficiency will be demonstrated using the example of a meandered dipole discussed in the previous section. The impedance matrix obtained by the in-house MoM tool is decomposed into characteristic modes [9]. The beta matrix (16) and the modal power loss matrix (17) are computed from this set of modes. Using these inputs, the total radiation efficiency η is computed using (20), and is compared with the MoM solution. The structure was approximated by 213 basis functions, and all 213 numerically computed modes were used in the superposition. The two results are almost equivalent (see Fig. 8), which is in correspondence with the theoretical development of Section 3.2. The small difference can be ascribed to numerical errors arising from computationally difficult decomposition.

The contribution of modal losses to the total radiation efficiency will be now investigated by studying the effect of the asymmetrical feeding point of the meandered dipole in Fig. 1 (position 'B'). It is clearly seen that a new minimum of radiation efficiency is present at 1.6 GHz, as shown in Fig. 9.

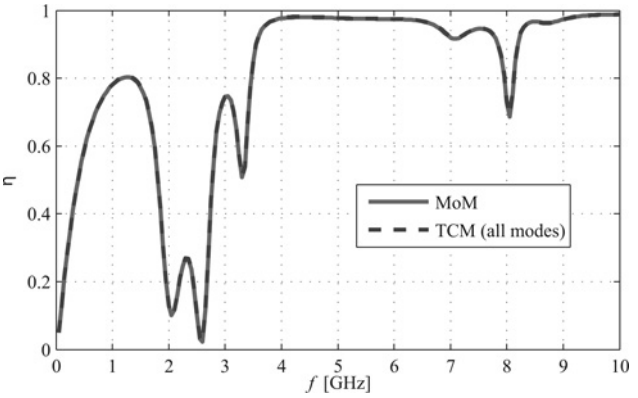

Fig. 8 *Radiation efficiency computed from the MoM result and through modal superposition*
Meandered dipole, $\sigma = 5.85 \times 10^6$ S/m, $t = 50$ μm

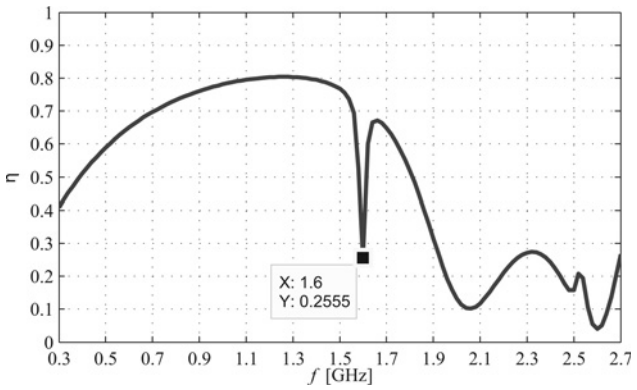

Fig. 9 *Radiation efficiency of the asymmetrically fed (feed point B)*
Meandered dipole, $\sigma = 5.85 \times 10^6$ S/m, t = 50 μm

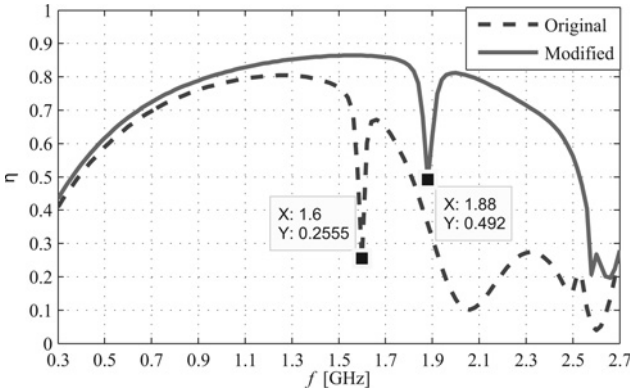

Fig. 12 *Comparison of the radiation efficiency of the modified and the original meandered dipole, feed point B, $\sigma = 5.85 \times 10^6$ S/m, t = 50 μm*

Table 1 Diagonal terms of the coupling matrix, the modal power loss matrix and the modal radiation efficiency at 1.6 GHz

U	β_{uu}	P^{L}_{uu}	η_{uu}	$\beta_{uu}P^{L}_{uu}$
1	8.62×10^5	0.084	**0.92**	7.25×10^6
2	2.03×10^4	2.25	**0.31**	4.56×10^4
3	2.36×10^7	0.05	0.95	1.19×10^8
4	1.71×10^6	1.16	0.46	1.98×10^6
5	1.65×10^7	1.83	0.35	3.00×10^7
6	8.75×10^{11}	5.85	0.15	5.12×10^{10}
7	1.60×10^8	61.96	0.016	9.91×10^7

The modal efficiencies of the significant modes are bold

The structure was decomposed into characteristic modes; see β_{uu} and P^{L}_{uu} in Table 1 for the first seven modes. Although the cross terms, that is, the β_{uv}, P^{L}_{uv}; $u \neq v$ are necessary in (20), the main information about the significance in the sum of radiation efficiencies is readable from the diagonal terms only. From Table 1, it is evident that the dominantly excited modes are modes 2 and 1. While mode 1 is desired and radiates well, mode 2 has low modal radiation efficiency ($\eta_{22} = 31\%$) and thus it contributes strongly to power loss.

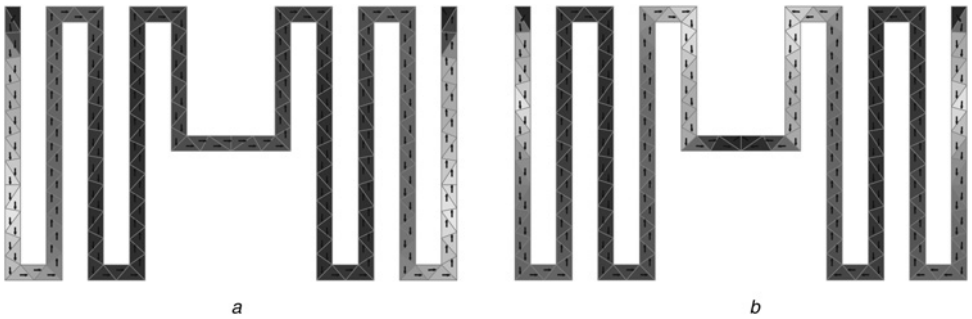

Fig. 10 *Characteristic current at 1.6 GHz*
a Mode 1
b Mode 2

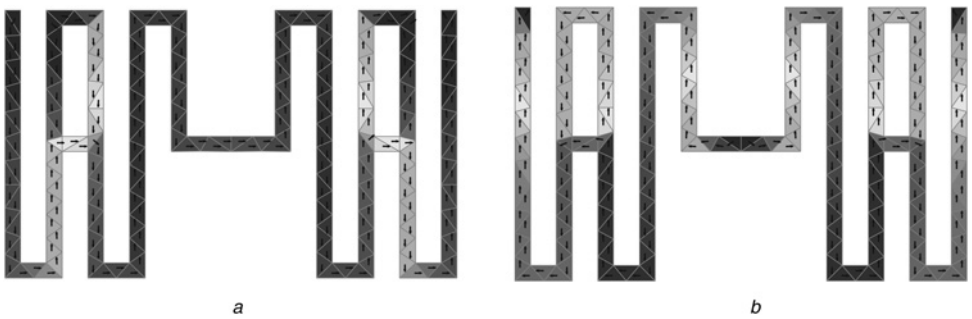

Fig. 11 *Modified meandered dipole, characteristic current, 1.88 GHz*
a Mode 1
b Mode 2

doi: 10.1049/iet-map.2013.0473

Table 2 Diagonal terms of the coupling matrix, modal power loss matrix and modal radiation efficiency of the modified meander at 1.88 GHz

u	β_{uu}	P^{L}_{uu}	η_{uu}	$\beta_{uu}P^{L}_{uu}$
1	1.25×10^4	0.068	**0.94**	8.57×10^6
2	1.06×10^3	0.51	**0.66**	5.44×10^4
3	1.22×10^9	793	0.0013	9.64×10^7
4	4.20×10^6	0.073	0.93	3.08×10^7
5	2.63×10^6	0.84	0.54	2.22×10^6
6	3.12×10^9	0.85	0.54	2.67×10^9
7	1.66×10^6	2.85	0.26	4.75×10^6

The modal efficiencies of the significant modes are bold

Next, it would be useful to eliminate the efficiency drop at 1.6 GHz. This is a difficult task from the design point of view, since it is not clear how to achieve this goal from the MoM solution. However, TCM gives guidance that mode 2 should be suppressed or shifted in frequency. Thus the meander should be modified to affect mode 2, while not affecting mode 1; see Fig. 10. A good position for the modification is in the area where the currents of mode 2 are at their maximum, that is, approx. at the centre of the meander arm. The modes on a modified structure are shown in Fig. 11.

The positive effect of the modification on η can be seen in Fig. 12. The current path for mode 2 is shortened, which shifts its resonant frequency from 1.6 to 1.88 GHz. The resonance of mode 1 is also slightly shifted from 0.96 to 1.02 GHz (computed by TCM). Since the current of mode 2 on the modified structure flows less in the opposing directions, η_{22} rises from 31 to 66%, see Table 2. This is reflected in the η in Fig. 12, where the efficiency drop is not as deep as for the original meander.

Another interesting fact is that $\eta = 49.2\%$ at 1.88 GHz, whereas the modal $\eta_2 = 66.12\%$. One would achieve $\eta = \eta_2$ if only mode 2 was excited. However, non-zero contributions to P^{L} from all modes are shown in Table 2. Thus in practice, the η at the resonant frequency of a certain mode u is always lower than the corresponding η_u.

5 Conclusions

The theory for evaluating radiation efficiency from characteristic currents has been presented. It has been shown that the conduction loss (and thus the radiation efficiency) can be understood as the weighted sum of the losses associated with the characteristic modes. The assumptions made in the derivation hold very well for the test structures, namely a meandered dipole, coupled dipoles and PIFA over a finite ground plane and several different metalisation thicknesses and conductivities.

The main advantage of the proposed technique lies in the physical interpretation of the sources of conduction losses which contribute to the overall radiation efficiency. This has been demonstrated on a simple example of an asymmetrically fed meandered dipole, which was modified to improve the radiation efficiency. Another benefit of the technique is the easy implementation to any MoM code. The radiation efficiency computation can be performed as a post processing step, which is particularly useful for TCM. This method can also be used in a very fast optimisation loop.

It is assumed that the extension to the dielectrics bodies is possible following a similar approach. This is a subject of further research, where the formulation of volumetric currents in the dielectrics is utilised.

6 Acknowledgments

The authors would like to thank Dr. M. Polivka for the initial tests in the IE3D software, and Professor J. Vrba and Mr. P. Hamouz for their comments. Also, we would like to thank two anonymous reviewers who suggested valuable improvements to the paper. This work was supported by the Project P102/12/2223 of the Czech Science Foundation, and by the Project SGS14/190/OHK3/3 T/13 of the Grant Agency of the Czech Technical University in Prague.

7 References

1 Balanis, C.A.: 'Antenna theory analysis and design' (Wiley, 2005, 3rd edn.)
2 Volakis, J.L., Chen, C., Fujimoto, K.: 'Small antennas: miniaturization techniques and applications' (McGraw-Hill, 2010)
3 Qian, Z.G., Chew, W.C., Suaya, R.: 'Generalized impedance boundary condition for conductor modeling in surface integral equation', *IEEE Trans. Microw. Theory Tech.*, 2007, **55**, (11), pp. 2354–2364
4 Karlsson, A.: 'Approximate boundary conditions for thin structures', *IEEE Trans. Antennas Propag.*, 2009, **57**, (1), pp. 144–148
5 Harrington, R.F., Mautz, J.R.: 'Theory of characteristic modes for conducting bodies', *IEEE Trans. Antennas Propag.*, 1971, **19**, (5), pp. 622–628
6 Cabedo-Fabres, M.: 'Systematic design of antennas using the theory of characteristic modes', Ph.D. dissertation, UPV, February 2007
7 Cabedo-Fabres, M., Antonino-Daviu, E., Valero-Nogueira, A., Bataller, M.F.: 'The theory of characteristic modes revisited: a contribution to the design of antennas for modern applications', *IEEE Antennas Propag. Mag.*, 2007, **49**, (5), pp. 52–68
8 Capek, M., Hazdra, P., Eichler, J.: 'A method for the evaluation of radiation Q based on modal approach', *IEEE Trans. Antennas Propag.*, 2012, **60**, (10), pp. 4556–4567
9 Capek, M., Hamouz, P., Hazdra, P., Eichler, J.: 'Implementation of the theory of characteristic modes in Matlab', *IEEE Antennas Propag. Mag.*, 2013, **55**, (2), pp. 176–189
10 Hamouz, P., Hazdra, P., Polivka, M., Capek, M., Mazanek, M.: 'Radiation efficiency and Q factor study of franklin antenna using the theory of characteristic modes'. Proc. Fifth European Conf. on Antennas and Propagation (EUCAP), Rome, Italy, April 2011, pp. 1974–1977
11 Rao, S.M., Wilton, D.R., Glisson, A.W.: 'Electromagnetic scattering by surfaces of arbitrary shape', *IEEE Trans. Antennas Propag.*, 1982, **30**, (3), pp. 409–418
12 Gibson, W.C.: 'The method of moments in electromagnetics' (Chapman and Hall/CRC, 2007, 1st edn.)
13 Harrington, R.F.: 'Time-harmonic electromagnetic fields' (IEEE Press, Wiley, 2001, 2nd edn.)
14 Safin, E., Martens, R., Manteuffel, D.: 'Modal source reconstruction based on radiated far-field for antenna design'. Proc. Sixth European Conf. on Antennas and Propagation (EuCAP), 2012, pp. 1645–1649
15 Harrington, R.F.: 'Field computation by moment methods' (IEEE Press, Wiley, 1993)
16 Rowell, C., Lam, E.Y.: 'Mobile-phone antenna design', *IEEE Antennas Propag. Mag.*, 2012, **54**, (4), pp. 14–34
17 EM Software & Systems-S.A. FEKO. Available at: www.feko.info
18 The MathWorks. The Matlab. Available at: www.mathworks.com
19 Makarov, S.N.: 'Antenna and EM modeling with Matlab' (Wiley, 2002)
20 (2013, February) Feko, user's Manual, suite 6.2.2. EM Software & Systems-S.A. (Pty) Ltd. 32 Techno Avenue, Technopark, Stellenbosch, 7600, South Africa. Available at: www.feko.info

IV

M. Capek, L. Jelinek, and G. A. E. Vandenbosch, "Stored Electromagnetic Energy and Quality Factor of Radiating Structures,", 2015, submitted, arXiv: 1403.0572. [47∗]

PROCEEDINGS A

rspa.royalsocietypublishing.org

Research

Article submitted to journal

Subject Areas:
electromagnetism, mathematical physics, electrical engineering

Keywords:
electromagnetic theory, antenna theory, stored electromagnetic energy, quality factor

Author for correspondence:
Miloslav Capek
e-mail: miloslav.capek@fel.cvut.cz

Stored Electromagnetic Energy and Quality Factor of Radiating Structures

Miloslav Capek[1], Lukas Jelinek[1] and Guy A. E. Vandenbosch[2]

[1]Department of Electromagnetic Field, Faculty of Electrical Engineering, Czech Technical University in Prague, Technicka 2, 16627, Prague, Czech Republic
[2]Department of Electrical Engineering, Division ESAT-TELEMIC (Telecommunications and Microwaves), Katholieke Universiteit Leuven, B-3001, Leuven, Belgium

This paper deals with the old yet unsolved problem of defining and evaluating the stored electromagnetic energy – a quantity essential for calculating the quality factor, which reflects the intrinsic bandwidth of the considered electromagnetic system. A novel paradigm is proposed to determine the stored energy in the time domain leading to the method, which exhibits positive semi-definiteness and coordinate independence, i.e. two key properties actually not met by the contemporary approaches. The proposed technique is compared with two up-to-date frequency domain methods that are extensively used in practice. All three concepts are discussed and compared on the basis of examples of varying complexity, starting with lumped RLC circuits and finishing with realistic radiators.

1. Introduction

In physics, an oscillating system is traditionally characterized [1] by its oscillation frequency and quality factor Q, which gives a measure of the lifetime of free oscillations. At its high values, the quality factor Q is also inversely proportional to the intrinsic bandwidth in which the oscillating system can effectively be driven by external sources [2, 3].

THE ROYAL SOCIETY PUBLISHING

The concept of quality factor Q as a single frequency estimate of relative bandwidth is most developed in the area of electric circuits [4] and electromagnetic radiating systems [3]. Its evaluation commonly follows two paradigms. As far as the first one is concerned, the quality factor is evaluated from the knowledge of the frequency derivative of input impedance [5, 6, 7]. As for the second paradigm, the quality factor is defined as 2π times the ratio between the cycle mean stored energy and the cycle mean lost energy [5, 8]. Generally, these two concepts yield distinct results, but come to identical results in the case of vanishingly small losses, the reason being the Foster's reactance theorem [9, 10].

The evaluation of quality factor by means of frequency derivative of input impedance was made very popular by the work of Yaghjian and Best [11] and is widely used in engineering practice [12, 13] thanks to its property of being directly measurable. Recently, this concept of quality factor has also been expressed as a bilinear form of source current densities [14], which is very useful in connection with modern numerical software tools [15]. Regardless of the mentioned advantages, the impedance concept of quality factor suffers from a serious drawback of being zero in specific circuits [16, 17] and/or radiators [17, 18] with evidently non-zero energy storage. This unfortunately prevents its usage in modern optimization techniques [19].

The second paradigm, in which the quality factor is evaluated via the stored energy and lost energy, is not left without difficulties either. In the case of non-dispersive components, the cycle mean lost energy does not pose a problem and may be evaluated as a sum of the cycle mean radiated energy and the cycle mean energy dissipated due to material losses [20]. Unfortunately, in the case of a non-stationary electromagnetic field associated with radiators, the definition of stored (non-propagating) electric and magnetic energies presents a problem that has not yet been satisfactorily solved [3]. The issue comes from the radiation energy, which does not decay fast enough in radial direction, and is in fact infinite in stationary state [21].

In order to overcome the infinite values of total energy, the evaluation of stored energy in radiating systems is commonly accompanied by the technique of extracting the divergent radiation component from the well-known total energy of the system [20]. This method is somewhat analogous to the classical field [22] re-normalization. Most attempts in this direction have been performed in the domain of time-harmonic fields. The pioneering work in this direction is the equivalent circuit method of Chu [21], in which the radiation and energy storage are represented by resistive and reactive components of a complex electric circuit describing each spherical mode. This method was later generalized by several works of Thal [24, 25]. Although powerful, this method suffers from fundamental drawback of spherical harmonics expansion, which is unique solely in the exterior of the sphere bounding the sources. Therefore, the circuit method cannot provide any information on the radiation content of the interior region, nor on the connection of energy storage with the actual shape of radiator.

The radiation extraction for spherical harmonics has also been performed directly at the field level. The classical work in this direction comes from Collin and Rothschild [26]. Their proposal leads to good results for canonical systems [26, 27, 28], and has been analytically shown self-consistent outside the radian-sphere [29]. Similarly to the work of Chu, this procedure is limited by the use of spherical harmonics to the exterior of the circumscribing sphere.

The problem of radiation extraction around radiators of arbitrary shape has been for the first time attacked by Fante [30] and Rhodes [31], giving the interpretation to the Foster's theorem [10] in open problems. The ingenious combination of the frequency derivative of input impedance and the frequency derivative of far-field radiation pattern led to the first general evaluation of stored energy. Fante's and Rhodes' works have been later generalized by Yaghjian and Best [11], who also pointed out an unpleasant fact that this method is coordinate-dependent. A scheme for minimisation of this dependence has been developed [11], but it was not until the work of Vandenbosch [32] who, generalizing the expressions of Geyi for small radiators [33] and rewriting the extraction technique into bilinear forms of currents, was able to reformulate the original extraction method into a coordinate-independent scheme. A noteworthy discussion of various forms of this extraction technique can be found in the work of Gustafsson and Jonsson

[34]. It was also Gustafsson et al. who emphasized [19] that under certain conditions, this extraction technique fails, giving negative values for specific current distributions. Hence the aforementioned approach remains incomplete too [35].

The problem of stored energy has seldom been addressed directly in the time domain. Nevertheless, there are some interesting works dealing with time-dependent energies. Shlivinski expanded the fields into spherical waves in time domain [36, 37], introducing time domain quality factor that qualifies the radiation efficiency of pulse-fed radiators. Collarday [38] proposed a brute force method utilizing the finite differences technique. In [39], Vandenbosch derived expressions for electric and magnetic energies in time domain that however suffer from an unknown parameter called storage time. A notable work of Kaiser [40] then introduced the concept of rest electromagnetic energy, which resembles the properties of stored energy, but is not identical to it [41].

The knowledge of the stored electromagnetic energy and the capability of its evaluation are also tightly connected with the question of its minimization [21, 42, 43, 44, 45]. Such lower bound of the stored energy would imply the upper bound to the available bandwidth, a parameter of great importance for contemporary communication devices.

In this paper, a scheme for radiation energy extraction is proposed following a novel line of reasoning in the time domain. The scheme aims to overcome the handicaps of the previously published works, and furthermore is able to work with general time-dependent source currents of arbitrary shape. It is presented together with the two most common frequency domain methods, the first being based on the time-harmonic expressions of Vandenbosch [32] and the second using the input impedance approximation introduced by Yaghjian and Best [11]. All three concepts are closely investigated and compared on the basis of examples of varying complexity. The working out of all three concepts starts solely from the currents flowing on a radiator, which are usually given as a result in modern electromagnetic simulators. This raises challenging possibilities of modal analysis [46] and optimization [47].

The paper is organized as follows. Two different concepts of quality factor Q that are based on electromagnetic energies (in both, the frequency and time domain), are introduced in §2. Subsequently, the quality factor Q derived from the input impedance is formulated in terms of currents on a radiator in §3. The following two sections present numerical examples: §4 treats non-radiating circuits and §5 deals with radiators. The results are discussed in §6 and the paper is concluded in §7.

2. Energy concept of quality factor Q

In the context of energy, the quality factor is most commonly defined as

$$Q = 2\pi \frac{\langle \mathcal{W}_{\mathrm{sto}}(t) \rangle}{W_{\mathrm{lost}}} = 2\pi \frac{W_{\mathrm{sto}}}{W_{\mathrm{lost}}}, \tag{2.1}$$

where a time-harmonic steady state with angular frequency ω_0 is assumed, with $\mathcal{W}_{\mathrm{sto}}(t)$ as the electromagnetic stored energy, $\langle \mathcal{W}_{\mathrm{sto}}(t) \rangle = W_{\mathrm{sto}}$ as the cycle mean of $\mathcal{W}_{\mathrm{sto}}(t)$ and W_{lost} as the lost electromagnetic energy during one cycle [20]. In conformity with the font convention introduced above, in the following text, the quantities defined in the time domain are stated in calligraphic font, while the frequency domain quantities are indicated in the roman font.

A typical Q-measurement scenario is depicted in figure 1, which shows a radiator fed by a shielded power source. The input impedance in the time-harmonic steady state at the frequency ω_0 seen by the source is Z_{in}. Assuming that the radiator is made of conductors with ideal non-dispersive conductivity σ and lossless non-dispersive dielectrics, we can state that the lost energy during one cycle, needed for (2.1), can be evaluated as

$$W_{\mathrm{lost}} = \int_{\alpha}^{\alpha+T} i_0(t)\, u_0(t)\, \mathrm{d}t = \frac{\pi}{\omega_0} \mathrm{Re}\{Z_{\mathrm{in}}\} I_0^2 = W_{\mathrm{r}} + W_{\sigma}, \tag{2.2}$$

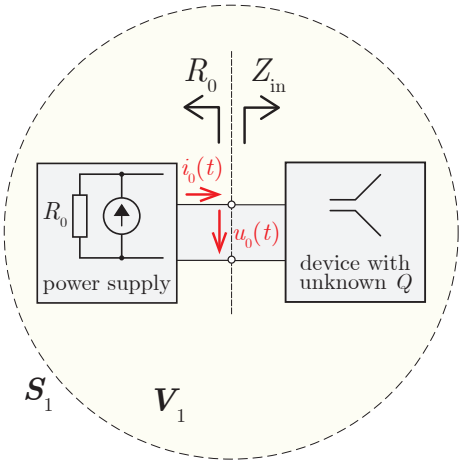

Figure 1. A device with unknown Q that is fed by a shielded power source with internal resistance R_0.

where I_0 is the amplitude of $i_0\,(t)$ (see figure 1), $W_{\rm r}$ represents the cycle mean radiation loss and W_σ stands for the energy lost in one cycle via conduction. The part W_σ of (2.2) can be calculated as

$$W_\sigma = \frac{\pi}{\omega_0}\int\limits_V \sigma\,|\boldsymbol{E}\,(\boldsymbol{r},\omega_0)|^2\;\mathrm{d}V, \tag{2.3}$$

with V being the shape of radiator and $\boldsymbol{E}$ being the time-harmonic electric field intensity under the convention $\boldsymbol{\mathcal{E}}\,(t) = \mathrm{Re}\{\boldsymbol{E}\,(\omega)\,\mathrm{e}^{\mathrm{i}\omega t}\}$, $\mathrm{i} = \sqrt{-1}$. At the same time, the near-field of the radiator [48] contains the stored energy $\mathcal{W}_{\rm sto}\,(t)$, which is bound to the sources and does not escape from the radiator towards infinity. The evaluation of the cycle mean energy $W_{\rm sto}$ is the goal of the following §2(a) and §2(b), in which the power balance [10] is going to be employed.

(a) Stored energy in time domain

This subsection presents a new paradigm of stored energy evaluation. The first step consists in imagining the spherical volume V_1 (see figure 1) centred around the system, whose radius is large enough to lie in the far-field region [48]. The total electromagnetic energy content of the sphere (it also contains heat W_σ) is

$$\mathcal{W}\,(V_1,t) = \mathcal{W}_{\rm sto}\,(t) + \mathcal{W}_{\rm r}\,(V_1,t)\,, \tag{2.4}$$

where $\mathcal{W}_{\rm r}\,(V_1,t)$ is the energy contained in the radiation fields that have already escaped from the sources. Let us assume that the power source is switched on at $t=-\infty$, bringing the system into a steady state, and then switched off at $t=t_{\rm off}$. For $t\in[t_{\rm off},\infty)$ the system is in a transient state, during which all the energy $\mathcal{W}\,(V_1,t_{\rm off})$ will either be transformed into heat at the resistor R_0 and the radiator's conductors or radiated through the bounding envelope S_1. Explicitly, Poynting's theorem [10] states that the total electromagnetic energy at time $t_{\rm off}$ can be calculated as

$$\begin{aligned}\mathcal{W}\,(V_1,t_{\rm off}) = {}& R_0\int\limits_{t_{\rm off}}^{\infty} i_{\rm R_0}^2(t)\,\mathrm{d}t + \int\limits_{t_{\rm off}}^{\infty}\int\limits_V \boldsymbol{\mathcal{E}}\,(\boldsymbol{r},t)\cdot\boldsymbol{\mathcal{J}}\,(\boldsymbol{r},t)\;\mathrm{d}V\,\mathrm{d}t\\ &+\int\limits_{t_{\rm off}}^{\infty}\oint\limits_{S_1}\Big(\boldsymbol{\mathcal{E}}_{\rm far}\,(\boldsymbol{r},t)\times\boldsymbol{\mathcal{H}}_{\rm far}\,(\boldsymbol{r},t)\Big)\cdot\mathrm{d}\boldsymbol{S}_1\,\mathrm{d}t,\end{aligned} \tag{2.5}$$

in which S_1 lies in the far-field region.

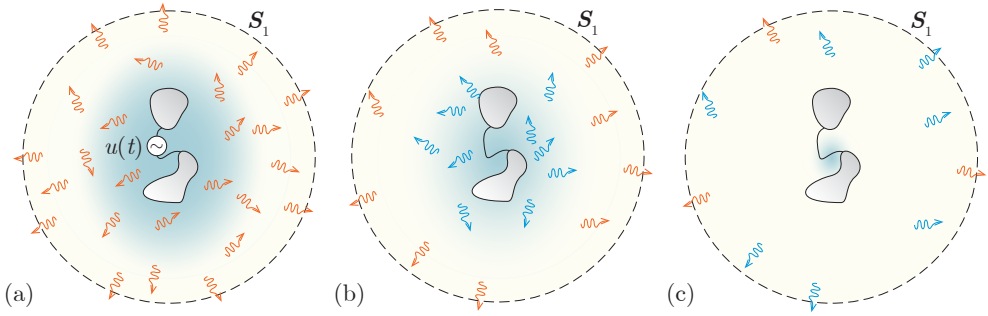

Figure 2. Graphical representation of the total electromagnetic energy evaluation via (2.8) for a loss-less radiator excited by ideal voltage source. Panel (a) shows a steady state just before $t = t_{\text{off}}$, when the steady state radiation (orange wavelets) as well as the steady state stored energy (blue cloud) were maintained by the source. Panel (b) shows that after the source is switched off, the existing radiation travels to S_1 (and some of it also passes S_1) while a new radiation (blue wavelets) emerges at the expense of the stored energy. Panel (c) depicts the time $t \gg t_{\text{off}}$ when the stored energy is almost exhausted. Capturing all wavelets for $t > t_{\text{off}}$ by means of integral (2.8) gives the total energy within the capturing surface S_1.

As a special yet important example, let us assume a radiating device made exclusively of perfect electric conductors (PEC). In that case, the far-field can be expressed as [20]

$$\boldsymbol{\mathcal{H}}_{\text{far}}(\boldsymbol{r},t) = -\frac{1}{4\pi c_0}\int\limits_{V'}\frac{\boldsymbol{n}_0\times\dot{\boldsymbol{\mathcal{J}}}(\boldsymbol{r}',t')}{R}\,\mathrm{d}V', \tag{2.6a}$$

$$\boldsymbol{\mathcal{E}}_{\text{far}}(\boldsymbol{r},t) = -\frac{\mu}{4\pi}\int\limits_{V'}\frac{\dot{\boldsymbol{\mathcal{J}}}(\boldsymbol{r}',t') - \left(\boldsymbol{n}_0\cdot\dot{\boldsymbol{\mathcal{J}}}(\boldsymbol{r}',t')\right)\boldsymbol{n}_0}{R}\,\mathrm{d}V' \tag{2.6b}$$

in which c_0 is the speed of light, $R = |\boldsymbol{r}-\boldsymbol{r}'|$, $\boldsymbol{n}_0 = (\boldsymbol{r}-\boldsymbol{r}')/R$, $t' = t - R/c_0$ stands for the retarded time and the dot represents the derivative with respect to the time argument, i.e.

$$\dot{\boldsymbol{\mathcal{J}}}(\boldsymbol{r}',t') = \left.\frac{\partial\boldsymbol{\mathcal{J}}(\boldsymbol{r}',\tau)}{\partial\tau}\right|_{\tau=t'}. \tag{2.7}$$

Since we consider the far-field, we can further write [49] $R \approx r$ for amplitudes, $R \approx r - \boldsymbol{r}_0\cdot\boldsymbol{r}'$ for time delays, with $\boldsymbol{n}_0 \approx \boldsymbol{r}_0$ and $r = |\boldsymbol{r}|$. Using (2.6*a*)–(2.7) and the above-mentioned approximations, the last term in (2.5) can be written as

$$\begin{aligned}\int\limits_{t_{\text{off}}}^{\infty}\oint\limits_{S_1}\left(\boldsymbol{\mathcal{E}}_{\text{far}}(\boldsymbol{r},t)\times\boldsymbol{\mathcal{H}}_{\text{far}}(\boldsymbol{r},t)\right)\cdot\boldsymbol{r}_0\,\mathrm{d}S_1\,\mathrm{d}t &= \frac{1}{Z_0}\int\limits_{t_{\text{off}}}^{\infty}\oint\limits_{S_1}|\boldsymbol{\mathcal{E}}_{\text{far}}(\boldsymbol{r},t)|^2\,\mathrm{d}S_1\,\mathrm{d}t\\ &= \frac{\mu^2}{Z_0(4\pi)^2}\int\limits_{t_{\text{off}}}^{\infty}\int\limits_0^{\pi}\int\limits_0^{2\pi}\left|\int\limits_{V'}\left(\dot{\boldsymbol{\mathcal{J}}}(\boldsymbol{r}',t') - \left(\boldsymbol{r}_0\cdot\dot{\boldsymbol{\mathcal{J}}}(\boldsymbol{r}',t')\right)\boldsymbol{r}_0\right)\mathrm{d}V'\right|^2\sin\theta\,\mathrm{d}\varphi\,\mathrm{d}\theta\,\mathrm{d}t,\end{aligned} \tag{2.8}$$

where $t' = t - r/c_0 + \boldsymbol{r}_0\cdot\boldsymbol{r}'/c_0$, where Z_0 is the free space impedance and where the relation

$$\boldsymbol{\mathcal{H}}_{\text{far}}(\boldsymbol{r},t) = \frac{\boldsymbol{r}_0\times\boldsymbol{\mathcal{E}}_{\text{far}}(\boldsymbol{r},t)}{Z_0} \tag{2.9}$$

has been used. Utilizing (2.5) and (2.8), we are thus able to find the total electromagnetic energy inside S_1, see figure 2 for graphical representation.

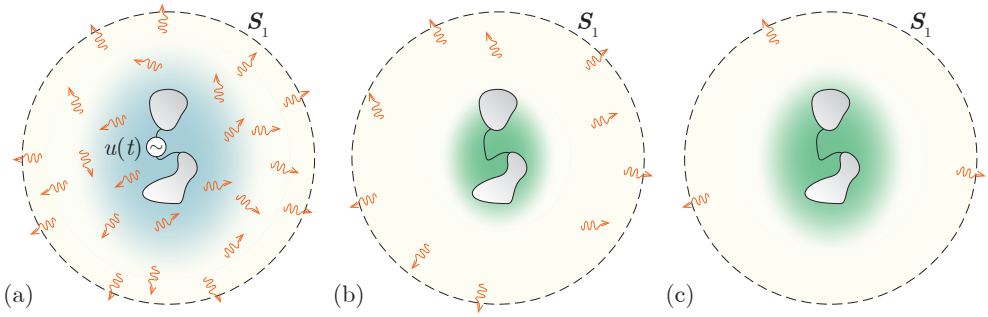

Figure 3. Graphical representation of the radiated energy evaluation via (2.8) for a loss-less radiator excited by ideal voltage source. Panel (a) shows a steady state just before $t = t_{\mathrm{off}}$, when the steady state radiation (orange wavelets) as well as the steady state stored energy (blue cloud) were maintained by the source. Panel (b) shows that at $t \geq t_{\mathrm{off}}$, the radiating currents are modified so to inhibit any radiation, although they possibly create a new energy storage (green cloud). The radiation emitted before $t = t_{\mathrm{off}}$ (orange wavelets) is unaffected by this modification. Panel (c) depicts the time $t \gg t_{\mathrm{off}}$ when almost all radiation passed S_1. The radiation content of the sphere S_1 is evaluated via (2.8). The green stored energy does not participate as it is not represented by radiation, and is consequently not captured by the integral (2.8).

Note here that the total electromagnetic energy content of the sphere could also be expressed as

$$\mathcal{W}\left(V_1, t_{\mathrm{off}}\right) = \frac{1}{2} \int\limits_{V_1} \left(\mu \left| \boldsymbol{\mathcal{H}}\left(\boldsymbol{r}, t_{\mathrm{off}}\right) \right|^2 + \epsilon \left| \boldsymbol{\mathcal{E}}\left(\boldsymbol{r}, t_{\mathrm{off}}\right) \right|^2 \right) \mathrm{d}V \tag{2.10}$$

which can seem to be simpler than the aforementioned scheme. The simplicity is, however, just formal. The main disadvantage of (2.10) is that the integration volume includes also the near-field region, where the fields are rather complex (and commonly singular). Furthermore, contrary to (2.8), the radius of the sphere plays an important role in (2.10) unlike in (2.8), where it appears only via a static time shift r/c_0. In fact, it will be shown later on that this dependence can be completely eliminated in the calculation of stored energy.

In order to obtain the stored energy $\mathcal{W}_{\mathrm{sto}}\left(t_{\mathrm{off}}\right)$ inside S_1 we, however, need to know the radiation content of the sphere at $t = t_{\mathrm{off}}$. A thought experiment aimed at attaining it is presented in figure 3. It exploits the properties of (2.8). Consulting the figure, let us imagine that during the calculation of $\mathcal{W}\left(V_1, t_{\mathrm{off}}\right)$ we were capturing the time course of the current $\boldsymbol{\mathcal{J}}\left(\boldsymbol{r}', t\right)$ at every point. In addition, let us assume that we define an artificial current $\boldsymbol{\mathcal{J}}_{\mathrm{freeze}}\left(\boldsymbol{r}', t\right)$ as

$$\boldsymbol{\mathcal{J}}_{\mathrm{freeze}}\left(\boldsymbol{r}', t\right) = \begin{cases} \boldsymbol{\mathcal{J}}\left(\boldsymbol{r}', t\right), & t < t_{\mathrm{off}} \\ \boldsymbol{\mathcal{J}}\left(\boldsymbol{r}', t_{\mathrm{off}}\right), & t \geq t_{\mathrm{off}} \end{cases} \tag{2.11}$$

and use it inside (2.8) instead of the true current $\boldsymbol{\mathcal{J}}\left(\boldsymbol{r}', t\right)$. The expression (2.8) then claims that for $t < t_{\mathrm{off}}$ the artificial current $\boldsymbol{\mathcal{J}}_{\mathrm{freeze}}\left(\boldsymbol{r}', t\right)$ is radiating in the same way as in the case of the original problem, but for $t > t_{\mathrm{off}}$, the radiation is instantly stopped. Therefore, if we now evaluate (2.8) over the new artificial current, it will give exactly the radiation energy $\mathcal{W}_{\mathrm{r}}\left(V_1, t_{\mathrm{off}}\right)$, which has escaped from the sources before t_{off}. Subtracting it from $\mathcal{W}\left(V_1, t_{\mathrm{off}}\right)$, we obtain the stored energy $\mathcal{W}_{\mathrm{sto}}\left(t_{\mathrm{off}}\right)$ and averaging over one period, we obtain the cycle mean stored energy

$$W_{\mathrm{sto}} = \left\langle \mathcal{W}_{\mathrm{sto}}\left(t_{\mathrm{off}}\right) \right\rangle = \frac{1}{T} \int\limits_{\alpha}^{\alpha+T} \mathcal{W}_{\mathrm{sto}}\left(t_{\mathrm{off}}\right) \mathrm{d}t_{\mathrm{off}}. \tag{2.12}$$

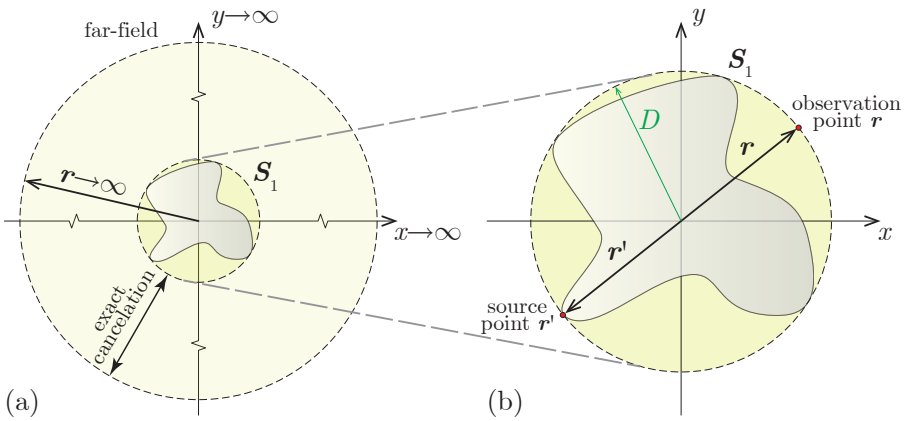

Figure 4. Sketch of the far-field cancellation. The circumscribing sphere $\boldsymbol{S}_1$ can be advantageously stretched right around the radiator, since outside this smallest sphere, the first and the second run are identically subtracted.

With respect to the freezing of the current, it is important to realize that this could mean an indefinite accumulation of charge at a given point. However, it is necessary to consider this operation as to be performed on the artificial impressed sources, which can be chosen freely.

When subtracting the radiated energy from the total energy, it is important to take into account that for $t < t_{\text{off}}$, the currents were the same in both situations. Thus defining $D = \max\{|\boldsymbol{r}'|\}$, we can state that for $t < t_{\text{off}} + (r - D)/c_0$, the integrals (2.8) will exactly cancel during the subtraction, see figure 4. The relation (2.8) can then be safely evaluated only for $t' = t - D/c_0 + \boldsymbol{r}_0 \cdot \boldsymbol{r}'/c_0$ (the worst-case scenario depicted in figure 4b), which means that the currents need to be saved only for $t > t_{\text{off}} - 2D/c_0$. It is crucial to take into consideration that this is equivalent to say that, after all, the bounding sphere S_1 does not need to be situated in the far-field. It is sufficient (and from the computational point of view also advantageous), if S_1 is the smallest circumscribing sphere centred in the coordinate system, for the rest of the far-field is cancelled anyhow, see figure 4a.

As a final note, we mention that even though the above-described method relies on the integration on a spherical surface, the resulting stored energy properly takes into account the actual geometry of the radiator, representing thus a considerable generalization of the time domain prescription for the stored energy proposed in [29] which is able to address only the regions outside the smallest circumscribing sphere. Further properties of the method are going to be presented on numerical results in §5 and will be detailed in §6.

(b) Stored Energy in Frequency Domain

This subsection rephrases the stored energy evaluation by Vandenbosch [32], which approaches the issue in the frequency domain, utilizing the complex Poynting's theorem that states [20] that

$$-\frac{1}{2}\langle \boldsymbol{E}, \boldsymbol{J}\rangle = P_{\text{m}} - P_{\text{e}} + 2\text{i}\omega\,(W_{\text{m}} - W_{\text{e}}) = P_{\text{in}}, \tag{2.13}$$

in which P_{in} is the cycle mean complex power, the terms P_{m} and P_{e} form the cycle mean radiated power $P_{\text{m}} - P_{\text{e}}$ and $2\omega\,(W_{\text{m}} - W_{\text{e}})$ is the cycle mean reactive net power, and

$$\langle \boldsymbol{u}, \boldsymbol{v}\rangle = \int_V \boldsymbol{u}\,(\boldsymbol{r}) \cdot \boldsymbol{v}^*\,(\boldsymbol{r})\ \text{d}V \tag{2.14}$$

is the inner product [50]. In the classical treatment of (2.13), W_{m} and W_{e} are commonly taken [20] as $\mu\,|\boldsymbol{H}|^2/4$ and $\epsilon\,|\boldsymbol{E}|^2/4$ that are integrated over the entire space. Both of them are infinite for

the radiating system. Nonetheless, when electromagnetic potentials are utilized [51], the complex power balance (2.13) can be rewritten as

$$P_{\mathrm{in}} = P_{\mathrm{m}}^{\boldsymbol{A}} - P_{\mathrm{e}}^{\varphi} + 2\mathrm{i}\omega\left(W_{\mathrm{m}}^{\boldsymbol{A}} - W_{\mathrm{e}}^{\varphi}\right) = \frac{\mathrm{i}\omega}{2}\left(\langle \boldsymbol{A}, \boldsymbol{J}\rangle - \langle \varphi, \rho\rangle\right), \tag{2.15}$$

where $\boldsymbol{A}$ represents the vector potential, φ represents the scalar potential, and ρ stands for the charge density. As an alternative to the classical treatment, it is then possible to write

$$W_{\mathrm{m}}^{\boldsymbol{A}} - \mathrm{i}\frac{P_{\mathrm{m}}^{\boldsymbol{A}}}{2\omega} = \frac{1}{4}\langle \boldsymbol{A}, \boldsymbol{J}\rangle \tag{2.16}$$

and

$$W_{\mathrm{e}}^{\varphi} - \mathrm{i}\frac{P_{\mathrm{e}}^{\varphi}}{2\omega} = \frac{1}{4}\langle \varphi, \rho\rangle \tag{2.17}$$

without altering (2.13). However, it is important to stress that in such case, $W_{\mathrm{m}}^{\boldsymbol{A}}$ in (2.16) and W_{e}^{φ} in (2.17) generally represent neither stored nor total magnetic and electric energies [20]. Some attempts have been undertaken to use (2.16) and (2.17) as stored magnetic and electric energies even in non-stationary cases [52]. These attempts were however faced with extensive criticism [53], [54], mainly due to the variance of separated energies under gauge transformations.

Regardless of the aforementioned issues, (2.16) and (2.17) were modified [32] in an attempt to obtain the stored magnetic and electric energies. This modification reads

$$\widetilde{W}_{\mathrm{m}} \equiv W_{\mathrm{m}}^{\boldsymbol{A}} + \frac{W_{\mathrm{rad}}}{2}, \tag{2.18a}$$

$$\widetilde{W}_{\mathrm{e}} \equiv W_{\mathrm{e}}^{\varphi} + \frac{W_{\mathrm{rad}}}{2}, \tag{2.18b}$$

where the particular term

$$W_{\mathrm{rad}} = \mathrm{Im}\left\{k\left(k^2\langle L_{\mathrm{rad}}\boldsymbol{J}, \boldsymbol{J}\rangle - \langle L_{\mathrm{rad}}\nabla\cdot\boldsymbol{J}, \nabla\cdot\boldsymbol{J}\rangle\right)\right\} \tag{2.19}$$

is associated with the radiation field, and the operator

$$L_{\mathrm{rad}}\boldsymbol{U} = \frac{1}{16\pi\epsilon\omega^2}\int\limits_{V'}\boldsymbol{U}\left(\boldsymbol{r}'\right)\mathrm{e}^{-\mathrm{i}kR}\,\mathrm{d}V' \tag{2.20}$$

is defined using $k = \omega/c_0$ as the wavenumber. The electric currents $\boldsymbol{J}$ are assumed to flow in a vacuum. For computational purposes, it is also beneficial to use the radiation integrals for vector and scalar potentials [48], and rewrite (2.16), (2.17) as [14]

$$W_{\mathrm{m}}^{\boldsymbol{A}} - \mathrm{i}\frac{P_{\mathrm{m}}^{\boldsymbol{A}}}{2\omega} = k^2\langle L\boldsymbol{J}, \boldsymbol{J}\rangle \tag{2.21}$$

and

$$W_{\mathrm{e}}^{\varphi} - \mathrm{i}\frac{P_{\mathrm{e}}^{\varphi}}{2\omega} = \langle L\nabla\cdot\boldsymbol{J}, \nabla\cdot\boldsymbol{J}\rangle, \tag{2.22}$$

with

$$L\boldsymbol{U} = \frac{1}{16\pi\epsilon\omega^2}\int\limits_{V'}\boldsymbol{U}\left(\boldsymbol{r}'\right)\frac{\mathrm{e}^{-\mathrm{i}kR}}{R}\,\mathrm{d}V'. \tag{2.23}$$

It is suggested in [32] that $\widetilde{W}_{\mathrm{sto}} = \widetilde{W}_{\mathrm{m}} + \widetilde{W}_{\mathrm{e}}$ is the stored energy W_{sto}. Yet this statement cannot be considered absolutely correct, since as it was shown in [19, 55], $\widetilde{W}_{\mathrm{sto}}$ can be negative. Consequently, it is necessary to conclude that $\widetilde{W}_{\mathrm{sto}}$, defined by the frequency domain concept

[32], can only approximately be equal to the stored energy W_{sto}, resulting in

$$\widetilde{W}_{\mathrm{sto}} \approx W_{\mathrm{sto}}, \tag{2.24}$$

and then by analogy with (2.1)

$$\widetilde{Q} = 2\pi \frac{\widetilde{W}_{\mathrm{sto}}}{W_{\mathrm{lost}}} = 2\pi \frac{\widetilde{W}_{\mathrm{m}} + \widetilde{W}_{\mathrm{e}}}{W_{\mathrm{lost}}} \approx Q \tag{2.25}$$

is defined.

3. Fractional bandwidth concept of quality factor Q

It is well-known that for $Q \gg 1$, the quality factor Q is approximately inversely proportional to the fractional bandwidth (FBW)

$$Q_Z \approx \frac{\chi}{\mathrm{FBW}}, \tag{3.1}$$

where χ is a given constant and $\mathrm{FBW} = (\omega^+ - \omega^-)/\omega_0$, [11]. The quality factor Q, which is known to fulfil (3.1), was found by Yaghjian and Best [11] utilizing an analogy with RLC circuits and using the transition from conductive to voltage standing wave ratio bandwidth. Its explicit definition reads

$$Q_Z = \frac{\omega}{2\,\mathrm{Re}\{P_{\mathrm{in}}\}} \left| \frac{\partial P_{\mathrm{in}}}{\partial \omega} \right| = |Q_R + \mathrm{i} Q_X|\,, \tag{3.2}$$

where the total input current at the radiator's port is assumed to be normalized to $I_0 = 1\mathrm{A}$.

The differentiation of the complex power in the form of (2.15) can be used to find the source definition of (3.2), and leads to [14]

$$Q_R = \frac{\pi}{\omega} \frac{P_{\mathrm{m}}^{\boldsymbol{A}} + P_{\mathrm{e}}^{\varphi} + P_{\mathrm{rad}} + P_{\partial\omega}}{W_{\mathrm{lost}}}, \tag{3.3a}$$

$$Q_X = 2\pi \frac{\widetilde{W}_{\mathrm{sto}} + W_{\partial\omega}}{W_{\mathrm{lost}}}, \tag{3.3b}$$

in which

$$\frac{P_{\mathrm{rad}}}{2\omega} = \mathrm{Re}\left\{ k \left(k^2 \langle L_{\mathrm{rad}} \boldsymbol{J}, \boldsymbol{J} \rangle - \langle L_{\mathrm{rad}} \nabla \cdot \boldsymbol{J}, \nabla \cdot \boldsymbol{J} \rangle \right) \right\}, \tag{3.4}$$

and

$$W_{\partial\omega} - \mathrm{i}\frac{P_{\partial\omega}}{2\omega} = k^2 \left(\langle L\boldsymbol{J}, D\boldsymbol{J} \rangle + \langle L\boldsymbol{J}^*, D\boldsymbol{J}^* \rangle \right) - \left(\langle L\nabla \cdot \boldsymbol{J}, D\nabla \cdot \boldsymbol{J} \rangle + \langle L\nabla \cdot \boldsymbol{J}^*, D\nabla \cdot \boldsymbol{J}^* \rangle \right). \tag{3.5}$$

The operator D is defined as

$$D\boldsymbol{U} = \omega \frac{\partial \boldsymbol{U}}{\partial \omega}. \tag{3.6}$$

As particular cases of (3.3*b*), we obtain the Rhodes' definition [5] of the quality factor Q as $|Q_X|$ and the definition (2.25) as Q_X, omitting the $W_{\partial\omega}$ term from (3.3*b*).

For the purposes of this paper, we can observe in (2.1), (3.2), (3.3*a*) and (3.3*b*) that the stored energy in the case of the FBW concept is equivalent to

$$W_{\mathrm{sto}}^{\mathrm{FBW}} \equiv \frac{1}{2} \left| \frac{\partial P_{\mathrm{in}}}{\partial \omega} \right| = \left| \widetilde{W}_{\mathrm{sto}} + W_{\partial\omega} - \mathrm{i}\frac{P_{\mathrm{m}}^{\boldsymbol{A}} + P_{\mathrm{e}}^{\varphi} + P_{\mathrm{rad}} + P_{\partial\omega}}{2\omega} \right|, \tag{3.7}$$

but we remark here that (3.7) was not intended to be the stored energy [11].

4. Non-radiating circuits

The previous §§2 and 3 have defined three generally different concepts of stored energy, namely W_{sto}, $\widetilde{W}_{\mathrm{sto}}$ and $W_{\mathrm{sto}}^{\mathrm{FBW}}$. Given that W_{lost} is uniquely defined, we can benefit from the use of the corresponding dimensionless quality factors Q, $\widetilde{Q}$ and Q_Z for comparing them. This is performed

in §4 for non-radiating circuits and in §5 for radiating systems. Particularly, in §4, we assume passive lossy but non-dispersive and non-radiating one-ports.

(a) Time domain stored energy for lumped elements

Following the general procedure indicated in §2(a), let us assume a general RLC circuit that was for $t \in (-\infty, t_{\mathrm{off}})$ fed by a time-harmonic source (current or voltage) $s(t) = \sin(\omega_0 t)$ which was afterwards switched off for $t \in [t_{\mathrm{off}}, \infty)$. Since the circuit is non-radiating, the total energy $\mathcal{W}(V_1, t_{\mathrm{off}})$ is directly equal to $\mathcal{W}_{\mathrm{sto}}(t_{\mathrm{off}})$. Furthermore, a careful selection of the voltage (or current) source for a given circuit helps us to eliminate the internal resistance of the source. So we get

$$W_{\mathrm{sto}} = \sum_k \frac{R_k}{T} \int_{\alpha}^{\alpha+T} \int_{t_{\mathrm{off}}}^{\infty} i_{\mathrm{R},k}^2(t)\, \mathrm{d}t\, \mathrm{d}t_{\mathrm{off}}, \tag{4.1}$$

where $i_{\mathrm{R},k}(t)$ is the transient current in the k-th resistor.

The currents $i_{\mathrm{R},k}$ are advantageously evaluated in the frequency domain. The Fourier transform of the source reads [56]

$$S(\omega) = \frac{\mathrm{i}\pi}{2}\left(\delta(\omega+\omega_0) - \delta(\omega-\omega_0)\right) + \frac{\mathrm{e}^{-\mathrm{i}\omega t_{\mathrm{off}}}}{2}\left(\frac{\mathrm{e}^{\mathrm{i}\omega_0 t_{\mathrm{off}}}}{\omega-\omega_0} - \frac{\mathrm{e}^{-\mathrm{i}\omega_0 t_{\mathrm{off}}}}{\omega+\omega_0}\right). \tag{4.2}$$

We can then write $I_{\mathrm{R},k}(\omega) = T_{\mathrm{R}_k}(\omega)\, S(\omega)$, where $T_{\mathrm{R}_k}(\omega)$ represents the transfer function. Consequently

$$\begin{aligned} i_{\mathrm{R},k}(t) &= \frac{1}{2\pi}\int_{-\infty}^{\infty} T_{\mathrm{R}_k}(\omega)\, S(\omega)\, \mathrm{e}^{\mathrm{i}\omega t}\, \mathrm{d}\omega \\ &= \frac{1}{2}\mathrm{Im}\left\{T_{\mathrm{R}_k}(\omega_0)\, \mathrm{e}^{\mathrm{i}\omega_0 t}\right\} + \frac{\omega}{4\pi}\int_{-\infty}^{\infty} T_{\mathrm{R}_k}(\omega)\left(\frac{\mathrm{e}^{\mathrm{i}\omega_0 t_{\mathrm{off}}}}{\omega-\omega_0} - \frac{\mathrm{e}^{-\mathrm{i}\omega_0 t_{\mathrm{off}}}}{\omega+\omega_0}\right)\mathrm{e}^{\mathrm{i}\omega(t-t_{\mathrm{off}})}\, \mathrm{d}\omega. \end{aligned} \tag{4.3}$$

As the studied circuit is lossy, $T_{\mathrm{R}_k}(\omega)$ has no poles on the real ω-axis and the second integral can be evaluated by the standard contour integration in the complex plane of ω along the semi-circular contour in the upper ω half-plane, while omitting the points $\omega = \pm\omega_0$. The result of the contour integration for $t > t_{\mathrm{off}}$ can be written as

$$i_{\mathrm{R},k}(t) = \frac{\mathrm{i}}{2}\sum_m \operatorname*{res}_{\omega\to\omega_{m,k}} \left\{T_{\mathrm{R}_k}(\omega)\left(\frac{\mathrm{e}^{\mathrm{i}\omega_0 t_{\mathrm{off}}}}{\omega-\omega_0} - \frac{\mathrm{e}^{-\mathrm{i}\omega_0 t_{\mathrm{off}}}}{\omega+\omega_0}\right)\mathrm{e}^{\mathrm{i}\omega(t-t_{\mathrm{off}})}\right\}, \tag{4.4}$$

where $\omega_{m,k}$ are the poles of $T_{\mathrm{R}_k}(\omega)$ with $\mathrm{Im}\{\omega_{m,k}\} > 0$. The substitution of (4.4) into (4.1) gives the mean stored energy. It is also important to realize that in this case, it is easy to analytically carry out both integrations involved in (4.1). The result is obviously identical to the cycle mean of the classical definition of stored energy.

$$\mathcal{W}_{\mathrm{sto}}(t_{\mathrm{off}}) = \frac{1}{2}\left(\sum_m L_m i_{\mathrm{L},m}^2(t_{\mathrm{off}}) + \sum_n C_n u_{\mathrm{C},n}^2(t_{\mathrm{off}})\right), \tag{4.5}$$

which is the lumped circuit form of (2.10), with $i_{\mathrm{L},m}(t)$ being the current in the m-th inductor L_m and $u_{\mathrm{C},n}(t)$ being the voltage on the n-th capacitor C_n.

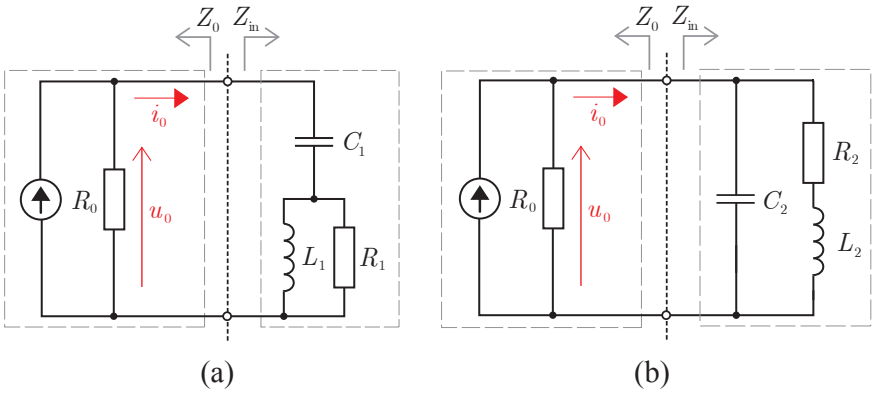

Figure 5. Studied RLC circuits: (a) C_1 in series with parallel L_1 and R_1, and (b) C_2 in parallel with serial R_2 and L_2

.

(b) Frequency domain stored energy for lumped elements

Without the radiation ($P_{\text{rad}} = 0, \omega W_{\text{rad}} = 0$), the cycle mean of (2.10), which is also equal to the cycle mean (4.5), is identical to the frequency domain expression

$$\widetilde{W}_{\text{sto}} = W_{\text{m}}^{\boldsymbol{A}} + W_{\text{e}}^{\varphi} = \frac{1}{4}\left(\sum_m L_m |I_{\text{L},m}|^2 + \sum_n C_n |U_{\text{C},n}|^2\right) = \frac{1}{4}\int_V \left(\mu\,|\boldsymbol{H}|^2 + \epsilon\,|\boldsymbol{E}|^2\right)\,\mathrm{d}V, \quad (4.6)$$

where $W_{\text{m}}^{\boldsymbol{A}}$ and W_{e}^{φ} are defined by (2.21) and (2.22) respectively. We thus conclude that $W_{\text{sto}} = \widetilde{W}_{\text{sto}}$ and $Q = \widetilde{Q}$ for non-radiating circuits.

(c) Frequency domain stored energy for lumped elements derived from FBW concept

In order to evaluate (3.2), the same procedure as in the derivation of Foster's reactance theorem [10] can be employed (keeping in mind the unitary input current, no radiation and assuming non-zero conductivity). It results in

$$\begin{aligned} W_{\text{sto}}^{\text{FBW}} &= \left|\frac{1}{4}\int_V \left(\mu\,|\boldsymbol{H}|^2 + \epsilon\,|\boldsymbol{E}|^2\right)\,\mathrm{d}V - \frac{\mathrm{i}\sigma}{2}\int_V \boldsymbol{E}^* \cdot \frac{\partial \boldsymbol{E}}{\partial \omega}\,\mathrm{d}V\right| \\ &= \left|\frac{1}{4}\left(\sum_m L_m |I_{\text{L},m}|^2 + \sum_n C_n |U_{\text{C},n}|^2\right) - \frac{\mathrm{i}}{2}\sum_k R_k I_{\text{R},k}^* \frac{\partial I_{\text{R},k}}{\partial \omega}\right|, \end{aligned} \quad (4.7)$$

where $I_{\text{R},k}$ is the amplitude of the current through the k-th resistor. The formula indicated above clearly reveals the fundamental difference between W_{sto} and $W_{\text{sto}}^{\text{FBW}}$, which consists in the last term of RHS in (4.7). It means that, in general, $W_{\text{sto}}^{\text{FBW}}$ does not represent the time-averaged stored energy.

(d) Results

In the previous §§4(a)–4(c) we have shown that for non-radiating circuits there is no difference between the quality factor defined in the time domain (Q) and the one defined in the frequency domain ($\widetilde{Q}$). Nevertheless, there is a substantial difference between Q and Q_Z, which is going to be presented in §4(d) using two representative examples depicted in figure 5. We do not explicitly consider simple series and parallel RLC circuits in this paper, since the three definitions of the

stored energy and quality factor Q deliver exactly the same results, i.e. $Q = \omega_0 L/R = \omega_0 RC$. This is attributable to the frequency independence of the current flowing through the resistor (the series resonance circuit), or of the voltage on the resistor (the parallel resonance circuit). In those cases, the last term of (4.7) vanishes identically. This fact is the very reason why the FBW approach works perfectly for radiators that can be approximated around resonance by a parallel or series RLC circuit. However, it also means that for radiators that need to be approximated by other circuits, the approach may not deliver the correct energy. This is probably the reason why this method seems to fail in the case of wideband radiators and radiators with slightly separated resonances.

In the case of circuits depicted in figure 5, the input impedances are

$$Z_{\text{in}}^{(a)} = \frac{1}{\mathrm{i}\omega C_1} + \frac{1}{\dfrac{1}{R_1} + \dfrac{1}{\mathrm{i}\omega L_1}}, \quad Z_{\text{in}}^{(b)} = \frac{1}{\dfrac{1}{R_2 + \mathrm{i}\omega L_2} + \mathrm{i}\omega C_2}, \tag{4.8}$$

and the corresponding resonance frequencies read

$$\omega_0^{(a)} = \frac{R_1}{L_1}\frac{1}{\sqrt{\dfrac{C_1 R_1^2}{L_1} - 1}}, \quad \omega_0^{(b)} = \frac{R_2}{L_2}\sqrt{\frac{L_2}{C_2 R_2^2} - 1}, \tag{4.9}$$

respectively. Utilizing the method from §2(a), it can be demonstrated that the energy quality factors are

$$Q^{(a)} = \widetilde{Q}^{(a)} = \frac{R_1}{\omega_0^{(a)} L_1}, \quad Q^{(b)} = \widetilde{Q}^{(b)} = \frac{\omega_0^{(b)} L_2}{R_2}, \tag{4.10}$$

while the FBW quality factors equal

$$Q_Z^{(a)} = \kappa^{(a)} Q^{(a)}, \quad Q_Z^{(b)} = \kappa^{(b)} Q^{(b)}, \tag{4.11}$$

where

$$\kappa^{(a)} = \frac{1}{\omega_0^{(a)}\sqrt{L_1 C_1}}, \quad \kappa^{(b)} = \omega_0^{(b)}\sqrt{L_2 C_2}. \tag{4.12}$$

For the sake of completeness, it is useful to indicate that the quality factors proposed by Rhodes [5] are found to be

$$\left|Q_X^{(a)}\right| = \left(\kappa^{(a)}\right)^2 \mathcal{Q}^{(a)}, \quad \left|Q_X^{(b)}\right| = \left(\kappa^{(b)}\right)^2 \mathcal{Q}^{(b)}. \tag{4.13}$$

The comparison of the above-mentioned quality factors is depicted in figure 6 using the parametrization by R_i/L_i and $R_i C_i$, where $i \in \{1, 2\}$. The circuit (a) in figure 5 is resonant for $R_1 C_1 > L_1/R_1$, whilst the circuit (b) in the same figure is resonant for $R_1 C_1 < L_1/R_1$. It can be observed that the difference between the depicted quality factors decreases as the quality factor rises and finally vanishes for $Q \to \infty$. On the other hand, there are significant differences for $Q < 2$.

Therefore, we can conclude that for general RLC circuits made of lumped (non-radiating) elements

$$W_{\text{sto}} \equiv \widetilde{W}_{\text{sto}} \neq W_{\text{sto}}^{\text{FBW}} \Longrightarrow Q \equiv \widetilde{Q} \neq Q_Z. \tag{4.14}$$

5. Radiating structures

The evaluation of the quality factor Q for radiating structures is far more involved than for non-radiating circuits. This is due to the fact that the radiating energy should be subtracted correctly. Hence, the method proposed in §2(a) was implemented according to the flowchart depicted in figure 7.

The evaluation is done in Matlab [57]. The current density $\boldsymbol{\mathcal{J}}\left(\boldsymbol{r}', t\right)$ and the current $i_{\text{R}_0}\left(t\right)$ flowing through the internal resistance of the source are the only input quantities used, see

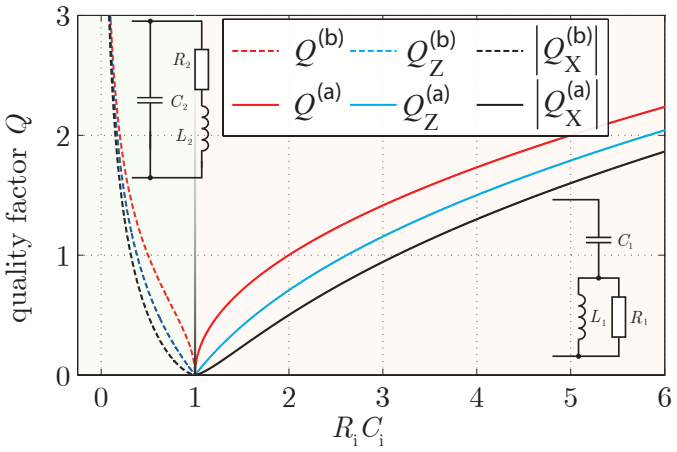

Figure 6. The quality factors for the two particular lumped RLC circuits of figure 5. The curves correspond to $R_i/L_i = 1\,\mathrm{s}^{-1}$, with $i \in \{1, 2\}$.

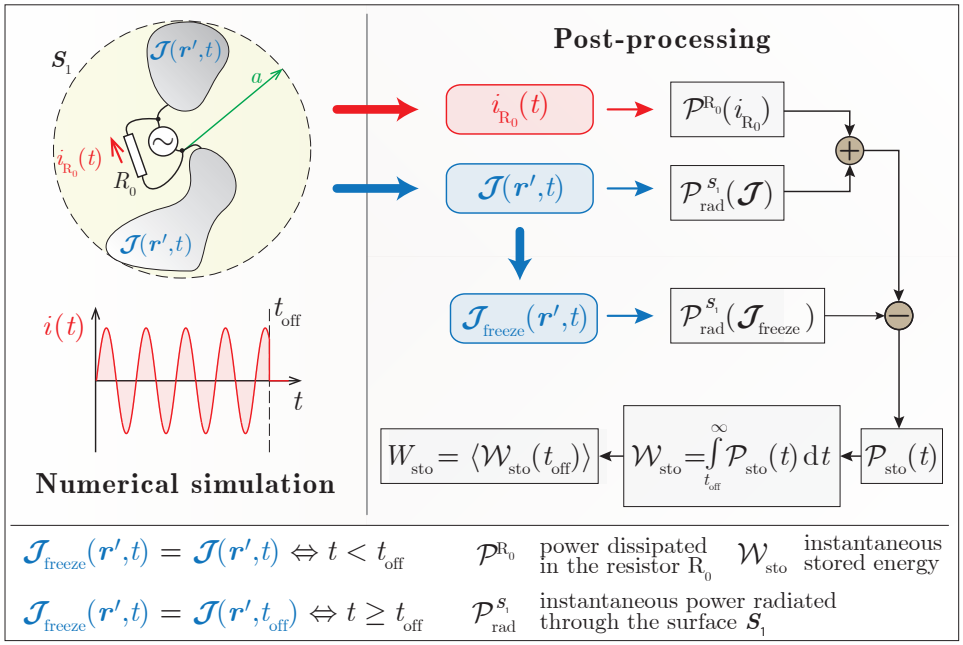

Figure 7. Flowchart of the method proposed in §2(a). The time domain currents are processed according to the right-hand side of the flowchart.

figure 7. In particular cases treated in this section, we utilize the ideal voltage source that invokes $i_{\mathrm{R}_0}(t) \equiv 0$, and thus the first integral in RHS of (2.5) vanishes.

In order to verify the proposed approach, three types of radiators are going to be calculated, namely the centre-fed dipole, off-centre-fed dipole and Yagi-Uda antenna. All these radiators are made of an infinitesimally thin-strip perfect electric conductor and operate in vacuum background. Consequently, the second integral in RHS of (2.5) also vanishes. The quality factor Q calculated with the help of the novel method is going to be compared with the results of two

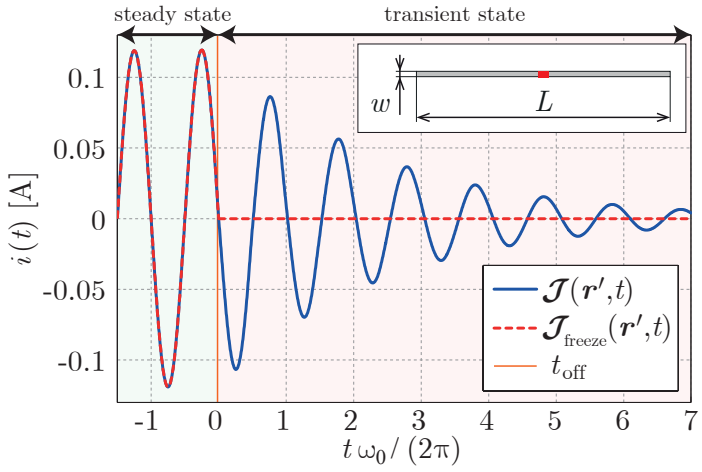

Figure 8. Current flowing through the voltage gap of dipole (exact proportions of the antenna are indicated in the inset). The blue line shows the steady state and the transient state of the original currents $\boldsymbol{\mathcal{J}}(\boldsymbol{r}',t)$, whilst the red line corresponds to the modified currents $\boldsymbol{\mathcal{J}}_{\text{freeze}}(\boldsymbol{r}',t)$. The depicted curves correspond to the source with the voltage $u(t) = U_0 \sin(\omega_0 t)\, H(t_{\text{off}} - t)$, where the U_0 was chosen so that the mean radiated power equals 0.5 W.

remaining classical approaches detailed in §2(b) and §3, which produced the quality factors $\widetilde{Q}$ (2.25) and Q_Z (3.2) respectively.

All essential steps of the method are going to be explained using the example of a centre-fed dipole in §5(a). Subsequently, in §5(b) and §5(c), the method is going to be directly applied to more complicated radiators. The most important properties of the novel method are going to be examined in the subsequent discussion §6.

(a) Centre-fed thin-strip dipole

The first structure to be calculated is a canonical radiator: a dipole of the length L and width $w = L/200$. The dipole is fed by a voltage source [48] located in its centre.

The calculation starts in FEKO commercial software [58] in which the dipole is simulated. The dipole is fed by a unitary voltage and the currents $\boldsymbol{J}(\boldsymbol{r}',\omega)$ are evaluated within the frequency span from $ka = 0$ to $ka \approx 325$ for 8192 samples. The resulting currents are imported into Matlab. We define the normalized time $t_{\text{n}} = t\omega_0/(2\pi)$ (see x-axis of figures 8 and 9), where ω_0 is the angular frequency that the quality factor Q is going to be calculated at. Then iFFT over $S(\omega)\,\boldsymbol{J}(\boldsymbol{r}',\omega)$, see (4.2), is applied, and the time domain currents $\boldsymbol{\mathcal{J}}(\boldsymbol{r}',t)$ with $\Delta t_n = 0.02$ for $t_n \in (0, 163)$ are obtained. The implementation details of iFFT, which must also contain singularity extraction of the source spectrum $S(\omega)$, are not discussed here, as they are not of importance to the method of quality factor calculation itself. The next step consists in the evaluation of (2.8) for both, the original currents $\boldsymbol{J}(\boldsymbol{r}',t)$ and frozen currents $\boldsymbol{J}_{\text{freeze}}(\boldsymbol{r}',t)$, see figure 7.

At this point, it is highly instructive to explicitly show the time course of the current at the centre of the dipole (see figure 8), as well as the time course of the power passing through the surface S_1 in both aforementioned scenarios (original and frozen currents), see figure 9. The source was switched off at $t_{\text{n}} = 0$. During the following transient (blue lines in figure 8 and figure 9), all energy content of the sphere is lost by the radiation. Within the second scenario, with all currents constant for $t \geq t_{\text{off}}$, the radiation of the dipole is instantaneously stopped at $t_{\text{off}} = 0$. The power radiated for $t_{\text{off}} > 0$ (red line in figure 9) then represents the radiation that existed at $t = t_{\text{off}}$ within the sphere, but needed some time to leave the volume. Subtracting the blue and red curves in figure 9 and integrating in time for $t \geq t_{\text{off}}$ then gives the stored energy at

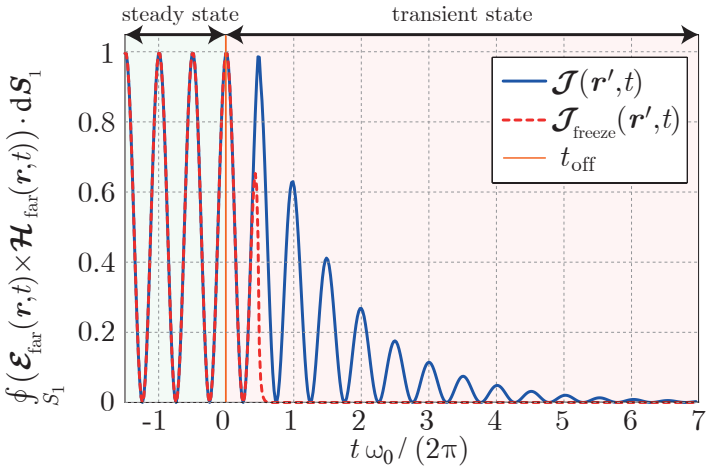

Figure 9. Radiated power passing through the surface $\boldsymbol{S}_1$ for a centre-fed dipole. The meaning of the blue and red lines as well as the normalization of input voltage is the same as in figure 8.

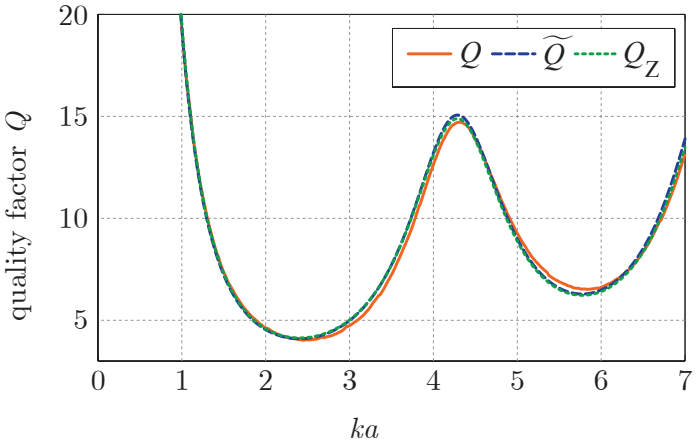

Figure 10. Frequency dependence of the quality factors for a centre-fed dipole.

$t = t_{\text{off}}$. In order to construct the course of $\mathcal{Q}(t_{\text{off}})$, the stored energy is evaluated for six different switch-off times t_{off}. The resulting $\mathcal{Q}(t_{\text{off}})$ is then fitted by

$$\mathcal{Q}(t_{\text{off}}, \omega_0) = A + B\sin(2\omega_0 t_{\text{off}} + \beta). \tag{5.1}$$

The fitting was exact (within the used precision) in all fitted points, which allowed us to consider (5.1) as an exact expression for all t_{off}. The constant A then equals $Q(\omega_0)$.

We are typically interested in the course of Q with respect to the frequency. Repeating the above-explained procedure for varying ω_0, we obtain the red curve in figure 10. In the same figure, the comparison with $\widetilde{Q}$ from §2(b) (blue curve) and Q_Z from §3 (green curve) is depicted. To calculate $\widetilde{Q}$ by means of (2.21), (2.22), (2.19), (2.24) in the frequency domain, we used the currents $\boldsymbol{J}(\boldsymbol{r}', \omega)$ from FEKO and renormalized them with respect to the input current $I_0 = 1$ A. Similarly, the calculation of the FBW quality factor Q_Z (3.2) is performed for the same source currents with identical normalization, and is based on expression (3.7) and all subsequent relations integrated in Matlab.

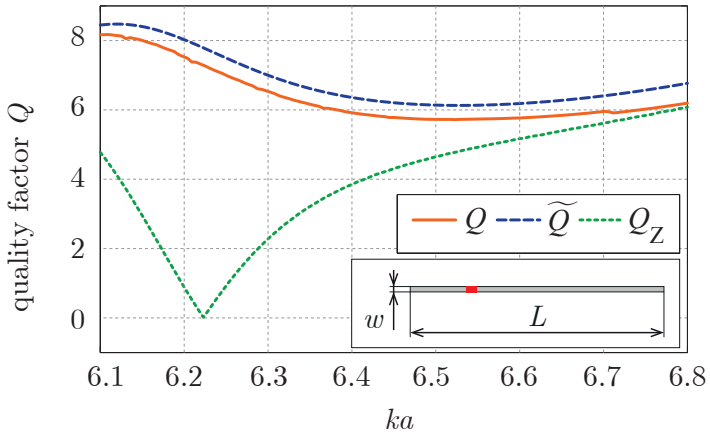

Figure 11. Comparison of all quality factors in the case of off-centre-fed dipole (see the inset for exact proportions of the antenna).

(b) Off-centre-fed thin-strip dipole

The second example is represented by an off-centre-fed dipole, which is known to exhibit the zero value of Q_Z [18], for $ka \approx 6.2$ provided that the delta gap is placed at $0.23L$ from the bottom of the dipole. The dipole has the same parameters as in the previous example, except the position of feeding (see the inset in figure 11).

It is apparent from figure 11 that the quality factor Q based on the new stored energy evaluation does not suffer from drop-off around $ka \approx 6.2$, and in fact yields similar values as $\widetilde{Q}$, including the same trend.

(c) Yagi-Uda antenna

Yagi-Uda antenna was selected as a representative of quite complex structure that the method can ultimately be tested on. The antenna has the same dimensions as in [11] and is depicted in the inset in figure 13. Since this antenna has non-unique phase centre, it can serve as an ideal candidate for verification of the coordinate independence of the novel method. The results were calculated in the same way as in the previous examples, and are indicated in figures 12 and 13. The comparison between the results in figure 12 and those related to the dipole in figure 9 clearly reveals that the transient state is remarkably longer in the case of Yagi-Uda antenna, which means that the longer integration time is required. Furthermore, it can be seen (red curve for $t > t_{\mathrm{off}}$) that the bounding sphere contains a considerable amount of radiation that should be subtracted. The accuracy of this subtraction is embodied in figure 13, which shows the quality factors Q, $\widetilde{Q}$, and Q_Z. Notice the similarity between Q and $\widetilde{Q}$.

6. Discussion

Based on the previous sections, important properties of the novel time domain technique can be isolated and discussed. This discussion also poses new and so far unanswered questions that can be addressed in future.

The coordinate independence / dependence constitutes an important issue of many similar techniques evaluating the stored electromagnetic energy. Contrary to the radiation energy subtraction of Fante [30], Rhodes [31], Yaghjian and Best [11], or Gustafsson and Jonsson [34], the new time-domain method can be proved to be coordinate-independent. It means that the same results are obtained irrespective of the position and rotation of the coordinate system. Due to the

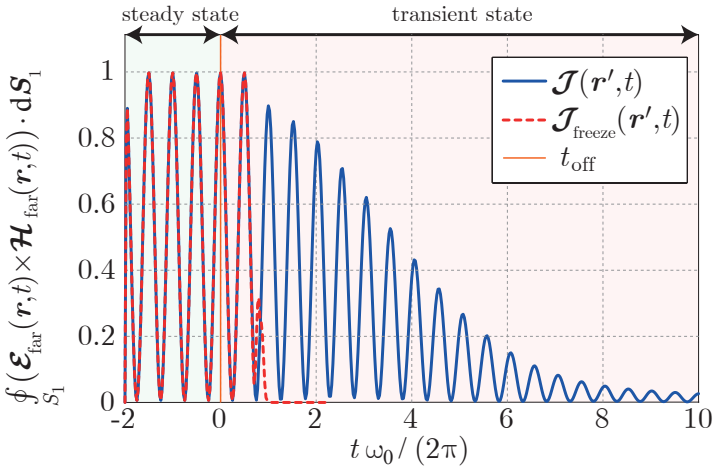

Figure 12. Radiated power passing through the surface $\boldsymbol{S}_1$ in the case of Yagi-Uda antenna. The meaning of the blue and red lines as well as the normalization of input voltage is the same as in figure 8. The antenna proportions are depicted in the inset of figure 13.

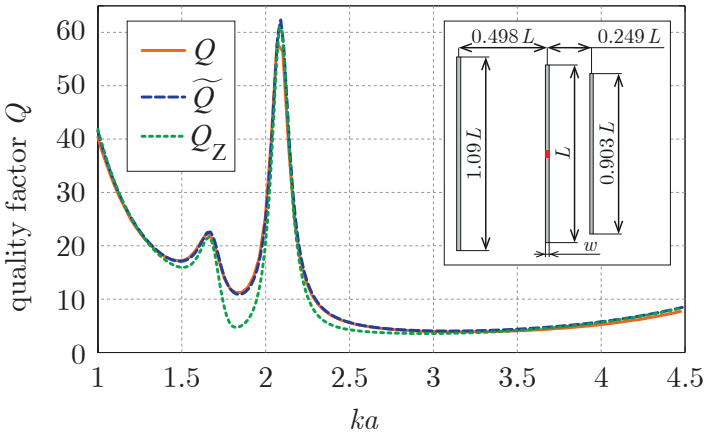

Figure 13. Comparison of all Q factors of Yagi-Uda antenna (antenna proportions are stated in the inset).

explicit reference to coordinates, this statement in question may not be completely obvious from (2.8). However it should be noted that any potential spatial shift or rotation of coordinate system emerges only as a static time shift of the received signal at the capturing sphere. Such static shift is irrelevant to the energy evaluation due to the integration over semi-infinite time interval.

The positive semi-definiteness represents another essential characteristic. It should be immanent in all theories concerning the stored energy. Although (2.8) contains the absolute value, it is difficult to mathematically prove the positive semi-definiteness of the stored energy evaluation as a whole, because it is not automatically granted that the integration during the second run integrates smaller amount of energy than the integration during the first run. Despite that, we can anticipate the expected behaviour from the physical interpretation of the method, which stipulates that the energy integrated in the second run must have been part of the first run as well. At worst, the subtraction of both runs can give null result. This observation is in perfect agreement with the numerical results. Nevertheless, the exact and rigorous proof admittedly remains an unresolved issue that is to be addressed in the future.

Unlike the methods of Fante [30], Rhodes [5] or Collin and Rothschild [26], the obvious benefit of the novel method consists in its ability to account for a shape of the radiator, not being restricted to the exterior of circumscribing sphere.

Finally, it is crucial to realize that the novel method is not restricted to the time-harmonic domain, but can evaluate the stored energy in any general time-domain state of the system. This raises new possibilities for analyzing radiators in the time domain, namely the ultra-wideband radiators and other systems working in the pulse regime.

7. Conclusion

Three different concepts aiming to evaluate the stored electromagnetic energy and the resulting quality factor Q of radiating system were investigated. The novel time domain scheme constitutes the first one, while the second one utilizes time-harmonic quantities and classical radiation energy extraction. The third one is based on the frequency variation of radiator?s input impedance. All methods were subject to in-depth theoretical comparison and their differences were presented on general non-radiating RLC networks as well as common radiators.

It was explicitly shown that the most practical scheme based on the frequency derivative of the input impedance generally fails to give the correct quality factor, but may serve as a very good estimate of it for structures that are well approximated by series or parallel resonant circuits. In contrast, the frequency domain concept with far-field energy extraction was found to work correctly in the case of general RLC circuits and simple radiators. Unlike the newly proposed time domain scheme, it could however yield negative values of stored energy, which is actually known to happen for specific current distributions. In this respect, the novel time domain method proposed in this paper could be denoted as reference, since it exhibits the coordinate independence, positive semi-definiteness, and most importantly, takes into account the actual radiator shape. Another virtue of the novel scheme is constituted by the possibility to use it out of the time-harmonic domain, e.g. in the realm of radiators excited by general pulse.

The follow-up work should focus on the radiation characteristics of separated parts of radiators or radiating arrays, the investigation of different time domain feeding pulses and their influence on performance of ultra-wideband radiators and, last but not least, on the theoretical formulation of the stored energy density generated by the new time domain method.

Data accessibility. This manuscript does not contain primary data and as a result has no supporting material associated with the results presented.

Authors' contributions. All authors contributed to the formulation, did numerical simulations and drafted the manuscript. All authors gave final approval for publication.

Acknowledgements. The authors are grateful to Ricardo Marques (Department of Electronics and Electromagnetism, University of Seville) and Raul Berral (Department of Applied Physics, University of Seville) for many valuable discussions that stimulated some of the core ideas of this contribution. The authors are also grateful to Jan Eichler (Department of Electromagnetic Field, Czech Technical University in Prague) for his help with the simulations.

Funding statement. The authors would like to acknowledge the support of COST IC1102 (VISTA) action and of project 15-10280Y funded by the Czech Science Foundation.

Conflict of interests. We declare to have no competing interests.

References

1 Morse, P. M. & Feshbach, H. 1953 *Methods of Theoretical Physics*. McGraw-Hill.
2 Hallen, E. 1962 *Electromagnetic Theory*. Chapman & Hall.
3 Volakis, J. L., Chen, C. & Fujimoto, K. 2010 *Small Antennas: Miniaturization Techniques & Applications*. McGraw-Hill.
4 Collin, R. E. 1992 *Foundations for Microwave Engineering*. John Wiley - IEEE Press, 2nd edn.

5 Rhodes, D. R. 1976 Observable stored energies of electromagnetic systems. *J. Franklin Inst.*, **302**(3), 225–237. doi:10.1016/0016-0032(79)90126-1.

6 Kajfez, D. & Wheless, W. P. 1986 Invariant definitions of the unloaded Q factor. *IEEE Antennas Propag. Magazine*, **34**(7), 840–841.

7 Harrington, R. F. 1958 On the gain and beamwidth of directional antennas. *IRE Trans. Antennas Propag.*, **6**(3), 219–225. doi:10.1109/TAP.1958.1144605.

8 Standard definitions of terms for antennas 145 - 1993.

9 Foster, R. M. 1924 A reactance theorem. *Bell System Tech. J.*, **3**, 259–267. doi:10.1098/rspa.1977.0018.

10 Harrington, R. F. 2001 *Time-Harmonic Electromagnetic Fields*. John Wiley - IEEE Press, 2nd edn.

11 Yaghjian, A. D. & Best, S. R. 2005 Impedance, bandwidth and Q of antennas. *IEEE Trans. Antennas Propag.*, **53**(4), 1298–1324. doi:10.1109/TAP.2005.844443.

12 Best, S. R. & Hanna, D. L. 2010 A performance comparison of fundamental small-antenna designs. *IEEE Antennas Propag. Magazine*, **52**(1), 47–70. doi:10.1109/MAP.2010.5466398.

13 Sievenpiper, D. F., Dawson, D. C., Jacob, M. M., Kanar, T., Sanghoon, K., Jiang, L. & Quarfoth, R. G. 2012 Experimental validation of performance limits and design guidelines for small antennas. *IEEE Trans. Antennas Propag.*, **60**(1), 8–19. doi:10.1109/TAP.2011.2167938.

14 Capek, M., Jelinek, L., Hazdra, P. & Eichler, J. 2014 The measurable Q factor and observable energies of radiating structures. *IEEE Trans. Antennas Propag.*, **62**(1), 311–318. doi:10.1109/TAP.2013.2287519.

15 Jin, J.-M. 2010 *Theory and Computation of Electromagnetic Fields*. John Wiley.

16 Gustafsson, M. & Nordebo, S. 2006 Bandwidth, Q factor and resonance models of antennas. *Progress In Electromagnetics Research*, **62**, 1–20. doi:10.2528/PIER06033003.

17 Capek, M., Jelinek, L. & Hazdra, P. 2015 On the functional relation between quality factor and fractional bandwidth. *IEEE Trans. Antennas Propag.*, **63**(6), 2787–2790. doi:10.1109/TAP.2015.2414472.

18 Gustafsson, M. & Jonsson, B. L. G. 2015 Antenna Q and stored energy expressed in the fields, currents, and input impedance. *IEEE Trans. Antennas Propag.*, **63**(1), 240–249. doi:10.1109/TAP.2014.2368111.

19 Gustafsson, M., Cismasu, M. & Jonsson, B. L. G. 2012 Physical bounds and optimal currents on antennas. *IEEE Trans. Antennas Propag.*, **60**(6), 2672–2681. doi:10.1109/TAP.2012.2194658.

20 Jackson, J. D. 1998 *Classical Electrodynamics*. John Wiley, 3rd edn.

21 Chu, L. J. 1948 Physical limitations of omni-directional antennas. *J. Appl. Phys.*, **19**, 1163–1175. doi:10.1063/1.1715038.

22 Dirac, P. A. M. 1938 Classical theory of radiating electrons. *Proc. of Royal Soc. A*, **167**, 148–169. doi:10.1098/rspa.1938.0124.

23 Dyson, F. J. 1949 The radiation theories of Tomonaga, Schwinger, and Feynman. *Phys. Rev.*, **75**, 486. doi:10.1103/PhysRev.75.486.

24 Thal, H. L. 1978 Exact circuit analysis of spherical waves. *IEEE Trans. Antennas Propag.*, **26**(2), 282–287. doi:10.1109/TAP.1978.1141822.

25 Thal, H. L. 2012 Q bounds for arbitrary small antennas: A circuit approach. *IEEE Trans. Antennas Propag.*, **60**(7), 3120–3128. doi:10.1109/TAP.2012.2196920.

26 Collin, R. E. & Rothschild, S. 1964 Evaluation of antenna Q. *IEEE Trans. Antennas Propag.*, **12**(1), 23–27. doi:10.1109/TAP.1964.1138151.

27 McLean, J. S. 1996 A re-examination of the fundamental limits on the radiation Q of electrically small antennas. *IEEE Trans. Antennas Propag.*, **44**(5), 672–675.

28 Manteghi, M. 2010 Fundamental limits of cylindrical antennas. Tech. Rep. 1, Virginia Tech.

29 Collin, R. E. 1998 Minimum Q of small antennas. *Journal of Electromagnetic Waves and Applications*, **12**(10), 1369–1393. doi:10.1163/156939398X01457.

30 Fante, R. L. 1969 Quality factor of general ideal antennas. *IEEE Trans. Antennas Propag.*, **17**(2), 151–157. doi:10.1109/TAP.1969.1139411.

31 Rhodes, D. R. 1977 A reactance theorem. *Proc. R. Soc. Lond. A.*, **353**, 1–10. doi:10.1098/rspa.1977.0018.

32 Vandenbosch, G. A. E. 2010 Reactive energies, impedance, and Q factor of radiating structures. *IEEE Trans. Antennas Propag.*, **58**(4), 1112–1127. doi:10.1109/TAP.2010.2041166.

33 Geyi, W. 2003 A method for the evaluation of small antenna Q. *IEEE Trans. Antennas Propag.*, **51**(8), 2124–2129. doi:10.1109/TAP.2003.814755.

34 Gustafsson, M. & Jonsson, B. L. G. 2014 Stored electromagnetic energy and antenna Q. *Prog. Electromagn. Res.*, **150**, 13–27.

35 Vandenbosch, G. A. E. 2013 Reply to "Comments on 'Reactive energies, impedance, and Q factor of radiating structures'". *IEEE Trans. Antennas Propag.*, **61**(12), 6268. doi:10.1109/TAP.2013.2281573.

36 Shlivinski, A. & Heyman, E. 1999 Time-domain near-field analysis of short-pulse antennas - part I: Spherical wave (multipole) expansion. *IEEE Trans. Antennas Propag.*, **47**(2), 271–279. doi:10.1109/8.761066.

37 Shlivinski, A. & Heyman, E. 1999 Time-domain near-field analysis of short-pulse antennas - part II: Reactive energy and the antenna Q. *IEEE Trans. Antennas Propag.*, **47**(2), 280–286. doi:10.1109/8.761067.

38 Collardey, S., Sharaiha, A. & Mahdjoubi, K. 2006 Calculation of small antennas quality factor using FDTD method. *IEEE Antennas Wireless Propag. Lett.*, **5**, 191–194. doi:10.1109/LAWP.2006.873947.

39 Vandenbosch, G. A. E. 2013 Radiators in time domain, part I: Electric, magnetic, and radiated energies. *IEEE Trans. Antennas Propag.*, **61**(8), 3995–4003. doi:10.1109/TAP.2013.2261044.

40 Kaiser, G. 2011 Electromagnetic inertia, reactive energy and energy flow velocity. *J. Phys. A.: Math. Theor.*, **44**, 1–15. doi:10.1088/1751-8113/44/34/345206.

41 Capek, M. & Jelinek, L. 2015 Various interpretations of the stored and the radiated energy density. Submitted, arXiv: 1503.06752.

42 Harrington, R. F. 1960 Effects of antenna size on gain, bandwidth, and efficiency. *J. Nat. Bur. Stand.*, **64-D**, 1–12.

43 Yaghjian, A. D., Gustafsson, M. & Jonsson, B. L. G. 2013 Minimum Q for lossy and losseless electrically small dipole antenna. *Progress In Electromagnetics Research*, **143**, 641–673. doi:10.2528/PIER13103107.

44 Jonsson, B. L. G. & Gustafsson, M. 2015 Stored energies in electric and magnetic current densities for small antennas. *Proc. of Royal Soc. A*, **471**, 1–23. doi:10.1098/rspa.2014.0897.

45 Jelinek, L., Capek, M., Hazdra, P. & Eichler, J. 2015 An analytical evaluation of the quality factor Q_Z for dominant spherical modes. *IET Microw. Antennas Propag.*, **9**(10), 1096–1103. doi:10.1049/iet-map.2014.0302. ArXiv: 1311.1750v1.

46 Capek, M., Hazdra, P. & Eichler, J. 2012 A method for the evaluation of radiation Q based on modal approach. *IEEE Trans. Antennas Propag.*, **60**(10), 4556–4567. doi:10.1109/TAP.2012.2207329.

47 Gustafsson, M. & Nordebo, S. 2013 Optimal antenna currents for Q, superdirectivity, and radiation patterns using convex optimization. *IEEE Trans. Antennas Propag.*, **61**(3), 1109–1118. doi:10.1109/TAP.2012.2227656.

48 Balanis, C. A. 1989 *Advanced Engineering Electromagnetics*. John Wiley.

49 Balanis, C. A. 2005 *Antenna Theory Analysis and Design*. John Wiley, 3rd edn.

50 Akhiezer, N. I. & Glazman, I. M. 1993 *Theory of Linear Operators in Hilbert Space*. Dover, 2nd edn.

51 Morgenthaler, F. R. 2011 *The Power and Beauty of Electromagnetic Fields*. Wiley-IEEE Press.

52 Carpenter, C. J. 1989 Electromagnetic energy and power in terms of charges and potentials instead of fields. *Proc. of IEE A*, **136**(2), 55–65.

53 Uehara, M., Allen, J. E. & Carpenter, C. J. 1992 Comments to 'Electromagnetic energy and power in terms of charges and potentials instead of fields'. *Proc. of IEE A*, **139**(1), 42–44.

54 Endean, V. G. & Carpenter, C. J. 1992 Comments to 'Electromagnetic energy and power in terms of charges and potentials instead of fields'. *Proc. of IEE A*, **139**(6), 338–342.

55 Jelinek, L., Capek, M., Hazdra, P. & Eichler, J. 2014 Lower bounds of the quality factor Q_Z. In *IEEE International Symposium on Antennas and Propagation and USNC-URSI Radio Science Meeting*. Accepted.

56 Rothwell, E. J. & Cloud, M. J. 2001 *Electromagnetics*. CRC Press.

57 The MathWorks 2015 The Matlab.

58 EM Software & Systems-S.A. FEKO.

V

M. Capek and L. Jelinek, "Various interpretations of the stored and the radiated energy density," 2015, submitted, arXiv: 1503.06752. [46∗]

Various Interpretations of the Stored and the Radiated Energy Density

Miloslav Capek, *Member, IEEE,* and Lukas Jelinek

***Abstract*—Three contradictory but state-of-the-art concepts for defining and evaluating stored electromagnetic energy are treated in this communication, and are collated with the widely accepted definition of stored energy, which is the total energy minus the radiated energy. All three concepts are compared, and the results are discussed on an example of a dominant spherical mode, which is known to yield dissimilar results for the concepts dealt with here. It is shown that various definitions of stored energy density immanently imply diverse meanings of the term "radiation".**

***Index Terms*—Antenna theory, electromagnetic theory, electrically small antennas, Q factor.**

I. Introduction

The evaluation of stored electromagnetic energy and its density is one of the old but as yet unsolved problems of classical electromagnetism. This is true despite its straightforward and generally accepted definition: stored electromagnetic energy is that part of the total electromagnetic energy that is, in comparison with the radiated energy, bound to the sources of the field, being unable to escape towards infinity. In other words, the stored electromagnetic energy is the difference between the total and the radiated electromagnetic energies, representing a "rest mass" seen by the force exerted by the source.

In the case of a static field and a quasi-static field, the evaluation of the stored energy is immediate, as it is just equal to the total energy [1], the physical interpretation of which is directly inferred from Poynting's theorem [1]. The problem arises for fields generated by general radiators. One of the core problems is that within the time harmonic steady state, the total energy is infinite [1]. This infinite energy is contained in the radiation field, and the goal of the evaluation of the stored energy is to subtract this infinite radiation energy. The second problem is that Poynting's theorem gives us no clue of what radiation energy really is. One can only rely on some general properties like the positive semi-definiteness of the energy, and the fact that the far field of the radiator placed in the lossless media carries solely radiation energy [2].

Probably the first treatment of stored electromagnetic energy dates back to the work of Bateman [3], who pointed out that the electromagnetic energy in a vacuum does not in general move with the speed of light in a vacuum, being slowed down by a kind of "rest mass". This "rest mass" vanishes only in the case of pure radiation fields, i.e. only at an infinite distance from a finite source. This work has however been forgotten and it was not until recent years that it was recovered and generalized by Kaiser [4], into the form of stored electromagnetic energy density.

Manuscript received XXX, 2015; revised XXX, 2015. This work was supported by the Czech Science Foundation under project No. 15-10280Y

M. Capek and L. Jelinek are with the Department of Electromagnetic Field, Faculty of Electrical Engineering, Czech Technical University in Prague, Technicka 2, 16627, Prague, Czech Republic (e-mail: miloslav.capek@fel.cvut.cz, lukas.jelinek@fel.cvut.cz).

In parallel, the problem of stored energy has also been extensively studied in the community of electrical engineering, mostly in connection with antennas. In particular, antenna designers commonly aim at the lowest energy storage in order to maximize the radiation efficiency of an antenna, and for this purpose one actually encounters the problem of stored energy evaluation [5]. To that point, Chu [6] proposed a circuit equivalent of the spherical modes, and with its help subtracted the radiation energy and established fundamental lower bounds of the radiation quality factor. His method has been generalized by several works of Thal [7], [8], [9]. Radiation energy subtraction has also been attempted directly on the field level. Among the most prominent works we mention [10], [11], [12], [13], [14], and also [15], in which subtraction is taken from another point of view, claiming that separation of total energy into stored energy and radiated energy is unphysical, as it cannot be derived from Maxwell's equations.

The works of Bateman [3], Kaiser [4], and Collin [11] attempted to define stored energy locally via its density, while the works of Rhodes [16], Yaghjian and Best [17], Vandenbosch [14], and Gustafsson and Jonsson [18] operated solely with stored energy as a whole. The local approach however offers certain benefits: first, radiation energy extraction is carried out at every space-time point, avoiding cumbersome operations with ill-defined infinite space integrations [14], and second, the definition via the density is also more physical, as within classical relativistic theory all laws should be formulated strictly locally.

The concepts mentioned above yield similar values of stored energy for common radiators. However, there exist specific cases for which the methods are profoundly different. One such case is the dominant TE spherical mode, which has been shown to lead to apparently incorrect negative stored energies within some evaluation schemes [19].

This paper has two main purposes: to compare different interpretations of radiated energy, and to recall the possibility of a local definition of stored energy, which, despite its appealing properties, has not found its place within the antenna community.

The paper is organized as follows. The necessary definitions and nomenclature are introduced in Sec. II. Sec. III recalls several radiation energy extraction techniques. The techniques are compared on an example of the dominant spherical mode in Sec. IV. The results are discussed in Sec. V. Conclusions are drawn in Sec. VI.

II. Definitions

In this paper, we will strictly omit dispersive media, in which the concept of stored energy is problematic, even without radiation [20]. Furthermore, as is common in the theory of electromagnetic radiators, this paper will deal with time harmonic fields represented by field phasors $\boldsymbol{F}(\boldsymbol{r},\omega)$ at angular frequency ω, which relates to the time domain quantities as $\boldsymbol{\mathcal{F}}(\boldsymbol{r},t) = \mathrm{Re}\left\{\boldsymbol{F}(\boldsymbol{r},\omega)\exp(\mathrm{j}\omega t)\right\}$. We will also use cycle mean averages, which are defined as $\langle f(t)\rangle = (1/T)\int_{t_0}^{t_0+T} f(t)\,\mathrm{d}t$, with $T = 2\pi/\omega$, and are widely employed in the case of power quantities, where

$\langle \boldsymbol{\mathcal{F}}(\boldsymbol{r},t)\cdot\boldsymbol{\mathcal{G}}(\boldsymbol{r},t)\rangle = (1/2)\,\mathrm{Re}\{\boldsymbol{F}(\boldsymbol{r},\omega)\cdot\boldsymbol{G}^{*}(\boldsymbol{r},\omega)\}$ within the time harmonic domain [21], and in which symbol $*$ denotes complex conjugate. Note, however, that the results detailed below and summarized in Table I hold for a general time domain field.

For the purpose of comparing various concepts of stored energy, we will advantageously use a dimensionless quality factor, defined as

$$Q = \frac{\omega W_{\mathrm{sto}}}{P_{\mathrm{r}}}, \tag{1}$$

where

$$W_{\mathrm{sto}} = \int_{V} \langle w_{\mathrm{sto}}(\boldsymbol{r},t)\rangle \,\mathrm{d}V \tag{2}$$

is the total cycle mean stored energy, defined via its density $w_{\mathrm{sto}}(\boldsymbol{r},t)$, and where

$$\begin{aligned} P_{\mathrm{r}} &= \oiint_{S} \langle \boldsymbol{\mathcal{E}}(\boldsymbol{r},t)\times\boldsymbol{\mathcal{H}}(\boldsymbol{r},t)\rangle\cdot\,\mathrm{d}\boldsymbol{S} \\ &= \frac{1}{2}\oiint_{S}\mathrm{Re}\{\boldsymbol{E}(\boldsymbol{r},\omega)\times\boldsymbol{H}^{*}(\boldsymbol{r},\omega)\}\cdot\,\mathrm{d}\boldsymbol{S} \end{aligned} \tag{3}$$

is the cycle mean radiated power [1].

III. Various Definitions of Stored Energy Density and Radiated Energy Density

This section briefly reviews three major definitions of stored electromagnetic energy density used in the literature. The three concepts are summarized in Table I, and their general properties are discussed in the following section.

A. The Concept of Collin-Rothschild

The classical scheme for radiation energy extraction was defined by Collin and Rothschild in [10], and was later refined in [11] into the form of energy density exposed in the first column of Table I. The corresponding cycle mean energy density for a time harmonic field can also easily be written as

$$\begin{aligned} \langle w_{\mathrm{sto}}^{\mathrm{CR}}(\boldsymbol{r},\omega)\rangle =& \frac{1}{4}\left(\epsilon\|\boldsymbol{E}(\boldsymbol{r},\omega)\|^{2}+\mu\|\boldsymbol{H}(\boldsymbol{r},\omega)\|^{2}\right) \\ &-\frac{1}{2c_0}\mathrm{Re}\{\boldsymbol{E}(\boldsymbol{r},\omega)\times\boldsymbol{H}^{*}(\boldsymbol{r},\omega)\}\cdot\mathbf{n}_0, \end{aligned} \tag{4}$$

where $\boldsymbol{n}_0$ is the normal to the far field wave-front.

This radiation energy extraction is the most common method used in the literature [5], despite its immediate deficiency of using $\boldsymbol{n}_0$ as the direction of the power flow. This poses no problem for specific geometries (pure modes in separable coordinate systems), but cannot suffice in general. Any general radiator will clearly in its near field emit radiation in directions different from the far field.

For the sake of comparison, the quantity

$$Q^{\mathrm{RC}} = \frac{\omega W_{\mathrm{sto}}^{\mathrm{RC}}}{P_{\mathrm{r}}} \tag{5}$$

is defined as advantageously normalized total stored energy within this concept.

B. The Concept of Kaiser-Bateman

A very interesting way of evaluating stored energy was proposed by Kaiser [4], generalizing the previous work of Bateman [3]. Within this concept, the relativistic energy-momentum relation [1] is used to define the stored energy density exposed in the second row of Table I.

To the best of the authors' knowledge, this is the first time that stored energy density has been defined strictly locally with no reference to the position of the sources, i.e. radiation energy extraction is carried out locally at every point of the space-time.

Using time harmonic fields, the cycle mean stored energy within this concept can be written explicitly as

$$\langle w_{\mathrm{sto}}^{\mathrm{KB}}(\boldsymbol{r},t)\rangle = \left\langle \sqrt{U^{2}(\boldsymbol{r},t)-W_{\mathrm{rad}}^{2}(\boldsymbol{r},t)}\right\rangle, \tag{6}$$

in which

$$\begin{aligned} U^{2}(\boldsymbol{r},t)-W_{\mathrm{rad}}^{2}(\boldsymbol{r},t) =& \frac{1}{16}\Big(\epsilon\|\boldsymbol{E}(\boldsymbol{r},\omega)\|^{2}+\mu\|\boldsymbol{H}(\boldsymbol{r},\omega)\|^{2} \\ &+\frac{1}{2}\mathrm{Re}\Big\{\big(\epsilon\boldsymbol{E}(\boldsymbol{r},\omega)\cdot\boldsymbol{E}(\boldsymbol{r},\omega) \\ &+\mu\boldsymbol{H}(\boldsymbol{r},\omega)\cdot\boldsymbol{H}(\boldsymbol{r},\omega)\big)\mathrm{e}^{2\mathrm{j}\omega t}\Big\}\Big)^{2} \\ &-\frac{1}{4}\left\|\frac{1}{c_0}\big(\mathrm{Re}\{\boldsymbol{E}(\boldsymbol{r},\omega)\times\boldsymbol{H}^{*}(\boldsymbol{r},\omega)\} \right. \\ &\left.+\mathrm{Re}\left\{\boldsymbol{E}(\boldsymbol{r},\omega)\times\boldsymbol{H}(\boldsymbol{r},\omega)\,\mathrm{e}^{2\mathrm{j}\omega t}\right\}\big)\right\|^{2} \end{aligned} \tag{7}$$

with the corresponding quality factor

$$Q^{\mathrm{KB}} = \frac{\omega W_{\mathrm{sto}}^{\mathrm{KB}}}{P_{\mathrm{r}}}. \tag{8}$$

Two crucial differences immediately appear when comparing (4) and (6). First, in (6) the entire power flow is subtracted from the field energy, while in (4) only the power flow along the direction of wave-front at infinity is subtracted. Second, in (6) the subtraction in done is squares, while in (4) the subtraction is direct. As a result of the squared subtraction in (7), the cycle mean cannot be simply performed a priori.

With respect to this concept of Kaiser-Bateman, it is worth mentioning a situation in which the general time domain definition, see Table I, can be greatly simplified [4]. This happens in the case when $\boldsymbol{\mathcal{E}}(\boldsymbol{r},t)\cdot\boldsymbol{\mathcal{H}}(\boldsymbol{r},t)=0$, which is the case for the example in this paper, and it is not rare even in realistic situations (at least in an approximate sense). Under this specific condition, the definition from the second row of Table I can be rewritten as

$$w_{\mathrm{sto}}^{\mathrm{KB}}(\boldsymbol{r},t) = \frac{1}{2}\left|\epsilon\|\boldsymbol{\mathcal{E}}(\boldsymbol{r},t)\|^{2}-\mu\|\boldsymbol{\mathcal{H}}(\boldsymbol{r},t)\|^{2}\right| \tag{9}$$

which is a rather curious form. Not being the absolute value, (9) would correspond to the energy excess appearing in the complex Poynting's theorem [1]. The absolute value, however, makes it (according to Kaiser and Bateman) the stored energy density.

TABLE I
VARIOUS CONCEPTS OF EXTRACTION AND SUBTRACTION OF RADIATED ENERGY.

Concept	$\mathcal{W}_{\mathrm{sto}}(\boldsymbol{r},t)$	$\mathcal{W}_{\mathrm{rad}}(\boldsymbol{r},t)$
Collin and Rothschild [10]	$\mathcal{U}(\boldsymbol{r},t)-\mathcal{W}_{\mathrm{rad}}(\boldsymbol{r},t)$	$\frac{\boldsymbol{\mathcal{S}}(\boldsymbol{r},t)}{c_0}\cdot\mathbf{n}_0$
Kaiser [4], Bateman [3]	$\sqrt{\mathcal{U}^2(\boldsymbol{r},t)-\mathcal{W}^2_{\mathrm{rad}}(\boldsymbol{r},t)}$	$\left\|\frac{\boldsymbol{\mathcal{S}}(\boldsymbol{r},t)}{c_0}\right\|$
Rhodes [16], Yaghjian and Best [17], Vandenbosch [14], Gustafsson and Jonsson [18]	$\mathcal{U}(\boldsymbol{r},t)-\mathcal{W}_{\mathrm{rad}}(\boldsymbol{r},t)$	$\epsilon_0\frac{\\|\boldsymbol{\mathcal{F}}(\boldsymbol{r},t)\\|^2}{r^2}$
$\mathcal{U}(\boldsymbol{r},t)=\frac{1}{2}\epsilon_0\\|\boldsymbol{\mathcal{E}}(\boldsymbol{r},t)\\|^2+\frac{1}{2}\mu_0\\|\boldsymbol{\mathcal{H}}(\boldsymbol{r},t)\\|^2,\quad \boldsymbol{\mathcal{S}}(\boldsymbol{r},t)=\boldsymbol{\mathcal{E}}(\boldsymbol{r},t)\times\boldsymbol{\mathcal{H}}(\boldsymbol{r},t),\quad \boldsymbol{\mathcal{F}}(\boldsymbol{r},t)=\lim_{r\to\infty}\left(r\boldsymbol{\mathcal{E}}\left(\boldsymbol{r},t+\frac{r}{c_0}\right)\right)$		

C. The Concept of Rhodes

Another well-established scheme for stored energy evaluation was used by Rhodes [16], was generalized by Yaghjian [17] and was later reworked into the source concept by Vandenbosh [14] for radiators of arbitrary shape. The definition of stored energy density within this concept is exposed in the third row of Table I. The formula can also easily be rewritten for time harmonic fields as

$$\langle w^{\mathrm{Rh}}_{\mathrm{sto}}(\boldsymbol{r},t)\rangle = \frac{1}{4}\left\langle \epsilon\left\|\boldsymbol{E}(\boldsymbol{r},\omega)\right\|^2+\mu\left\|\boldsymbol{H}(\boldsymbol{r},\omega)\right\|^2-2\epsilon\frac{\left\|\boldsymbol{F}\right\|^2}{r^2}\right\rangle, \tag{10}$$

in which $\boldsymbol{F}=\lim_{r\to\infty}(r\boldsymbol{E}\exp(\mathrm{j}kr))$. The corresponding normalization is defined as

$$Q^{\mathrm{Rh}}=\frac{\omega W^{\mathrm{Rh}}_{\mathrm{sto}}}{P_{\mathrm{r}}}. \tag{11}$$

IV. Stored Energy and Its Density For the Dominant Spherical TE Mode

The dominant spherical TE mode is defined as the field generated by the current density [1]

$$\boldsymbol{J}(\vartheta,a)=\frac{\sin(\vartheta)}{2a}\delta(r-a)\boldsymbol{\varphi}_0, \tag{12}$$

flowing on a spherical shell of radius a, see Fig. 1, and it provides interesting testing grounds for stored energy evaluation [18]. The fields generated by this source read [22] for $r<a$

$$\boldsymbol{E}=-\frac{\mu\omega}{2}ka\,\mathrm{h}^{(2)}_1(ka)\,\mathrm{j}_1(kr)\sin(\vartheta)\boldsymbol{\varphi}_0, \tag{13a}$$

$$\boldsymbol{H}=\mathrm{j}k\frac{ka\,\mathrm{h}^{(2)}_1(ka)}{kr}\Big(-\mathrm{j}_1(ka)\cos(\vartheta)\mathbf{r}_0+\frac{kr\,\mathrm{j}_0(kr)-\mathrm{j}_1(kr)}{2}\sin(\vartheta)\boldsymbol{\vartheta}_0\Big), \tag{13b}$$

and for $r\geq a$

$$\boldsymbol{E}=-\frac{\mu\omega}{2}ka\,\mathrm{j}_1(ka)\,\mathrm{h}^{(2)}_1(kr)\sin(\vartheta)\boldsymbol{\varphi}_0, \tag{14a}$$

$$\boldsymbol{H}=\mathrm{j}k\frac{ka\,\mathrm{j}_1(ka)}{kr}\Big(-\mathrm{h}^{(2)}_1(ka)\cos(\vartheta)\mathbf{r}_0+\frac{kr\,\mathrm{h}^{(2)}_0(kr)-\mathrm{h}^{(2)}_1(kr)}{2}\sin(\vartheta)\boldsymbol{\vartheta}_0\Big), \tag{14b}$$

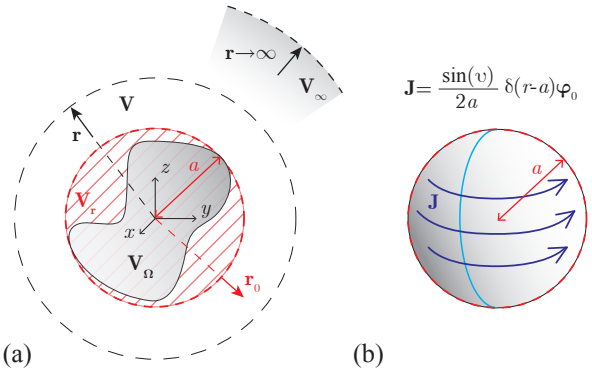

Fig. 1. Sketch of the coordinate system that is used throughout the paper (a) and a sketch of the TE_{10} current on a spherical shell of radius a. (b) The input current is normalized to $I_0=1\,\mathrm{A}$ with respect to the light blue contour.

where $k=\omega/c_0$ is the free space wave-number and c_0 is the speed of light.

The total energy of the fields W^{tot} (in the form of the corresponding quality factor) can be evaluated in a straightforward manner as

$$Q^{\mathrm{tot}}=\frac{\omega W^{\mathrm{tot}}}{P_{\mathrm{r}}}=Q^{\mathrm{tot}}_{\mathrm{int}}+Q^{\mathrm{tot}}_{\mathrm{ext}} \tag{15}$$

with

$$\begin{aligned}Q^{\mathrm{tot}}_{\mathrm{int}}&=\frac{\omega W^{\mathrm{tot}}_{\mathrm{int}}}{P_{\mathrm{r}}}=\int_0^{ka}Q^{\mathrm{tot}}_{\mathrm{int}}(kr)\,\mathrm{d}kr\\&=\frac{1}{2}\frac{\left|h^{(2)}_1(ka)\right|^2}{j^2_1(ka)}\int_0^{ka}\Big((kr)^2\left|j_1(kr)\right|^2+2\left|j_1(kr)\right|^2\\&\quad+\left|kr\,j_0(kr)-j_1(kr)\right|^2\Big)\mathrm{d}kr,\end{aligned} \tag{16a}$$

$$\begin{aligned}Q^{\mathrm{tot}}_{\mathrm{ext}}&=\frac{\omega W^{\mathrm{tot}}_{\mathrm{ext}}}{P_{\mathrm{r}}}=\int_{ka}^{\infty}Q^{\mathrm{tot}}_{\mathrm{ext}}(kr)\,\mathrm{d}kr\\&=\frac{1}{2}\int_{ka}^{\infty}\Big((kr)^2\left|h^{(2)}_1(kr)\right|^2+2\left|h^{(2)}_1(kr)\right|^2\\&\quad+\left|kr\,h^{(2)}_0(kr)-h^{(2)}_1(kr)\right|^2\Big)\mathrm{d}kr,\end{aligned} \tag{16b}$$

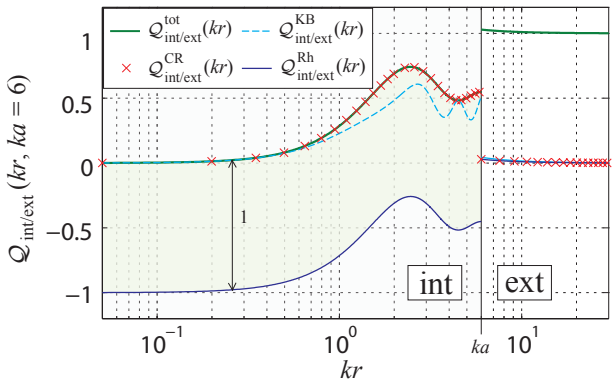

Fig. 2. The normalized total energy density and the normalized stored energy density of the spherical TE_{10} mode for $ka = 6$. Several approaches to obtain the stored energy density are depicted. The energy jump is given by the presence of the current shell at $r = a$. The surface of the shaded area is equal to ka, which is in exact correspondence with [18].

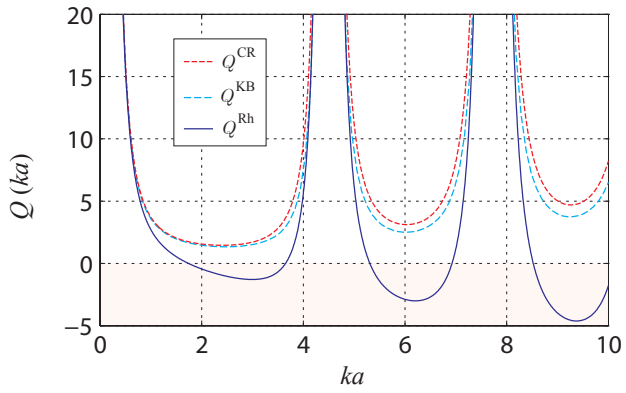

Fig. 3. The normalized total energy and the normalized stored energy as a function of ka. Several approaches to obtain the stored energy are depicted.

where subscript "int" denotes energies for $r < a$ and subscript "ext" denotes the energies for $r \geq a$. The integration in (16a)–(16b) can be carried out analytically (though it will lead to $Q^{\rm tot}_{\rm ext} \to \infty$), but we rather leave out the possibility to study the radial energy density represented by $Q\,(kr)$.

Similarly, we can evaluate the stored energy and its radial density within the scheme of Collin-Rothschild, Kaiser-Bateman and Rhodes as

$$Q^{\rm CR/KB/Rh} = Q^{\rm CR/KB/Rh}_{\rm int} + Q^{\rm CR/KB/Rh}_{\rm ext} \tag{17}$$

with

$$Q^{\rm CR/KB/Rh}_{\rm int} = \int_0^{ka} \mathcal{Q}^{\rm CR/KB/Rh}_{\rm int}\,(kr)\;{\rm d}kr, \tag{18a}$$

$$Q^{\rm CR/KB/Rh}_{\rm ext} = \int_{ka}^{\infty} \mathcal{Q}^{\rm CR/KB/Rh}_{\rm ext}\,(kr)\;{\rm d}kr. \tag{18b}$$

The densities $\mathcal{Q}^{\rm tot}_{\rm int}\,(kr)$, $\mathcal{Q}^{\rm tot}_{\rm ext}\,(kr)$, $\mathcal{Q}^{\rm CR/KB/Rh}_{\rm int}\,(kr)$, and $\mathcal{Q}^{\rm CR/KB/Rh}_{\rm ext}\,(kr)$ are depicted for $ka = 6$ in Fig. 2, while the $Q^{\rm tot}$ and $Q^{\rm CR/KB/Rh}$ are depicted in Fig. 3 as functions of ka.

V. Discussion

There are several important observations in Table I, Fig. 2 and Fig. 3 that will be discussed separately in the following subsections.

A. Over-subtraction

The curves in Fig. 2 reveal that radiation energy subtraction inside the circumscribing sphere brings serious issues, the significance of which will grow with the electrical size of the radiator.

Particularly, there is an observable difference between the stored energy density of Collin-Rothschild and that of Kaiser-Bateman. While the scheme of Collin-Rothschild does not subtract any radiation energy in the internal region (the power flow in the radial direction is strictly zero), the scheme of Kaiser-Bateman subtracts the entire Poynting's vector there, which is indeed non-zero also inside the sphere. A comparison of the stored energy density in Kaiser-Bateman's scheme with the total energy density reveals that there is an energy loss in the internal region provided by angular components of the Poynting's vector. This energy is however not radiated out of the sphere. This subtraction is clearly incorrect, as it will also be performed in the case of a spherical cavity, which does not contain radiation, at least not in the classical sense of an energy reaching infinity.

A different form of over-subtraction also burdens the scheme of Rhodes, but some care should be taken with the different interpretation of this scheme by various authors, namely, Rhodes [16], Yaghjian and Best [17], Vandenbosch [14], and Gustafsson [18]. In particular, Rhodes [16] divides the entire space similarly as in this paper, see (17), thus obtaining the internal stored energy and the external stored energy. Radiation subtraction according to the third row of Table I is used only in the external region, making this scheme identical to the scheme of Collin-Rothschild [10]. By contrast, Gustafsson's approach [18] uses subtraction everywhere, but adds ka to the resulting stored energy, which for spherical radiators gives the same result as the method of Collin-Rothschild, thought it generally differs. Finally, the approach of Yaghjian and Best [17] and the approach of Vandebosch [14] use subtraction everywhere, with no further compensation. This leads to over-subtraction of the order ka in normalized scale that is used.

B. Positive semi-definiteness

Figure 2 and Fig. 3 show that the stored energy density and the total stored energy are both positively semi-definite within the scheme of Collin-Rothschild and Kaiser-Bateman. In fact, the scheme of Kaiser-Bateman is manifestly positively semi-definite [4], and general positive semi-definiteness can also be expected from the scheme of Collin-Rothschild [11].

By contrast, the scheme of Rhodes within the paradigm of Yaghjian, Best and Vandebosch can lead to negative stored energies, which is clearly unphysical, see also [19]. This issue however comes as no surprise when we realize that

for a current distribution independent of frequency (the case presented in this paper), the aforementioned stored energy can be expressed as [23]

$$W_{\mathrm{sto}}^{\mathrm{Rh}} = -\frac{1}{4}\frac{\partial}{\partial\omega}\Im\left\{\int_V \boldsymbol{E}\cdot\boldsymbol{J}^*\,\mathrm{d}V\right\} \propto \frac{\partial X\left(\omega\right)}{\partial\omega}\left|I_0\right|^2, \quad (19)$$

where X is the reactance seen by the sources of the field, where I_0 corresponds to the appropriate current normalization, and where $\partial X/\partial\omega$ is well known to reach negative values in radiating systems [24]. The source of this negativity problem is clearly over-subtraction of the radiation energy, see Fig. 2.

C. Coordinate dependence

One of the basic requirements on a valid physical quantity is its independence from an absolute coordinate system. Unfortunately, this is not satisfied in the case of the first and the third line of Table I, where the radiation energy definition explicitly refers to absolute coordinates. A change of the coordinate origin then leads to a change in the value of the radiated and stored energy, which contradicts the idea of energy storage being a property of the radiator. This problem of the scheme of Rhodes is in fact well known, and some ways of minimizing it have already been published [17], [18]

VI. Conclusion

This communication has reviewed and discussed three up-to-date concepts of stored electromagnetic energy density. It has been shown on a particular example that, although sound, all three concepts yield results that to a certain degree contradict physical reality. It has been shown that the problems result from an improper definition of radiated energy density. Particularly, the concepts that have been discussed failed at least in some of the following prerequisites for a physically meaningful definition, which should

- be strictly local,
- be coordinate independent,
- be gauge invariant,
- give a positively semi-definite energy density,
- give a zero value everywhere in a closed cavity.

As a result, the correct definition of radiated energy density remains an open question, despite its long history and despite being a fundamental question in the classical theory of electrodynamics.

References

[1] J. D. Jackson, *Classical Electrodynamics*, 3rd ed. John Wiley, 1998.

[2] J. Schwinger, L. L. DeRaad, K. A. Milton, and T. W.-y., *Classical Electrodynamics*. Westview Press, 1998.

[3] H. Bateman, *The mathematical analysis of electrical and optical wave-motion on the basis of Maxwell's equations*. Forgotten Books, 2010.

[4] G. Kaiser, "Electromagnetic inertia, reactive energy and energy flow velocity," *J. Phys. A.: Math. Theor.*, vol. 44, pp. 1–15, 2011.

[5] J. L. Volakis, C. Chen, and K. Fujimoto, *Small Antennas: Miniaturization Techniques & Applications*. McGraw-Hill, 2010.

[6] L. J. Chu, "Physical limitations of omni-directional antennas," *J. Appl. Phys.*, vol. 19, pp. 1163–1175, 1948.

[7] H. L. Thal, "New radiation Q limits for spherical wire antennas," *IEEE Trans. Antennas Propag.*, vol. 54, no. 10, pp. 2757–2763, Oct. 2006.

[8] ——, "Polarization, gain, and Q for small antennas," *IEEE Trans. Antennas Propag.*, vol. 59, no. 12, pp. 4844–4848, Dec. 2011.

[9] ——, "Q bounds for arbitrary small antennas: A circuit approach," *IEEE Trans. Antennas Propag.*, vol. 60, no. 7, pp. 3120–3128, July 2012.

[10] R. E. Collin and S. Rothschild, "Evaluation of antenna Q," *IEEE Trans. Antennas Propag.*, vol. 12, no. 1, pp. 23–27, Jan. 1964.

[11] R. E. Collin, "Minimum Q of small antennas," *Journal of Electromagnetic Waves and Applications*, vol. 12, no. 10, pp. 1369–1393, 1998.

[12] D. R. Rhodes, "On the stored energy of planar apertures," *IEEE Trans. Antennas Propag.*, vol. 14, no. 6, pp. 676–684, Nov. 1966.

[13] ——, "A reactance theorem," *Proc. R. Soc. Lond. A.*, vol. 353, pp. 1–10, Feb. 1977.

[14] G. A. E. Vandenbosch, "Reactive energies, impedance, and Q factor of radiating structures," *IEEE Trans. Antennas Propag.*, vol. 58, no. 4, pp. 1112–1127, Apr. 2010.

[15] S. M. Mikki and Y. Antar, "A theory of antenna electromagnetic near field – part I," *IEEE Trans. Antennas Propag.*, vol. 59, no. 12, pp. 4691–4705, Dec. 2011.

[16] D. R. Rhodes, "Observable stored energies of electromagnetic systems," *J. Franklin Inst.*, vol. 302, no. 3, pp. 225–237, 1976.

[17] A. D. Yaghjian and S. R. Best, "Impedance, bandwidth and Q of antennas," *IEEE Trans. Antennas Propag.*, vol. 53, no. 4, pp. 1298–1324, April 2005.

[18] M. Gustafsson and B. L. G. Jonsson, "Stored electromagnetic energy and antenna Q," *Prog. Electromagn. Res.*, vol. 150, pp. 13–27, 2014.

[19] M. Gustafsson, M. Cismasu, and B. L. G. Jonsson, "Physical bounds and optimal currents on antennas," *IEEE Trans. Antennas Propag.*, vol. 60, no. 6, pp. 2672–2681, June 2012.

[20] L. D. Landau, E. M. Lifshitz, and L. P. Pitaevskii, *Electrodynamics of Continuous Media*, 2nd ed. Butterworth-Heinemann, 1979.

[21] R. F. Harrington, *Time-Harmonic Electromagnetic Fields*, 2nd ed. John Wiley - IEEE Press, 2001.

[22] J. A. Stratton, *Electromagnetic Theory*. John Wiley - IEEE Press, 2007.

[23] M. Capek, L. Jelinek, P. Hazdra, and J. Eichler, "The measurable Q factor and observable energies of radiating structures," *IEEE Trans. Antennas Propag.*, vol. 62, no. 1, pp. 311–318, Jan. 2014.

[24] S. R. Best, "The Foster reactance theorem and quality factor for antennas," *IEEE Antennas Wireless Propag. Lett.*, vol. 3, no. 1, pp. 306–309, Dec. 2004.

VI

M. Capek, L. Jelinek, and P. Hazdra, "On the functional relation between quality factor and fractional bandwidth," *IEEE Trans. Antennas Propag.*, vol. 63, no. 6, pp. 2787–2790, June 2015. [40∗]

On the Functional Relation Between Quality Factor and Fractional Bandwidth

Miloslav Capek, Lukas Jelinek, and Pavel Hazdra

***Abstract*—The functional relation between the fractional bandwidth and the quality factor of a radiating system is investigated in this communication. Several widely used definitions of the quality factor are compared with two examples of RLC circuits that serve as a simplified model of a single-resonant antenna tuned to its resonance. It is demonstrated that for a first-order system, only the quality factor based on differentiation of the input impedance has unique proportionality to the fractional bandwidth, whereas, e.g., the classical definition of the quality factor, i.e., the ratio of the stored energy to the lost energy per one cycle, is not uniquely proportional to the fractional bandwidth. In addition, it is shown that for higher order systems, the quality factor based on differentiation of the input impedance ceases to be uniquely related to the fractional bandwidth.**

***Index Terms*—Antenna theory, electromagnetic theory, Q factor.**

I. Introduction

The fractional bandwidth (FBW) is a parameter of primary importance in any oscillating system [1], since it is a relative frequency band in which the system can be effectively driven by an external source. In the case of an antenna, a fractional bandwidth is a frequency band in which the power incident upon the input port can be effectively radiated [2].

Based on an analytical evaluation of the basic RLC circuits in the time-harmonic domain [3], FBW is believed to be inversely proportional to the quality factor, which is commonly defined as 2π times the ratio of the cycle mean stored energy and the lost energy, see e.g., IEEE Std. 145-1993, [4]. This relation is known to be very precise for high values of the quality factor (Q factor), and has been shown to be exact for the Q factor tending to infinity, i.e., a lossless oscillating system cannot be driven by an external source, since its FBW is equal to zero. However, this inverse proportionality is known to fail at low values of the Q factor and, in fact, it is not clear whether there exists any functional relation of FBW and the Q factor, which would be valid in all ranges of the Q factor. It is, however, important to stress that if such a relation were to exist, it would be of crucial importance, since there exists a fundamental lower bound of the Q factor of a lossless electromagnetic radiator [5], [6], which would then imply a fundamental upper bound of its FBW, an essential theoretical limitation for electrically small radiators.

This communication serves two purposes. First, a proof is given of the nonexistence of a general functional relation between traditionally defined FBW and the Q factor. The proof is based on an analytical evaluation of the functional relation for two distinct RLC circuits. It is given by contradiction, and it also covers some other commonly used prescriptions of the Q factor. Second, it is pointed out that the so-called Q_Z quality factor defined in [7] and further generalized in [8] is inversely proportional to FBW for first-order systems, but ceases to have this behavior for higher order (multiresonance) systems with closely spaced resonances [9].

Manuscript received December 04, 2014; revised February 04, 2015; accepted March 14, 2015. Date of publication March 20, 2015; date of current version May 29, 2015. This work was supported in part by the Czech Science Foundation under project 13-09086S and in part by the COST IC1102 (VISTA) action.

The authors are with the Department of Electromagnetic Field, Faculty of Electrical Engineering, Czech Technical University in Prague, 16627 Prague, Czech Republic (e-mail: miloslav.capek@fel.cvut.cz).

Color versions of one or more of the figures in this communication are available online at http://ieeexplore.ieee.org.

Digital Object Identifier 10.1109/TAP.2015.2414472

II. Definition of the Q Factor

This section defines several widely used prescriptions of the Q factor that will be used later:

1) classical quality factor $Q_{\rm cl}$ [4];
2) modified quality factor $Q_{\rm rev}$, based on the concept of recoverable energy [10]–[12];
3) Q_X quality factor, based on differentiation of the input reactance [13];
4) Q_Z quality factor, based on differentiation of the input impedance [7], [8].

A. Definition of the Classical Quality Factor $Q_{\rm cl}$

The classical Q factor is conventionally defined as [4]

$$Q_{\rm cl} = \frac{\omega_0 W_{\rm sto}}{P_{\rm lost}} \tag{1}$$

in which ω_0 is the resonant frequency, $W_{\rm sto}$ is the cycle mean stored energy, and $P_{\rm lost}$ is the cycle mean power loss. This prescription of the Q factor is traditionally encumbered with difficulties in identifying the stored energy of a general electromagnetic radiator [14]. This problem is, however, left aside in this communication, as $W_{\rm sto}$ is used only for nonradiating circuits, for which the concept of stored energy is well established [3]. Namely, the cycle mean stored energy of a nonradiating circuit can generally be written as

$$W_{\rm sto} = \frac{1}{4}\sum_n \left(L_n \left| I_{{\rm L}_n} \right|^2 + C_n \left| U_{{\rm C}_n} \right|^2 \right) \tag{2}$$

and the cycle mean lost power can be written as

$$P_{\rm lost} = \frac{1}{2}\sum_n R_n \left| I_{{\rm R}_n} \right|^2 . \tag{3}$$

In (2) and (3), L, C, and R are the inductance, capacitance, and resistance of the circuit, and $I_{\rm L}$, $U_{\rm C}$, and $I_{\rm R}$ are the corresponding currents and voltages. The convention $\mathcal{F}(t) = {\rm Re}\{F(\omega){\rm exp}({\rm j}\omega t)\}$ for time-harmonic quantities has been utilized.

B. Quality Factor $Q_{\rm rev}$ Based on Recoverable Energy

The original definition of the Q factor (1) can be slightly modified to

$$Q_{\rm rev} = \frac{\omega_0 W_{\rm rev}}{P_{\rm lost}} \tag{4}$$

in which $W_{\rm rev}$ (the so-called recoverable energy) is that part of the stored energy $W_{\rm sto}$, which can be recovered back from the input port by a matched load. This recoverable energy can in essence be evaluated by bringing the system into a time-harmonic steady state at frequency ω_0 by a voltage source with matched internal impedance, and afterward switching OFF the source and capturing all the energy returned to the internal impedance [10]–[12].

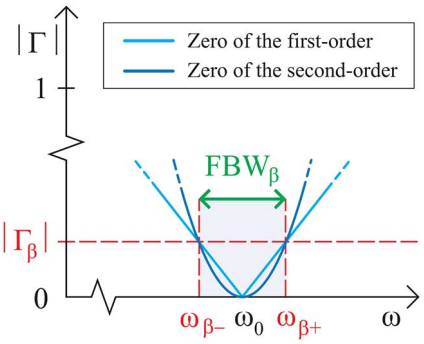

Fig. 1. Course of the reflectance from a device under test in the vicinity of the resonance frequency ω_0. The device under test is assumed to be matched ($Z_{\mathrm{in}}(\omega_0) = R_0$) to the measurement device at the resonance frequency ω_0, so that $|\Gamma(\omega_0)| = 0$.

C. Reactance Quality Factor Q_X

A different approach in defining the Q factor is based on the assumption that Foster's reactance theorem [15] also holds for lossy systems [16], [17]. In that case, the Q factor can be defined by the frequency derivative of the input reactance as

$$Q_X = \frac{\omega_0}{2\,\mathrm{Re}\{Z_{\mathrm{in}}\}} \left| \frac{\partial\,\mathrm{Im}\{Z_{\mathrm{in}}\}}{\partial\omega} \right|_{\omega=\omega_0} \tag{5}$$

where Z_{in} is the input impedance of the circuits. This definition was proposed by Harrington [18], and was refined by Rhodes [13], and it is commonly used even nowadays.

D. Impedance Quality Factor Q_Z

A prescription that is widely used in antenna practice gives the Q factor in terms of the input impedance [7], [8]. The relation reads

$$Q_Z = \frac{\omega_0}{2\,\mathrm{Re}\{Z_{\mathrm{in}}\}} \left| \frac{\partial Z_{\mathrm{in}}}{\partial\omega} \right|_{\omega=\omega_0} \tag{6}$$

and it is known to correspond well to FBW [8].

III. Functional Relation of Q Factor and FBW

The major purpose of this communication is to investigate the functional relation

$$\mathrm{FBW}_\beta = f(Q) \tag{7}$$

where f is an as yet unknown function

$$\mathrm{FBW}_\beta = \frac{\omega_{\beta+} - \omega_{\beta-}}{\omega_0} \tag{8}$$

where $\omega_{\beta+}$ and $\omega_{\beta-}$ delimit the range of frequencies for which the reflectance at the input port of the device under test

$$|\Gamma| = \left| \frac{Z_{\mathrm{in}} - R_0}{Z_{\mathrm{in}} + R_0} \right| \tag{9}$$

is smaller than a given threshold $|\Gamma_\beta|$ (see Fig. 1). The resistance R_0 in (9) belongs to the input port of the measurement device.

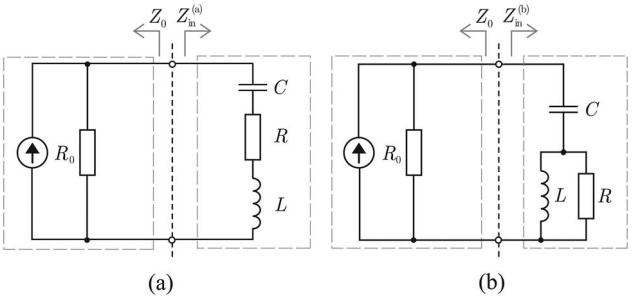

Fig. 2. Studied RLC circuits connected to a voltage source with internal resistance R_0. (a) R, C, and L in series. (b) C in series with parallel L and R.

A. First-Order Systems

Instead of directly analyzing relationship (7) for a complex system such as an antenna, we start with two single-resonant RLC circuits, depicted in Fig. 2. If it is proved that a given definition of the Q factor is not uniquely proportional to FBW for the simple circuits in Fig. 2, it can be concluded that this Q factor is not proportional to FBW at all.

Assuming a circuit tuned to resonance and matched to the measuring device ($Z_{\mathrm{in}}(\omega_0) = R_0$), see Fig. 1, we utilize a simple consideration, in which the reflection coefficient Γ is expanded to its Taylor series around resonance frequency ω_0 and only the first nonzero term is kept. Under such conditions and using (9), the reflectance can be written as

$$\begin{aligned} |\Gamma| &= |\omega - \omega_0| \left| \frac{\partial\Gamma}{\partial\omega} \right|_{\omega=\omega_0} + \mathcal{O}(\omega^2) \\ &= \frac{|\omega - \omega_0|}{\omega_0} \frac{\omega_0}{2\,\mathrm{Re}\{Z_{\mathrm{in}}\}} \left| \frac{\partial Z_{\mathrm{in}}}{\partial\omega} \right|_{\omega=\omega_0} + \mathcal{O}(\omega^2). \end{aligned} \tag{10}$$

Comparing (10) with (6) and (8) gives the required functional relation (7), which reads

$$\mathrm{FBW}_\beta = 2\frac{|\Gamma_\beta|}{Q_Z} \tag{11}$$

and which is valid at least for $|\Gamma_\beta| \to 0$. This means that the quality factor Q_Z (6) is uniquely proportional to the FBW (at least in this differential sense). Furthermore, if the other Q factors are to follow relation (7), they must necessarily be functionally dependent on quality factor Q_Z. This property is investigated as follows.

The quality factor Q_Z of the two circuits under consideration can easily be calculated from the input impedances, which yields

$$Q_Z^{(\mathrm{a})} = \frac{\omega_0^{(\mathrm{a})} L}{R}, \qquad \omega_0^{(\mathrm{a})} = \frac{1}{\sqrt{LC}} \tag{12a}$$

$$Q_Z^{(\mathrm{b})} = \frac{R}{\omega_0^{(\mathrm{b})} L} \cdot \frac{1}{\omega_0^{(\mathrm{b})}\sqrt{LC}}, \qquad \omega_0^{(\mathrm{b})} = \frac{R}{L\sqrt{\dfrac{CR^2}{L} - 1}} \tag{12b}$$

where superscripts (a) and (b) refer to the two circuits in Fig. 2.

The other Q factors can be evaluated in a straightforward manner as

$$Q_{\mathrm{cl}}^{(\mathrm{a})} = Q_Z^{(\mathrm{a})} \tag{13a}$$

$$Q_X^{(\mathrm{a})} = Q_Z^{(\mathrm{a})} \tag{13b}$$

$$Q_{\mathrm{rev}}^{(\mathrm{a})} = \frac{Q_Z^{(\mathrm{a})}}{2} \tag{13c}$$

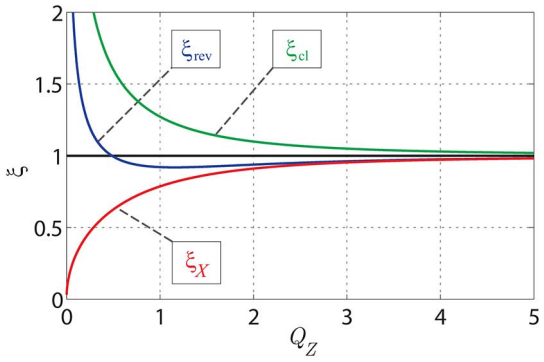

Fig. 3. ξ factors of (15a)–(15c) as a function of quality factor Q_Z.

and

$$Q_{\rm cl}^{\rm (b)} = \xi_{\rm cl}\, Q_Z^{\rm (b)} \tag{14a}$$

$$Q_X^{\rm (b)} = \xi_X\, Q_Z^{\rm (b)} \tag{14b}$$

$$Q_{\rm rev}^{\rm (b)} = \xi_{\rm rev}\, \frac{Q_Z^{\rm (b)}}{2} \tag{14c}$$

where

$$\xi_{\rm cl} = \sqrt{\chi}, \tag{15a}$$

$$\xi_X = \sqrt{\chi}\, \frac{\chi}{\chi + \left(Q_Z^{\rm (b)}\right)^{-2}} \tag{15b}$$

$$\xi_{\rm rev} = \sqrt{\chi}\, \frac{\chi + \left(Q_Z^{\rm (b)}\right)^{-2}}{\chi + 2\left(Q_Z^{\rm (b)}\right)^{-2}} \tag{15c}$$

$$\chi = \frac{1 + \sqrt{1 + 4\left(Q_Z^{\rm (b)}\right)^{-2}}}{2}. \tag{15d}$$

The above results offer a simple interpretation. Since the quality factor Q_Z factor has been shown to have a unique functional relation to FBW [see (11)], the other quality factors could have such a unique functional relation only if the functional relations corresponding to circuit (a) and circuit (b) [see (13) and (14)] are the same, i.e., if the corresponding ξ coefficients in (15a)–(15c) are equal to unity. That this is not the case is clear from their analytical prescription, and also from their graphical representation in Fig. 3. By means of contradiction, it must then be stated that there is no general functional relation between FBW and quality factors $Q_{\rm cl}, Q_X, Q_{\rm rev}$, the only exception being $Q \to \infty$.

B. Higher Order (Multiresonance) Systems

Section III-A has shown that, in the case of first-order systems, only quality factor Q_Z is a potential candidate for having a general functional relation to FBW. The purpose of this section is to test this property on higher order systems.

Higher order systems offer more degrees of freedom. This in general makes approximation (10) invalid. In fact, it can be shown [19] that a circuit of order n can always be tuned so that the first $n-1$ terms of the Taylor expansion (10) vanish (binomial transformer).

An example of such a second-order system [20] is depicted in Fig. 4, which for $Q_{\rm P} = Q_{\rm S}$ results in $Q_Z = 0$. Another example [21], [22] is a thin-strip dipole of length L and width $w = L/100$ (see Fig. 5), which is tuned to resonance by a lumped reactance connected in series

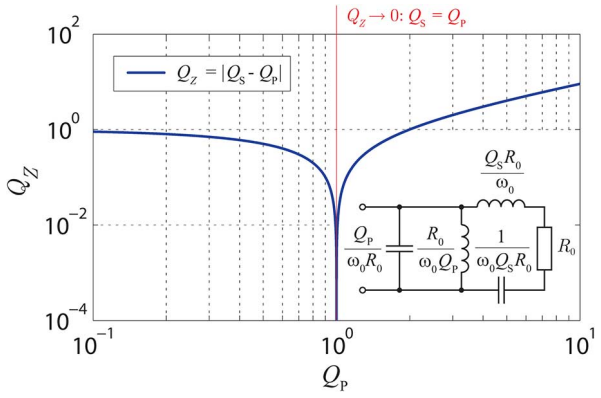

Fig. 4. Quality factor Q_Z of a second-order RLC circuit proposed in [20]. The Q_Z quality factor is evaluated at the resonance frequency ω_0, where the input impedance of the circuit is equal to R_0 irrespective of constants $Q_{\rm P}$ and $Q_{\rm S}$, which represent the quality factors of the serial and parallel branch of the circuit, respectively. The equality $Q_{\rm S} = Q_{\rm P}$ provides a zero of second order in the reflectance (9) and results in a vanishingly small quality factor Q_Z. The depicted curve assumes $Q_{\rm S} = 1$.

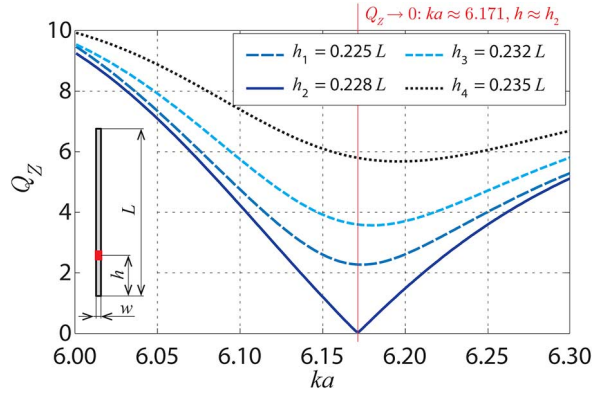

Fig. 5. Quality factor Q_Z of a thin-strip dipole as a function of electrical size and as a function of feeding position. The dipole is kept in resonance by a lumped reactance connected in series with the feed.

with a voltage gap feed. If the voltage gap is placed at $h \approx 0.228L$, it can be seen that $Q_Z = 0$ at $ka \approx 6.171$, in which $k = \omega/c_0$ is the wavenumber, c_0 is the speed of light, and a is the radius of the smallest circumscribing sphere.

The occurrence of $Q_Z \to 0$ mentioned above is an extreme case of the behavior of quality factor Q_Z in a general multiresonance system in which the resonances coincide. The quality factor Q_Z is, however, a smooth function of the frequency distance of the resonances, and there exist a whole range of distances for which it does not represent the fractional bandwidth well [9].

These results, and especially the awkward property of a possibly zero value of quality factor Q_Z in the case of circuits with clearly finite FBW, unfortunately exclude this Q factor from prescriptions with a possibly unique relation to FBW.

IV. Conclusion

It has been shown that, contrary to common belief, the classical quality factor defined by the stored and lost energy is not related to the fractional bandwidth by a general and unambiguous functional relation. This is also true for Q factors resulting from recoverable energy

and input reactance. Considering the first-order system, only the Q factor based on differentiation of the input impedance has been shown to be a possible candidate for such a general functional relation. It has, however, been demonstrated that for higher order systems, including elementary radiators such as dipoles, no quality factor has, in general, exact proportionality to the fractional bandwidth.

ACKNOWLEDGMENT

The authors would like to thank to M. Gustafsson from Lund University, Sweden for a fruitful discussion about the topic, and for pointing out the possibility of minimizing quality factor Q_Z by off-center feeding of a dipole. They would also like to thank the two anonymous reviewers whose remarks improved the clarity of this communication.

REFERENCES

[1] P. M. Morse and H. Feshbach, *Methods of Theoretical Physics*. New York, NY, USA: McGraw-Hill, 1953.
[2] C. A. Balanis, *Antenna Theory Analysis and Design*, 3rd ed. Hoboken, NJ, USA: Wiley, 2005.
[3] E. Hallen, *Electromagnetic Theory*. London, U.K.: Chapman & Hall, 1962.
[4] *Standard Defintions of Terms for Antennas*, IEEE Antennas and Propagation Society Standard 145, 1993.
[5] L. J. Chu, "Physical limitations of omni-directional antennas," *J. Appl. Phys*., vol. 19, pp. 1163–1175, 1948.
[6] R. C. Hansen and R. E. Collin, "A new Chu formula for Q," *IEEE Antennas Propag. Mag*., vol. 51, no. 5, pp. 38–41, Oct. 2009,
[7] D. Kajfez and W. P. Wheless, "Invariant definitions of the unloaded Q factor," *IEEE Antennas Propag. Mag*., vol. 34, no. 7, pp. 840–841, Jul. 1986.
[8] A. D. Yaghjian and S. R. Best, "Impedance, bandwidth and Q of antennas," *IEEE Trans. Antennas Propag*., vol. 53, no. 4, pp. 1298–1324, Apr. 2005.
[9] H. R. Stuart, S. R. Best, and A. D. Yaghjian, "Limitations in relating quality factor to bandwidth in a double resonance small antenna," *IEEE Antennas Wireless Propag. Lett*., vol. 6, pp. 460–463, 2007.
[10] V. G. Polevoi, "Maximum energy extractable from an electromagnetic field," *Radiophys. Quantum Electron*., vol. 33, no. 7, pp. 603–609, 1990.
[11] C. A. Grimes, G. Liu, F. Tefiku, and D. M. Grimes, "Time-domain measurement of antenna Q," *Microwave Opt. Technol. Lett*., vol. 25, no. 2, pp. 95–100, Apr. 2000.
[12] R. H. Direen, "Fundamental limitations on the terminal behavior of antennas and nonuniform transmission lines," Ph.D. dissertation, Dept. of Electrical, Computer, and Energy Engineering, Univ. Colorado, Boulder, CO, 2010.
[13] D. R. Rhodes, "Observable stored energies of electromagnetic systems," *J. Franklin Inst*., vol. 302, no. 3, pp. 225–237, 1976.
[14] G. A. E. Vandenbosch, "Reply to "Comments on 'Reactive energies, impedance, and Q factor of radiating structures," *IEEE Trans. Antennas Propag*., vol. 61, no. 12, p. 6268, Dec. 2013.
[15] R. M. Foster, "A reactance theorem," *Bell System Tech. J*., vol. 3, pp. 259–267, 1924.
[16] D. R. Rhodes, "A reactance theorem," *Proc. R. Soc. Lond. A*., vol. 353, pp. 1–10, Feb. 1977.
[17] W. Geyi, P. Jarmuszewski, and Y. Qi, "The Foster reactance theorem for antennas and radiation Q," *IEEE Trans. Antennas Propag*., vol. 48, no. 3, pp. 401–408, Mar. 2000.
[18] R. F. Harrington and J. R. Mautz, "Control of radar scattering by reactive loading," *IEEE Trans. Antennas Propag*., vol. 20, no. 4, pp. 446–454, Jul. 1972.
[19] R. E. Collin, *Foundations for Microwave Engineering*, 2nd ed. Hoboken, NJ, USA: Wiley/IEEE Press, 1992.
[20] M. Gustafsson and S. Nordebo, "Bandwidth, Q factor and resonance models of antennas," *Progr. Electromagn. Res*., vol. 62, pp. 1–20, 2006.
[21] M. Gustafsson, D. Tayli, and M. Cismasu. (2014). *Q Factors for Antennas in Dispersive Media*. eprint arXiv: 1408.6834v2 [Online]. Available: http://arxiv.org/abs/1408.6834
[22] M. Gustafsson, M. Cismasu, D. Tayli, S. Nordebo, and L. Jonsson. (2013). *An Overview of Current Optimization and Physical Bounds on Antennas* [Online]. Available: www.eit.lth.se/index.php?uhpuid=scd.mgu&hpuid=139&L=1

Design of a Wideband Millimeter Wave Micromachined Rotman Lens

Nathan Jastram and Dejan S. Filipovic

***Abstract*—Design, fabrication, and performance of a micromachined millimeter wave Rotman lens are presented. To achieve wide instantaneous bandwidth with $\pm 30^\circ$ scan range, five different transmission lines with carefully designed transitions are monolithically integrated within the same process. Theoretical bandwidth of over 70 GHz is verified with a narrower bandwidth W-band measurements of VSWR ($< 2.75{:}1$), and 65–115 GHz measurements of realized gain (5–11 dBi), 3 dB beamwidth (20°–40°), and beam-peak locations in E-plane. Demonstrated results indicate that wideband Rotman lenses can now be engineered for emerging millimeter and submillimeter wave applications.**

***Index Terms*—Array feeds, micromachining, Rotman lens.**

I. INTRODUCTION

An increased interest in components and subsystems for millimeter and submillimeter wave applications, such as biomedical imaging, automotive anticollision radars, electronic warfare, and communications [1]–[3], has been recently observed. For many of these applications, beam steering is highly desired. The most popular traditional beam-steering approach is phased array which uses a network of active and passive components to set required amplitude and phase distributions for pointing beam in a desired direction. However, at millimeter wave frequencies, active phase shifters can have high loss [4], [5] while wideband passive components are more challenging to realize [6]. An array configuration with lower loss and wider bandwidth is the Rotman lens [7]; a planar electromagnetic lens with inherently broadband performance and frequency invariant beams.

Several Rotman lenses operating above 60 GHz using microstrip [8]–[10] or waveguide [11], [12] based topologies have been reported. In [8], a V-band $3\ (\text{beam port}) \times 5\ (\text{array port})$ device is built using low-temperature cofired ceramic (LTCC). While there is no reported data on the loss of the stand-alone lens, the insertion loss in (only)

Manuscript received July 31, 2014; revised February 04, 2015; accepted March 14, 2015. Date of publication March 19, 2015; date of current version May 29, 2015. This work was supported by the Office of Naval Research under Grant N00014-11-1-0010. PolyStrata is trademark of Nuvotronics, LLC.

The authors are with are with the Department of Electrical, Computer, and Energy Engineering, University of Colorado Boulder, Boulder, CO 80309, USA (e-mail: Nathan.Jastram@colorado.edu; Dejan@colorado.edu).

Color versions of one or more of the figures in this communication are available online at http://ieeexplore.ieee.org.

Digital Object Identifier 10.1109/TAP.2015.2414475

VII

L. Jelinek, M. Capek, P. Hazdra, and J. Eichler, "An analytical evaluation of the quality factor Q_Z for dominant spherical modes," *IET Microw. Antennas Propag.*, vol. 9, no. 10, pp. 1096–1103, 2015. [31∗]

IET Microwaves, Antennas & Propagation

Research Article

IET Journals
The Institution of Engineering and Technology

An analytical evaluation of the quality factor Q_Z for dominant spherical modes

ISSN 1751-8725
Received on 6th May 2014
Revised on 7th November 2014
Accepted on 28th February 2015
doi: 10.1049/iet-map.2014.0302
www.ietdl.org

Lukas Jelinek ✉, *Miloslav Capek*, *Pavel Hazdra*, *Jan Eichler*

Department of Electromagnetic Field, Faculty of Electrical Engineering, Czech Technical University in Prague, Technicka 2, 16627, Prague, Czech Republic

✉ *E-mail: lukas.jelinek@fel.cvut.cz*

Abstract: This study describes an analytical evaluation of the quality factor Q_Z in a separable system in which the vector potential is known. The proposed method uses a potential definition of active and reactive power, implicitly avoiding infinite entire space integration and extraction of radiation energy. As a result, all the used quantities are finite, and the calculated Q_Z is always non-negative function of frequency. The theory is presented on the canonical example of the currents flowing on a spherical shell. The Q_Z for the dominant spherical transverse magnetic and transverse electric modes and their linear combination are found in closed forms, including both internal and external energies. The proposed analytical method and its results are compared with previously published limits of the quality factor Q.

1 Introduction

The quality factor (Q factor) is recognised as one of the most significant parameters of a radiating system, especially if the electrical dimensions are small, see for example [1] and references therein. The reason is its approximate inverse proportionality to a fractional bandwidth (FBW) and a possibility of establishing the lower bounds of Q factor [1]. This implies an upper bound of FBW, a restriction of substantial importance for electrically small antennas (ESAs).

The classical work on lower bounds of Q factor is the work of Chu [2], which considers a sphere of radius a that encloses an ESA. The normalised radial wave impedance for the dominant spherical transverse magnetic (TM) mode is expressed as a continued fraction equivalent to a ladder network with particular R, L, C elements. In this way, the lower bound of Q can be found. However, the Chu's method is restricted to the spherical modes only and does not include the internal energy of the sphere, making the limit overly optimistic. Later, Wheeler [3] reduced the basic radiators, dipole and loop, to the circuit elements and derived practically oriented limits. Expansion to the spherical harmonics was also used by Harrington [4] to evaluate the electric and magnetic energy for each mode. The same approach was presented by Collin and Rothschild [5] for spherical and cylindrical modes. McLean [6] verified the Chu's formula. He obtained the same results, but his approach is based on the field radiated by the Hertzian dipole. Thiele *et al*. [7] used the 'far-field method', based on the separation of the far-field pattern into its visible and invisible parts [8]. Thal [9–11] used the ladder network to extend the Chu's limit by including the energies inside the enclosing sphere. Hansen and Collin [12] also included internal energies, but they used $\boldsymbol{E}$- and $\boldsymbol{H}$-fields together with the subtraction of the radial power flow. Hansen *et al*. [13] generalised the results of Hansen and Collin for any spherical TM and transverse electric (TE) modes and for a sphere filled with an isotropic medium. The limitations of the dual-mode case were studied by Fante [14] and recently by Kim [15].

The most recent approaches to the Q factor calculation utilised the source current distribution. There are obvious benefits: the resultant functionals are of bilinear forms, the calculation is very effective and it is possible to use any current distribution that is available thanks to modern EM simulators or that could even be user defined. This opens new possibilities in optimisation [16] and modal decomposition [17]. The work by Vandenbosch [18] is inspired by the pioneering research of Geyi [19], and directly uses Maxwell equations and the source currents. The same theory has been generalised in the time domain [20]. However, some non-observable terms [21] were neglected. Another approach by Gustafsson *et al*. [22] utilised static polarisability. Gustaffson and Jonsson [23] also postulated the uncertainty in Vandenbosch's definition of Q. Unfortunately, their contribution opens a new question about the coordinate-dependent term which is strictly non-physical.

Some attempts have also been made to obtain the lower bound of Q by utilising the sources. This limit was investigated by Vandenbosch and Volski [24], but the method is encumbered with the difficulties mentioned above, and thus the results are provided only for a small radiator. Very interesting work has been done by Seshadri [25], closely related with [26], where the complex power of the spherical modes is already known analytically.

Together with the theoretical achievements, many scientists have sought for an antenna prototype that achieves the given limits, see for example [27, 28]. The folded multi-arm spherical helix antenna designed by Best [29] achieved roughly 1.5 times the Chu's limit and almost exactly the limit predicted by Hansen and Collin. An attempt to reach the Chu's limit was undertaken by Kim and Breinbjerg [30], using a magnetic-coated perfectly electrically conducting (PEC) core.

The above-mentioned history however evoke a question, whether the classical Q limits, based on the far-field energy extraction, are the only possibility how to establish an upper bound of FBW or whether there exist a simpler way. In fact, there exists another widely used concept of so-called Q_Z factor proposed by Yaghjian and Best [31], which should closely follow an inverse proportionality to FBW. Its source concept is already established [32], however works on its lower bounds are scarce [23, 33]. Particularly [33], there exists an explicit evaluation of the Q_Z of the separated TE and TM spherical modes with internal region excluded and there are signs of Q_Z not having an absolute lower bound other than $Q_Z = 0$.

This paper makes amendments to the current state of the topic of the lower bounds of the Q_Z factor. The method of Q_Z evaluation is based on the differentiation of the complex power expressed by electromagnetic potentials rather than fields [32]. In this way, the issues with divergent integrals [18] are automatically eliminated, since the subtraction of the far-field energy is not needed (it is implicitly included in the Q_Z definition). The complex power differentiation also avoids non-physical quantities like coordinate-dependent terms or negative energies [23].

The proposed theory is presented on an example of spherical modes, which have been in the spotlight in recent decades for their ability to establish a general lower bound of Q factor. It is important to stress that the whole process is completely analytical, without any approximations. The final expressions, presented in the closed form, are easy to work with and are compatible with all previous observations. Furthermore, the proposed methodology can be applied not only to the spherical coordinate system, but also to any system in which the vector wave equation is separable [34] and thus the vector potential is analytically known. This gives a possibility of practical Q_Z limits tailored for a particular antenna design.

The paper is organised as follows. The definition of the Q_Z factor is briefly recapitulated in Section 2. The complex power and all necessary power and energy terms of the dominant spherical TM and TE modes are presented in Sections 3 and 4. Section 5 presents the practically available limits for single-mode radiators in free space, which are represented by the dominant spherical modes, further denoted as TM_{10} and TE_{10} and compares them with the classical Q limits. Section 6 deals with the Q_Z factor of the combination of the modes and compares it with the results for the classical Q factor. Section 7 then gives some important remarks on the presented derivations and results. The paper is concluded in Section 8.

2 Definition of Q_Z

The exact derivation of the Q_Z factor [31] in terms of sources is provided in [32], including the related discussion and numerical verification, and reads

$$Q_Z = |Q_R + \jmath Q_X| = \frac{ka}{2(P_\mathrm{m} - P_\mathrm{e})} \left| \frac{\partial\big((P_\mathrm{m} - P_\mathrm{e}) + \jmath\omega(W_\mathrm{m} - W_\mathrm{e})\big)}{\partial ka} \right| \tag{1}$$

where subscripts Z, R and X represent impedance, resistance and reactance of the antenna, respectively, and where $\jmath = \sqrt{-1}$, ω is the angular frequency of the time harmonic field [35] under the convention $\mathcal{F}(t) = \sqrt{2}\Re\{\boldsymbol{F}(\omega)\mathrm{e}^{\jmath\omega t}\}$, where $\mathcal{F}$ is any time-harmonic quantity, $k = \omega/c_0$ is the wavenumber, c_0 is the speed of light, a is the smallest radius of a sphere circumscribing all the sources, $P_\mathrm{m} - P_\mathrm{e}$ is the total radiated power [36], $\omega(W_\mathrm{m} - W_\mathrm{e})$ is the total reactive power [36] and the total input current at the antenna's port is normalised to $I_0 = 1$ A. Considering an arbitrary source current distribution $\boldsymbol{J}$ and charge density ρ inside a source region Ω, and $\boldsymbol{A}$ and φ as the vector and scalar potentials [36], the separated Q_R and Q_X terms in (1) can be written as

$$Q_R = \frac{P_\mathrm{m} + P_\mathrm{e} + P_\mathrm{rad} + P_\omega}{2\big(P_\mathrm{m} - P_\mathrm{e}\big)} \tag{2}$$

and

$$Q_X = \frac{\omega\big(W_\mathrm{m} + W_\mathrm{e} + W_\mathrm{rad} + W_\omega\big)}{2\big(P_\mathrm{m} - P_\mathrm{e}\big)} \tag{3}$$

where the particular terms are expressed as

$$W_\mathrm{m} - \jmath\frac{P_\mathrm{m}}{\omega} = \int_\Omega \boldsymbol{A}\cdot\boldsymbol{J}^*\,\mathrm{d}\boldsymbol{r} \tag{4a}$$

$$W_\mathrm{e} - \jmath\frac{P_\mathrm{e}}{\omega} = \int_\Omega \varphi\rho^*\,\mathrm{d}\boldsymbol{r} \tag{4b}$$

$$W_\mathrm{rad} - \jmath\frac{P_\mathrm{rad}}{\omega} = -\jmath k\big(k^2\mathcal{L}_\mathrm{rad}(\boldsymbol{J},\boldsymbol{J}) - \mathcal{L}_\mathrm{rad}(\nabla\cdot\boldsymbol{J},\nabla\cdot\boldsymbol{J})\big) \tag{4c}$$

$$W_\omega - \jmath\frac{P_\omega}{\omega} = k^2\mathcal{L}_\omega(\boldsymbol{J},\boldsymbol{J}) - \mathcal{L}_\omega(\nabla\cdot\boldsymbol{J},\nabla\cdot\boldsymbol{J}) \tag{4d}$$

with

$$\mathcal{L}_\mathrm{rad}(\boldsymbol{U},\boldsymbol{V}) = \frac{1}{4\pi\epsilon\omega^2} \int_{\Omega'}\int_\Omega \boldsymbol{U}(\boldsymbol{r})\cdot\boldsymbol{V}^*(\boldsymbol{r}')\mathrm{e}^{-\jmath kR}\,\mathrm{d}\boldsymbol{r}\,\mathrm{d}\boldsymbol{r}' \tag{5a}$$

$$\mathcal{L}_\omega(\boldsymbol{U},\boldsymbol{V}) = \frac{1}{4\pi\epsilon\omega} \int_{\Omega'}\int_\Omega \frac{\partial\big(\boldsymbol{U}(\boldsymbol{r})\cdot\boldsymbol{V}^*(\boldsymbol{r}')\big)}{\partial\omega}\frac{\mathrm{e}^{-\jmath kR}}{R}\,\mathrm{d}\boldsymbol{r}\,\mathrm{d}\boldsymbol{r}' \tag{5b}$$

in which $R = \|\boldsymbol{r} - \boldsymbol{r}'\|$ is the Euclidean distance, ϵ is the vacuum permittivity and * denotes complex conjugation. The detailed derivation of the above relations is described in [32].

The Q_X in (3) and Q_Z in (1) are Q factors of an untuned antenna [1] and thus they will be denoted as Q_X^untuned and Q_Z^untuned in the rest of the paper. One can, however, tune the antenna to its resonance at angular frequency ω_0 by a reactive lumped element. Then, the Q factors of tuned antenna will be denoted as Q_X^tuned and Q_Z^tuned, and they can be evaluated as [32]

$$Q_X^\mathrm{tuned} = \omega_0\frac{2\max\{W_\mathrm{m}, W_\mathrm{e}\} + W_\mathrm{rad} + W_\omega}{2(P_\mathrm{m} - P_\mathrm{e})} \tag{6a}$$

$$Q_Z^\mathrm{tuned} = \big|Q_R + \jmath Q_X^\mathrm{tuned}\big| \tag{6b}$$

Note that tuning by purely reactive elements leaves the Q_R factor unchanged.

3 Complex power and the Q_Z of the TM_{10} mode

Let us consider the TM_{10} mode, which is described by the current density

$$\boldsymbol{J} = \frac{\sin(\vartheta)}{2\pi a}\delta(r-a)\boldsymbol{\vartheta}_0 \tag{7}$$

flowing on a spherical shell of radius a situated in a vacuum, where δ is the Dirac delta and $\boldsymbol{\vartheta}_0$ is the unit vector codirectional with ϑ, see Fig. 1. The current density (7) is normalised so that the current flowing through the x–y plane is $I_0 = 1$ A. The corresponding

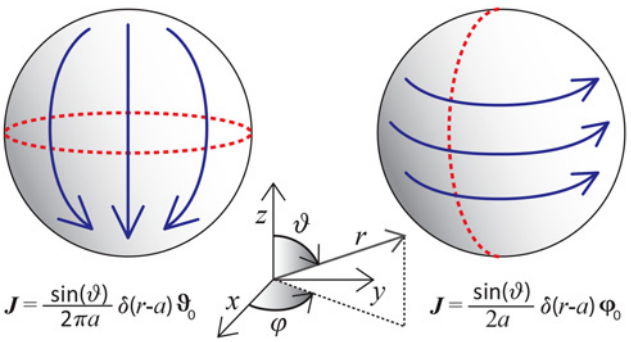

Fig. 1 *Sketch of modal currents on a sphere of radius a: dipole mode (TM_{10}) on the left and loop mode (TE_{10}) on the right. The input current is normalised with respect to the dashed contours. The coordinate system considered throughout the paper is depicted in the middle of the figure*

charge density is

$$\rho = J\frac{\cos(\vartheta)}{\omega\pi a^2}\delta(r-a) \tag{8}$$

The vector and scalar potentials of the TM_{10} mode are (see Appendix 1)

$$\begin{aligned} A_\vartheta = -\frac{J\mu}{2\pi ka}\sin(\vartheta)\Big(&2h_1^{(2)}(ka)j_1(ka) \\ &+\Big(h_1^{(2)}(ka)-kah_0^{(2)}(ka)\Big)\Big(j_1(ka)-kaj_0(ka)\Big)\Big) \end{aligned} \tag{9}$$

and

$$\varphi = \frac{\omega\mu}{\pi k}h_1^{(2)}(ka)j_1(ka)\cos(\vartheta) \tag{10}$$

where j_n and $h_n^{(2)} = j_n - jy_n$ are the spherical Bessel and Hankel functions of the nth order [37]. Substituting the potentials into (4a) and (4b) leads to

$$P_{\mathrm{m}} = \frac{4}{6\pi}Z_0\Big(2j_1^2(ka)+\big(j_1(ka)-kaj_0(ka)\big)^2\Big) \tag{11a}$$

$$P_{\mathrm{e}} = \frac{4}{3\pi}Z_0 j_1^2(ka) \tag{11b}$$

$$\begin{aligned} \omega W_{\mathrm{m}} = -\frac{4}{6\pi}Z_0\big(&2y_1(ka)j_1(ka) \\ &+\big(y_1(ka)-kay_0(ka)\big)\big(j_1(ka)-kaj_0(ka)\big)\big) \end{aligned} \tag{11c}$$

$$\omega W_{\mathrm{e}} = -\frac{4}{3\pi}Z_0 y_1(ka)j_1(ka) \tag{11d}$$

where $Z_0 = \sqrt{\mu/\epsilon}$ is the free space impedance. Note here that the distribution (7), by definition, does not vary with the frequency, $\partial \boldsymbol{J}(\vartheta)/\partial\omega = 0$, and thus from (4d) we have

$$P_\omega = \omega W_\omega = 0 \tag{12}$$

Finally, by comparing (1) with (2) and (3), and using (12), we can deduce that

$$P_{\mathrm{rad}} = ka\frac{\partial(P_{\mathrm{m}}-P_{\mathrm{e}})}{\partial ka} - (P_{\mathrm{m}}+P_{\mathrm{e}}) \tag{13a}$$

$$\omega W_{\mathrm{rad}} = ka\frac{\partial\omega(W_{\mathrm{m}}-W_{\mathrm{e}})}{\partial ka} - \omega(W_{\mathrm{m}}+W_{\mathrm{e}}) \tag{13b}$$

The above expressions have been simplified in Mathematica [38] and evaluated in Matlab [39], and the results are depicted in Fig. 2. The

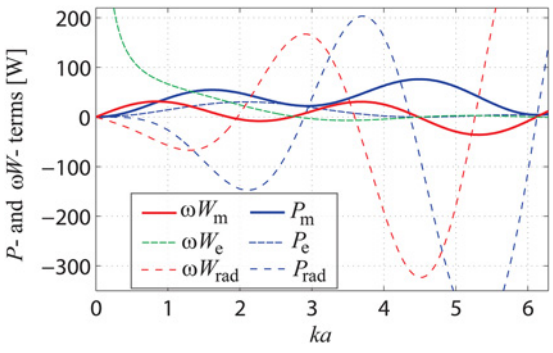

Fig. 2 *Radiated power terms P_m and P_e, the reactive power terms ωW_m and ωW_e, and the power terms associated with radiation P_{rad} and ωW_{rad} for the TM_{10} mode*

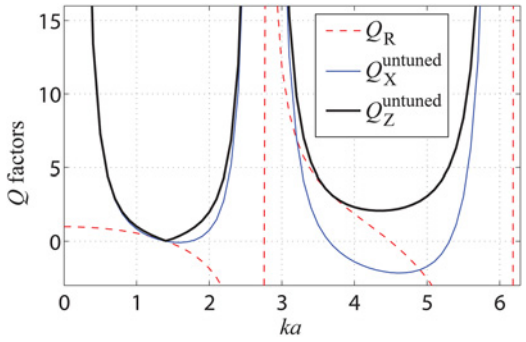

Fig. 3 *Comparison of the Q_Z^{untuned} and its parts Q_R and Q_X^{untuned} for the TM_{10} mode. Both Q_R and Q_X^{untuned} can be negative. They can only be interpreted according to (1)*

corresponding Q_R, Q_X^{untuned} and Q_Z^{untuned} factors of the TM_{10} mode are depicted in Fig. 3.

4 Complex power and the Q_Z of the TE_{10} mode

The procedure from the previous section can be used for the TE_{10} mode as well. In that case, the current density is

$$\boldsymbol{J} = \frac{\sin(\vartheta)}{2a}\delta(r-a)\boldsymbol{\varphi}_0 \tag{14}$$

where φ_0 is the unit vector codirectional with φ, see Fig. 1. The current density is normalised so that the current flowing through the $z-(x>0)$ half-plane is $I_0 = 1$ A. The corresponding charge density vanishes, $\rho = 0$, and so

$$\varphi = 0 \tag{15a}$$

$$P_{\mathrm{e}} = 0 \tag{15b}$$

$$\omega W_{\mathrm{e}} = 0 \tag{15c}$$

Furthermore, as the current is frequency independent, (12) and (13b) still holds. The vector potential is again found by the method described in Appendix 1, and is equal to

$$A_\varphi = -\frac{J\mu}{2}\sin(\vartheta)kaj_1(ka)h_1^{(2)}(ka) \tag{16}$$

which leads to

$$P_{\mathrm{m}} = \frac{2\pi}{3}Z_0(ka)^2 j_1^2(ka) \tag{17a}$$

$$\omega W_{\mathrm{m}} = -\frac{2\pi}{3}Z_0(ka)^2 j_1(ka)y_1(ka) \tag{17b}$$

All non-zero terms related to the TE_{10} mode are depicted in Fig. 4. The Q_Z^{untuned} and its parts Q_R and Q_X^{untuned} of the TE_{10} mode are depicted in Fig. 5.

5 The limitations for ESA and asymptotic behaviour of the Q_Z factor for the TM_{10} and the TE_{10} mode

In this section, we will discuss the Q and the Q_Z factors for the spherical TM_{10} and TE_{10} modes that are tuned to its resonance at given ka by the external reactive lumped element. Particularly, the Q_Z^{tuned} obtained from (6b) is compared with the classical Chu's limit [2] Q_{Chu} (formula (8) in [5]), with the limit found by Hansen

IET Microw. Antennas Propag., 2015, Vol. 9, Iss. 10, pp. 1096–1103

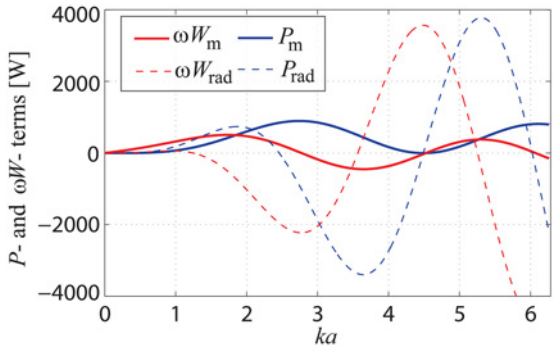

Fig. 4 *Radiated power term P_m, the reactive power term ωW_m and the power terms associated with radiation P_{rad} and ωW_{rad} for the TE_{10} mode*

and Collin [12] Q_{HC} (formulas (9) and (12) of [12]) and with the recent limits found by Vandenbosch [18]. Note that within the context of frequency-independent modes (with $P_\omega = \omega W_\omega = 0$) the quality factor used by Vandenbosch [18] is just the Q_X^{tuned}.

The results for the TM_{10} mode are depicted in Fig. 6, whereas the results for the TE_{10} mode are depicted in Fig. 7. The region of ESA ($ka < 0.5$), which is of interest for Q factor limits, is highlighted. The observed agreement between Q_Z^{tuned}, Q_X^{tuned} and Q_{HC} can be denoted as excellent in this region. On the other hand, the Chu's limit is clearly too optimistic because of the fact that Chu excluded the reactive power inside the bounding sphere. This is particularly significant in the case of the TE_{10} mode, which stores approximately one-third of the total stored energy inside the sphere.

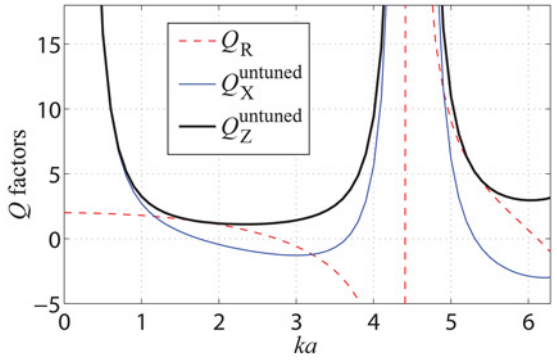

Fig. 5 *Comparison of the Q_Z^{untuned} and its parts Q_R and Q_X^{untuned} for the TE_{10} mode. Both Q_R and Q_X^{untuned} can be negative. They can only be interpreted according (1)*

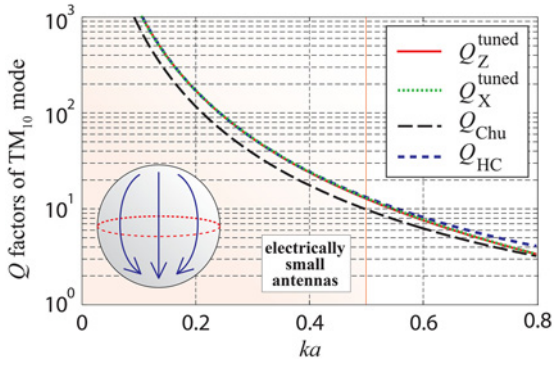

Fig. 6 *Comparison of the Q and the Q_Z factors for the spherical TM_{10} mode: the Q_Z^{tuned} of this paper, the Q_{Chu} from [5], the Q_{HC} from [12] and Q_X^{tuned} of this paper which is equivalent to that of [18]*

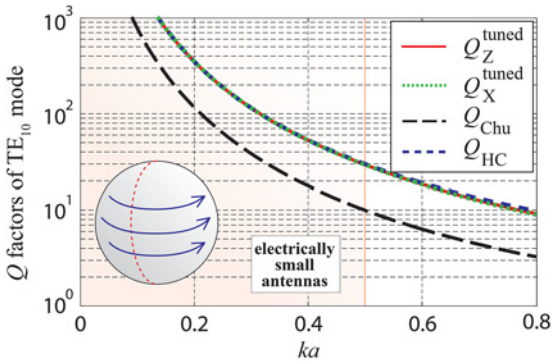

Fig. 7 *Comparison of the Q and the Q_Z factors for the spherical TE_{10} mode: the Q_Z^{tuned} of this paper, the Q_{Chu} from [5], the Q_{HC} from [12] and Q_X^{tuned} of this paper which is equivalent to that of [18]*

The explicit forms of the Q_Z^{tuned} and Q_{HC} of the TM_{10} and of the TE_{10} mode are rather lengthy and are thus left for Appendix 3. Within the region of interest (the ESA region of $ka < 0.5$) their series expansion provides an excellent approximation and the series expansion can furthermore be directly compared with the published results of the classical Q limits. As for the Q_R, Q_X^{tuned} and Q_Z^{tuned} factors derived in this paper, the series for the TM_{10} mode read

$$Q_R = 1 - \frac{2}{5}(ka)^2 + \mathcal{O}(ka)^4 \tag{18a}$$

$$Q_X^{\text{tuned}} = \frac{3}{2(ka)^3} + \frac{3}{5(ka)} - \frac{813}{1400}ka + \mathcal{O}(ka)^3 \tag{18b}$$

$$Q_Z^{\text{tuned}} = Q_X^{\text{tuned}} + \mathcal{O}(ka)^3 \tag{18c}$$

while the series for the TE_{10} mode read

$$Q_R = 2 - \frac{(ka)^2}{5} + \mathcal{O}(ka)^4 \tag{19a}$$

$$Q_X^{\text{tuned}} = \frac{3}{(ka)^3} + \frac{3}{ka} - \frac{174}{175}ka + \mathcal{O}(ka)^3 \tag{19b}$$

$$Q_Z^{\text{tuned}} = Q_X^{\text{tuned}} + \mathcal{O}(ka)^3 \tag{19c}$$

The Q_Z^{tuned} is almost identical to Q_X^{tuned} for $ka \to 0$, since $Q_X^{\text{tuned}} \gg Q_R$, see Figs. 3 and 5. For comparison we also present series of the classical Chu's limit [2] in the version of [5] which reads

$$Q_{\text{Chu}} = \frac{1}{(ka)^3} + \frac{1}{ka} \tag{20}$$

(note that this expansion is an exact formula) and the series of Q_{HC} of the TM_{10} mode [12] which reads

$$Q_{\text{HC}} \simeq \frac{3}{2(ka)^3} + \frac{1}{\sqrt{2}ka} \tag{21}$$

Lastly, the Q_{HC} of the TE_{10} mode [12] reads

$$Q_{\text{HC}} \simeq 3Q_{\text{Chu}} \tag{22}$$

Comparing the above expressions, a good correspondence between (21), (18c) and (22), (19c) is now evident.

6 The Q_Z factor of the linear combination of the TM_{10} and the TE_{10} modes

Let us now assume more complicated example consisting of a linear combination of collinear magnetic and electric dipole forming a generalised Huygens source. In such case, the surface current density on the spherical shell can be expressed as

$$\boldsymbol{J} = \boldsymbol{J}_{\mathrm{TM}} + Y(ka)\boldsymbol{J}_{\mathrm{TE}} \tag{23}$$

where $\boldsymbol{J}_{\mathrm{TM}}$ and $\boldsymbol{J}_{\mathrm{TE}}$ are given by (7) and (14), respectively, that is the current normalisation is performed over the TM_{10} mode only. As formulated, the coefficient $Y(ka)$ has to represent a transfer function of a causal system (being analytical in the lower half-plane of complex k), but otherwise can be arbitrary.

The current density (23) is frequency dependent and thus (12), (13a), (13b) are not valid any more. We can, however, follow a similar scheme and by comparing (1) with (2) and (3), and using (6a) and (6b) we can easily deduce that

$$Q_Z^{\mathrm{tuned}} = \frac{1}{2(P_{\mathrm{m}} - P_{\mathrm{e}})} \times \left| ka \frac{\partial\big((P_{\mathrm{m}} - P_{\mathrm{e}}) + \jmath\omega(W_{\mathrm{m}} - W_{\mathrm{e}})\big)}{\partial ka} + \jmath\omega\big|W_{\mathrm{m}} - W_{\mathrm{e}}\big| \right| \tag{24}$$

which could be taken as a general formula for the Q_Z^{tuned} evaluation. The resulting Q_Z^{tuned} will also be compared with the Q_{HC} evaluated by the classical extraction method of Collin and Rothschild [5] (refined by Hansen and Collin [12]).

The final formulas are rather clumsy in both cases to be shown explicitly and we will thus stick only to graphical results. In this respect, it is very interesting to use the new degree of freedom gained by the coefficient $Y(ka)$ in (23). More specifically, it is straightforward to show that the Q_{HC} depends solely on $|Y(ka)|^2$, whereas the Q_Z^{tuned} depends on both, $|Y(ka)|^2$ and $\partial|Y(ka)|^2/\partial ka$. The Q_Z^{tuned} thus, in fact, gained two new degrees of freedom. With respect to this paper it is then interesting to ask whether the coefficient $Y(ka)$ and its derivative cannot be optimised so that the Q_Z^{tuned} and the Q_{HC} of the combined current (23) would, at a given ka, reach lower values than the Q_Z^{tuned} and the Q_{HC} of the pure TM_{10} mode. The results are depicted in Figs. 8 and 9 for minimised values of the Q factors at four different values of ka. As a word of caution it is important to note here that the curves in Figs. 8 and 9 were obtained in such a way that the Q_Z^{tuned} and the Q_{HC} were optimised at a selected value of ka by the variation of $|Y(ka)|^2$ and $\partial|Y(ka)|^2/\partial ka$ and the optimal values of the variables were then kept in the rest of the depicted ka interval. This represents no problem for the Q_{HC}, which depends solely on

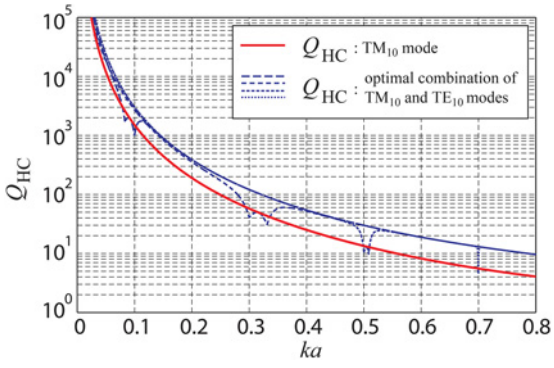

Fig. 8 *Comparison of the Q_{HC} factor of a combination of the TM_{10} and the TE_{10} modes for several optimal realisations of Y(ka) (dashed lines) and of the Q_{HC} of the pure TM_{10} mode (full line)*

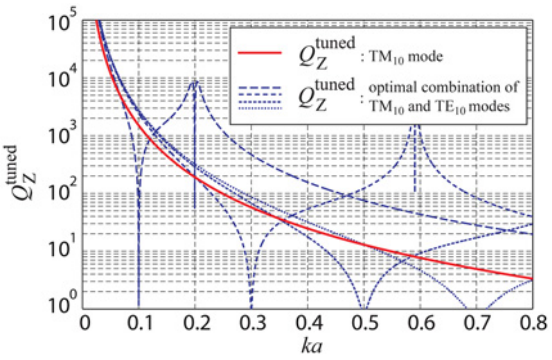

Fig. 9 *Comparison of the Q_Z^{tuned} factor of a combination of the TM_{10} and the TE_{10} modes for several optimal realisations of Y(ka) (dashed line) and of the Q_Z^{tuned} of the pure TM_{10} mode (full line)*

$|Y(ka)|^2$, but can only be approximately satisfied in the case of Q_Z^{tuned}, which depends on both, $|Y(ka)|^2$ and $\partial|Y(ka)|^2/\partial ka$.

The curves in Figs. 8 and 9 clearly show that both, the Q_{HC} and the Q_Z^{tuned}, can be lowered by a proper combination of the TM_{10} and the TE_{10} modes. The results for the Q_{HC} are coherent with [40, 41] and show just a mild drop. On the other hand, the Q_Z^{tuned} can be cast to values as low as $Q_Z^{\mathrm{tuned}} \simeq 1$, which, against all odds, can be done even for $ka \to 0$. Moreover, it can be shown that for approximately $ka > 1.3$, the Q_Z^{tuned} can always be made equal to zero, which follows the predictions of [23, 33].

7 Interpretation of the results

In this section, we will briefly comment and offer an interpretation for the above derived results in order to make the message of the paper perspicuous.

- The presented method describes a general scheme for the Q_Z^{tuned} evaluation in separable coordinate systems [42]. Since no explicit far-field energy extraction is needed, the method provides much simpler evaluation scheme than the classical derivation. In particular, the presented method avoids the complicated integration in the 'radial' direction. The only underlying integrals (4a) and (4b) can easily be evaluated in-hand for all common separable systems (spherical, cylindrical, spheroidal, ellipsoidal) since the integrands are polynomials of trigonometric functions. As a consequence, the evaluation of the Q_Z^{tuned} can, in principle, be done analytically in the separable systems.
- The good correspondence of the Q_Z^{tuned} with the classical Q for the TM_{10} and the TE_{10} modes is reported for $ka < 1$. This fact has, up to now, been only known for the Q_Z^{tuned} and the Q referring to the fields external to the spherical shell of sources [33], but has only been in the realm of a hypothesis for the fields including the internal region. The above given derivation puts this claim on solid grounds.
- Section 6 reveals, following the predictions of [23, 33], that when dealing with the combination of at least two modes, the Q_Z^{tuned} can become problematic. Although the Q_Z^{tuned} of the combination of the TM_{10} and the TE_{10} modes is mostly higher than the Q_Z^{tuned} of the pure TM_{10} mode, it can be locally lowered. The reduction can be much stronger than $Q_Z^{\mathrm{tuned}}/2$ of the pure TM_{10} mode, which would be expected for the classical Q factor [40, 41]. The reduction can cover many orders in magnitude and the Q_Z^{tuned} can in fact reach even zero value. Nevertheless, it should be recognised that this phenomenon does not reflect a physical reality of enhancing the FBW, but rather represents a shortcoming of the Q_Z^{tuned}. In practical designs of ESAs, the Q_Z^{tuned} of the pure TM_{10} mode should still be considered as a reasonable lower bound.
- The previous observation implies that the following statement on the Q_Z factor from the IEEE Std. [43]: 'NOTE – For an electrically small antenna, it is numerically equal to one-half the magnitude of the ratio of the incremental change in impedance to the

IET Microw. Antennas Propag., 2015, Vol. 9, Iss. 10, pp. 1096–1103

corresponding incremental change in frequency at resonance, divided by the ratio of the antenna resistance to the resonant frequency.' should be revisited, since the counter-example is provided in this paper and in [23, 33].

- Despite of the above shortcomings, the Q_Z^{tuned} still remains one of the best estimation of the FBW, since it can be measured, it is easy to evaluate and provides good results in the majority of the cases. It is however recommended to antenna designers to be aware of the above-mentioned problems, specifically in all the cases in which the measured/calculated Q_Z^{tuned} yields smaller value than the Q_Z^{tuned} of the pure TM_{10} mode.

8 Conclusion

The potential theory has been employed to obtain the quality factor Q_Z of important spherical current distributions, particularly of the fundamental TM and TE modes and their combination. It has been shown that the presented approach is effective, leading to unique and finite-energy terms with the far-field extraction implicitly included. For the presented cases of the spherical coordinate system, the Q_Z was obtained in closed form for any ka. The lower limit of the Q_Z of electrically small single-mode antennas was then obtained by series expansion of these expressions for small ka. Excellent agreement with the previous work of Thal and Hansen has been observed. On contrary, the analysis of multimodal currents revealed that Q_Z of the pure TM_{10} mode cannot be considered as a true lower bound of Q_Z of a general current radiating in free space. A particular example of linear combination of the TM_{10} and the TE_{10} modes has in fact showed that the Q_Z can be tuned to values as low as $Q_Z^{\text{tuned}} \simeq 1$ even for electrically very small structures.

The proposed approach has been presented on spherical modes, but it is not restricted to them, and can easily be extended to other separable coordinate systems. In this respect, the elliptic coordinates may be of considerable interest, as they can closely match the shape of many realistic antennas. The Q_Z obtained in this way could then represent practically oriented limitations for antenna designers.

9 Acknowledgments

This work has been supported by the Czech Science Foundation under projects nos. P102/12/2223 and 13-09086S. The authors would like to thank Mats Gustafsson from Lund University, Sweden for pointing out the possibility of Q_Z minimisation by the combination of modes.

10 References

1 Volakis, J.L., Chen, C.-C., Fujimoto, K.: 'Survey of small antenna theory' (Small Antennas: Miniaturization Techniques & Applications) (McGraw-Hill, 2010, 1st edn.)
2 Chu, L.J.: 'Physical limitations of omni-directional antennas', *J. Appl. Phys.*, 1948, **19**, pp. 1163–1175
3 Wheeler, H.A.: 'The radiansphere around a small antenna', *Proc. IRE*, 1959, **47**, (8), pp. 1325–1331
4 Harrington, R.F.: 'Effects of antenna size on gain, bandwidth, and efficiency', *J. Res. Natl. Bur. Stand.*, 1960, **64-D**, pp. 1–12
5 Collin, R.E., Rothschild, S.: 'Evaluation of antenna Q', *IEEE Trans. Antennas Propag.*, 1964, **12**, pp. 23–27
6 McLean, J.S.: 'A re-examination of the fundamental limits on the radiation Q of electrically small antennas', *IEEE Trans. Antennas Propag.*, 1996, **44**, (5), pp. 672–675
7 Thiele, G.A., Detweiler, P.T., Penno, R.P.: 'On the lower bound of the radiation Q for electrically small antennas', *IEEE Trans. Antennas Propag.*, 2003, **51**, (6), pp. 1263–1269
8 Rhodes, D.R.: 'On the stored energy of planar apertures', *IEEE Trans. Antennas Propag.*, 1966, **14**, (6), pp. 676–684
9 Thal, H.L.: 'New radiation Q limits for spherical wire antennas', *IEEE Trans. Antennas Propag.*, 2006, **54**, (10), pp. 2757–2763
10 Thal, H.L.: 'Comments on 'A New Chu Formula for Q'', *IEEE Antennas Propag. Mag.*, 2010, **52**, (1), pp. 214–215
11 Thal, H.L.: 'Q bounds for arbitrary small antennas: a circuit approach', *IEEE Trans. Antennas Propag.*, 2012, **60**, (7), pp. 3120–3128
12 Hansen, R.C., Collin, R.E.: 'A new Chu formula for Q', *IEEE Antennas Propag. Mag.*, 2009, **51**, (5), pp. 38–41
13 Hansen, T.V., Kim, O.S., Breinbjerg, O.: 'Stored energy and quality factor of spherical wave functions – in relation to spherical antennas with material cores', *IEEE Trans. Antennas Propag.*, 2012, **60**, (3), pp. 1281–1290
14 Fante, R.L.: 'Quality factor of general ideal antennas', *IEEE Trans. Antennas Propag.*, 1969, **17**, (2), pp. 151–157
15 Kim, O.S.: 'Minimum Q electrically small antennas', *IEEE Trans. Antennas Propag.*, 2012, **60**, (8), pp. 3551–3558
16 Gustafsson, M., Nordebo, S.: 'Optimal antenna currents for Q, superdirectivity, and radiation patterns using convex optimization', *IEEE Trans. Antennas Propag.*, 2013, **61**, (3), pp. 1109–1118
17 Capek, M., Hazdra, P., Eichler, J.: 'A method for the evaluation of radiation Q based on modal approach', *IEEE Trans. Antennas Propag.*, 2012, **60**, (10), pp. 4556–4567
18 Vandenbosch, G.A.E.: 'Reactive energies, impedance, and Q factor of radiating structures', *IEEE Trans. Antennas Propag.*, 2010, **58**, (4), pp. 1112–1127
19 Geyi, Y.: 'A method for the evaluation of small antenna Q', *IEEE Trans. Antennas Propag.*, 2003, **51**, (8), pp. 2124–2129
20 Vandenbosch, G.A.E.: 'Radiators in time domain, part I: Electric, magnetic, and radiated energies', *IEEE Trans. Antennas Propag.*, 2013, **61**, (8), pp. 3995–4003
21 Rhodes, D.R.: 'Observable stored energies of electromagnetic systems', *J. Franklin Inst.*, 1976, **302**, (3), pp. 225–237
22 Gustafsson, M., Sohl, C., Kristensson, G.: 'Physical limitations on antennas of arbitrary shape', *Proc. of R. Soc. A: Math., Phys. Eng. Sci.*, 2007, **463**, pp. 2589–2607
23 Gustafsson, M., Jonsson, B.L.G.: 'Stored electromagnetic energy and antenna Q', *Prog. Electromagn. Res.*, 2014, **150**, pp. 13–27
24 Vandenbosch, G.A.E., Volski, V.: 'Lower bounds for radiation Q of very small antennas of arbitrary topology'. Proc. of the Fourth European Conf. on Antennas and Propagation (EUCAP), Barcelona, Spain, April 2010, pp. 1–4
25 Seshadri, S.R.: 'Resonances of a spherical antenna'. Radio Science Meeting (USNC-URSI NRSM), 2013
26 Seshadri, S.R.: 'Constituents of power of an electric dipole of finite size', *J. Opt. Soc. Am. A*, 2008, **25**, (3), pp. 805–810
27 Sievenpiper, D.F., Dawson, D.C., Jacob, M.M., *et al.*: 'Exprerimental validation of performance limits and design guidelines for small antennas', *IEEE Trans. Antennas Propag.*, 2012, **60**, (1), pp. 8–19
28 Best, S.R., Hanna, D.L.: 'A performance comparison of fundamental small-antenna designs', *IEEE Antennas Propag. Mag.*, 2010, **52**, (1), pp. 47–70
29 Best, S.R.: 'The radiation properties of electrically small folded spherical helix antennas', *IEEE Trans. Antennas Propag.*, 2004, **52**, (4), pp. 953–960
30 Kim, O.S., Breinbjerg, O.: 'Reaching the Chu lower bound on Q with magnetic dipole antennas using a magnetic-coated PEC core', *IEEE Trans. Antennas Propag.*, 2011, **59**, (8), pp. 2799–2805
31 Yaghjian, A.D., Best, S.R.: 'Impedance, bandwidth and Q of antennas', *IEEE Trans. Antennas Propag.*, 2005, **53**, (4), pp. 1298–1324
32 Capek, M., Jelinek, L., Hazdra, P., Eichler, J.: 'The measurable Q factor and observable energies of radiating structures', *IEEE Trans. Antennas Propag.*, 2014, **62**, (1), pp. 311–318
33 Gustafsson, M., Nordebo, S.: 'Bandwidth, Q factor and resonance models of antennas'. *Prog. Electromag. Res.*, 2006, **62**, pp. 1–20
34 Morse, P.M., Feshbach, H.: 'Methods of theoretical physics' (McGraw-Hill, 1953)
35 Harrington, R.F.: 'Time-harmonic electromagnetic fields' (John Wiley - IEEE Press, 2001, 2nd edn.)
36 Jackson, J.D.: 'Classical electrodynamics' (John Wiley, 1998, 3rd edn.)
37 Jeffrey, A., Dai, H.-H.: 'Handbook of mathematical formulas and integrals' (Academic Press, 2008, 4th edn.)
38 Wolfram: Mathematica. [Online]. Available: http://www.wolfram.com/mathematica/
39 The MathWorks: The Matlab. [Online]. Available: www.mathworks.com
40 Thal, H.L.: 'Gain and Q bounds for coupled TM-TE modes', *IEEE Trans. Antennas Propag.*, 2009, **57**, pp. 1879–1885
41 Pozar, D.M.: 'New results for minimum Q, maximum gain, and polarization properties of electrically small arbitrary antennas'. Proc. of the Third European Conf. on Antennas and Propagation (EUCAP), Berlin, Germany, March 2009, pp. 23–27
42 Stratton, J.A.: 'Electromagnetic theory' (John Wiley, IEEE Press, 2007)
43 'Standard definitions of terms for antennas 145' (IEEE Antennas and Propagation Society Std., 1993)
44 Hansen, W.W.: 'A new type of expansion in radiation problems', *Phys. Rev.*, 1935, **47**, (2), pp. 139–143

11 Appendix

11.1 Appendix 1: Vector and scalar potentials of the TM_{10} and TE_{10} mode

The vector and scalar potentials are found by the expansion method of Appendix 2. For the particular case of the TM_{10} and the TE_{10} modes, we obtain the corresponding vector and scalar potentials regular for $r = [0, \infty)$ by using (36a)–(36c) with $\boldsymbol{a} = \boldsymbol{z}_0$, $\psi_{00} = z_0(kr)$ for $\boldsymbol{M}$-, $\boldsymbol{N}$-terms and with $\psi_{10} = z_1(kr)\cos(\vartheta)$ for $\boldsymbol{L}$-terms, where $z_n(x)$ is a spherical Bessel function of order n and where we will use $z_n(x) = j_n(x)$ for $r < a$ and $z_n = h_n^{(2)}$ for $r > a$. The resulting

vector wave functions read

$$\boldsymbol{M}_{10} = \boldsymbol{\varphi}_0 k z_1(kr)\sin(\vartheta) \tag{25a}$$

$$\boldsymbol{N}_{10} = \boldsymbol{r}_0 \frac{2}{r} z_1(kr)\cos(\vartheta) + \boldsymbol{\vartheta}_0 \frac{1}{r}\big(z_1(kr) - krz_0(kr)\big)\sin(\vartheta) \tag{25b}$$

$$\boldsymbol{L}_{10} = \boldsymbol{r}_0 \frac{1}{r}\big(z_1(kr) - krz_2(kr)\big)\cos(\vartheta) - \boldsymbol{\vartheta}_0 \frac{1}{r} z_1(kr)\sin(\vartheta) \tag{25c}$$

The vector potential of the TM_{10} mode will be expressed as a linear combination of (25b) and (25c) because of the non-vanishing charge density and the need for the $\boldsymbol{L}_{10}$-term. The vector potential of the TE_{10} mode will be expressed in terms of (25a) only, since there is no charge density and thus no scalar potential.

According to the above, in order to find the vector and the scalar potential of the TM_{10} mode, we choose

$$\left.\begin{aligned} \boldsymbol{A} &= C_1\boldsymbol{N}_{10} + D_1\boldsymbol{L}_{10} \\ \varphi &= -\jmath\omega D_1\psi_{10} \end{aligned}\right\} r < a \tag{26a}$$

$$\left.\begin{aligned} \boldsymbol{A} &= C_2\boldsymbol{N}_{10} + D_2\boldsymbol{L}_{10} \\ \varphi &= -\jmath\omega D_2\psi_{10} \end{aligned}\right\} r > a \tag{26b}$$

where C, D are constants to be determined. The $C_{1,2}$ can be determined from the boundary conditions on the current shell at $r = a$, that is by continuity of the tangential electric field $\boldsymbol{n}_0 \times (\boldsymbol{E}_1 - \boldsymbol{E}_2) = 0$ and discontinuity of the tangential magnetic field $\boldsymbol{n}_0 \times (\boldsymbol{H}_1 - \boldsymbol{H}_2) = \boldsymbol{K}$, where $\boldsymbol{K}$ is the surface current density and where the normal $\boldsymbol{n}_0$ points to the region 1 [36]. The boundary conditions lead to

$$C_1 = -\frac{\jmath\mu}{2\pi k}\left(h_1^{(2)}(ka) - kah_0^{(2)}(ka)\right) \tag{27a}$$

$$C_2 = -\frac{\jmath\mu}{2\pi k}\left(j_1(ka) - kaj_0(ka)\right) \tag{27b}$$

For the unknown constants $D_{1,2}$ in (26a) and (26b), the only condition that needs to be satisfied is the wave equation for the scalar potential in the Lorentz gauge

$$\nabla^2\varphi + k^2\varphi = -\frac{\rho}{\epsilon} \tag{28}$$

Choosing then the scalar potential being continuous at $r = a$, (28) dictates

$$\frac{\partial\varphi}{\partial r}\Big|_{r=a^+} - \frac{\partial\varphi}{\partial r}\Big|_{r=a^-} = -\jmath\frac{\cos(\vartheta)}{\omega\epsilon\pi a^2} \tag{29}$$

which leads to

$$D_1 = \frac{\jmath\mu}{k\pi}h_1^{(2)}(ka) \tag{30a}$$

$$D_2 = \frac{\jmath\mu}{k\pi}j_1(ka) \tag{30b}$$

Putting all together we have for $r < a$

$$\begin{aligned} A_\vartheta = -\frac{\jmath\mu}{2\pi kr}\sin(\vartheta)\Big(&2h_1^{(2)}(ka)j_1(kr) \\ &+\Big(h_1^{(2)}(ka) - kah_0^{(2)}(ka)\Big)\big(j_1(kr) - krj_0(kr)\big)\Big) \end{aligned} \tag{31a}$$

$$\varphi = \frac{\omega\mu}{\pi k}h_1^{(2)}(ka)j_1(kr)\cos(\vartheta) \tag{31b}$$

and for $r > a$

$$\begin{aligned} A_\vartheta = -\frac{\jmath\mu}{2\pi kr}\sin(\vartheta)\Big(&2h_1^{(2)}(kr)j_1(ka) \\ &+\Big(h_1^{(2)}(kr) - krh_0^{(2)}(kr)\Big)\big(j_1(ka) - kaj_0(ka)\big)\Big) \end{aligned} \tag{32a}$$

$$\varphi = \frac{\omega\mu}{\pi k}h_1^{(2)}(kr)j_1(ka)\cos(\vartheta) \tag{32b}$$

where the first terms in the vector potential come from $\boldsymbol{L}_{10}$ and the second terms come from $\boldsymbol{N}_{10}$.

The derivation of the scalar and vector potential of the TE_{10} mode is analogous to the above, and results in

$$A_\varphi = -\frac{\jmath\mu}{2}\sin(\vartheta)kaj_1(kr)h_1^{(2)}(ka) \tag{33a}$$

$$\varphi = 0 \tag{33b}$$

for $r < a$, and

$$A_\varphi = -\frac{\jmath\mu}{2}\sin(\vartheta)kaj_1(ka)h_1^{(2)}(kr) \tag{34a}$$

$$\varphi = 0 \tag{34b}$$

for $r < a$.

11.2 Appendix 2: Expansion of the vector wave equation in separable systems

In this appendix, we recall the expansion of the vector wave equation and point out some aspects important for a consistent definition of Q. This approach leads to the analytical calculation of the Q factor for the separable systems.

According to [44], the general solution of $\nabla^2\boldsymbol{A} + k^2\boldsymbol{A} = 0$ can be written as

$$\boldsymbol{A} = \sum_n \left(\alpha_n\boldsymbol{M}_n + \beta_n\boldsymbol{N}_n + \gamma_n\boldsymbol{L}_n\right) \tag{35}$$

where

$$\boldsymbol{M}_n = \nabla \times (\boldsymbol{a}\psi_n) \tag{36a}$$

$$\boldsymbol{N}_n = \frac{1}{k}\nabla \times \boldsymbol{M}_n \tag{36b}$$

$$\boldsymbol{L}_n = \nabla\psi_n \tag{36c}$$

$\boldsymbol{a}$ is a constant vector, and scalar function ψ_n satisfies

$$\nabla^2\psi_n + k^2\psi_n = 0 \tag{37}$$

The conventional notation from [42] is used for clarity of the paper. Taking now the vector field $\boldsymbol{A}$ as a magnetic vector potential in the Lorentz gauge, one can verify that the scalar potential is

$$\varphi = -\frac{1}{\jmath\omega\epsilon\mu}\nabla\cdot\boldsymbol{A} = -\jmath\omega\sum_n \gamma_n\psi_n \tag{38}$$

where μ is the permeability of the vacuum, and that the field quantities read

$$\boldsymbol{E} = -\frac{\jmath\omega}{k^2}(\nabla\nabla\cdot\boldsymbol{A} + k^2\boldsymbol{A}) = -\jmath\omega\sum_n(\alpha_n\boldsymbol{M}_n + \beta_n\boldsymbol{N}_n) \tag{39a}$$

$$\boldsymbol{H} = \frac{1}{\mu}\nabla\times\boldsymbol{A} = \frac{k}{\mu}\sum_n(\alpha_n\boldsymbol{N}_n + \beta_n\boldsymbol{M}_n) \tag{39b}$$

where we used the fact that $\nabla\times\boldsymbol{N}_m = k\boldsymbol{M}_n$.

It is worth noting that any measurable quantity is independent of $\boldsymbol{L}_n$-terms (which is equivalent to gauge invariance). Particularly, if a volume is chosen so that it contains all the sources and if the vector potential (35) is divided as $\boldsymbol{A} = \boldsymbol{A}^{M,\,N} + \boldsymbol{A}^{L}$, with $\boldsymbol{A}^{M,\,N}$ belonging to $\boldsymbol{M}_n$-, $\boldsymbol{N}_n$-terms and $\boldsymbol{A}^{L}$ belonging to $\boldsymbol{L}_n$-terms, then, one can easily realise that

$$\int_{\Omega} \left(\boldsymbol{A}^{L} \cdot \boldsymbol{J}^{*} - \varphi\rho^{*}\right) \mathrm{d}\boldsymbol{r} = 0 \tag{40}$$

and thus that only the $\boldsymbol{M}_n$-, $\boldsymbol{N}_n$-terms participate in the definition of the complex power [36]

$$\jmath\omega \int_{\Omega} \left(\boldsymbol{A} \cdot \boldsymbol{J}^{*} - \varphi\rho^{*}\right) \mathrm{d}\boldsymbol{r} = \jmath\omega \int_{\Omega} \left(\boldsymbol{A}^{M,N} \cdot \boldsymbol{J}^{*}\right) \mathrm{d}\boldsymbol{r} \tag{41}$$

11.3 Analytical expressions for the Q_Z^{tuned} and the Q_{HC} of the TM_{10} and the TE_{10} modes

This appendix presents the analytical expressions for the Q_{HC} and the Q_Z^{tuned} for the dominant spherical TM_{10} and TE_{10} modes. The Q_Z^{tuned} is evaluated according to the method introduced in this paper (Sections 3–5). The Q_{HC} is evaluated using the classical extraction method of Collin and Rothschild [5] (Hansen and Collin [12]).

Particularly, the expressions for the TM_{10} mode read (see (42) and (43))

whereas the expressions for the TE_{10} mode read

$$Q_{\text{HC}} = \max\left\{ \begin{array}{c} \dfrac{2x(x^2+1) + 4x\cos(2x) + (x^2-3)\sin(2x)}{4\left(\sin(x) - x\cos(x)\right)^2}, \\ \dfrac{(x^2+1)\left(2x - \sin(2x)\right)}{4\left(\sin(x) - x\cos(x)\right)^2} \end{array} \right\} \tag{44}$$

(see (45))

$$Q_{\text{HC}} = \max\left\{ \begin{array}{c} \dfrac{2(x^5 - x^3 + x) - 4x(x^2-2)\cos(2x) - (x^4 - 9x^2 + 5)\sin(2x)}{4\left(x\cos(x) + (x^2-1)\sin(x)\right)^2}, \\ \dfrac{2(x^5 - x^3 + x) + 4x\cos(2x) + (x^4 + 3x^2 - 3)\sin(2x)}{4\left(x\cos(x) + (x^2-1)\sin(x)\right)^2} \end{array} \right\} \tag{42}$$

$$Q_Z^{\text{tuned}} = \frac{\left|x^5 - 2\jmath x^4 - 4x^3 + 5\jmath x^2 + 4x - 2\jmath + \mathrm{e}^{2\jmath x}\left(2\jmath - \jmath x^2 + \cdots\right.\right.}{2\left(x\cos(x) + \cdots\right.} \\ \frac{\left.\left. \ldots + \left|\left(x\sin(x) - (x^2-1)\cos(x)\right)\left(x\cos(x) + (x^2-1)\sin(x)\right)\right|\right)\right|}{\left.\cdots + (x^2-1)\sin(x)\right)^2} \tag{43}$$

$$Q_Z^{\text{tuned}} = \frac{\left|x^3 - 2\jmath x^2 - 2x + \jmath - \mathrm{e}^{2\jmath x}\left(\jmath + \left|\left(x\cos(x) - \sin(x)\right)\left(x\sin(x) + \cos(x)\right)\right|\right)\right|}{2\left(\sin(x) - x\cos(x)\right)^2} \tag{45}$$

VIII

M. Capek and L. Jelinek, "Comments on 'On Stored Energies and Radiation Q'," *IEEE Trans. Antennas Propag.*, vol. 63, 2015. [41∗]

Comments on "On Stored Energies and Radiation Q"

Miloslav Capek, *Member, IEEE,* and Lukas Jelinek

The commented paper [1] claims to provide a new expression for an energy stored around a general radiator. The major purpose of this comment is to show that the claim is unjustified. Alongside with this issue, it is pointed out that some of the core formulas of [1] are not completely correct, and that their correct form has in fact been derived elsewhere, though for the purpose of evaluating the quality factor Q_Z and not the stored energies.

The major outcome of the commented paper [1] is claimed to be equations (29)–(31), which should represent the total stored energy $\widetilde{W}_\mathrm{m}+\widetilde{W}_\mathrm{e}$, the stored magnetic energy $\widetilde{W}_\mathrm{m}$, and the stored electric energy $\widetilde{W}_\mathrm{e}$ (using the notation of [1]), and their connection with (2), (4), (5) of [1]. Equations (4), (5) of [1] are however not valid under the assumptions of [1], see [2] and [3].

In order to be more specific, we will first recall here a well-established result [4], [5]

$$\frac{\partial X}{\partial\omega}\left|I_0\right|^2=\int_0^\infty\int_\Omega\left(\mu\|\boldsymbol{H}\|^2+\epsilon\|\boldsymbol{E}\|^2-2\epsilon\frac{\|\boldsymbol{F}\|^2}{r^2}\right)r^2\,\mathrm{d}\Omega\,\mathrm{d}r+2\sqrt{\frac{\epsilon}{\mu}}\,\mathrm{Im}\int_\Omega\left.\frac{\partial\boldsymbol{F}}{\partial\omega}\right|_{I_0}\cdot\boldsymbol{F}^*\,\mathrm{d}\Omega, \tag{1}$$

where X is the input reactance of the considered radiator, which is fed by a frequency independent[1] current I_0, and which is surrounded by an homogeneous, isotropic and non-dispersive medium of permittivity ϵ and permeability μ. Equation (1) further assumes r to be the radial coordinate, $\mathrm{d}\Omega=\sin\theta\,\mathrm{d}\theta\,\mathrm{d}\varphi$ being the solid angle differential, $\boldsymbol{E}$, $\boldsymbol{H}$ being the electric and magnetic intensity generated by the antenna, respectively, and $\boldsymbol{F}(\boldsymbol{r})=\lim_{r\to\infty}\{r\boldsymbol{E}(\boldsymbol{r})\exp(\mathrm{j}kr)\}$ with k being the wave-number. The total radiated power can be written as [4], [5]

$$P_\mathrm{rad}=\frac{1}{2}\sqrt{\frac{\epsilon}{\mu}}\int_\Omega\|\boldsymbol{F}\|^2\,\mathrm{d}\Omega. \tag{2}$$

Manuscript received XXX, 2015; revised XXX, 2015.

The authors are with the Department of Electromagnetic Field, Faculty of Electrical Engineering, Czech Technical University in Prague, Technicka 2, 16627, Prague, Czech Republic (e-mail: miloslav.capek@fel.cvut.cz, lukas.jelinek@fel.cvut.cz).

[1]The assumption of the frequency independent current at the input port is essential for the validity of (1) and of (8), (9) later on. This assumption is not used in [1]. However, as the system at hand is linear, this input current normalization can always be made. Any result claimed in [1] as valid for general input current thus must be valid also for the frequency independent input current. It is also important to stress that the frequency independence of the input current does not imply the frequency independence of the current density on the entire radiator.

It follows from (2) that (2) of [1] can be rewritten as

$$\widetilde{W}_\mathrm{m}+\widetilde{W}_\mathrm{e}=\lim_{r\to\infty}\left(W_\mathrm{m}+W_\mathrm{e}-\frac{r}{\nu}P_\mathrm{rad}\right)=\\=\frac{1}{4}\int_0^\infty\int_\Omega\left(\mu\|\boldsymbol{H}\|^2+\epsilon\|\boldsymbol{E}\|^2-2\epsilon\frac{\|\boldsymbol{F}\|^2}{r^2}\right)r^2\,\mathrm{d}\Omega\,\mathrm{d}r, \tag{3}$$

in which $\nu=1/\sqrt{\mu\epsilon}$. Equation (3) together with (4), (5) of [1] thus results in

$$\frac{\partial X}{\partial\omega}\left|I_0\right|^2\stackrel{?}{=}\int_0^\infty\int_\Omega\left(\mu\|\boldsymbol{H}\|^2+\epsilon\|\boldsymbol{E}\|^2-2\epsilon\frac{\|\boldsymbol{F}\|^2}{r^2}\right)r^2\,\mathrm{d}\Omega\,\mathrm{d}r, \tag{4}$$

which is not generally correct as it lacks the last term on the RHS of (1), which is generally non-zero [5, Fig. 10]. This omission has in fact already been mentioned in [5, text above Eq. (72)] and [3, text above Eq. (4)], but has been missed by the author of [1] despite of [5] being cited in [1].

Alongside with the above argumentation, it is worth noting that the questionable association (result of (4), (5) of [1])

$$\frac{1}{4}\frac{\partial X}{\partial\omega}\left|I_0\right|^2\stackrel{?}{=}\widetilde{W}_\mathrm{m}+\widetilde{W}_\mathrm{e}, \tag{5}$$

can be tested directly. To this point, the solid line in Figs. 1, 2 shows that $\partial X/\partial\omega$ can be negative for radiating systems, unlike to the stored electromagnetic energy. This well established theoretical and experimental fact (see for example [3]) is omitted by the author of [1].

The next commentary concerns the seemingly erroneous relation of (29)–(31) of [1] with (4), (5) of [1], which can be written as

$$\frac{1}{4}\frac{\partial X}{\partial\omega}\left|I_0\right|^2\stackrel{?}{=}W^{(\mathrm{Vandenbosch})}\\-\frac{\omega\eta\nu}{8\pi}\int_{V_1}\int_{V_2}\mathrm{Im}\left\{\rho^*(\boldsymbol{r}_1)\frac{\partial\rho(\boldsymbol{r}_2)}{\partial\omega}\right\}\frac{\sin(kR)}{R}\,\mathrm{d}V_2\,\mathrm{d}V_1\\+\frac{\omega\eta\nu}{8\pi}\int_{V_1}\int_{V_2}\frac{1}{\nu^2}\mathrm{Im}\left\{\boldsymbol{J}^*(\boldsymbol{r}_1)\cdot\frac{\partial\boldsymbol{J}(\boldsymbol{r}_2)}{\partial\omega}\right\}\frac{\sin(kR)}{R}\,\mathrm{d}V_2\,\mathrm{d}V_1, \tag{6}$$

where

$$W^{(\mathrm{Vandenbosch})}=\\\frac{\eta\nu}{16\pi}\int_{V_1}\int_{V_2}\left(\rho^*(\boldsymbol{r}_1)\rho(\boldsymbol{r}_2)+\frac{1}{\nu^2}\boldsymbol{J}^*(\boldsymbol{r}_1)\cdot\boldsymbol{J}(\boldsymbol{r}_2)\right)\frac{\cos(kR)}{R}\,\mathrm{d}V_2\,\mathrm{d}V_1\\+\frac{\omega\eta}{16\pi}\int_{V_1}\int_{V_2}\left(\rho^*(\boldsymbol{r}_1)\rho(\boldsymbol{r}_2)-\frac{1}{\nu^2}\boldsymbol{J}^*(\boldsymbol{r}_1)\cdot\boldsymbol{J}(\boldsymbol{r}_2)\right)\sin(kR)\,\mathrm{d}V_2\,\mathrm{d}V \tag{7}$$

is an energy defined in [6, Eq. (63), (64)], $\rho(\boldsymbol{r})$ is the charge density, and η is the wave impedance. In fact, the correct version of (6) has previously been derived in [7], [8] and reads

(using the notation of this comment)

$$\begin{aligned}&\frac{1}{4}\frac{\partial X}{\partial \omega}\left|I_0\right|^2 = W^{(\text{Vandenbosch})}\\&-\frac{\omega\eta\nu}{8\pi}\int\limits_{V_1}\int\limits_{V_2}\operatorname{Re}\left\{\frac{1}{\omega}\rho^*\left(\boldsymbol{r}_1\right)\frac{\partial\omega\rho\left(\boldsymbol{r}_2\right)}{\partial\omega}\right\}\frac{\cos\left(kR\right)}{R}\,\mathrm{d}V_2\,\mathrm{d}V_1\\&+\frac{\omega\eta\nu}{8\pi}\int\limits_{V_1}\int\limits_{V_2}\frac{1}{\nu^2}\operatorname{Re}\left\{\boldsymbol{J}^*\left(\boldsymbol{r}_1\right)\cdot\frac{\partial\boldsymbol{J}\left(\boldsymbol{r}_2\right)}{\partial\omega}\right\}\frac{\cos\left(kR\right)}{R}\,\mathrm{d}V_2\,\mathrm{d}V_1,\end{aligned}\tag{8}$$

where the input current I_0 is assumed to be frequency independent. Formula (6) differs from (8) in the last two terms. The Figs. 1, 2 show which of the two formulas better represents the frequency change of the input reactance calculated as a ratio between voltage and current at the input port. The comparison is performed on an example of thin dipole similar to that of [1] and on an example of Yagi-Uda antenna treated in [5]. In order to further support our claims, an additional and independent evaluation of $\partial X/\partial\omega$ can be found. This evaluation relies on a combination of (1) and results of [9, Eqs. (4), (5)] or similarly [10, Eqs. (25), (26), (28)], which reads

$$\begin{aligned}&\frac{1}{4}\frac{\partial X}{\partial \omega}\left|I_0\right|^2 = W^{(\text{Vandenbosch})}\\&-\frac{\eta\nu}{16\pi}\int\limits_{V_1}\int\limits_{V_2}\operatorname{Im}\left\{\rho^*\left(\boldsymbol{r}_1\right)\rho\left(\boldsymbol{r}_2\right)\right\}\mathcal{G}\left(\boldsymbol{r}_1,\boldsymbol{r}_2\right)\,\mathrm{d}V_2\,\mathrm{d}V_1\\&+\frac{\eta\nu}{16\pi}\int\limits_{V_1}\int\limits_{V_2}\frac{1}{\nu^2}\operatorname{Im}\left\{\boldsymbol{J}^*\left(\boldsymbol{r}_1\right)\cdot\boldsymbol{J}\left(\boldsymbol{r}_2\right)\right\}\mathcal{G}\left(\boldsymbol{r}_1,\boldsymbol{r}_2\right)\,\mathrm{d}V_2\,\mathrm{d}V_1\\&+\frac{1}{2}\sqrt{\frac{\epsilon}{\mu}}\operatorname{Im}\int\limits_{\Omega}\left.\frac{\partial\boldsymbol{F}}{\partial\omega}\right|_{I_0}\cdot\boldsymbol{F}^*\,\mathrm{d}\Omega,\end{aligned}\tag{9}$$

in which

$$\mathcal{G}\left(\boldsymbol{r}_1,\boldsymbol{r}_2\right)=\frac{k^2\left(\|\boldsymbol{r}_2\|^2-\|\boldsymbol{r}_1\|^2\right)\mathrm{j}_1\left(kR\right)}{R},\tag{10}$$

with $\mathrm{j}_1\left(kR\right)$ being the spherical Bessel function of the 1st order. The results of (9) are also depicted in Fig. 1 and Fig. 2. The error in (6) observed in Figs. 1, 2 is however not visible in [1], the reason most probably being the assumption of an unrealistic current distribution with a purely reactive input impedance at the driving port. In contrast, Figs. 1, 2 consider a rigorous full-wave solution.

As a final comment, it is important to mention that the results of [7], [8], for example (8), are not mentioned in [1], although they address the related problem of the source concept of the quality factor Q_Z.

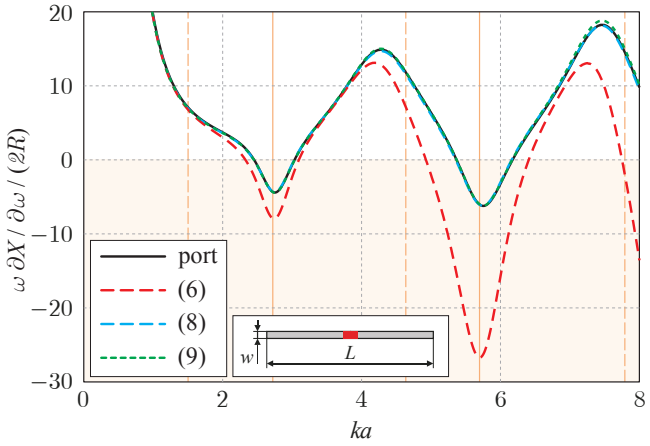

Fig. 1. The normalized frequency derivative of the input reactance of a thin dipole made of a perfectly electrically conducting strip of width $w = L/200$ and of infinitesimal thickness. The dipole is fed in its center by a delta gap source with the input current normalized to 1 A. The quantity R denotes the input resistance of the antenna. The calculation has been performed in the FEKO full-wave integral equation solver [11]. The frequency derivative of the input reactance is calculated from the port impedance (solid line), from (6) (red dashed line), from (8) (blue dashed line), and from (9) (green dashed line). The dashed orange lines highlight resonances, while the full orange lines highlight antiresonances.

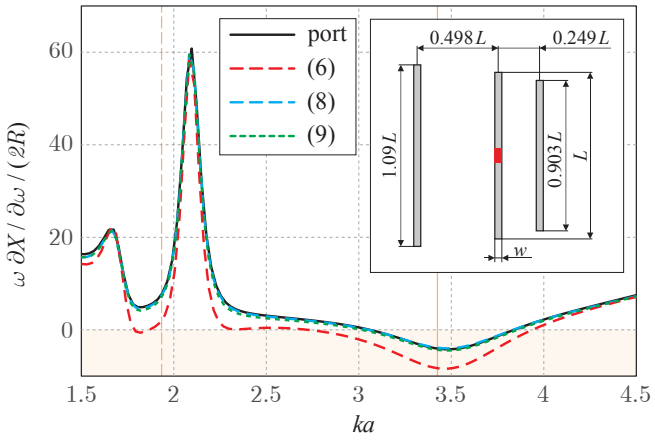

Fig. 2. The normalized frequency derivative of the input reactance of a thin-strip Yagi-Uda antenna (see the inset). The width of the strip and its thickness, as well as the meaning of depicted curves, are the same as in Fig. 1.

REFERENCES

[1] W. Geyi, "On stored energies and radiation Q," *IEEE Trans. Antennas Propag.*, vol. 63, no. 2, pp. 636–645, Feb. 2015.
[2] J. B. Andersen and S. Berntsen, "Comments to 'The Foster Reactance Theorem for Antennas and Radiation Q'," *IEEE Trans. Antennas Propag.*, vol. 55, no. 3, pp. 1013–1014, March 2007.
[3] S. R. Best, "The Foster reactance theorem and quality factor for antennas," *IEEE Antennas Wireless Propag. Lett.*, vol. 3, no. 1, pp. 306–309, Dec. 2004.
[4] D. R. Rhodes, "Observable stored energies of electromagnetic systems," *J. Franklin Inst.*, vol. 302, no. 3, pp. 225–237, 1976.
[5] A. D. Yaghjian and S. R. Best, "Impedance, bandwidth and Q of antennas," *IEEE Trans. Antennas Propag.*, vol. 53, no. 4, pp. 1298–1324, April 2005.
[6] G. A. E. Vandenbosch, "Reactive energies, impedance, and Q factor of radiating structures," *IEEE Trans. Antennas Propag.*, vol. 58, no. 4, pp. 1112–1127, Apr. 2010.
[7] M. Capek, L. Jelinek, P. Hazdra, and J. Eichler, "The measurable Q factor and observable energies of radiating structures," *IEEE Trans. Antennas Propag.*, vol. 62, no. 1, pp. 311–318, Jan. 2014.
[8] ——. The measurable Q factor and observable energies of radiating structures. eprint arXiv: 1309.6122. [Online]. Available: http://arxiv.org/abs/1309.6122
[9] M. Gustafsson and B. L. G. Jonsson, "Antenna Q and stored energy expressed in the fields, currents, and input impedance," *IEEE Trans. Antennas Propag.*, vol. 63, no. 1, pp. 240–249, Jan. 2015.
[10] ——, "Stored electromagnetic energy and antenna Q," *Prog. Electromagn. Res.*, vol. 150, pp. 13–27, 2014.
[11] EM Software & Systems-S.A. FEKO. [Online]. Available: www.feko.info

IX

P. Hazdra, M. Capek, J. Eichler, and M. Mazanek, "The radiation Q-factor of a horizontal $\lambda/2$ dipole above ground plane," *IEEE Antennas Wireless Propag. Lett.*, vol. 13, pp. 1073–1075, 2014. [43∗]

The Radiation Q-Factor of a Horizontal $\lambda/2$ Dipole Above Ground Plane

Pavel Hazdra, *Member, IEEE*, Miloslav Capek, *Member, IEEE*, Jan Eichler, *Student Member, IEEE*, and Milos Mazanek, *Member, IEEE*

***Abstract*—Closed-form equations are given for radiation quality factor of a thin-wire $\lambda/2$ dipole above an infinite electric ground plane. Particular results of interest include a simple formula for a small separation between the dipole and the ground and for one dipole in free space.**

***Index Terms*—Antenna theory, dipole antennas, Q-factor.**

I. Introduction

In [1], the radiation Q-factor of coupled dipoles with sinusoidal current distribution has been numerically investigated by using the work of Vandenbosch [2]. This letter presents a slightly different approach allowing us to easily find the Q-factor of side-by-side coupled dipoles in closed form. It is assumed that the dipoles are thin and operating at a $\lambda/2$ resonance. The derivation is based on an analytical knowledge of the input impedance of such antenna configuration, and the Q is evaluated from the frequency changes of the impedance at the feeding port [3], [4]. For simplicity, we deal only with the case of two out-of-phase dipoles, a situation equivalent to the practically important case (see, e.g., Kraus [5]) of one horizontal dipole above the infinite electric ground plane.

II. Q-Factor of a Dipole Above Infinite Ground

Using the method of images and the concept of self- and mutual impedances, the input driving impedance $Z_{\rm in}$ of a horizontal dipole placed at a height h above an infinite perfect electric ground plane (see Fig. 1) is given by [5]

$$Z_{\rm in} = Z_{11} - Z_{12}(h) \tag{1}$$

where the self- and mutual impedance parts for sinusoidal current distribution are obtained by the Induced EMF method [6] as [7]

$$R_{11} = 30\left[\gamma + \ln(2\pi) - {\rm Ci}(2\pi)\right] \tag{2}$$

Manuscript received February 27, 2014; revised April 29, 2014; May 13, 2014; and May 30, 2014; accepted June 02, 2014. Date of publication June 06, 2014; date of current version June 13, 2014. This work was supported by the Czech Science Foundation under Grant No. P102/12/2223.

The authors are with the Department of Electromagnetic Field, Faculty of Electrical Engineering, Czech Technical University in Prague, 16627 Prague, Czech Republic (e-mail: hazdrap@fel.cvut.cz).

Color versions of one or more of the figures in this letter are available online at http://ieeexplore.ieee.org.

Digital Object Identifier 10.1109/LAWP.2014.2329421

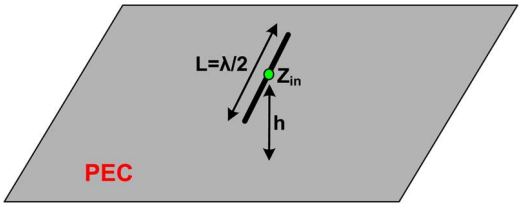

Fig. 1. Center-fed $\lambda/2$ horizontal dipole above PEC ground plane.

$$X_{11} = 30\left\{2{\rm Si}(kL) + \cos(kL)\left\{2{\rm Si}(kL) - {\rm Si}(2kL)\right\} - \sin(kL)\left[2{\rm Ci}(kL) - {\rm Ci}(2kL) - {\rm Ci}\left(\frac{2ka^2}{L}\right)\right]\right\} \tag{3}$$

$$R_{12} = 30\left[2{\rm Ci}(4\pi u) - {\rm C}(u)\right] \tag{4}$$

$$X_{12} = -30\left[2{\rm Si}(4\pi u) - {\rm S}(u)\right]. \tag{5}$$

In the above, Si and Ci are the sine and cosine integral functions [6], a is dipole radius, $u = h/\lambda$ is distance of the dipole above the ground in terms of wavelength, k is wavenumber, and $\gamma \doteq 0.577$ is the Euler constant. Furthermore, we define

$${\rm C}(u) = {\rm Ci}\left[\pi(\sqrt{16u^2+1}+1)\right] + {\rm Ci}\left[\pi(\sqrt{16u^2+1}-1)\right] \tag{6}$$

and

$${\rm S}(u) = {\rm Si}\left[\pi(\sqrt{16u^2+1}+1)\right] + {\rm Si}\left[\pi(\sqrt{16u^2+1}-1)\right]. \tag{7}$$

Around resonance, we may assume that the change in resistance with frequency is negligible, so according to [3], we have

$$Q_{\rm Z} \cong Q_{\rm X} = \frac{\omega_0}{2R_{in}}\frac{\partial X_{in}}{\partial \omega} = \frac{k}{2}\frac{\frac{\partial(X_{11}-X_{12})}{\partial k}}{R_{11}-R_{12}} \tag{8}$$

where $k = 2\pi/\lambda$. Working out (8) yields the main result

$$Q_{\rm X} = \frac{1}{2}\frac{\pi\left[2{\rm Ci}(\pi) - {\rm Ci}(2\pi) - {\rm Ci}\left(8\pi\frac{a^2}{\lambda^2}\right)\right] + {\rm s}(u)}{\gamma + \ln(2\pi) - {\rm Ci}(2\pi) - 2{\rm Ci}(4\pi u) + {\rm C}(u)}, \tag{9}$$

where

$${\rm s}(u) = 2\left\{\sin(4\pi u) - \sin\left[\pi(\sqrt{16u^2+1}+1)\right]\right\}. \tag{10}$$

The (9) is valid for $\lambda/2$ dipole with sinusoidal linear current distribution, and the usual thin-wire approximation $(a/\lambda \ll 1)$

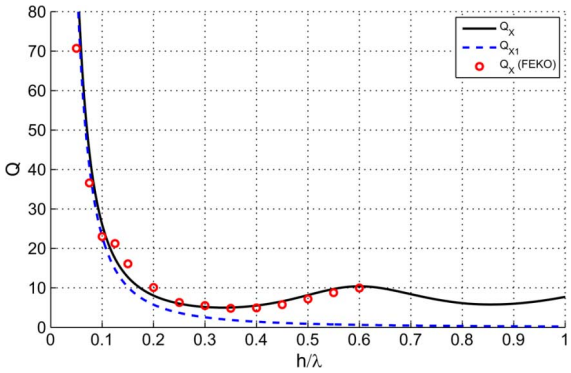

Fig. 2. Quality factors calculated by (9) and (12), compared to the numerical results from FEKO software. A dipole of length $\lambda/2$ with $a/\lambda = 5 \cdot 10^{-4}$.

is required. Consequently, we may expand the Ci function for small arguments as

$$\mathrm{Ci}\left(8\pi\frac{a^2}{\lambda^2}\right) \cong \gamma + \ln(8\pi) + 2\ln\left(\frac{a}{\lambda}\right). \tag{11}$$

Indeed, it is possible to take into account the frequency variations of R_{in} and to evaluate the Q_{Z} too, but the resulting expressions are tricky, and (as already shown in [1] and [4]) the differences between Q_{Z} and Q_{X} are very small in resonance.

A. Asymptotic Case of $u \to 0$

Equation (9) is still quite complex, but may be significantly simplified by assuming very small distances above the ground $u = h/\lambda \to 0$. Then, (9) reduces to asymptotical result of practical interest

$$Q_{\mathrm{X1}} = \frac{1}{16\pi}\frac{2\mathrm{Ci}(\pi) - \mathrm{Ci}(2\pi) - \gamma - \ln(8\pi) - 2\ln\left(\frac{a}{\lambda}\right)}{u^2} \tag{12}$$

where it is noted that $Q_{\mathrm{X1}} \propto u^{-2} = (\lambda/h)^2$.

Evaluating the various constants in nominator gives the following simple formula:

$$Q_{X1} = \frac{1}{16\pi}\frac{-3.631 - 2\ln\left(\frac{a}{\lambda}\right)}{u^2}. \tag{13}$$

The dependence of (9) and its "small-distance" approximation (12) on h/λ are shown in Fig. 2, together with a few values numerically obtained by the full-wave method-of-moments software FEKO [8]. A thin dipole with radius $a/\lambda = 5 \cdot 10^{-4}$ has been considered. It is observed that (12) differs from (9) by less than 10% for $h/\lambda < 0.1$.

B. Radiated and Reactive Powers and Minimum of Q

The numerically obtained minimum of (9) occurs at $h/\lambda \cong 0.33$. The corresponding Q is lower than for free space (Q_{fs}) for this radius by a factor of $Q_{\mathrm{gnd}}/Q_{\mathrm{fs}} \cong 0.67$. The minimum is predominantly caused by interaction of the radiated power between the dipole and its image, rather than by variation of stored energy. This has been noted in [1], where an optimal separation between an elementary source and PEC ground is analytically found as $h/\lambda \cong 0.36$. The position of minimum seems to agree very well with results from [9], where their value is around $kh = 2$, i.e., $h/\lambda \cong 0.32$.

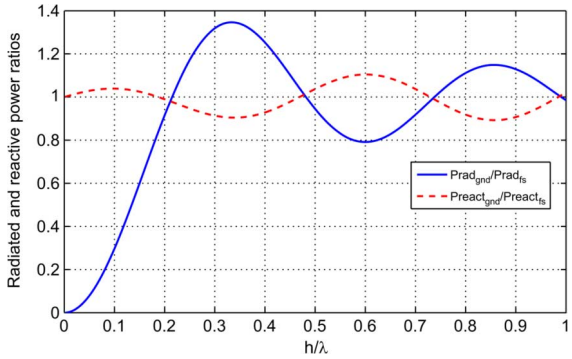

Fig. 3. Radiated and reactive power for horizontal $\lambda/2$ dipole normalized to free-space values.

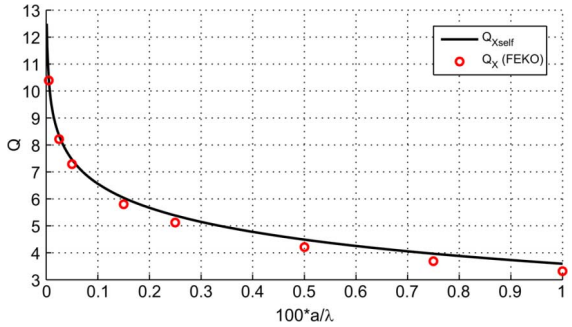

Fig. 4. Quality factor for $\lambda/2$ dipole in free space calculated by (15) and compared to the numerical results from the FEKO software.

Equation (8) may be interpreted as a power ratio

$$Q_X = \frac{\omega W_{\mathrm{stored}}}{P_{\mathrm{radiated}}} = \frac{P_{\mathrm{reactive}}}{P_{\mathrm{radiated}}} \tag{14}$$

so we are able to plot the above power quantities separately and normalize them to their free-space values (dipole without the ground); see Fig. 3. A very similar picture as that in [9] is obtained. We note again the special point $h/\lambda \cong 0.33$ that maximizes radiated power while minimizing reactive ("stored") power.

C. Case of $u \to \infty$, Dipole in Free Space

The dipole in free space may be treated similarly, using just the self-impedance Z_{11} in (8). However, we can advantageously use the general result (9) where it is seen that by letting $u \to \infty$ in (9), the interaction terms containing h vanish. This results in the special case of the Q-factor for the $\lambda/2$ dipole in free space, which reads

$$Q_{\mathrm{Xself}} = \frac{\pi}{2}\frac{2\mathrm{Ci}(\pi) - \mathrm{Ci}(2\pi) - \gamma - \ln(8\pi) - 2\ln\left(\frac{a}{\lambda}\right)}{\gamma + \ln(2\pi) - \mathrm{Ci}(2\pi)}. \tag{15}$$

Evaluating the various constants gives simple formula

$$Q_{\mathrm{Xself}} \cong -2.34 - 1.29\ln\left(\frac{a}{\lambda}\right). \tag{16}$$

The logarithmic nature of Q on a dipole radius a is clearly observed. Surprisingly, (15) gives reasonable results for wide ranges of dipole thickness as demonstrated by comparison to FEKO in Fig. 4. The error is less than 10% for $a/\lambda < 1.5 \cdot 10^{-3}$.

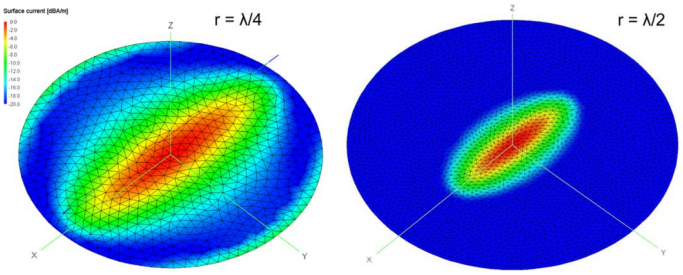

Fig. 5. Surface currents at the circular ground planes of different radii. The dipole is at height of $h = \lambda/20$.

TABLE I
QUALITY FACTORS FOR $\lambda/2$ DIPOLE WITH RADIUS $a/\lambda = 5 \cdot 10^{-3}$ ABOVE CIRCULAR FINITE GROUNDS OF DIFFERENT EXTENT

h	Q_{X}	Q_{X} ($r_{\mathrm{gnd}} = \lambda/2$)	Q_{X} ($r_{\mathrm{gnd}} = \lambda/4$)
$\lambda/10$	16.1	21.5	30.9
$\lambda/20$	59.4	61.3	65.3
$\lambda/30$	130.3	109.8	98.6

TABLE II
QUALITY FACTORS FOR $\lambda/2$ DIPOLE WITH RADIUS $a/\lambda = 5 \cdot 10^{-4}$ ABOVE CIRCULAR FINITE GROUNDS OF DIFFERENT EXTENT

h	Q_{X}	Q_{X} ($r_{\mathrm{gnd}} = \lambda/2$)	Q_{X} ($r_{\mathrm{gnd}} = \lambda/4$)
$\lambda/10$	26.1	30.8	49.1
$\lambda/20$	96.8	97.3	121.3
$\lambda/30$	213.5	195.5	207

III. Q-FACTOR OF A DIPOLE ABOVE FINITE CIRCULAR GROUND

The applicability of derived formulas for finite ground is studied in this section. A circular ground of two different radii r has been chosen for simplicity, and the situation has been modeled in FEKO again. The results are presented for radius of dipole $a/\lambda = 5 \cdot 10^{-3}$ (Table I) and $a/\lambda = 5 \cdot 10^{-4}$ (Table II). Height of the dipole is considered $h = \{\lambda/10, \lambda/20, \lambda/30\}$.

It is seen that even for small ground plane size, the agreement is quite satisfactory. A proposed explanation follows from simulation of surface currents for different ground radii shown at Fig. 5. For low heights, the current distribution has elliptical core located mostly under the dipole. Indeed as the height increases, the "projection" of radiator requires bigger extent of ground plane to be mirrored.

However, carefully observing results in Tables I and II, it is somewhat surprising that the agreement is not generally better with smaller heights (actually the best match accidentally occurs for $h = \lambda/20$). This issue is also present when an infinite plane is used as shown in detail for small h in Fig. 6. Actually, the discrepancy between (8) and FEKO simulation starts to increase for heights smaller than $\lambda/20$.

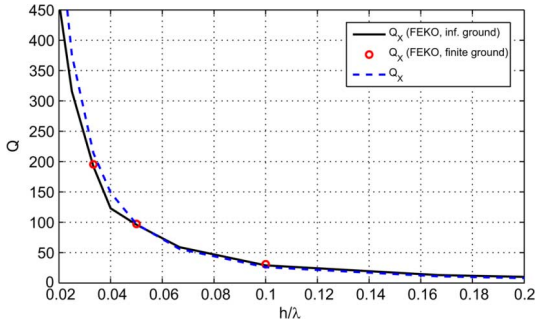

Fig. 6. Quality factor for small distances above ground. Comparison of calculated values from (8) to FEKO simulations (for both infinite and finite $r_{\mathrm{gnd}} = \lambda/2$ ground). The dipole radius is $a/\lambda = 5 \cdot 10^{-4}$.

The most likely reason for this behavior seems to be addressed to an image theory treatment of currents located very close to a ground in FEKO. The simulated currents on dipole were also checked, and they were found to be sinusoidal as assumed in the analytical derivation.

IV. CONCLUSION

Closed-form equations for the radiation Q-factor of a dipole above a perfect electric ground and in free space have been derived. The presented approach could be similarly employed for other antenna arrangements where the input driving impedance is known in a closed form and the Q is analytically studied as a function of various geometrical parameters.

We focused on the case of a resonant antenna, but by employing complete impedance expressions, more general formulas may be derived. It has to be noted that away from resonance, the Q became untuned, and consequently the resulting workout will be very tedious.

REFERENCES

[1] P. Hazdra, M. Capek, and J. Eichler, "Radiation Q-factors of thin-wire dipole arrangements," *IEEE Antennas Wireless Propag. Lett.*, vol. 10, pp. 556–560, 2011.

[2] G. A. E. Vandenbosch, "Reactive energies, impedance, Q factor of radiating structures," *IEEE Trans. Antennas Propag.*, vol. 58, no. 4, pp. 1112–1127, Apr. 2010.

[3] D. Yaghjian and S. R. Best, "Impedance, bandwidth and Q of antennas," *IEEE Trans. Antennas Propag.*, vol. 53, no. 4, pp. 1298–1324, Apr. 2005.

[4] M. Capek, L. Jelinek, P. Hazdra, and J. Eichler, "The measurable Q factor and observable energies of radiating structures," *IEEE Trans. Antennas Propag.*, vol. 62, no. 1, pp. 311–318, Jan. 2014.

[5] J. D. Kraus and R. J. Marhefka, *Antennas For All Applications*, 3rd ed. New York, NY, USA: McGraw-Hill, 2001.

[6] E. C. Jordan and K. G. Balmain, *Electromagnetic Waves and Radiating Systems*, 2nd ed. Upper Saddle River, NJ, USA: Prentice-Hall, 1968.

[7] C. A. Balanis, *Antenna Theory: Analysis and Design*, 3rd ed. Hoboken, NJ, USA: Wiley, 2005.

[8] FEKO. ver. 6.0, EM Software & Systems-S.A. (Pty) Ltd., Stellenbosch, South Africa [Online]. Available: http://www.feko.info

[9] H. Chang, Y. H. Cho, and D. Kwon, "Radiation Q bounds for small electric dipoles over a conducting ground plane," *IEEE Trans. Antennas Propag.*, vol. 62, no. 4, pp. 2031–2040, Apr. 2014.

X

J. Eichler, P. Hazdra, and M. Capek, "Aspects of mesh generation for characteristic mode analysis," *IEEE Antennas Propag. Magazine*, vol. 56, no. 6, pp. 172–183, June 2014. [128∗]

David B. Davidson
Dept. E&E Engineering
University of Stellenbosch
Stellenbosch 7600, South Africa
Tel: +27 21 808 4458;
Fax: +27 21 808 4981
E-mail: davidson@sun.ac.za

Foreword by the Editor

The recently re-discovered theory of characteristic modes continues to receive much attention in computational electromagnetics. In the April 2013 column, the authors described a *MATLAB* implementation of the method. In this present contribution, they address efficient mesh generation for accurate solutions. Extensive results using both their implementation and a commercial package (*FEKO*) are presented. As always, we thank the authors for their support of this column.

Aspects of Mesh Generation for Characteristic-Mode Analysis

Jan Eichler, Pavel Hazdra, and Miloslav Capek

Department of Electromagnetic Field, Faculty of Electrical Engineering
Czech Technical University in Prague
Technicka 2, 16627, Prague, Czech Republic
E-mail: eichljan@fel.cvut.cz, hazdrap@fel.cvut.cz, miloslav.capek@fel.cvut.cz

Abstract

This paper deals with practical aspects of mesh generation for the theory of characteristic modes. First, we describe a tool for surface-mesh generation in *MATLAB*. The tool is afterwards used for an analysis of relative convergence of modal results computed by an in-house modal analyzer in *MATLAB*. Different meshing scenarios are selected for a dipole, a rectangular patch, and a rectangular patch with a slot, and a recommendation for a mesh-refinement strategy is given. The study is supported by a simple error analysis, considering the approximation error in the evaluation of moment-matrix elements. It is shown that the results are also applicable for the commercial implementation in *FEKO* software.

Keywords: Characteristic modes; Method of Moments; mesh generation; mesh refinement; convergence; approximation error

1. Introduction

Numerical electromagnetics has been a subject of research since the emergence of the first computers. Highly developed numerical methods, in conjunction with the capabilities of modern computers, have enabled the simulation of larger structures than ever before. However, for larger and more complex structures, cut-and-try methods, a brute-force optimization, and a design based on the experience of the engineer, become increasingly inefficient. For instance, designing an antenna array without using the pattern-multiplication principle would become a quite complex task. Methods that can separate the independent effects of the particular parts of a high-frequency device or provide a deeper understanding of physical principles are thus of great interest.

One class of such methods is the modal methods that compute field solutions for a particular structure without an excitation. A suitable modal method for radiating structures is the theory of characteristic modes (TCM). It states that for each perfectly electrically conducting surface, it is possible to find a set of functions – orthogonal with respect to radiated power – that decompose the electric current flowing on the surface, and diagonalize the electric-field integral equation (EFIE) impedance operator [1]. Such modes are useful from a theoretical as well as a practical point of view, since they make it easier to understand the physical principles underlying the operation of an antenna, especially if the dimensions are small.

The theory was developed by Garbacz and Turpin [2, 3], who have shown that it is possible to expand the fields radiated or scattered by a perfect electrically conducting (PEC) surface, S, into a set of eigenfunctions (characteristic modes). The key properties of these characteristic currents are that they are real (equiphasal), orthogonal with respect to the radiated power, and usually only a few modes are necessary to characterize the radiated or scattered fields with sufficient accuracy.

The theory was formulated from an alternative viewpoint by Harrington and Mautz [1], whose approach was to diagonalize the electric-field integral-equation operator. This formulation of the theory of characteristic modes provides explicit formulas for determining the characteristic functions (modes). A numerical computational method with a convergence study of the sum of the modal radiation patterns was also provided by the same authors in [4].

The aim of this paper is to present a practical study of the convergence of different modal parameters with mesh density. The important parameters are resonant frequency, the eigen radiation quality factor, and maximum directivity. The main output of the study is a recommendation for mesh generation for the theory of characteristic modes. Sources of the error will be discussed in the following, and will be applied to the in-house tool [5] and also to the *FEKO* commercial software [6]. The influence of segmentation on the eigenvalues of two half-wavelength dipoles can be found in [7]. It should be also noted that convergence of modal results with mesh density was demonstrated in [8], but the scope of that paper was limited to calculating the modal radiation quality factor, and interpreting the results. The analysis was therefore done with a lower number of basis functions and a uniform mesh. A graph of the convergence of the modal radiation, Q, calculated from the current density on a rectangular patch can also be found in [9]. However, none of these papers was dedicated to mesh generation and error sources, or presented any guidelines for mesh generation.

2. Mesh Generation for the Theory of Characteristic Modes

The inputs for the in-house tool [5] are the matrices $\mathbf{p}$ and $\mathbf{t}$, containing the surface mesh. Each column of $\mathbf{p}$ contains the Cartesian coordinates of a mesh node, and each column of $\mathbf{t}$ contains the indices of three points, creating a triangle.

A tool called *MeshGen* was developed in *MATLAB* in order to easily define and parameterize the geometry and to generate its surface mesh. A suitable algorithm for mesh generation is `distmesh` [10], written in *MATLAB*. It allows full mesh control (fixed points, mesh-density control), but the biggest advantage is that it is simple to understand and to integrate into our *MATLAB* tools. On the other hand, unlike the advanced version of the code (written in *C++*), the basic version is not fully robust, and the generation of the initial set of nodes is not deterministic [10].

MeshGen is capable of the surface meshing of three-dimensional planar structures by executing the following steps for each two-dimensional plane of the structure (It is possible to create a mesh of an arbitrary non-planar surface in three dimensions, e.g., on a Beziér surface, by applying a transformation on $\mathbf{p}$, as was done in [11, p. 64]):

- Automatic fixed points are placed on the border to respect the mesh-density function, $h(\mathbf{x})$, and to avoid small distances from user-defined fixed points.
- Mesh points from previously generated two-dimensional planes are used as fixed points.
- An initial set of mesh points is created.
- The mesh-point distribution is optimized by the `distmesh` algorithm.
- The two-dimensional mesh is validated to be conformal with the boundary of the shape. If the validation is not successful, the mesh will be refined.
- Transformations are applied to the two-dimensional mesh, and the result is merged with the previously generated mesh.

Due to the `distmesh` algorithm, *MeshGen* produces

meshes of high mean triangle quality, as well as high minimal triangle quality. (The triangle quality is $q = 2r_{\text{in}}/r_{\text{out}}$, $q \in \langle 0,1 \rangle$, where r_{in} is the radius of the biggest inscribed circle, and r_{out} is the radius of the smallest circumscribed circle [11]).

The following improvements to the basic *MATLAB* code [10] have been implemented:

- A deterministic algorithm to generate the initial point set.
- A check that the mesh is conformal with the boundary.
- A function that moves points in the proximity of the boundary of the shape to the boundary.
- A possibility of adding points to the center of the edge that is longer than the required edge length.
- An edge that is shorter than the required edge length is replaced with a center point.

All of these features rapidly increase the convergence of the algorithm to a high-quality mesh, as well as the algorithm's robustness. The initial mesh and the optimized mesh, including simple examples of the local mesh improvements, are plotted in Figure 1.

The progress of the generation is plotted in Figure 2, where it can be seen that the mean triangle quality is improved with increasing iterations. The minimal triangle quality is generally improved as well, but there are step increases in the curve due to local mesh improvements and re-triangulation if the nodes change position.

The structure is implicitly parameterized, so it is not necessary to write any additional function to change the structure. Instead, an internal parameter of the *MeshGen* object is modified. All features of *MeshGen* can be started from the *MATLAB* command line, and can therefore be used in a parametric sweep or optimization. *MeshGen* also supports importing and exporting of the *NASTRAN* mesh format, so the meshes can be exchanged with other computational tools. The interested reader can download *MeshGen* from [12]. An example of a mesh generated for an L-probe-fed patch antenna is shown in Figure 3.

3. Numerical Computation of Characteristic Modes

The characteristic modes, $\mathbf{J}_n$, of the surface S satisfy the operator equation

$$X\mathbf{J}_n = \lambda_n R\mathbf{J}_n, \tag{1}$$

where X and R are the imaginary and real parts of the electric-field integral-equation operator relating the tangential components of the surface current and scattered electric field. Corresponding to each mode is the eigennumber, λ_n. Harrington and Mautz [4] proposed to numerically solve Equation (1) by the Method of Moments. The current density of mode n is thus approximated by a set of basis functions, $\mathbf{w}_v$, multiplied by unknown coefficients, $I_{v,n}$:

$$\mathbf{J}_n \approx \sum_n I_{v,n}\mathbf{w}_v. \tag{2}$$

Applying the usual MoM procedure with testing functions $\mathbf{w}_u$, we obtain the following matrix equation [4]:

$$\mathbf{X}\mathbf{I}_n = \hat{\lambda}_n \mathbf{R}\mathbf{I}_n. \tag{3}$$

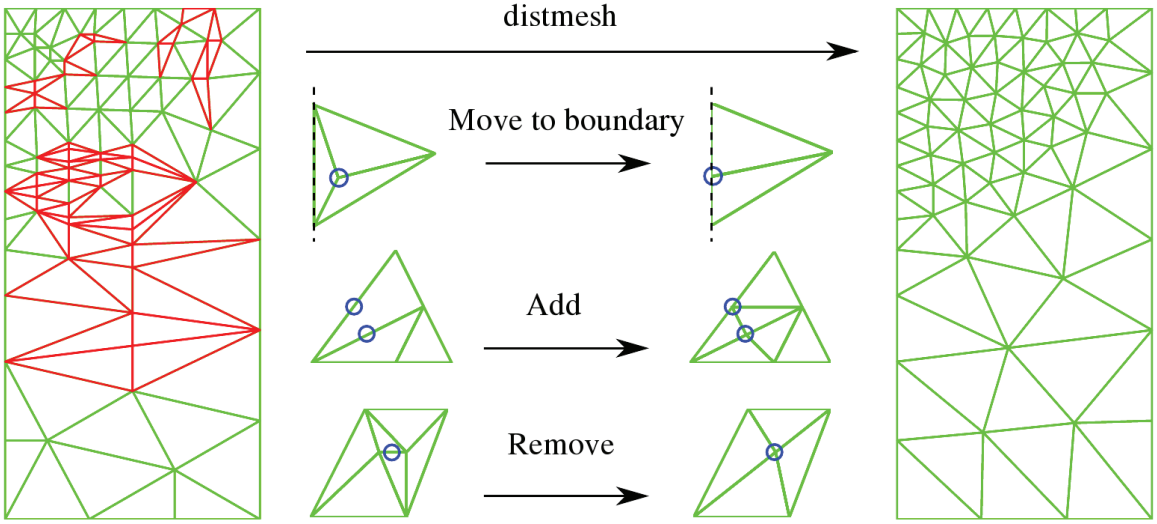

Figure 1. (l) The initial mesh: triangles with low quality are marked with a red contour. (middle) Operations improving algorithm convergence to a high-quality mesh. (r) The final mesh.

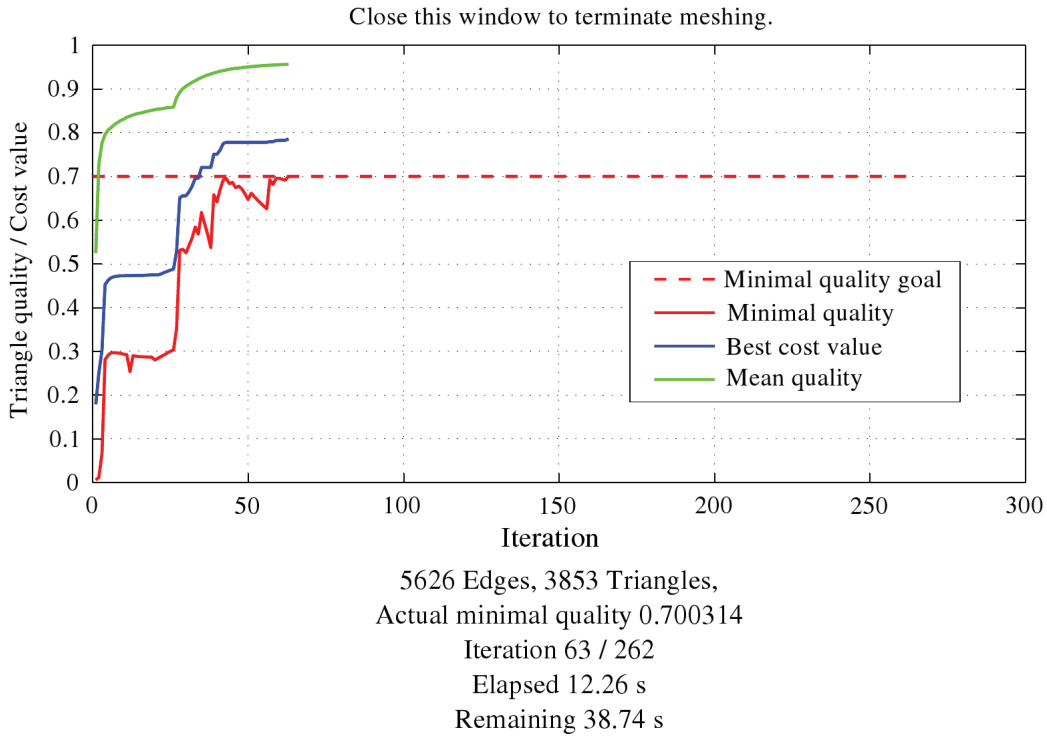

Figure 2. A graphical representation of the mesh-generation progress.

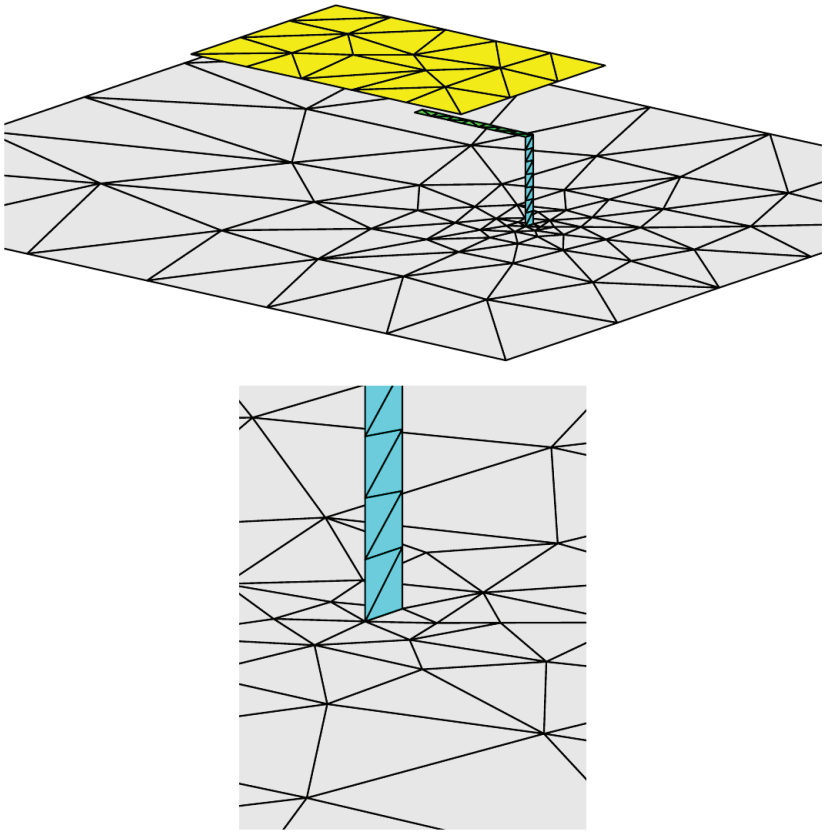

Figure 3. An example of the mesh generated by *MeshGen*: (top) an L-probe-fed patch antenna; (bottom) a detailed view of the connection between the ground plane and the probe.

Note that λ_n is not exactly equal to $\hat{\lambda}_n$, due to an approximation made in Equation (2).

The integrals involved in calculating matrix elements are usually evaluated by numerical quadrature, and thus contain errors. Such errors (perturbations) were mathematically studied in [13], with the following result. Consider a perturbed problem,

$$\tilde{\mathbf{X}}\tilde{\mathbf{I}}_n = \tilde{\lambda}_n \tilde{\mathbf{R}}\tilde{\mathbf{I}}_n , \tag{4}$$

where the matrices are of the form $\tilde{\mathbf{X}} = \mathbf{X} + \varepsilon\mathbf{G}$ and $\tilde{\mathbf{R}} = \mathbf{R} + \varepsilon\mathbf{H}$, and $\|\mathbf{G}\| = \|\mathbf{H}\| = 1$. Supposing that $\hat{\lambda}_n$ is a simple eigenvalue, $\mathbf{R}$ is nonsingular [13] (note that for certain frequencies, the electric-field integral-equation impedance matrix can be close to singular [14]). Considering that both $\mathbf{R}$ and $\mathbf{X}$ are symmetrical,

$$\tilde{\lambda}_n - \hat{\lambda}_n = \varepsilon \frac{\mathbf{I}_n^{\mathrm{T}} \left(\mathbf{G} - \hat{\lambda}_n \mathbf{H}\right) \mathbf{I}_n}{\mathbf{I}_n^{\mathrm{T}} \mathbf{R} \mathbf{I}_n} + O\left(\varepsilon^2\right). \tag{5}$$

Omitting the higher-order terms,

$$\tilde{\lambda}_n - \hat{\lambda}_n \approx \varepsilon \frac{\sum_u \sum_v I_{n,u} I_{n,v} \left(G_{u,v} - \hat{\lambda}_n H_{u,v}\right)}{\sum_u \sum_v I_{n,u} I_{n,v} R_{u,v}} . \tag{6}$$

From Equation (6), it is evident that to minimize the difference $\tilde{\lambda}_n - \hat{\lambda}_n$, one should minimize the term $\left(G_{u,v} - \hat{\lambda}_n H_{u,v}\right)$ in the regions with high $\mathbf{I}_n$. Note that the value of $I_{n,u}$ is related to the dot product of the $\mathbf{J}_n$ vector and the vector basis function $\mathbf{w}_u$. It is thus more robust to refine regions with high $\mathbf{J}_n$ than to refine regions with high $I_{n,u}$.

In the in-house tool [5], $\mathbf{w}_v$ and $\mathbf{w}_u$ are the RWG basis functions [15], and Equation (3) is computed by direct decomposition or by an iterative method in *MATLAB*. *FEKO* uses the Implicitly Restarted Arnoldi Method [16], an iterative procedure to obtain several most-significant characteristic numbers and vectors. The time consumption of both approaches for one frequency is plotted in Figure 4. The in-house tool uses a nine-point barycentric subdivision and centroid approximation [16, Chapter 2] in the computation of $\mathbf{Z}$ matrix elements. It is thus a bit faster than *FEKO*; however, one can expect more accurate results for the same mesh from *FEKO*.

The computational complexity of the direct solver is much higher than the complexity of the $\mathbf{Z}$ matrix computation as well as the iterative method (Figure 4). However, the iterative solver is preferred for structures larger than approximately 800 inner edges (i.e., RWG basis functions). All simulations were computed in a single-core mode on an Intel Core i7-3770K @ 3.5GHz CPU.

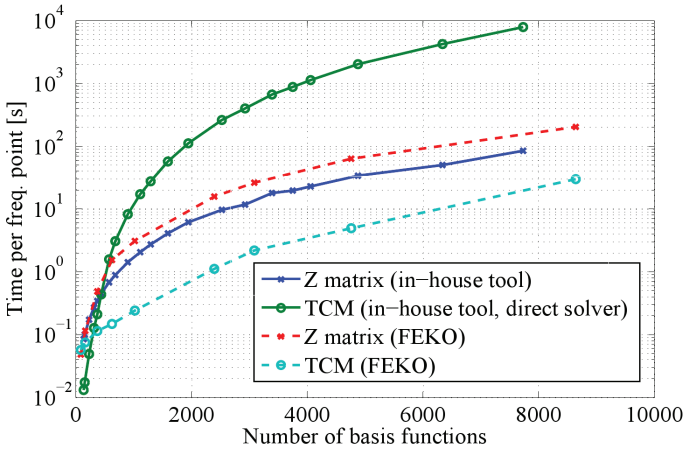

Figure 4. The computation time as a function of the number of basis functions: two modes were required in *FEKO*. The computations were performed in single-core mode on an Intel Core i7-3770K CPU @ 3.5 GHz.

4. Numerical Relative Convergence of Modal Parameters

This section presents a convergence study of the modal resonant frequency, $f_{\mathrm{res},n}$, defined as the frequency where $\lambda_n = 0$, the modal radiation quality factor

$$Q_{\mathrm{eig},n} = \frac{\omega}{2} \left| \frac{\partial \lambda_n}{\partial \omega} \right| , \tag{7}$$

and there is maximum modal directivity, $D_{\mathrm{max},n}$, with mesh density. The surrounding medium for all structures is a vacuum.

Convergence studies are necessary to eliminate the effect of the error-cancellation mechanism [18], which can be observed if several sources of error eliminate each other and the result thus appears to be accurate.

Let us define a relative error as

$$e(x) = \frac{\left| x - x_{\mathrm{ref}} \right|}{x_{\mathrm{ref}}} , \tag{8}$$

where x is one of the quantities of interest: $f_{\mathrm{res},n}$, or $Q_{\mathrm{eig},n}$, or $D_{\mathrm{max},n}$. The reference value, x_{ref}, should ideally be the precise value (as computed, for example, from an analytical formula) or a measured value. Analytical formulas for modes on a conducting sphere can be found in [19]. However, they will not be used here, since an RWG mesh cannot fully describe the geometry's curvature. Measured values are not available for the modal quantities. Other full-wave methods also cannot be used as a reference. For instance, the commonly used measure of resonance (the input susceptance of the antenna is equal to zero) is not equal to the modal resonance unless only one mode

is excited. There thus are two options: to use a result from a much denser RWG mesh as a reference, or to use a solution using higher-order basis functions as a reference. Results from *FEKO* software using a relatively fine mesh and basis functions denoted as order 2.5 were chosen as a reference in this paper.

In order to compare different mesh-refinement schemes for different structures, we used the following number associated with each mesh:

$$m = \frac{c_0}{f_{\mathrm{res,ref},n} \min(L)}, \tag{9}$$

where c_0 is the speed of light, $f_{\mathrm{res,ref},n}$ is the resonance frequency of mode n computed by the *FEKO* reference software, and L is the set of lengths of edges inside the structure. The number m thus has the meaning of the number of smallest edges per wavelength. Note that m does not take into account the actual distribution of the edge lengths in the structure, and that such criteria will be much more difficult to define, implement, and understand.

Meshes were generated using *MeshGen* requiring a minimal triangle quality of 0.8. While this criterion was not always satisfied (generation stopped because the maximum number of iterations was exceeded), the minimal quality for all the studied meshes was not lower than 0.6.

4.1 Strip Dipole

The first studied structure was a strip dipole, 30 mm in length and 0.6 mm in width. The structure was simulated using an adaptive frequency sweep [5], with increasing uniformly distributed mesh density.

Figure 5 showed that the dominant resonant frequency converged with an increased number of edges inside the structure. Even the coarsest mesh presented $e\left(f_{\mathrm{res},1}\right)$ smaller than 1.5%, and meshes with more than 91 edges had a relative error $e\left(f_{\mathrm{res},1}\right)$ under 0.5%. However, even for 16557 edges, there was still a small difference of 4 MHz (0.096%) from the *FEKO* result using 2.5th-order basis functions. This fact could indicate either very slow convergence of our tool for small relative errors, or that our tool converged to a slightly different value.

There was a very small dependence of the results on the number of triangles across the strip, with the exception of the step increase from one triangle per strip width to two triangles that appeared between $m = 107$ and $m = 223$ (Figure 5). In other words, proper discretization of the edge singularity of the charge (see, e.g., [20]) was not the crucial point for eigenvalue precision.

In the next step, the central part of the dipole was meshed with higher or lower density than the rest of the dipole, and the size of the central part was varied. However, the difference in convergence was disputable, and the uniform scheme converged more smoothly than the other schemes: it thus was recognized as the optimal refinement scheme for the dipole.

4.2 Rectangular Patch

The second structure was a rectangular patch 25 mm in length and 21.5 mm in width, placed 3 mm above an infinite PEC plane. Since the current density of the first mode was spread over the patch (Figure 6), the convergence of the uniformly refined mesh was generally better than for the locally refined mesh. The exception was the scenario denoted as V01, in which the mesh was coarser in the regions with a high magnitude of current density (Figure 6). This paradoxical behavior can be explained as follows. The two edges of the patch were discretized by bigger triangles, and thus the corresponding current density was lower (see Figure 6). This meant that according to Equation (5), these big triangles (with larger error) became less significant for computation of $\tilde{\lambda}_n$: in other words, the value of $\tilde{\lambda}_n$ was more affected by smaller triangles with smaller error.

Figures 7 and 8 showed very similar convergence of both uniform refinement (denoted as Uni) and the V01 refinement of the resonant frequency and Q_{eig}. This behavior was expected, since both results were related to the eigenvalue. In contrast, there was a difference in maximum directivity (Figure 9), which resulted from the difference in current density for Uni and V01 refinement. However, the difference between them was reduced with increasing m.

4.3 U-Shaped Patch

The next structure was the same patch as in the previous section, with a slot 15 mm in length and 2 mm in width. The dominant mode had a very localized current density (Figure 10). It was thus ideal for applying a nonuniform mesh-refinement scheme. To observe the differences between a properly refined mesh and an ineffective refinement, two schemes were proposed. Meshes that were properly refined in the regions with a high amplitude of the modal current density were denoted as V01 (Figure 10). In contrast, the scheme denoted as V02 was not refined near the maximum of $\|\mathbf{J}_n\|$ (see Figure 11), and was ineffective from the error-minimization point of view.

The slow convergence of V02 was clearly visible in Figures 12-14. On the other hand, the V01 results were very close to Uni with similar minimal edge length. Note that the total number of edges – which directly influenced the simulation speed (Figure 4) – was reduced by approximately a factor of three to four for the V01 mesh. Computing six frequencies therefore took 9.25 minutes and one minute for the uniform and V01 structures of Figure 10, respectively. The nice speedup

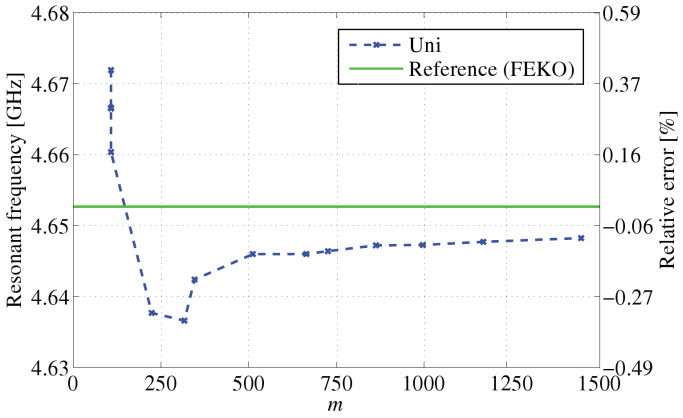

Figure 5. The convergence of the resonant frequency of mode 1 of the dipole, 30 mm in length and 0.6 mm in width. A uniformly refined mesh was used.

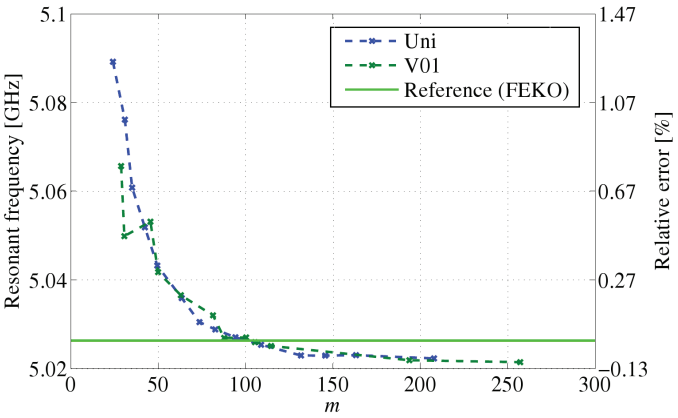

Figure 7. The convergence of the resonant frequency of the rectangular patch for different refinement schemes.

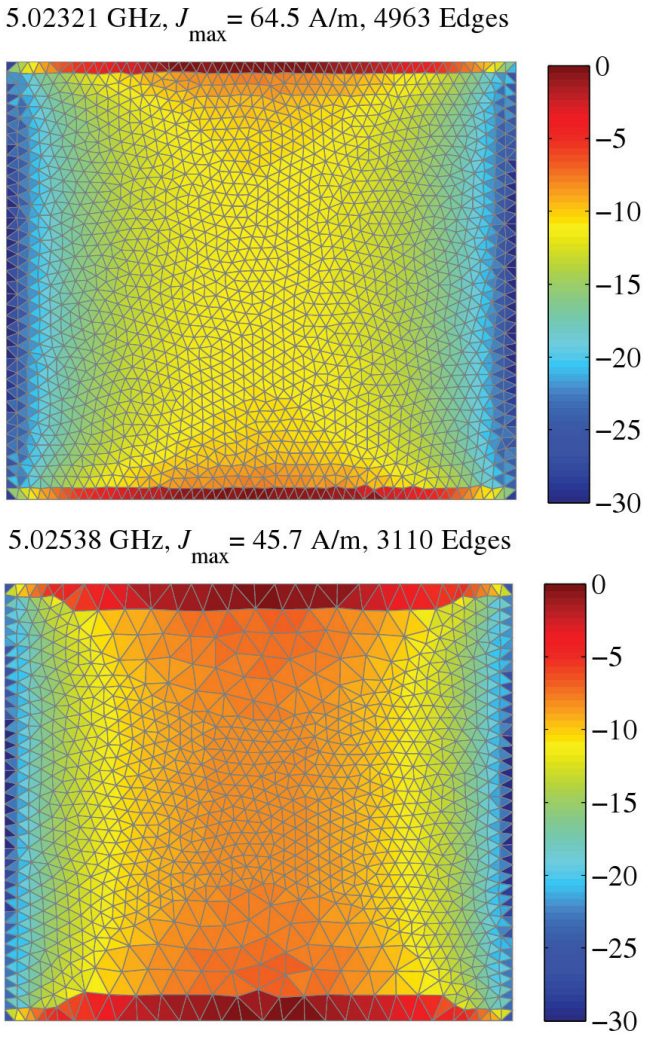

Figure 6. The first mode of a rectangular patch 3 mm above a ground plane at its resonance: (top) uniformly refined mesh, and (bottom) V01 refined mesh. A normalized logarithmic scale was used for both cases.

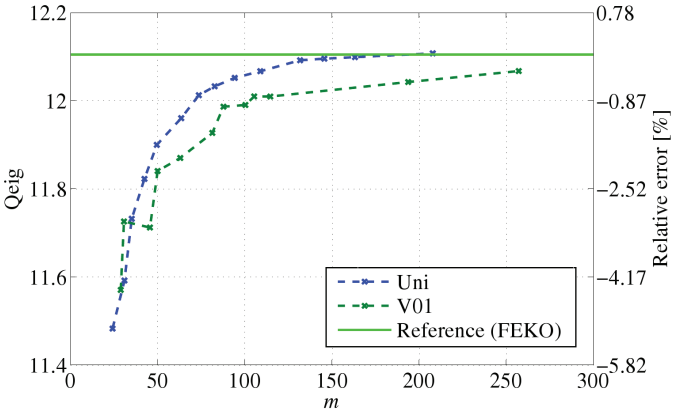

Figure 8. The convergence of Q_{eig} of the rectangular patch for different refinement schemes.

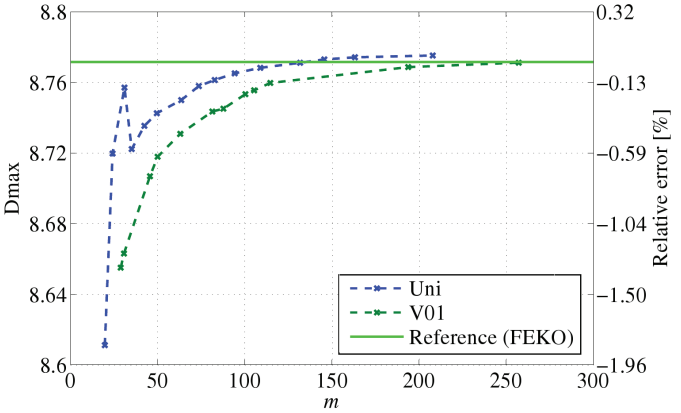

Figure 9. The convergence of the maximum directivity at resonance of the rectangular patch for different refinement schemes.

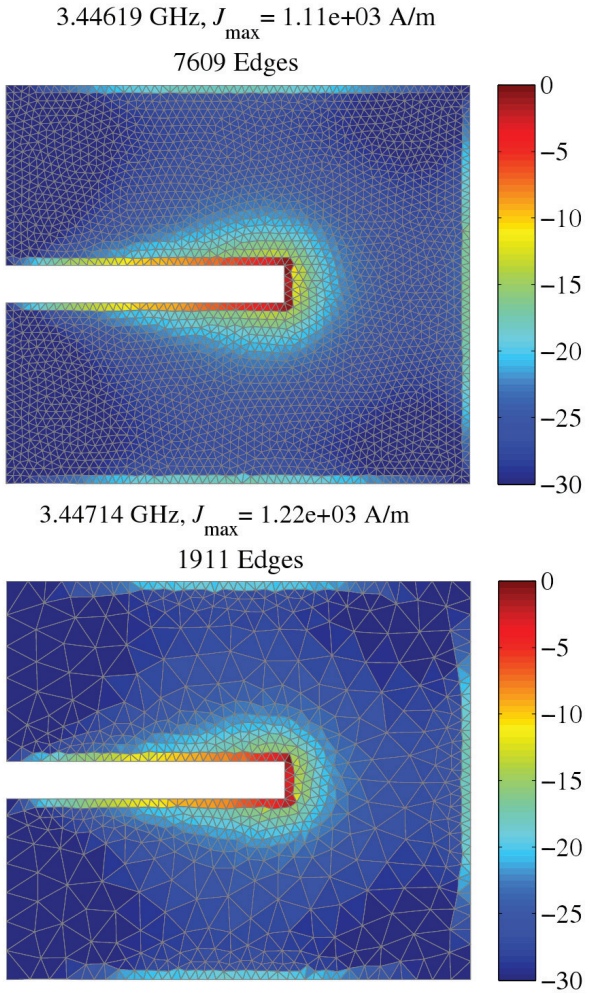

Figure 10. The first mode at its resonance: (top) uniformly refined mesh and (bottom) V01 mesh, normalized logarithmic scale.

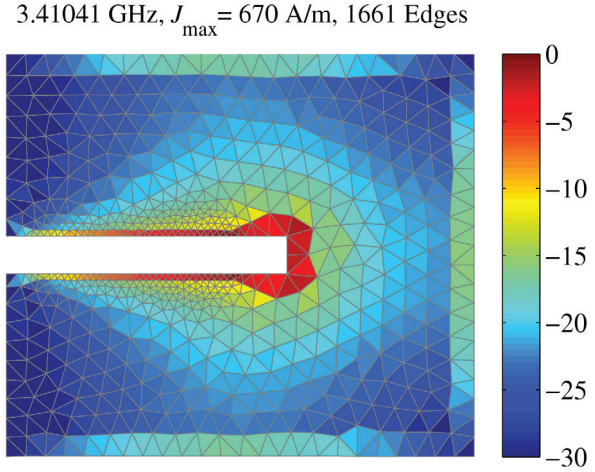

Figure 11. The first mode at its resonance: V02 refinement scheme, normalized logarithmic scale.

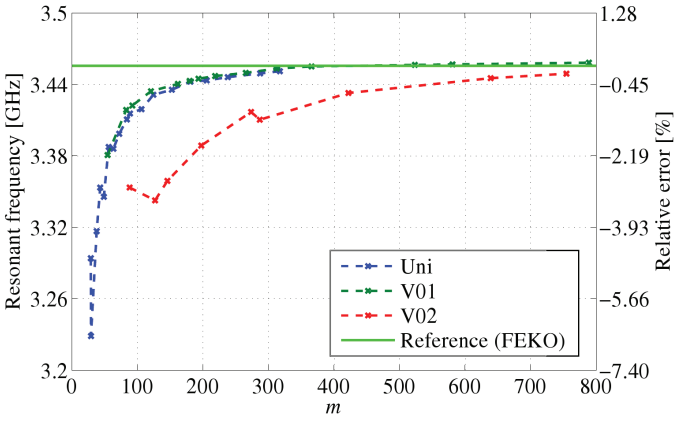

Figure 12. The convergence of the resonant frequency of the patch with a slot, for different refinement schemes.

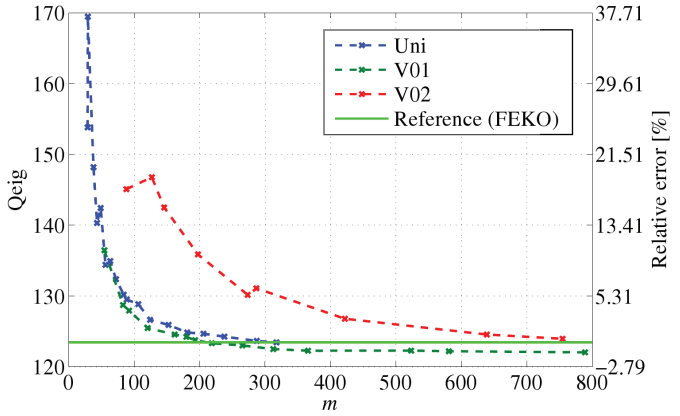

Figure 13. The convergence of Q_{eig} of the patch with a slot, for different refinement schemes.

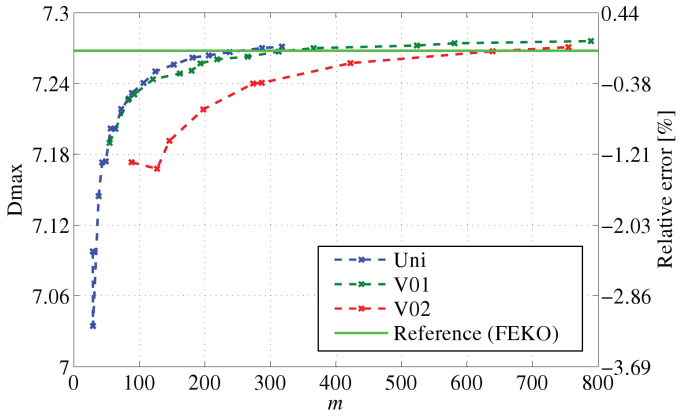

Figure 14. The convergence of the maximum directivity of the patch with a slot, for different refinement schemes.

of 9.25 was interesting, especially for an optimization. The difference would be enormous for the direct solver: 15.41 hours versus 10.74 minutes (six frequency samples).

4.4 Circularly Polarized Triangular Patch

In this section, a triangular patch with a slot will be analyzed, and convergence graphs both for the in-house tool and for *FEKO* will be presented. This type of patch can be used for circular polarization [21, Chapter 5]. For proper functionality, circularly polarized antennas combine two orthogonal modes in a specific way. In order to analyze (and design) such antennas, accurate results for both modes thus have to be obtained.

While the first mode of the triangle with a slot has the current density localized near the slot, the second mode is distributed over a dominant part of the patch (Figure 15). From the mesh-refinement point of view, mode 1 will resemble the dominant mode of a slotted patch, and mode 2 will resemble the mode of a rectangular patch. The mesh-refinement strategies from Sections 4.2 and 4.3 should therefore also apply for the triangle with a slot.

The mesh-refinement appropriate for mode 1 is denoted as V01 (Figure 16), and it reduced the number of edges by a factor of approximately 1.6 to 1.8 for a uniform mesh with similar accuracy. The convergence of $f_{\mathrm{res},1}$ was quite comparable for the Uni and the V01 mesh (Figure 17), while the convergence of $f_{\mathrm{res},2}$ was significantly better for Uni (Figure 18). Although the absolute values obtained for the same meshes imported into *FEKO* and using low-order basis functions differed, the trend of the curves in Figures 17 and 18 was the same as the trend of the curves computed by the in-house tool. The reason why $f_{\mathrm{res},2}$ differed for V01 and Uni was that the mode 2 current had high values in the regions with low mesh density of the V01 mesh (Figure 16).

The Q_{eig} of both modes was affected by the refinement strategy in the same manner as for f_{res}. Note that the eigen Q factor was somehow more sensitive to mesh density than the resonant frequency or the maximum directivity.

The V01 mesh was not suitable for obtaining the small e of mode 2 results; therefore, the mesh was additionally refined in the lower part of the triangle denoted as V02 (Figure 16). This refinement scheme preserved good convergence for both modes (Figures 17-22). However, the mesh density with respect to a uniform mesh was reduced only in the top part of the patch, and the reduction factor was only 1.1 to 1.2. Nonetheless, for a high number of edges, this factor will become more significant, e.g., a Uni mesh of 7625 edges was computed in 11.95 minutes, while a V02 mesh of 6521 edges took only 8.57 minutes (eight frequency points, iterative solver).

The V02 meshes were also imported to *FEKO*, and the results were quite close to the *FEKO* Uni mesh results. We

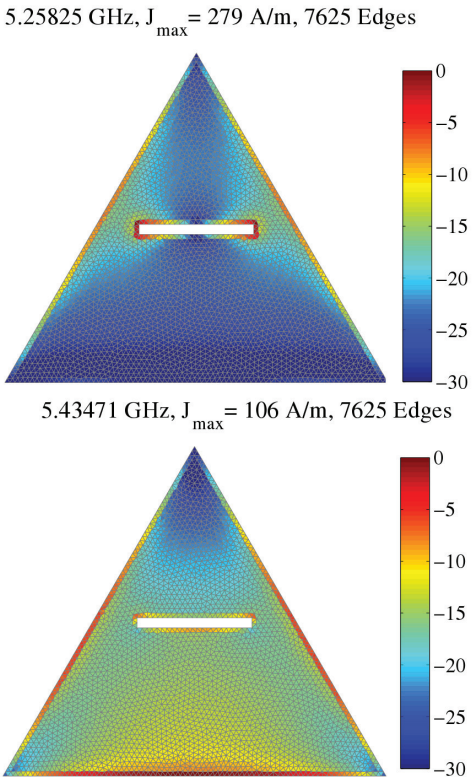

Figure 15. The first mode at its resonance: uniformly refined mesh, normalized logarithmic scale.

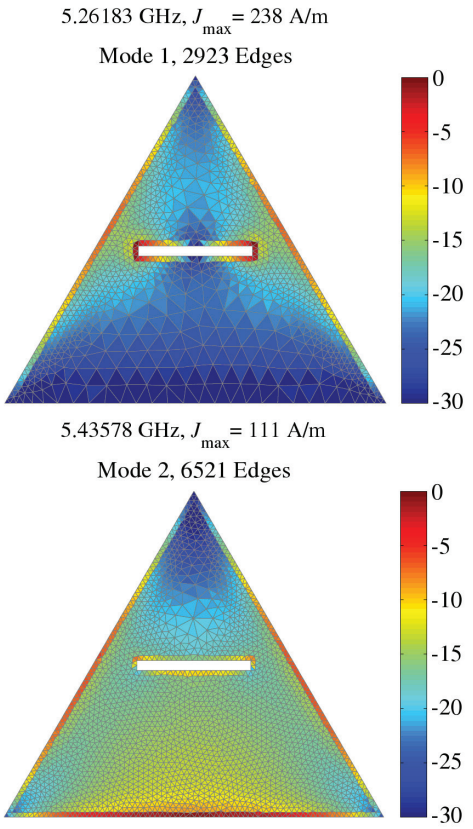

Figure 16. The first mode at its resonance: (top) V01 refined mesh, and (bottom) V02 refined mesh, normalized logarithmic scale.

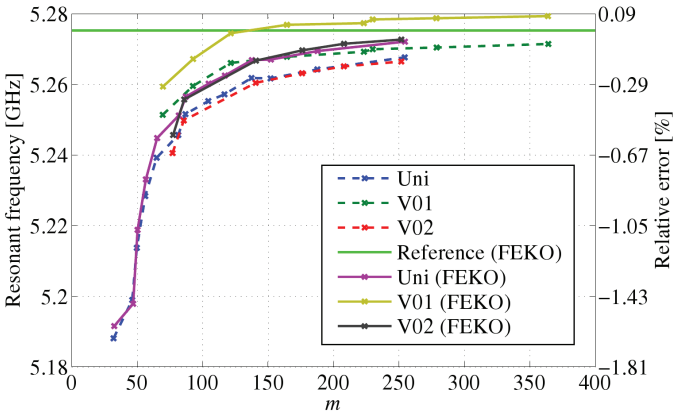

Figure 17. The convergence of the resonant frequency of the triangle with a slot, mode 1.

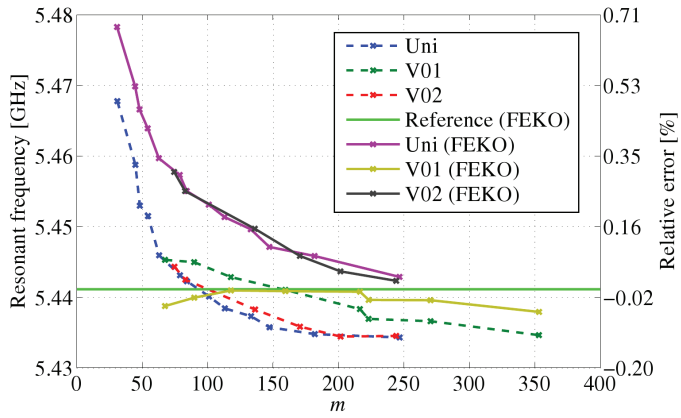

Figure 18. The convergence of the resonant frequency of the triangle with a slot, mode 2.

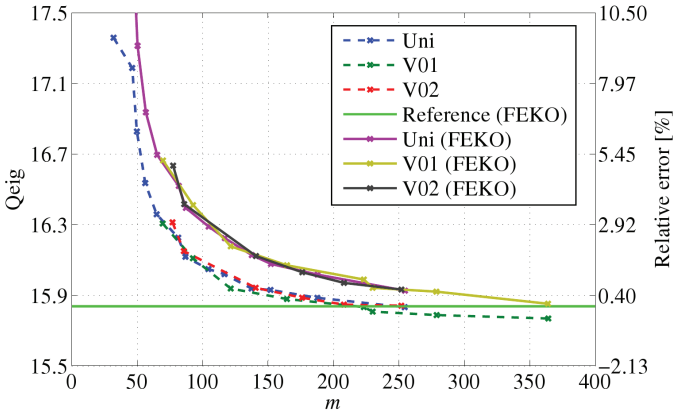

Figure 19. The convergence of Q_{eig} of the triangle with a slot, mode 1.

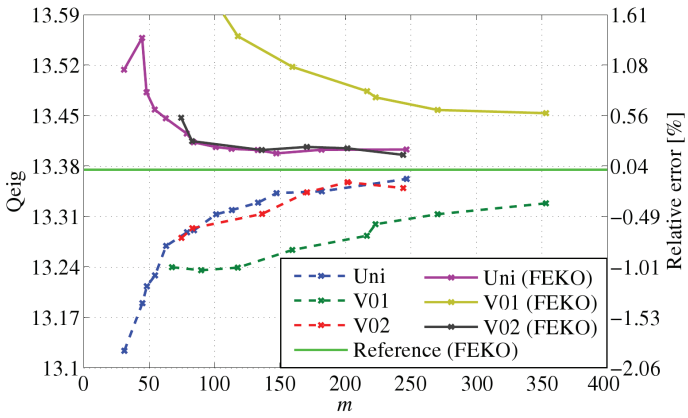

Figure 20. The convergence of Q_{eig} of the triangle with a slot, mode 2.

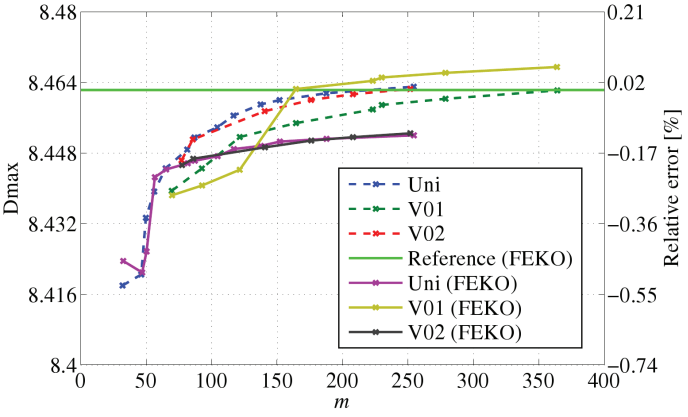

Figure 21. The convergence of D_{max} of the triangle with a slot, mode 1.

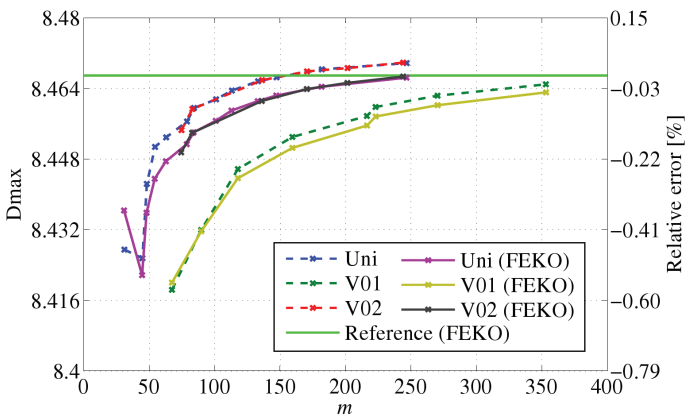

Figure 22. The convergence of D_{max} of the triangle with a slot, mode 2.

thus conclude that the presented results are applicable to the commercial implementation of characteristic modes theory [6].

5. Conclusion

In this paper, we have described a tool for surface-mesh generation in *MATLAB*. This tool was used in conjunction with an in-house theory-of-characteristic-modes tool to study the convergence of the numerical implementation with increased mesh density. A simple error analysis of the theory of characteristic modes formulation was presented. It revealed the interesting property that the eigenvalues are affected by the approximation errors in the matrix elements multiplied by $I_{n,u}I_{n,v}$. This result indicates that the mesh should be refined in the regions where the current magnitude is high.

The theory was tested on the dominant mode of a dipole, a rectangular patch, and a rectangular patch with a slot. Convergence curves for resonant frequency, Q_{eig}, and the maximum directivity for different mesh-refinement schemes were compared. The results were in accordance with the theoretical derivation. It was also observed that mesh refinement is much more suitable for modes with localized current, where high simulation speedup can be obtained for nonuniform mesh refinement with good relative accuracy.

Generally, the computation of characteristic modes by MoM converges with an increased number of basis functions (we suppose that the round-off errors were insignificant for all presented computations). However, no rule of thumb for the number of basis functions per wavelength for a given relative error was deduced. Specifically, the number, *m*, necessary to obtain a relative error $e(f_{\text{res}}) < 1\%$ for the dipole, the rectangular patch, the rectangular patch with a slot, and the circularly polarized triangle was (less than 100), 30, 109, and 53, respectively. Q_{eig} tends to be the most sensitive parameter, and needs careful choice of the mesh.

The recommendations for mesh refinement were tested on a circularly polarized patch in the in-house tool, and also in *FEKO* (using low-order basis functions). Although they were slightly different in absolute values – which may have been due to approximations in the in-house tool – the results were qualitatively equivalent, and preserved the same trends.

6. Acknowledgement

The authors would like to thank Dr. Lukas Jelinek for his comments. This work was supported by Czech Science Foundation project No. P102/12/2223 and by the COST LD 12055 AMTAS project.

7. References

1. R. F. Harrington and J. R. Mautz, "Theory of Characteristic Modes for Conducting Bodies," *IEEE Transactions on Antennas and Propagation*, **AP-19**, 5, September 1971, pp. 622-628.

2. R. J. Garbacz, *A Generalized Expansion for Radiated and Scattered Fields*, PhD dissertation, The Ohio State University, 1968.

3. R. J. Garbacz and R. H. Turpin, "A Generalized Expansion for Radiated and Scattered fields," *IEEE Transactions on Antennas and Propagation*, **AP-19**, 3, May 1971, pp. 348-358.

4. R. F. Harrington and J. R. Mautz, "Computation of Characteristic Modes for Conducting Bodies," *IEEE Transactions on Antennas and Propagation*, **AP-19**, 5, September 1971, pp. 629-639.

5. M. Capek, P. Hamouz, P. Hazdra, and J. Eichler, "Implementation of the Theory of Characteristic Modes in Matlab," *IEEE Antennas and Propagation Magazine*, **55**, 2, April 2013, pp. 176-189.

6. EM Software & Systems-S.A. FEKO; available online: www.feko.info.

7. B. Austin and K. P. Murray, "The Generation of Antenna Characteristic Modes from the Impedance Matrix Using the Moment Method," Seventh International Conference on Antennas and Propagation, ICAP 91, **2**, 1991**,** pp. 713-716.

8. J. Eichler, P. Hazdra, M. Capek, and M. Mazanek, "Modal Resonant Frequencies and Radiation Quality Factors of Microstrip Antennas," *International Journal of Antennas and Propagation*, **2012**, 2012, pp. 1-9.

9. M. Capek, P. Hazdra, and J. Eichler, "A Method for the Evaluation of Radiation *Q* Based on Modal Approach," *IEEE Transactions on Antennas and Propagation*, **AP-60**, 10, October 2012, pp. 4556-4567.

10. P.-O. Persson and G. Strang, "A Simple Mesh Generator in MATLAB," *SIAM Review*, **42**, 2004, pp. 329-345.

11. P.-O. Persson, *Mesh Generation for Implicit Geometries*, PhD dissertation, Massachusetts Institute of Technology, 2006.

12. Meshgen Web page, http://elmag.org/sites/default/files/users/eichler/files/MeshGenV03p.zip.

13. P. Kravanja, T. Sakurai, H. Sugiura, and M. V. Barel, "A Perturbation Result for Generalized Eigenvalue Problems and its Application to Error Estimation in a Quadrature Method for Computing Zeros of Analytic Functions," *Journal of Computational and Applied Mathematics*, **161**, 2003, pp. 339-347.

14. W. C. Gibson, *The Method of Moments in Electromagnetics*, Boca Raton, FL, Chapman and Hall, 2007.

15. S. M. Rao, D. R. Wilton, and A. W. Glisson, "Electromagnetic Scattering by Surfaces of Arbitrary Shape," *IEEE Transactions on Antennas and Propagation*, **AP-30**, 3, May 1982, pp. 409-418.

16. D. J. Ludick, E. Lezar, and U. Jakobus, "Characteristic Mode Analysis of Arbitrary Electromagnetic Structures Using FEKO," *ICEAA*, 2012, pp. 208-211.

17. S. N. Makarov, *Antenna and EM Modeling with Matlab*, New York, John Wiley, 2002.

18. J. C. Rautio, "An Investigation of an Error Cancellation Mechanism with Respect to Subsectional Electromagnetic Analysis Validation," *International Journal of Microwave and Millimeter-Wave Computer-Aided Engineering*, **6**, 1996, pp. 430-435.

19. E. A. Daviu, *Analysis and Design of Antennas for Wireless Communications Using Modal Methods*, PhD dissertation, Universidad Politécnica de Valencia, February 2008.

20. E. F. Kuester and D. D. Chang, "Closed-Form Expressions for the Current or Charge Distribution on Parallel Strips or Microstrip," *IEEE Transactions on Microwave Theory and Technique*, **28**, 3, 1980, pp. 254-259.

21. K.-L. Wong, *Compact and Broadband Microstrip Antennas*, New York, John Wiley & Sons, 2002.

XI

P. Hazdra, M. Capek, and J. Eichler, "Comments to 'Reactive Energies, Impedance, and Q Factor of Radiating Structures' by G. Vandenbosch," *IEEE Trans. Antennas Propag.*, vol. 61, no. 12, pp. 6266–6267, Dec. 2013. [99∗]

Comments and Replies

Comments to "Reactive Energies, Impedance, and Q Factor of Radiating Structures" by G. Vandenbosch

Pavel Hazdra, Miloslav Capek, and Jan Eichler

In an excellent paper [1], Prof. Vandenbosch derived rigorous equations for evaluating the radiated power and stored magnetic and electric energies explicit in terms of the source currents flowing on the radiating device. By integrating the radiated fields of an antenna it is easy to obtain the radiated power, but the evaluation of stored energies of a radiating system has been an issue since the early work of Chu [2]. The development presented in [1] involved advanced mathematics, however the resulting equations are easy to implement [3]. This letter shows simple alternative derivation of radiated power and stored energies, including the energy W_r associated with the radiated field. The results of our approach produce exactly the same equations as presented in [1]. We consider currents flowing in a vacuum, only losses due to radiation and the notation of [1] is used. The complex Poynting theorem states about the power balance that [4]:

$$-\frac{1}{2}\int_V \mathbf{E}\cdot\mathbf{J}^*\mathrm{d}V = P_r + j2\omega(\widehat{W}_m - \widehat{W}_e) \tag{1}$$

where V is the volume of an antenna, P_r is the radiated power and $\widehat{W}_m - \widehat{W}_e$ is the difference between magnetic and electric energies, which are both infinite due to radiation. Since we are interested in the complex power flow evaluated from source quantities, not from the fields in space, we insert

$$\mathbf{E} = -j\omega\mathbf{A} - \nabla\phi \tag{2}$$

where magnetic vector and electric scalar potentials are

$$\mathbf{A} = \frac{\mu_0}{4\pi}\int_{V'} \mathbf{J}(\mathbf{r}')G(\mathbf{r},\mathbf{r}')\mathrm{d}\mathbf{r}' \tag{3}$$

$$\phi = \frac{1}{4\pi\epsilon_0}\int_{V'} \rho(\mathbf{r}')G(\mathbf{r},\mathbf{r}')\mathrm{d}\mathbf{r}'. \tag{4}$$

$G(\mathbf{r},\mathbf{r}')$ is the free-space scalar Green's function

$$G(\mathbf{r},\mathbf{r}') = \frac{\mathrm{e}^{-jkR}}{R} = \frac{\cos(kR)}{R} - j\frac{\sin(kR)}{R} \tag{5}$$

where $R = |\mathbf{r}-\mathbf{r}'|$, $\mathbf{J}$ and ρ are the surface current distribution and charge distribution in the Lorenz gauge respectively. After a little manipulation it is easily shown that the real and imaginary part of the right-hand side of (1) are [4]:

$$P_r = \frac{1}{8\pi\omega\epsilon_0}\iint_{VV'}\left[k_0^2\mathbf{J}(\mathbf{r})\cdot\mathbf{J}^*(\mathbf{r}') - \nabla\cdot\mathbf{J}(\mathbf{r})\nabla\cdot\mathbf{J}^*(\mathbf{r}')\right] \times \frac{\sin(kR)}{R}\,\mathrm{d}\mathbf{r}\mathrm{d}\mathbf{r}' \tag{6}$$

$$2\omega(\widehat{W}_m - \widehat{W}_e) = \frac{1}{8\pi\omega\epsilon_0} \times \iint_{VV'}\left[k_0^2\mathbf{J}(\mathbf{r})\cdot\mathbf{J}^*(\mathbf{r}') - \nabla\cdot\mathbf{J}(\mathbf{r})\nabla\cdot\mathbf{J}^*(\mathbf{r}')\right] \times \frac{\cos(kR)}{R}\,\mathrm{d}\mathbf{r}\mathrm{d}\mathbf{r}'. \tag{7}$$

It is noted that (6) and (7) may be written using dynamic potentials (3), (4) (see also [5]):

$$P_r = -\frac{\omega}{2}\Im\left\{\int_V \mathbf{A}\cdot\mathbf{J}^* - \phi\rho^*\mathrm{d}V\right\} \tag{8}$$

$$2\omega(\widehat{W}_m - \widehat{W}_e) = \frac{\omega}{2}\Re\left\{\int_V \mathbf{A}\cdot\mathbf{J}^* - \phi\rho^*\mathrm{d}V\right\}. \tag{9}$$

The expression for radiated power given by (6) is quite known, so we concentrate on the net reactive power balance. When the imaginary part of the right side of (1) is evaluated from the fields and hence integrated over all of the space, both of its energy parts $\widehat{W}_m$ and $\widehat{W}_e$ contain infinities linked to the radiated energy [1], [4]. This issue is bypassed by integrating in (7) over the source domain V, which is finite, and so the energy terms are finite too. It is then interesting to discover that by splitting of (7) into its "current" and "charge" parts we obtain the same magnetic and electric energy expressions as in [1] (without the $W_{r,G}$ component, which is discussed later):

$$W_m = \frac{1}{16\pi\omega^2\epsilon_0}\iint_{VV'} k_0^2\mathbf{J}(\mathbf{r})\cdot\mathbf{J}^*(\mathbf{r}')\frac{\cos(kR)}{R}\mathrm{d}\mathbf{r}\mathrm{d}\mathbf{r}' \tag{10}$$

$$W_e = \frac{1}{16\pi\omega^2\epsilon_0}\iint_{VV'} \nabla\cdot\mathbf{J}(\mathbf{r})\nabla\cdot\mathbf{J}^*(\mathbf{r}')\frac{\cos(kR)}{R}\mathrm{d}\mathbf{r}\mathrm{d}\mathbf{r}'. \tag{11}$$

It should be noted that the above splitting is done *ad hoc*. There is no rigorous mathematical basis for such splitting—the difference of energies in (1) appears by definition in the Complex Poynting theorem.

Because of this difference, any common part W_r associated with radiation identically cancels out [6] and hence, another equation is needed. If we perform a ω derivation of (7) and assume that the currents do not vary with frequency as in [1], the result is composed of three contributions (as suggested by the reactance theorem, [7]):

$$\frac{\partial}{\partial\omega}2\omega(W_m - W_e) = 2W_m + 2W_e + 2W_{r,G}. \tag{12}$$

The first two terms in (12) are energies already found by (10) and (11), i.e.

$$W_m = \frac{\Re}{4}\int_V \mathbf{A}\cdot\mathbf{J}^*\mathrm{d}V \tag{13}$$

$$W_e = \frac{\Re}{4}\int_V \phi\rho^*\mathrm{d}V \tag{14}$$

and are the time-harmonic versions of the classic static expressions [8].

For the input reactance of an antenna we have from (1)

$$\frac{X|I|^2}{2} = 2\omega(W_m - W_e) \tag{15}$$

so (13) and (14) are the observable energies [6] in the sense that no other term has a measurable effect on the reactance. The third term in (12) is a new one, caused by the frequency derivative of the real

Manuscript received August 07, 2012; revised June 17, 2013; accepted July 31, 2013. Date of current version November 25, 2013. This work was supported by the project of the Czech Science Foundation, grant No. P102/12/2223 and by the COST VISTA (IC1102) action.

The authors are with the Department of Electromagnetic Field, Faculty of Electrical Engineering, Czech Technical University in Prague, 16627 Prague, Czech Republic (e-mail: hazdrap@fel.cvut.cz).

Digital Object Identifier 10.1109/TAP.2013.2281566

part of Green's function so therefore the kernel of $W_{r,G}$ contains $(\partial/\partial k)(\cos(kR)/R) = -\sin(kR)$. This term is obviously zero for a non-radiating system. It could be regarded as the finite residuum remaining after the subtraction of two infinite integrals (representing the total field energy and the far-field energy) in (58) of [1]. In our view this term reflects that the electric and magnetic fields are "energetically" coupled to form the electromagnetic wave radiating into an infinite spherical waveguide. Direct differentiation of (7) then yields

$$W_{r,G} = \frac{-1}{16\pi\omega\epsilon_0 c_0} \iint\limits_{VV'} \left[k_0^2 \mathbf{J}(\mathbf{r}) \cdot \mathbf{J}^*(\mathbf{r}') - \nabla \cdot \mathbf{J}(\mathbf{r}) \nabla \cdot \mathbf{J}^*(\mathbf{r}')\right] \sin(kR) \mathrm{d}\mathbf{r}\mathrm{d}\mathbf{r}'. \quad (16)$$

In terms of the potentials we have an interesting formula (see also [9])

$$W_{r,G} = \frac{\Re}{4} \int\limits_V k \left(\mathbf{J}^* \cdot \frac{\partial \mathbf{A}}{\partial k} - \rho^* \frac{\partial \phi}{\partial k}\right) \mathrm{d}V. \quad (17)$$

It is thus possible to define modified vacuum energies, same as in the original paper [1], with the radiated energy being equally distributed (because $W_{r,G,m} = W_{r,G,e}$) between the magnetic and electric components:

$$\begin{aligned} \widetilde{W_m} &= W_m + \frac{W_{r,G}}{2} \\ &= \frac{\Re}{4} \int\limits_V \mathbf{A}\cdot\mathbf{J}^* + \frac{k}{2}\left(\mathbf{J}^* \cdot \frac{\partial \mathbf{A}}{\partial k} - \rho^* \frac{\partial \phi}{\partial k}\right) \mathrm{d}V \quad (18) \\ \widetilde{W_e} &= W_e + \frac{W_{r,G}}{2} \\ &= \frac{\Re}{4} \int\limits_V \phi\rho^* + \frac{k}{2}\left(\mathbf{J}^* \cdot \frac{\partial \mathbf{A}}{\partial k} - \rho^* \frac{\partial \phi}{\partial k}\right) \mathrm{d}V. \quad (19) \end{aligned}$$

Consider now the frequency derivative of (15), where the current is held constant with frequency

$$\frac{\partial X}{\partial \omega} \frac{|I|^2}{2} = \frac{\partial}{\partial \omega} \left[2\omega(W_m - W_e)\right]. \quad (20)$$

Inserting (12) yields the Foster theorem [10]

$$\begin{aligned} \frac{\partial X}{\partial \omega} &= \frac{4(W_m + W_e + W_{r,G})}{|I|^2} \\ &= \frac{\Re}{|I|^2} \int\limits_V \mathbf{A}\cdot\mathbf{J}^* + \phi\rho^* + k\left(\mathbf{J}^* \cdot \frac{\partial \mathbf{A}}{\partial k} - \rho^* \frac{\partial \phi}{\partial k}\right) \mathrm{d}V. \quad (21) \end{aligned}$$

It is known [11] that the right side of (21) can be negative, thus the Foster theorem does not hold for antennas—because the radiation from the antenna acts as a loss. This is linked to the $W_{r,G}$ term (also called the "farfield dispersion energy" in [11]) which can be positive as well as negative.

The presented derivation is not as thorough as in [1], but is easy to understand since the energies are written in terms of dynamic potentials.

Last issue to be shortly addressed is about the radiation quality factor of an antenna. It is proposed that the only useful and reasonable Q factors of a radiator are the measurable ones, based on frequency changes of the input reactance Q_X, or more generally Q_Z, see [11]. Using (21) we have

$$\begin{aligned} Q_X &= \frac{\omega}{2R} \frac{\partial X}{\partial \omega} = \frac{\omega(W_m + W_e + W_{r,G})}{P_r} \\ &= \frac{\Re \int_V \mathbf{A}\cdot\mathbf{J}^* + \phi\rho^* + k\left(\mathbf{J}^* \cdot \frac{\partial \mathbf{A}}{\partial k} - \rho^* \frac{\partial \phi}{\partial k}\right) \mathrm{d}V}{-2\Im \int_V \mathbf{A}\cdot\mathbf{J}^* - \phi\rho^* \mathrm{d}V}. \quad (22) \end{aligned}$$

For Q_Z, the change of radiation resistance should be included too and we can write

$$Q_Z = \frac{\omega}{2R} \left|\frac{\partial Z}{\partial \omega}\right| = |Q_R + jQ_X| \quad (23)$$

which is worked out as

$$Q_Z = \frac{\left|\int_V \mathbf{A}\cdot\mathbf{J}^* + \phi\rho^* + k\left(\mathbf{J}^* \cdot \frac{\partial \mathbf{A}}{\partial k} - \rho^* \frac{\partial \phi}{\partial k}\right) \mathrm{d}V\right|}{-2\Im \int_V \mathbf{A}\cdot\mathbf{J}^* - \phi\rho^* \mathrm{d}V}. \quad (24)$$

It has been again assumed that the current is not changing with frequency in (22) and (24). It is shown [12] that for Q_Z the correction energy terms representing reconfiguration of sources with frequency are in practice negligible.

ACKNOWLEDGMENT

The authors would like to thank N. Bell and Dr. L. Jelinek for comments and Prof. G. A. E. Vandenbosch for fruitful discussions.

REFERENCES

[1] G. A. E. Vandenbosch, "Reactive energies, impedance, and Q factor of radiating structures," *IEEE Trans. Antennas Propag.*, vol. 58, no. 4, pp. 1112–1127, Apr. 2010.
[2] L. J. Chu, "Physical limitations of omni-directional antennas," *J. Appl. Phys.*, vol. 19, pp. 1163–1175, Dec. 1948.
[3] M. Capek, P. Hazdra, and J. Eichler, "A method for the evaluation of radiation Q based on modal approach," *IEEE Trans. Antennas Propag.*, vol. 60, no. 10, pp. 4556–4567, Oct. 2012.
[4] W. Geyi, *Foundations of Applied Electrodynamics*. Hoboken, NJ, USA: Wiley, 2010.
[5] C. Carpenter, "Electromagnetic energy and power in terms of charges and potentials instead of fields," *IEE Proc. A*, vol. 136, no. 2, pp. 55–65, 1989.
[6] D. R. Rhodes, "Observable stored energies of electromagnetic systems," *J. Franklin Inst.*, vol. 302, no. 3, pp. 225–237, Sep. 1976.
[7] D. R. Rhodes, "A reactance theorem," *Proc. R. Soc. London. A.*, vol. 353, no. 1672, pp. 1–10, Feb. 1977.
[8] J. D. Jackson, *Classical Electrodynamics*. Hoboken, NJ, USA: Wiley, 1998.
[9] M. Gustaffson and B. L. G. Jonsson, Stored Electromagnetic Energy and Antenna Q eprint arXiv:1211.5521 [Online]. Available: http://adsabs.harvard.edu/abs/2012arXiv1211.5521G
[10] W. Geyi, P. Jarmuszewski, and Y. Qi, "The Foster reactance theorem for antennas and radiation Q," *IEEE Trans. Antennas Propag.*, vol. 48, no. 3, pp. 401–408, Mar. 2000.
[11] D. Yaghjian and S. R. Best, "Impedance, bandwidth and Q of antennas," *IEEE Trans. Antennas Propag.*, vol. 53, pp. 1298–1324, Apr. 2005.
[12] M. Capek, L. Jelinek, P. Hazdra, and J. Eichler, "The measurable Q factor and observable energies of radiating structures," *IEEE Trans. Antennas Propag.*, to appear.

XII

J. Eichler, P. Hazdra, M. Capek, and M. Mazanek, "Modal resonant frequencies and radiation quality factors of microstrip antennas," *International J. of Antenas and Propag.*, vol. 2012, pp. 1–9, 2012. [42∗]

Hindawi Publishing Corporation
International Journal of Antennas and Propagation
Volume 2012, Article ID 490327, 9 pages
doi:10.1155/2012/490327

Research Article

Modal Resonant Frequencies and Radiation Quality Factors of Microstrip Antennas

Jan Eichler, Pavel Hazdra, Miloslav Capek, and Milos Mazanek

Department of Electromagnetic Field, Faculty of Electrical Engineering, Czech Technical University in Prague, Technická 2, 166 27, Prague, Czech Republic

Correspondence should be addressed to Pavel Hazdra, hazdrap@fel.cvut.cz

Received 9 August 2011; Revised 10 January 2012; Accepted 13 January 2012

Academic Editor: Charles Bunting

The chosen rectangular and fractal microstrip patch antennas above an infinite ground plane are analyzed by the theory of characteristic modes. The resonant frequencies and radiation Q are evaluated. A novel method by Vandenbosch for rigorous evaluation of the radiation Q is employed for modal currents on a Rao-Wilton-Glisson (RWG) mesh. It is found that the resonant frequency of a rectangular patch antenna with a dominant mode presents quite complicated behaviour including having a minimum at a specific height. Similarly, as predicted from the simple wire model, the radiation Q exhibits a minimum too. It is observed that the presence of out-of-phase currents flowing along the patch antenna leads to a significant increase of the Q factor.

1. Introduction

Evaluation of the basic properties of microstrip patch antennas (MPA) has been numerously discussed in literature, see, for example, [1–3]. The two main MPA attributes are resonant frequency (or frequencies but we will deal mostly with the dominant mode) and the radiation Q factor. So far, only approximate results and semianalytic equations have been published. To our knowledge, this is the first time that these important characteristics have been studied in a rigorous way. The antennas are treated by using a modal approach (hence we do not a priori consider any feeding to be connected), namely, by the theory of characteristic modes (TCM), [4, 5]. Evaluation of the radiation Q is performed both by the TCM from the eigenvalues slope and by novel rigorous equations derived by Vandenbosch [6] and Vandenbosch and Volski [7].

2. The Theory of Characteristic Modes

For completeness, let us formulate the basics of the characteristic modes for perfectly conducting bodies of area S. The scattered field $\mathbf{E}^s$ is related to the electric surface currents $\mathbf{J}$ by the electric field integral equation (EFIE) [8]

$$\left[L(\mathbf{J}) - \mathbf{E}^i\right]_{\tan} = 0. \tag{1}$$

Equation (1) is usually treated within the method of moments (MoMs) [8] framework and, due to the structure discretization, the $\mathbf{L}$ operator is known as the "complex impedance matrix" $[Z] = [R] + j[X]$.

Then the associated Euler's equation to be solved is

$$X\mathbf{J}_n = \lambda_n R\mathbf{J}_n. \tag{2}$$

Equation (2) is a standard weighted eigenvalue equation leading to a set of *real* characteristic eigencurrents $\mathbf{J}_n$ and associated eigenvalues λ_n. Properties of eigenvalues are described in [9], at this moment it is important to note that λ_n *reflects the amount of net reactive power* (thus $\lambda_n = 0$ means resonance). Instead of eigenvalues, the so-called characteristic angles α_n are introduced to show more visible behavior with frequency [9]. Characteristic currents form a complete orthogonal set, and hence the total current on a conducting body may be expressed as a linear combination of these mode currents [10].

2.1. Implementation of the Characteristic Modes Theory. Implementation of the modal decomposition process has been done in the MATLAB [11] environment using Makarov EFIE codes [12] with the RWG basis functions [13]. This usage is restricted to arbitrary 3D PEC structures with air

dielectrics. Our developed TCM tool [14] has the following main advantages:

(i) Comsol Multiphysics [15]/MATLAB's PDE TooLbox mesh import,

(ii) Optional Green's function for infinite ground plane simulations,

(iii) Single solver/multicore solver/distributed solver (within a computer network with installed MATLAB).

3. The Radiation Q Factor

In [6] a novel theory able to rigorously calculate radiated power and stored energies directly from currents flowing along the antenna has been presented. The radiation Q factor is then readily evaluated by the definition [16]:

$$Q = 2\omega \frac{\max\left(\widetilde{W}_m, \widetilde{W}_e\right)}{P_r}. \tag{3}$$

The equations for radiated power P_r and stored electric and magnetic energies $\widetilde{W}_e$, $\widetilde{W}_m$ are

$$P_r = \left(\frac{1}{8\pi\omega\varepsilon_0}\right) \int_{\Omega 1}\int_{\Omega 2} [k^2 \mathbf{J}(\mathbf{r}_1)\mathbf{J}(\mathbf{r}_2) - \nabla\cdot\mathbf{J}(\mathbf{r}_1)\nabla\cdot\mathbf{J}(\mathbf{r}_2)] \times \frac{\sin(kr_{21})}{r_{21}} d\Omega 1 d\Omega 2, \tag{4}$$

$$\widetilde{W}_e = \frac{1}{16\pi\omega^2\varepsilon_0}(I_e - I_R), \tag{5}$$

$$\widetilde{W}_m = \frac{1}{16\pi\omega^2\varepsilon_0}(I_m - I_R), \tag{6}$$

where

$$I_R = \frac{k}{2} \int_{\Omega 1}\int_{\Omega 2} [k^2 \mathbf{J}(\mathbf{r}_1)\mathbf{J}(\mathbf{r}_2) - \nabla\cdot\mathbf{J}(\mathbf{r}_1)\nabla\cdot\mathbf{J}(\mathbf{r}_2)] \times \sin(kr_{21}) d\Omega 1 d\Omega 2, \tag{7}$$

$$I_e = \int_{\Omega 1}\int_{\Omega 2} \nabla\cdot\mathbf{J}(\mathbf{r}_1)\nabla\cdot\mathbf{J}(\mathbf{r}_2)\frac{\cos(kr_{21})}{r_{21}} d\Omega 1 d\Omega 2, \tag{8}$$

$$I_m = k^2 \int_{\Omega 1}\int_{\Omega 2} \mathbf{J}(\mathbf{r}_1)\mathbf{J}(\mathbf{r}_2)\frac{\cos(kr_{21})}{r_{21}} d\Omega 1 d\Omega 2, \tag{9}$$

where k is a free-space wavenumber, $\mathbf{J}$ is the surface current density, and r_{21} is the distance between interacting current elements. The tilde denotes that the radiation contribution I_R has been subtracted from the stored energies at every point in space [17]. It is assumed that the currents are flowing in a vacuum.

3.1. The Modal Radiation Q Factor. The modal radiation Q factor may be evaluated from the slope of modal eigenvalues [18]:

$$Q_{\text{eig}} = \frac{\omega_0}{2}\frac{d\lambda}{d\omega}. \tag{10}$$

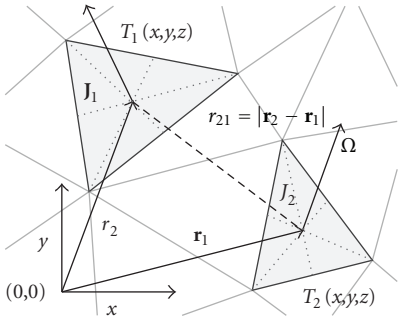

Figure 1: Distance between nonoverlapping current elements [23].

In [18], (10) is supposed to be an approximation of the radiation Q, but in resonance it is actually exact.

Since characteristic modes are normalized to radiate unit power $P_r = 1$ [4], (3) reduces to

$$Q = 2\omega \max\left(\widetilde{W}_e, \widetilde{W}_m\right). \tag{11}$$

For parallel or series RLC circuit (hence, for one mode), the "impedance Q_Z" equals the exact "current Q" [6]:

$$Q = Q_Z = \frac{\omega_0}{2}\left|\frac{\partial Z}{\partial\omega}\right| = \frac{\omega_0}{2}\left|\frac{\partial R}{\partial\omega} + \frac{\partial X}{\partial\omega}\right|. \tag{12}$$

Inserting

$$Z = R + jX = \frac{1}{|I^2|}\left[P_r + j2\omega\left(\widetilde{W}_m - \widetilde{W}_e\right)\right] \tag{13}$$

valid for lossless antennas [19] and using the fact that $P_r = 1$, (12) results in

$$Q = Q_X = \frac{\omega_0}{2}\left|\frac{\partial X}{\partial\omega}\right| = \frac{\omega_0}{2}\frac{\partial}{\partial\omega}\left[2\omega\left(\widetilde{W}_m - \widetilde{W}_e\right)\right] = \frac{\omega_0}{2}\frac{\partial\lambda}{\partial\omega} = Q_{\text{eig}}, \tag{14}$$

providing that

$$\lambda = 2\omega\left(\widetilde{W}_m - \widetilde{W}_e\right). \tag{15}$$

It is therefore concluded that the modal Q_{eig} equals the Q_X by definition, and it can be proven (using the reactance theorem [20, 21]) that in resonance it also equals the radiation Q defined from energies by (11).

3.2. Software Implementation. The above equations were implemented in MATLAB for the RWG triangular mesh where two different interaction situations occur:

(a) Distant Elements. When the triangular elements are not overlapping, current density on triangles may be simply approximated as point sources located at the centre of triangles [22], see Figure 1. No actual integration is then needed. This centroid approach is very fast with satisfactory accuracy as will be shown later (however it may fail for patches located very close to the ground plane).

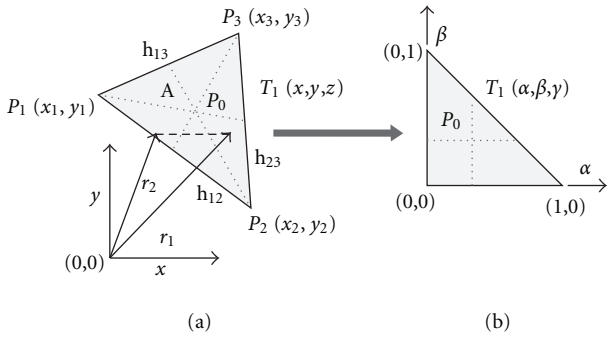

FIGURE 2: Self-term evaluation. (a) Original problem, (b) simplex coordinates transformation [23].

(b) Overlapping (Self) Elements. As known from the method of moments, the so-called "self" contributions are of great importance when dealing with calculations on discrete elements (meshes).

Here, the self-interaction occurs when two triangles are overlapping each other. Due to the behavior of integral kernels, only rapidly varying term $\cos(kr_{21})/r_{21}$ has to be carefully treated. Since $k_0 R_{21} \to 0$ (R_{21} being the longest side of the triangle T) is satisfied, one needs only to use the first term in the Taylor series expansion. The dominant singular static part is $1/r_{21}$ and the integral to be worked out is

$$I = \int_T \int_{T'} \frac{1}{\sqrt{(x-x')^2 + (y-y')^2}} dx\, dy\, dx'\, \mathrm{d}y', \tag{16}$$

where $T = T'$ is a triangular area. Using simplex coordinates transformation (Figure 2), the result is [23, 24]

$$I = -\frac{4}{3}A^2\left[\frac{\ln(1-2h_{12}/L)}{h_{12}} + \frac{\ln(1-2h_{13}/L)}{h_{13}} + \frac{\ln(1-2h_{23}/L)}{h_{23}}\right], \tag{17}$$

where A is the triangle area, h_{ij} are the edge lengths (see Figure 2), and L is the perimeter of the triangle.

4. Applications: Rectangular Patch Antenna

Let us first concentrate on a rectangular patch antenna of dimensions $L = 50$ mm and $W = 30$ mm (further noted as R50 × 30) placed in air at a height H above an infinite ground plane. Only the dominant TM_{01} mode will be studied. The reason for choosing a patch with $L/W \neq 1$ is that we do not have to deal with degenerated modes.

Using the image theory, the radiator in the XY plane at height $z = H$ above an infinite electric ground plane is modelled as two patches separated by $2H$. The total number of triangular elements is 676. In the TCM analyser, a proper out-of-phase mode is selected (Figure 3).

The resonant frequency of the dominant mode is shown as a function of height H, see Figure 4. It has been evaluated from a modal resonant condition for eigenvalues $\lambda = 2\omega(\widetilde{W}_m - \widetilde{W}_e) = 0$ employing an adaptive frequency sweep for each height. The behaviour is quite peculiar, especially for greater heights. For low heights ($H < 10$ mm or

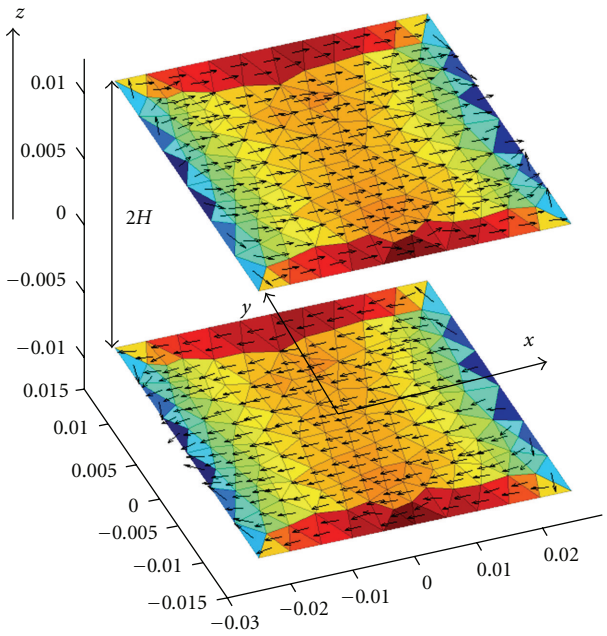

FIGURE 3: Model of MPA above infinite ground plane for $H = 10$ mm, dominant mode TM_{01} shown.

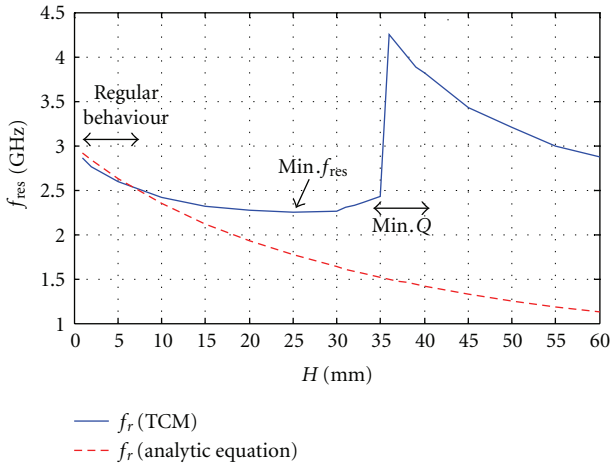

FIGURE 4: R50 × 30 resonant frequency of the dominant TM_{01} mode. The dashed red curve is a quasianalytical equation from [1].

$H/\lambda_{res} < 0.08$), the resonant frequency decreases "regularly," and quasianalytical formulas (see, e.g., [1, 3]) based on the fringing field concept are valid below this range. For $H \cong 25$ mm ($H/\lambda_{res} \cong 0.188$) there is absolute minimum of the TM_{01} resonant frequency. Further on, the resonant frequency rises to reach its maximum for $H \cong 40$ mm ($H/\lambda_{res} \cong 0.51$). Around this specific height the patch also shows the minimum of the radiation Q. The above described process repeats periodically. It is yet unclear to the authors as what is the physical background to the resonant frequency discontinuity around $H/\lambda_{res} \cong 0.5$.

The terms $2\omega\widetilde{W}_m, 2\omega\widetilde{W}_e$, and $2\omega(\widetilde{W}_m - \widetilde{W}_e)$ obtained from (5)–(9) and eigenvalues λ are plotted at Figure 5 for

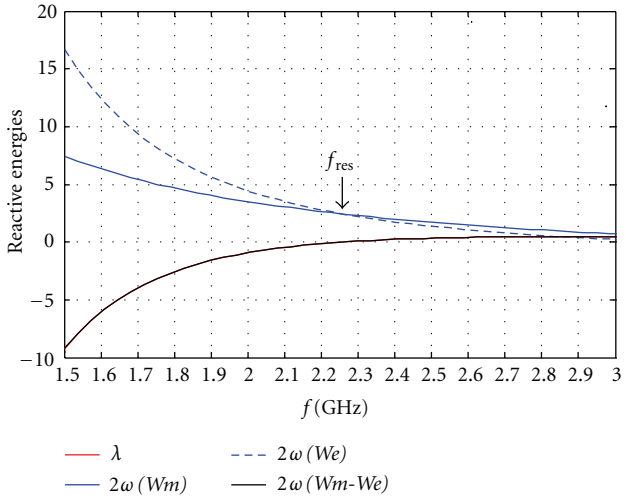

FIGURE 5: Reactive energies and their differences for an R50 × 30 patch at height of 25 mm.

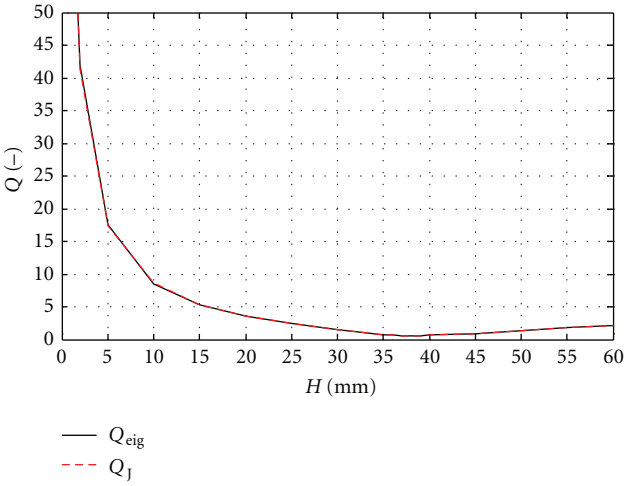

FIGURE 6: The radiation Q for dominant mode of an R50 × 30 patch as a function of height H.

$H = 25$ mm as a function of frequency. There is excellent agreement between the difference in stored energies and the eigenvalues, both obtained in a completely different manner.

There is also very good agreement between the exact Q_J and Q_{eig} confirming the validity of the proposed algorithm via (14), see Figure 6. Note that Q_{eig} in (10) does not require the currents to be calculated on the structure while Q_J is evaluated in a rigorous way from modal currents (11).

From Figure 6 it is seen that the radiation Q has a minimum for a specific height. It is deduced that the reason lies in the cancelling of the radiated power between the two out-of-phase currents. Similar behaviour has been observed in the case of two half-wave thin-wire dipoles with opposite sinusoidal currents, separated by $d = 2H$, see [25] for details. Actually these two out-of-phase dipoles may serve as a very simple model for a patch antenna with a dominant mode. When the dipoles are reduced to elementary (Hertzian) ones, an approximate analytical solution is available and in [25] we showed that the Q is led by the function

$$f_Q(H) \cong \frac{2H}{k2H - \sin(k2H)}. \tag{18}$$

After deriving (18), the condition is worked-out

$$\tan(k2H) = k2H, \tag{19}$$

and the first nontrivial root of (19) could be approximated as [25]

$$\left(\frac{H}{\lambda}\right)_{\min} \cong \frac{3}{8} - \frac{1}{6\pi^2} = 0.358. \tag{20}$$

For sinusoidal currents on dipoles the minimum (evaluated numerically) occurs for $H = 0.36\lambda$.

The minimum of the patch under study is obtained at $H \cong 0.4\lambda$, a value that is remarkably close to the simple dipole model.

4.1. Algorithm Convergence. Since no other methods for calculating modal Q are available, Q_{eig} is taken as a reference, and the relative error percentage is defined as:

$$\text{relative error} = \frac{\left|Q_J - Q_{eig}\right|}{Q_{eig}} \cdot 100, \tag{21}$$

where Q_J is calculated from the currents using (11). Four different heights H were chosen, $H = 1$ mm (0.01λ), $H = 2$ mm (0.0185λ), $H = 10$ mm (0.0803λ), and $H = 20$ mm (0.151λ), and the relative error was evaluated as a function of total triangular elements (including the mirror), see Figure 7. All quality factors were evaluated at the resonant frequency of the dominant mode for the R50 × 30 patch. As discussed earlier, the centroid approximation became more inaccurate with low heights H. However, even for the lowest analyzed value $H = 0.01\lambda$, the relative error is in the order of a few percent for reasonable mesh density (hundreds of elements). Further improvements to the integration routine are considered for the future.

4.2. Fractional Bandwidth of the R50 × 30 Patch Antenna. It is known that the fractional bandwidth (FBW) is related to the unloaded Q factor and the desired matching VSWR level. For VSWR < s we have [26]

$$\text{FBW} \cong \frac{s-1}{Q\sqrt{s}} \quad [\%]. \tag{22}$$

Using a full-wave simulator CST-MWS [27], an R50 × 30 patch has been simulated and the FBW_{CST} for VSWR < 2 was calculated as:

$$\text{FBW}_{CST} = \frac{f_2 - f_1}{f_0}, \tag{23}$$

where f_2 and f_1 are margins for VSWR < 2 and f_0 is the centre frequency. Only very low heights were studied since we used a simple probe feed which introduces an inductance component to the total input impedance. The comparison in Figure 8 shows good agreement of both fractional bandwidths.

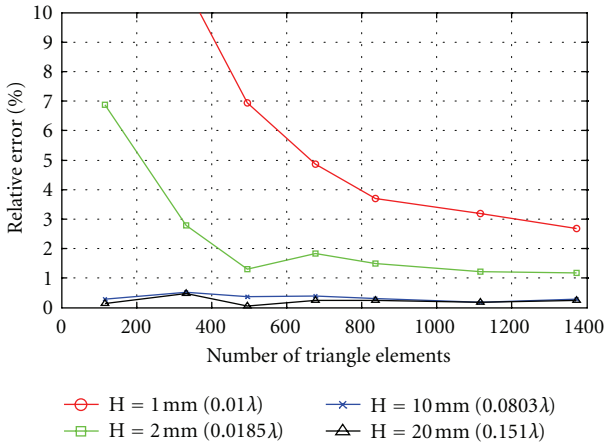

Figure 7: Relative error of the Q factor as a function of triangular elements (mesh density).

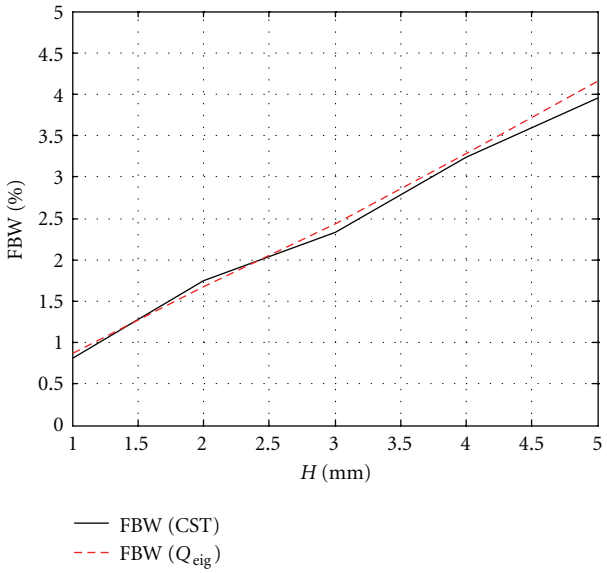

Figure 8: Fractional bandwidth FBW (VSWR < 2) for a R50 × 30 patch.

5. Applications: Fractal Antennas

In this section, a bit more complex structures will be studied. The first one (the "Self Affine U" fractal, SAU), has been described in [28] and further analyzed in [29]. This kind of radiating motif is employed as a dual-band radiator with mutually orthogonal radiation patterns at both bands. Therefore we are analyzing the first two modes, where the currents are orthogonal. These are depicted in Figures 9 and 10 for first (SAU1) and second (SAU2) fractal iteration, respectively. The current of the first (lower) mode $\mathbf{J}_1$ has two out-of-phase components (see Figure 11 for schematic current paths) while the second mode comprises inphase currents only. As we know from previous studies, opposite currents contribute to a rapid increase of the radiation Q, and it is expected that $\mathbf{J}_1$ will have a much higher Q than $\mathbf{J}_2$.

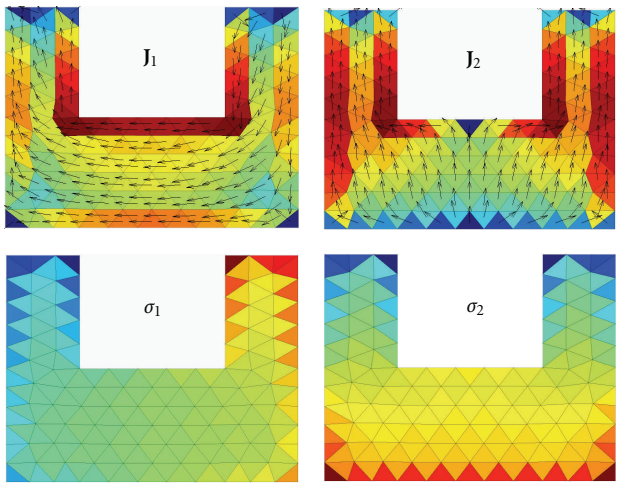

Figure 9: The first two characteristic modes (currents and charges) for the SAU1 structure.

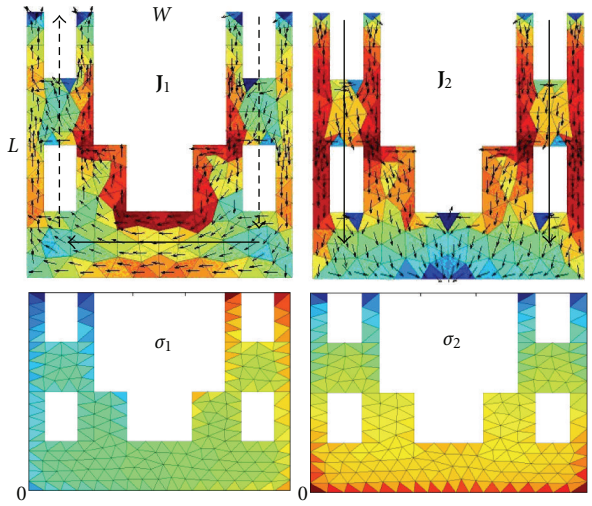

Figure 10: The first two characteristic modes (currents and charges) for the SAU2 structure.

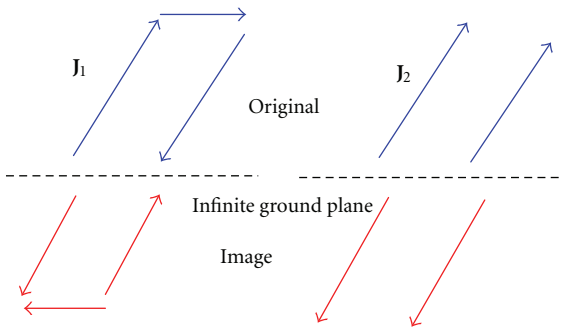

Figure 11: The main current paths for the first two modes of the SAU1/2 structure.

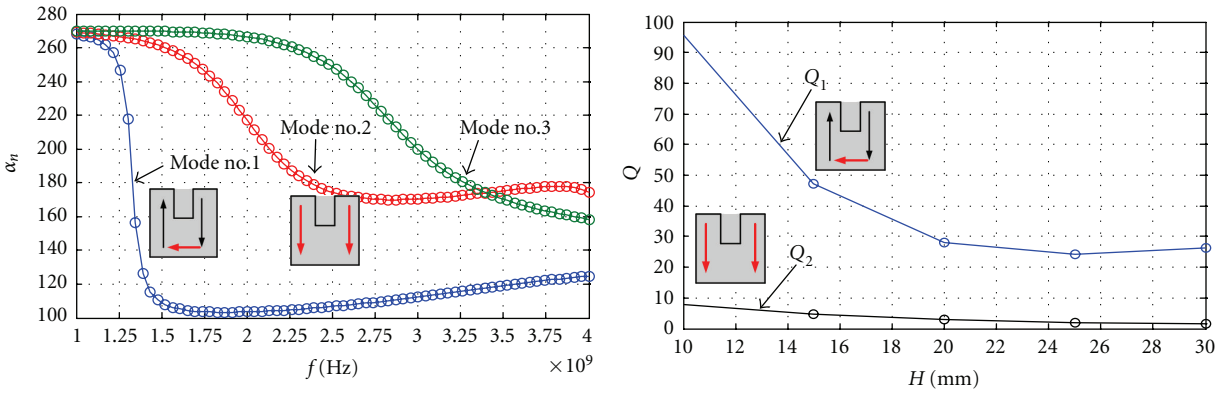

(a) (b)

Figure 12: Characteristic angles (left) and radiation Q for the SAU2.

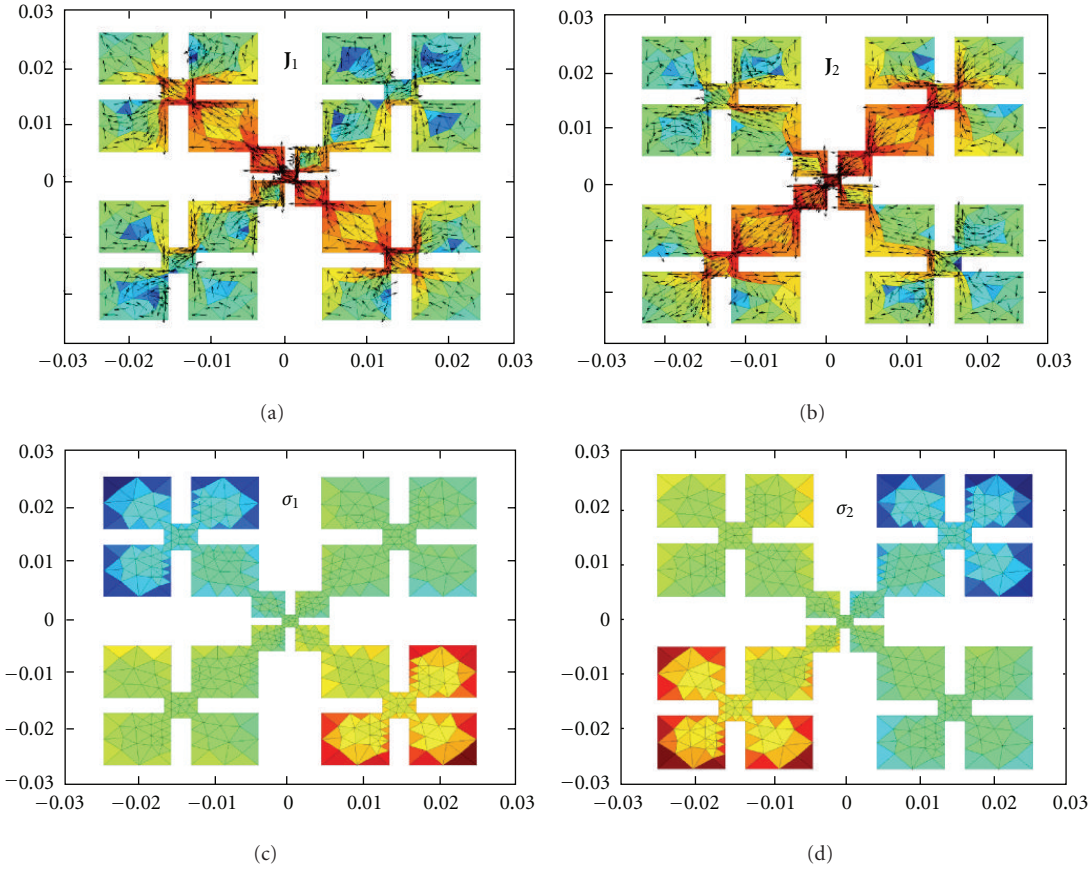

(a) (b) (c) (d)

Figure 13: Degenerated dominant mode $\mathbf{J}_1$, and $\mathbf{J}_2$ of the FCL2 antenna (currents and charges).

Figure 11 presents a very simple concept showing the main current paths for the $\mathbf{J}_1$ and $\mathbf{J}_2$ modes discussed above including the mirroring effect of the infinite ground plane. It could be simply stated that more opposing current paths lead to significant increase in Q.

We show detailed behaviour only for SAU2 (the situation is similar for SAU1)—see Figure 12 that confirms high Q for the $\mathbf{J}_1$ mode. Characteristic angles are calculated for $H = 29$ mm, the actual height for which the dual-band antenna was designed [29].

5.1. The FCL-2 Fractal Antenna. The second presented structure is the so-called fractal clover leaf (FCL) of the second iteration, [14]. The antenna is fed by an L-probe [30] that excites its dominant mode and is located at height $H = 36$ mm. Actually, the dominant mode is composed of two degenerated modes $\mathbf{J}_1$ and $\mathbf{J}_2$ (Figure 13). The second higher mode $\mathbf{J}_3$ is shown at Figure 14 for completeness.

Figure 15 shows the main current paths of these modes, and we can again deduce that the dominant mode will exhibit

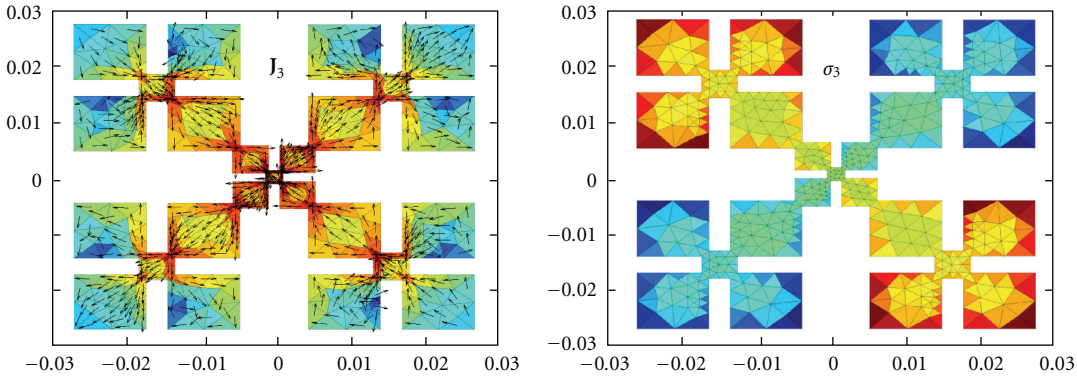

Figure 14: Second higher mode $\mathbf{J}_3$ (currents and charges).

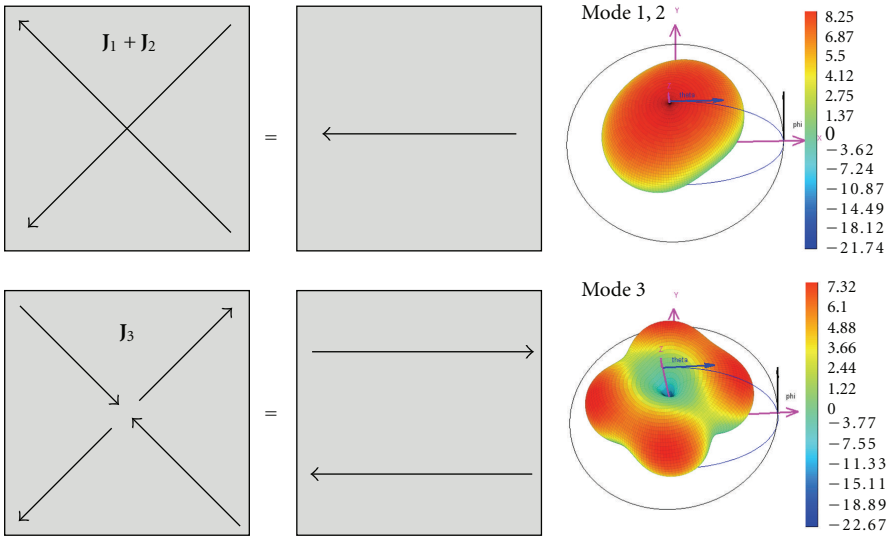

Figure 15: Schematic depiction of the dominant current paths for the dominant $(\mathbf{J}_1 + \mathbf{J}_2)$ and the second higher $\mathbf{J}_3$ modes together with their modal radiation patterns.

lower Q compared to $\mathbf{J}_3$. This is confirmed by Figure 16—$\mathbf{J}_3$ has more than 200x higher radiation Q.

6. Resonant Properties of Studied Antennas

The properties of studied antennas are summarized in this section. At first we observed that microstrip antenna could support different kinds of modes regarding their Q factors (see Figure 17):

(a) low Q modes with the current flowing in one direction and not changing its phase (dominant modes of simple shapes like rectangular, circular patch, and so forth.)

(b) high Q modes with part of the currents flowing in the opposite direction. These modes exist even on simple "U" shaped patch (Figure 9 left) and on complex (fractal) geometries.

Secondly, it has been observed that resonant frequency is quite a complicated function of height. Unfortunately we do not yet have any physical explanation as to why some modes present minimum values of f_r.

Looking at Figure 18, it is clear (and interesting) that the resonant frequency behaves quite differently for low-Q and high-Q modes. The resonant frequency of low-Q modes is much more sensitive to the height, whereas high-Q modes exhibit almost constant f_r when the height is varied. The proposed explanation is that the opposite currents (responsible for high Q) keep reactive fields very close to the radiating structure so the effect of a fringing field coupled to the ground plane becomes almost negligible.

7. Conclusions

Modal resonant properties of selected microstrip patch antennas have been studied with the help of characteristic

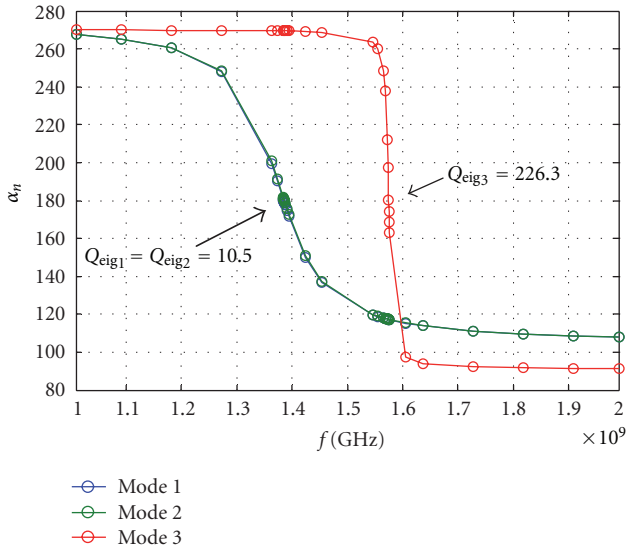

Figure 16: Characteristic angles for the FCL2 structure at $H = 29$ mm.

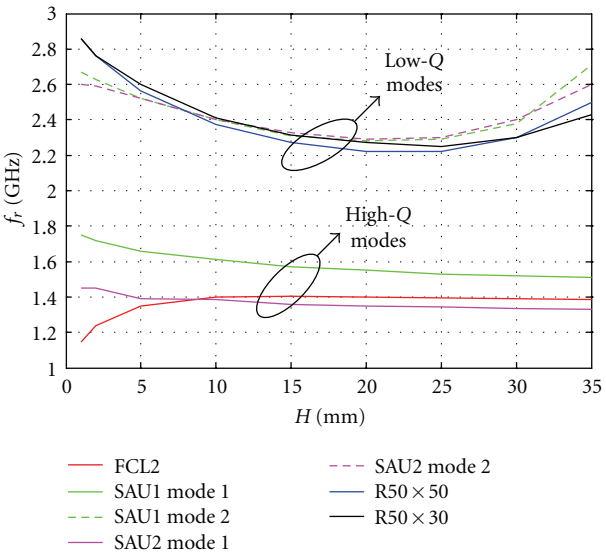

Figure 18: Resonant frequencies for different antennas/modes.

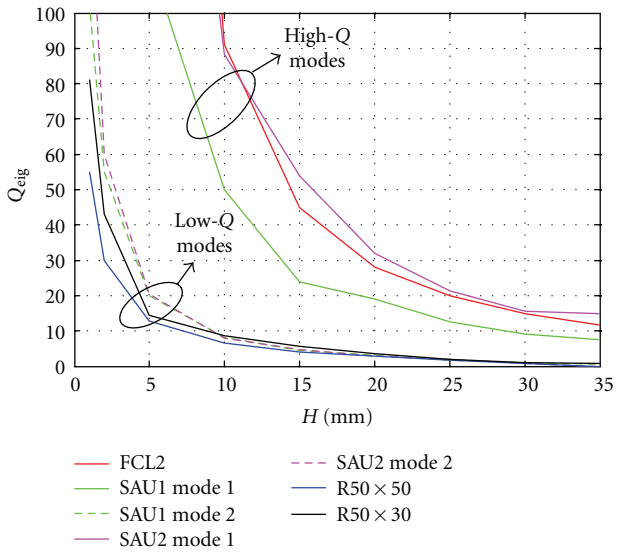

Figure 17: Radiation Qs for different antennas/modes.

modes and the novel theory published by Vandenbosch. It has been found that the resonant frequency of a simple rectangular patch antenna is quite a complicated function of its height above the infinite ground. Moreover, the dependency of resonant frequency is also found to be a function of the radiation Q factor (which is now possible to calculate in a rigorous way). Due to the complexity of the problem, no physical explanation for the resonant frequency behaviour has yet been found.

It is observed that the radiation Q factor decreases for "standard" heights ($<\sim 0.1\lambda$), however there exists an absolute minimum value of Q that has already been predicted by simple modeling of two elementary out-of-phase dipoles. Using proper feeding techniques (like the L-probe) allows us to design wideband compact antennas.

The theory now puts current distribution and the radiation Q factor into objective context. Whenever the current mode exhibits opposite components, high Q may appear.

Future work is needed to connect the presented theory with parameter sweeps or even optimization, so we will be able to design novel wideband/multimode compact antennas.

Acknowledgments

This work was supported by the Grant Agency of the Czech Technical University in Prague, grant no. SGS11/065/OHK3/1T/13 and by the Project COST 1102. The authors would like to thank professor Vandenbosch for fruitful discussions, Neil Bell for his comments, and two anonymous reviewers who suggested some improvements to the paper.

References

[1] P. Bhartia, I. Bahl, R. Garg, and A. Ittipiboon, *Microstrip Antenna Design Handbook*, Artech House, Norwood, Mass, USA, 2000.

[2] K. F. Lee and W. Chen, *Advances in Microstrip and Printed Antennas*, John Wiley & Sons, New York, NY, USA, 1997.

[3] J. R. James, P. S. Hall, and C. Wood, *Microstrip Antenna Theory and Design*, Peter Peregrinus, London, UK, 1986.

[4] R. F. Harrington and J. Mautz, "Theory of characteristic modes for conducting bodies," *IEEE Transactions on Antennas and Propagation*, vol. 19, no. 5, pp. 622–628, 1971.

[5] E. A. Daviu, *Analysis and design of antennas for wireless communications using modal methods*, Ph.D. dissertation, Universidad Politécnica de Valencia, Valencia, Spain, 2008.

[6] G. A. E. Vandenbosch, "Reactive energies, impedance, and Q factor of radiating structures," *IEEE Transactions on Antennas*

and Propagation, vol. 58, no. 4, Article ID 5398856, pp. 1112–1127, 2010.

[7] G. A. E. Vandenbosch and V. Volski, "Lower bounds for radiation Q of very small antennas of arbitrary topology," in *Proceedings of the 4th European Conference on Antennas and Propagation (EuCAP '10)*, pp. 1–4, Barcelona, Spain, April 2010.

[8] R. F. Harrington, *Field Calculation by the Method of Moments*, IEEE Press, New York, NY, USA, 1993.

[9] M. Cabedo-Fabres, E. Antonino-Daviu, A. Valero-Nogueira, and M. F. Bataller, "The theory of characteristic modes revisited: a contribution to the design of antennas for modern applications," *IEEE Antennas and Propagation Magazine*, vol. 49, no. 5, pp. 52–68, 2007.

[10] P. Hazdra and P. Hamouz, "On the modal superposition lying under the MoM matrix equations," *Radioengineering*, vol. 17, no. 3, pp. 42–46, 2008.

[11] Mathworks, http://www.mathworks.com/.

[12] S. N. Makarov, *Antenna and EM Modeling with Matlab*, John Wiley & Sons, New York, NY, USA, 2002.

[13] S. M. Rao, D. R. Wilton, and A. W. Glisson, "Electromagnetic scattering by surfaces of arbitrary shape ," *IEEE Transactions on Antennas and Propagation*, vol. 30, no. 3, pp. 409–418, 1982.

[14] M. Capek, P. Hazdra, P. Hamouz, and M. Mazanek, "Software tools for efficient generation, modelling and optimisation of fractal radiating structures," *IET Microwaves, Antennas and Propagation*, vol. 5, no. 8, pp. 1002–1007, 2011.

[15] Comsol Multiphysics, http://www.comsol.com/.

[16] J. L. Volakis, Ch. Chen, and K. Fujimoto, *Small Antennas: Miniaturization Techniques & Applications*, chapter 2, McGraw-Hill, New York, NY, USA, 1st edition, 2010.

[17] J. S. McLean, "A re-examination of the fundamental limits on the radiation q of electrically small antennas," *IEEE Transactions on Antennas and Propagation*, vol. 44, no. 5, pp. 672–676, 1996.

[18] R. F. Harrington and J. R. Mautz, "Control of radar scattering by reactive loading," *IEEE Transactions on Antennas and Propagation*, vol. 20, no. 4, pp. 446–454, 1972.

[19] R. F. Harrington, *Time-Harmonic Electromagnetic Fields*, IEEE Press, New York, NY, USA, 2001.

[20] D. R. Rhodes, "Observable stored energies of electromagnetic systems," *Journal of the Franklin Institute*, vol. 302, no. 3, pp. 225–237, 1976.

[21] D. R. Rhodes, "Reactance Theorem," *Proceedings of the Royal Society A*, vol. 353, no. 1672, pp. 1–10, 1977.

[22] J. Shaeffer, "MOM3D method of moments code theory manual," Research report 189594, Lockheed Advanced Development Company, 1992.

[23] M. Capek, P. Hazdra, and J. Eichler, "A method for the evaluation of radiation Q based on modal approach," *IEEE Transactions on Antennas and Propagation*. In press.

[24] P. Arcioni, M. Bressan, and L. Perregrini, "On the evaluation of the double surface integrals arising in the application of the boundary integral method to 3-D problems," *IEEE Transactions on Microwave Theory and Techniques*, vol. 45, no. 3, pp. 436–439, 1997.

[25] P. Hazdra, M. Capek, and J. Eichler, "Radiation Q-factors of thin-wire dipole arrangements," *IEEE Antennas and Wireless Propagation Letters*, vol. 10, pp. 556–560, 2011.

[26] A. D. Yaghjian and S. R. Best, "Impedance, bandwidth, and Q of antennas," *IEEE Transactions on Antennas and Propagation*, vol. 53, no. 4, pp. 1298–1324, 2005.

[27] CST Gmbh, http://www.cst.com/.

[28] S. N. Sinha and M. Jain, "A self-affine fractal multiband antenna," *IEEE Antennas and Wireless Propagation Letters*, vol. 6, Article ID 891519, pp. 110–112, 2007.

[29] J. Eichler, P. Hazdra, M. Čapek, T. Kořínek, and P. Hamouz, "Design of a dual-band orthogonally polarized l-probe-fed fractal patch antenna using modal methods," *IEEE Antennas and Wireless Propagation Letters*, vol. 10, pp. 1389–1392, 2011.

[30] C. L. Mak, K. M. Luk, K. F. Lee, and Y. L. Chow, "Experimental study of a microstrip patch antenna with an L-shaped probe," *IEEE Transactions on Antennas and Propagation*, vol. 48, no. 5, pp. 777–783, 2000.

XIII

J. Eichler, P. Hazdra, M. Capek, T. Korinek, and P. Hamouz, "Design of a dual-band orthogonally polarized l-probe-fed fractal patch antenna using modal methods," *IEEE Antennas Wireless Propag. Lett.*, vol. 10, pp. 1389–1392, 2011. [85∗]

Design of a Dual-Band Orthogonally Polarized L-Probe-Fed Fractal Patch Antenna Using Modal Methods

J. Eichler, *Student Member, IEEE*, P. Hazdra, *Member, IEEE*, M. Čapek, *Student Member, IEEE*, T. Kořínek, *Member, IEEE*, and P. Hamouz, *Student Member, IEEE*

***Abstract*—Modal methods are used to effectively design a dual-band orthogonally polarized fractal patch antenna. This letter summarizes the workflow from generating a fractal motif through modal analysis to feeding design and full-wave analysis. As the antenna's feeding and matching structure, a dual L-probe was proposed to widen its bandwidth. The full-wave simulation is in very good agreement with the measurement. The motif size is 50×50 mm^2, and the antenna operates at 1.25 and 2.1 GHz. The relative bandwidths are 4.18% and 11.4%, respectively.**

***Index Terms*—Bandwidth, dual-band, fractal antena, Iterated Function System (IFS), L-probe, modal analysis, theory of characteristic modes (TCM).**

I. Introduction

THE MODAL methods, namely the theory of characteristic modes [1] and the cavity model [2], represent powerful tools for analysis and design of microstrip antennas. They are especially useful for complex shapes like fractals. With modal analysis, it is possible to investigate properties of a wide range of microstrip motifs within a reasonable time and also to provide physical insights into their operation.

This letter follows the same procedure as in [3] and presents its application on the design of a dual-band antenna with a fractal motif. The other goals are specified as the following:

- radiation in the normal direction with gain >6 dBi;
- mutually orthogonal polarizations;
- small motif electrical size;
- wideband behavior on bands preferred.

Other antenna properties such as the ratio of two resonant frequencies f_2/f_1 and -10-dB relative frequency bandwidth will be discussed.

II. Modal Analysis

A. Modal Methods

In order to analyze planar motifs separately from an antenna feeding and to understand the physical principles of an antenna operation, two modal methods were used. The first is the well-known cavity model (CM) [2]. Drawbacks of this method are a restriction to low substrate heights h and low complexity of a motif shape.

More accurate but also slower than the CM is the theory of characteristic modes for conducting bodies (TCM), developed by Harrington and Mauz [1] and recently revised [4]. It can be applied to conducting bodies of arbitrary shape defined by a surface S. Also, an infinite conducting ground plane can be taken into account by the method of images. The characteristic currents $\mathbf{J}_n$ (modes) are given [1] by decomposition of the moment impedance matrix $\mathbf{Z} = \mathbf{R} + j\mathbf{X}$, i.e., by solving the associated eigenvalue problem

$$\mathbf{X}\mathbf{J}_n = \lambda_n \mathbf{R}\mathbf{J}_n. \tag{1}$$

The impedance matrix $\mathbf{Z}$ is obtained in a standard way by Galerkin method applied to the electric field integral equation on Rao–Wilton–Glisson elements [5]. The TCM provides information about the modal radiation quality factor $Q_{\mathrm{rad},n}$, which is dependent on the frequency variation of modal eigenvalues [1].

B. Analysis Procedure

At first, an analysis of a parametrized fractal motif was conducted using fast CM in order to find a suitable shape for dual-mode (dual-band) operation with the desired ratio of resonant frequencies. The results were subsequently refined by the TCM, which is also suitable for arbitrary air substrate heights (an infinite ground plane is considered). The CM and the TCM routines were programmed in MATLAB [6], [7].

The modal results were validated by a full-wave simulation, where the current distribution on patch is a superposition of all modes, i.e., theoretically an infinite series [8]. On the other hand, it is possible to obtain full-wave simulation results similar to the modal results if we choose feeding that predominantly excites the desired mode at its resonant frequency.

III. Fractal Motifs

A. Fractal Generation

A fractal is generated by the Iterated Function System (IFS) [9] implemented in MATLAB [7]. The IFS is defined by a finite family of contractions $S_1, S_2, \ldots, S_m$, where $m \geq 2$. For microstrip antennas (the two-dimensional case), each transformation is described by coefficients a, b, c, d, e, f

$$\begin{pmatrix} x_{i+1} \\ y_{i+1} \end{pmatrix} = \begin{pmatrix} a & b \\ c & d \end{pmatrix} \cdot \begin{pmatrix} x_i \\ y_i \end{pmatrix} + \begin{pmatrix} e \\ f \end{pmatrix} \tag{2}$$

Manuscript received October 07, 2011; accepted November 27, 2011. Date of publication December 08, 2011; date of current version December 19, 2011. This work was supported by the Grant Agency of the Czech Technical University in Prague under Grant SGS11/065/OHK3/1T/13 and the Grant Agency of the Czech Republic under Grant DG102/08/H018.

The authors are with the Department of Electromagnetic Field, Faculty of Electrical Engineering, Czech Technical University in Prague, 16627 Prague, Czech Republic (e-mail: eichljan@fel.cvut.cz).

Color versions of one or more of the figures in this letter are available online at http://ieeexplore.ieee.org.

Digital Object Identifier 10.1109/LAWP.2011.2178811

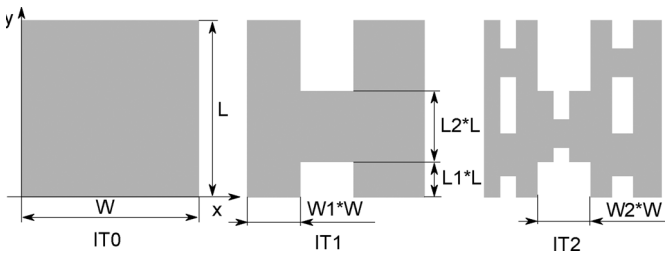

Fig. 1. Iterations of the SAU motif ($W1 = 0.3$, $W2 = 0.3$, $L1 = 0.2$, $L2 = 0.4$).

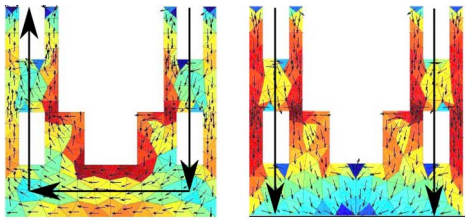

Fig. 2. Surface current on the SAU IT2 motif with dimensions $W = L = 50$ mm, $W1 = 0.25$, $W2 = 0.5$, $L1 = 0$, $L2 = 0.5$ (TCM). (a) Mode 1. (b) Mode 2.

TABLE I
IFS TRANSFORMATIONS FOR A GENERALIZED SAU FRACTAL, $b = c = 0$

T_n	a	d	e	f
T_1	$W1$	1-$L1$-$L2$	0	$L(L1+L2)$
T_2	1-$W1$-$W2$	1-$L1$-$L2$	$W(W1+W2)$	$L(L1+L2)$
T_3	$W1$	$L1+L2$	0	0
T_4	$W2$	$L2$	$W \cdot W1$	$L \cdot L1$
T_5	1-$W1$-$W2$	$L1+L2$	$W(W1+W2)$	0

where x, y are Cartesian coordinates and i is an iteration order. The zeroth iteration (IT0) denotes the chosen initial shape, e.g., triangle, rectangle, circle, etc. Each following iteration is a union of results of transformations $S_1, S_2, \ldots, S_m$ applied to the previous one. Rigorously, a fractal is generated after an infinite number of iterations. The nth iteration as an approximation of fractal will be used in the following text.

B. Chosen Fractal Motif

Based on previous experience, the fractal published in [10] was chosen as a potential candidate and will be called Self-affine "U" (SAU). The original motif was parametrized according to Fig. 1. The overall dimensions of the fractal were restricted not to exceed 50×50 mm^2.

The SAU fractal is created from a rectangle by four parameter-dependent IFS transformations according to Table I; see Fig. 1.

IV. MODAL RESULTS

Modal analysis revealed that modes 1 and 2 radiate in a normal direction if parameter L1 approaches 0 (the motif then resembles the letter "U"). Calculated characteristic currents are shown in Fig. 2, and the corresponding modal radiation patterns in Figs. 3 and 4.

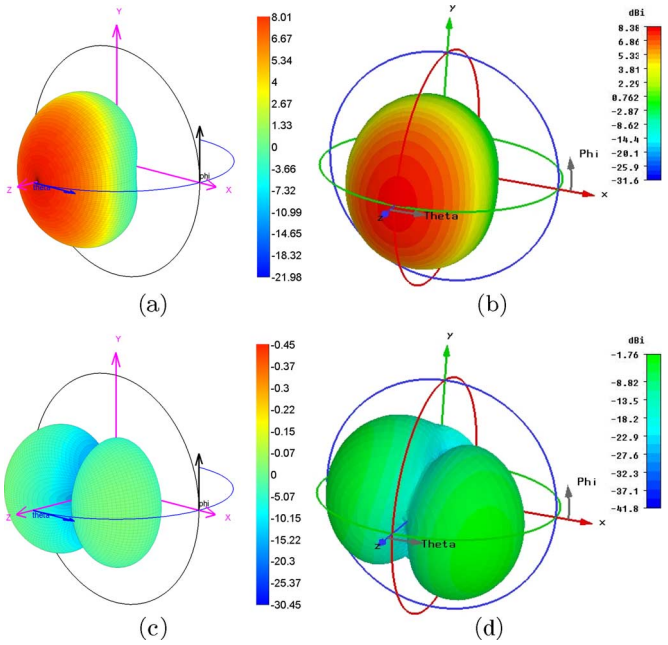

Fig. 3. Mode 1 Ludwig3 components of radiation pattern for the motif from Fig. 2, 5-mm air substrate, and a discrete port used in CST MWS. (a) Horizontal—MATLAB. (b) Horizontal—CST MWS. (c) Vertical—MATLAB. (d) Vertical—CST MWS.

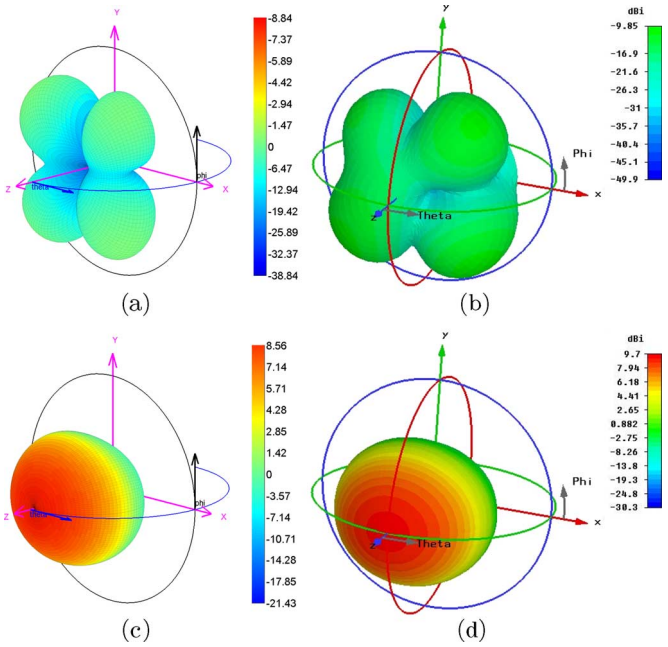

Fig. 4. Mode 2 Ludwig3 components of radiation pattern for the motif from Fig. 2, 5-mm air substrate, and a discrete port used in CST MWS. (a) Horizontal—MATLAB. (b) Horizontal—CST MWS. (c) Vertical—MATLAB. (d) Vertical—CST MWS.

Radiation patterns were also calculated in CST MWS [11], where the patch was fed by a discrete port. Modal radiation patterns can quite accurately predict polarization and the direction of maximal radiation; see Figs. 3 and 4. Orthogonality of polarizations could easily be explained by inspecting the dominant current lines for modes 1 and 2 from Fig. 2.

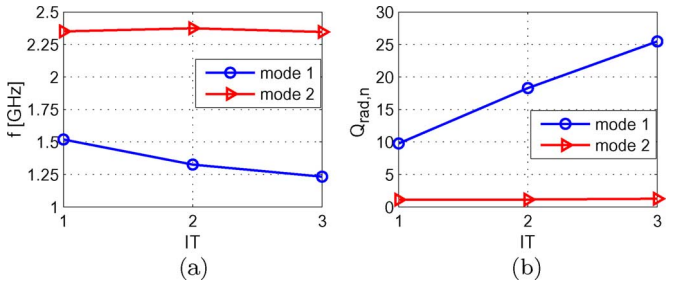

Fig. 5. Effect of iteration, SAU motif, $W = L = 50$ mm, $W1 = 0.25$, $W2 = 0.5$, $L1 = 0$, $L2 = 0.5$, $h = 30$ mm (TCM). (a) Effect on resonant frequency. (b) Effect on modal radiation quality factor.

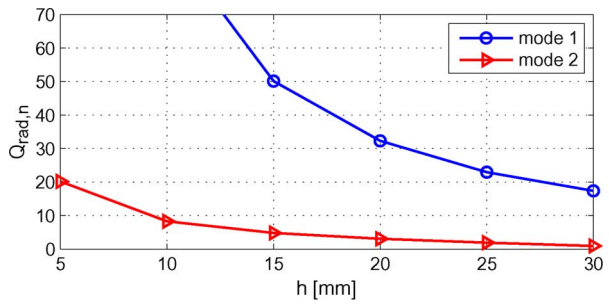

Fig. 6. Effect of substrate height on modal quality factor of SAU IT2, $W = L = 50$ mm, $W1 = 0.25$, $W2 = 0.5$, $L1 = 0$, $L2 = 0.5$ (TCM).

According to a parametric study of the SAU fractal, it is possible to achieve the modal ratio (CM) of f_2/f_1 to be approximately 1.6–3.5. The main influence on f_2/f_1 has the ratio W/L because the major part of the mode 1 current is orientated in the x-axis direction and mode 2 forms a standing wave in the y-axis direction (Fig. 2).

It is known [12] that the higher the iteration, the lower the resonant frequencies. A simple explanation is that higher iteration produces a more complex shape with a longer path for current. This effect is not linear with iteration and also affects different modes differently; see Fig. 5.

The fractional antenna bandwidth FBW [13] is inversely proportional to the quality factor Q, which consists of contributions caused by different types of loss [2], [13]. The only reasonable option is the lowering of the radiation Q_{rad}, otherwise radiation efficiency $\eta = P_{\mathrm{rad}}/P_{\mathrm{in}}$ decreases. The Q_{rad} of microstrip antennas depends on current distribution and is inversely proportional to the substrate height h and directly proportional to substrate relative permitivity ϵ_{r} [2]. The same effect of substrate height on modal $Q_{\mathrm{rad},n}$ could be seen in Fig. 6.

V. Full Wave Simulation

The SAU IT2 motif was chosen as a compromise between low resonant frequency and low modal quality factor; see Fig. 5. Modes 1 and 2 satisfy the demand on low resonant frequency and normal radiation. Here, we choose the patch with $W = L$, which corresponds to the modal $f_2/f_1 \approx 1.8$. However, the resonant frequency and the current density depend not only on patch shape, but also on substrate height h.

The selected motif is considerably electrically small ($0.208\times 0.208\lambda$ at f_1), therefore the FBW is quite narrow. To compensate this effect (Fig. 6), the patch is placed high enough above the ground plane and fed by an L-probe that acts also as a matching circuit. The optimal L-probe length and bend position is different in both bands [14], thus a modification leading to the dual L-probe (DL-probe) was proposed.

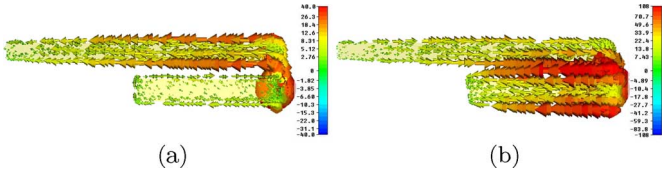

Fig. 7. Current density on the dual L-probe in both bands (CST MWS). (a) $f = 1.25$ GHz. (b) $f = 2.1$ GHz.

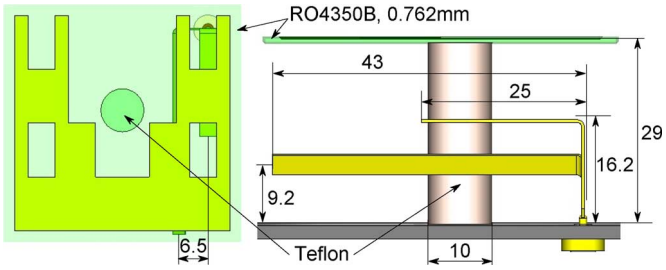

Fig. 8. SAU IT2 CST model with dimensions in millimeters.

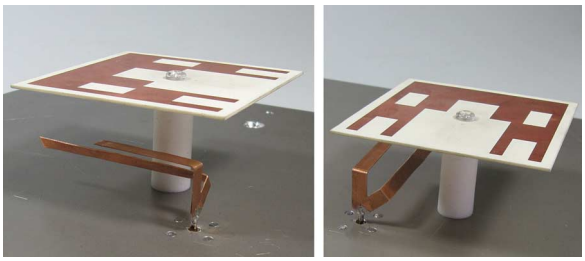

Fig. 9. Manufactured antenna.

Fig. 7 shows that the current density in both bands is concentrated on specific and more or less independent parts (arms) of the DL-probe. This allows us to design the arms separately for each working band. An overall view of the CST model with the actual orientation of the DL-probe is shown in Fig. 8.

The proper feeding position can be guessed from the current density computed by the TCM (or CM). The horizontal part of the DL-probe arm should be orientated parallel to the modal current on the patch surface (see Figs. 2 and 8).

VI. Measurement and Comparison of Results

An antenna with the SAU IT2 fractal motif was fabricated (see Fig. 9) and measured at the Department of Electromagnetic Field of FEE, CTU, in Prague, Czech Republic. The simulated and the measured S_{11} are in very good agreement; see Fig. 10. In the lower band, the motif dimensions are $0.208 \times 0.208\lambda$, which leads to quite a narrow bandwidth. This disadvantage was partially compensated by using DL-probe feeding, which allows 10-dB FBW to be 4.18%. The motif is electrically larger in the higher band ($0.34\times 0.34\lambda$), therefore the situation is easier, and the measured FBW is 11.4%.

The antenna feeding is optimized to maximal bandwidth in the lower band. However, by changing dimensions of the

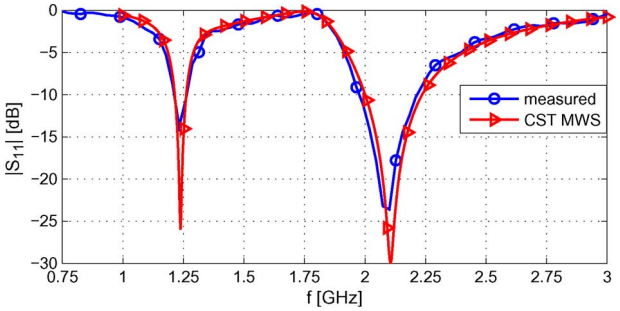

Fig. 10. Comparison of simulated and measured S_{11} of SAU IT2.

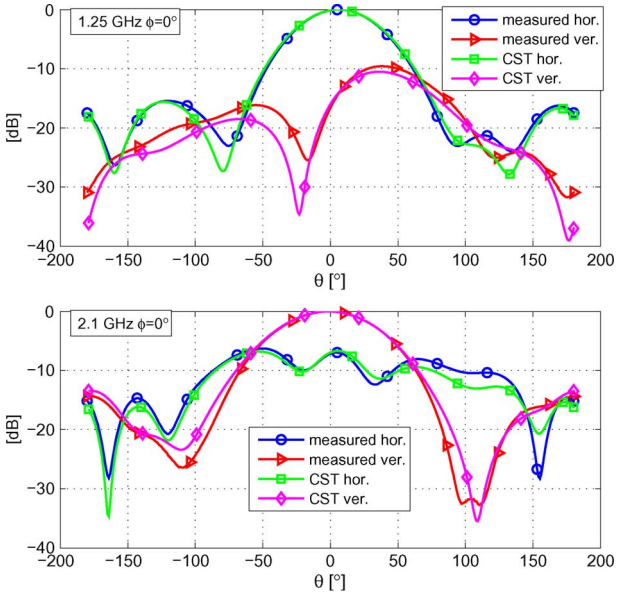

Fig. 11. Measured and simulated far-field cuts for horizontal and vertical polarization.

DL-probe, an antenna with the $\mathrm{FBW}_{\mathrm{lower}} = 3.42\%$ and the $\mathrm{FBW}_{\mathrm{upper}} = 18.7\%$ was designed in the CST MWS.

Farfield cuts for horizontal and vertical polarization are presented in Fig. 11. Due to unbalanced feeding, the radiation pattern is distorted, and the maximal directivity is slightly (5° and 8°) shifted from the normal direction (Fig. 11). Radiation pattern measurement confirms mutually orthogonal polarizations in both bands.

VII. Conclusion

This letter summarizes the procedure of planar antenna design using modal methods. They provide information about motif behavior and its suitability for the desired antenna. Because only patch motif is considered, it is possible to effectively analyze even quite complicated shapes like fractals. More importantly, modal decomposition shed some light on the physical behavior of the planar antenna. The last step is a design of patch feeding and a full-wave analysis.

Following the above-mentioned procedure, a dual-band antenna was developed, manufactured, and measured. It was found that modal radiation patterns could successfully predict antenna radiation properties such as polarization or main lobe direction. Motif dimensions are noticeably smaller than a $\lambda/2$ rectangular patch in both bands. The narrow bandwidth was partially compensated by the dual L-probe feeding structure. CST MWS simulation is in very good agreement with measurement.

The possible antenna applications are in point-to-point dual-band systems that could operate with linear polarization. The suggested structure is, after some dimension adjustments of the DL-probe and the motif, able to cover both WLAN bands 2.4 and 5 GHz with $\mathrm{FBW}_{\mathrm{lower}} > 3.2\%$ and $\mathrm{FBW}_{\mathrm{upper}} > 17\%$.

References

[1] R. F. Harrington and J. M. Mautz, "Theory of characteristic modes for conducting bodies," *IEEE Trans. Antennas Propag.*, vol. AP-19, no. 5, pp. 622–628, Sep. 1971.

[2] C. A. Balanis, *Antenna Theory—Analysis and Design*, 3rd ed. ed. Hoboken, NJ: Wiley, 2005.

[3] P. Hazdra, P. Hamouz, and M. Mazanek, "Theory of characteristic modes and its applications for analysis of fractal microstrip patch antennas," in *Proc. EuCAP*, Edinburgh, U.K., 2007, pp. 1–5.

[4] M. Cabedo, E. Antonino, A. Valero, and M. Ferrando, "The theory of characteristic modes revisited: A contribution to the design of antennas for modern applications," *IEEE Antennas Propag. Mag.*, vol. 49, no. 5, pp. 52–68, Oct. 2007.

[5] S. N. Makarov, *Antenna and EM Modelling With MATLAB*. New York: Wiley, 2002.

[6] MATLAB. ver. 2011b, MathWorks, Natick, MA [Online]. Available: http://www.mathworks.com

[7] M. Čapek, P. Hazdra, P. Hamouz, and M. Mazánek, "Software tools for efficient generation, modeling and optimisation of fractal radiating structures," *Microw., Antennas Propag.*, vol. 5, no. 8, pp. 1002–1007, 2011.

[8] P. Hazdra and P. Hamouz, "On the modal superposition lying under the MoM matrix equations," *Radioengineering*, vol. 17, no. 3, pp. 42–46, Sep. 2008.

[9] K. Falconer, *Fractal Geometry, Mathematical Foundations and Applications*, 2nd ed. Chichester, England: Wiley, 2003.

[10] S. N. Sinha and M. Jain, "A self-affine fractal multiband antenna," *IEEE Antennas Wireless Propag. Lett.*, vol. 6, pp. 110–113, 2007.

[11] CST. Microwave Studio Computer Simulation Technology, Framingham, MA, 2011 [Online]. Available: http://www.cst.com

[12] J. Anguera, "Fractal and broadband techniques on miniature, multifrequency, and high-directivity microstrip patch antennas," Ph.D. dissertation, Dept. Signal Theory Commun., UPC, Barcelona, Spain, 2003.

[13] A. D. Yaghjian and S. R. Best, "Impedance, bandwidth and Q of antennas," *IEEE Trans. Antennas Propag.*, vol. 53, no. 4, pp. 1298–1324, Apr. 2005.

[14] P. Hazdra, M. Mazánek, and J. Čermák, "Widemand rectangular microstrip patch antenna using L-probe feeding system," *Radioengineering*, vol. 16, no. 3, pp. 37–41, Sep. 2007.

XIV

P. Hazdra, M. Capek, and J. Eichler, "Radiation Q-factors of thin-wire dipole arrangements," *IEEE Antennas Wireless Propag. Lett.*, vol. 10, pp. 556–560, 2011. [44∗]

Radiation Q-Factors of Thin-Wire Dipole Arrangements

Pavel Hazdra, *Member, IEEE*, Miloslav Capek, *Member, IEEE*, and Jan Eichler, *Member, IEEE*

***Abstract*—In this letter, we present an investigation of the radiation Q-factors of two coupled thin dipole antennas with sinusoidal current distribution. The approach is based on novel rigorous equations for radiated power and stored energies recently derived by Vandenbosch. First, we study the validity of the used thin-wire approximation with a reduced kernel. Good agreement between the assumed sinusoidal current distribution and the real cylindrical antenna modeled with the full-wave method of moments (MoM) is observed. Then, radiation Q-factors are evaluated for half-wave side-by-side coupled dipole antennas with different feeding configurations. It is found that every such combination of studied coupled dipoles presents minimum Q for specific feeding arrangement and separation distance.**

***Index Terms*—Antenna coupling, dipole antenna, radiation Q-factor, thin-wire approximation.**

I. Introduction

THE RADIATION Q-factor is an important characteristic of a radiating system because of its connection to relative frequency bandwidth potential. Recently, Vandenbosch [1], [2] presented a rigorous method for evaluating radiated power P_{r} and stored electric/magnetic energies $\widetilde{W}_{\mathrm{e}}$, $\widetilde{W}_{\mathrm{m}}$ due to an arbitrary electric current density. We utilize his equations for the investigation of radiation Q of half-wave coupled dipole arrangements. Such an antenna arrangement is a textbook case, but it is of importance due to the representative nature of this topology (a dipole above an electric/magnetic ground plane or close to a metallic plate, the study of dipole antenna diversity, etc.). The results presented give a deeper physical insight of multiple dipole arrangements than that offered by "classical" approaches for evaluating on the antenna Q based on input impedance variation.

II. Radiation Q Formulation for the Thin-Wire Dipole Antenna

Consider linear z-oriented real sinusoidal currents flowing along a lossless dipole with an overall length $2L$

$$J(z) = \sin\left[k\left(L - |z|\right)\right]. \tag{1}$$

General equations for radiated power and stored energies from [1] are now reduced to the following double linear integrals:

$$P_{\mathrm{r}} = \left(\frac{1}{8\pi\omega\varepsilon_0}\right)\int_{-L}^{L}\int_{-L}^{L}\left[k^2 J(z)\,J(z') - \nabla\cdot J(z)\,\nabla\cdot J(z')\right]\frac{\sin(kr)}{r}\,dzdz' \tag{2}$$

$$\widetilde{W}_{\mathrm{e}} = \frac{1}{16\pi\omega^2\varepsilon_0}\left(I_{\mathrm{e}} - I_{\mathrm{R}}\right) \tag{3}$$

$$\widetilde{W}_{\mathrm{m}} = \frac{1}{16\pi\omega^2\varepsilon_0}\left(I_{\mathrm{m}} - I_{\mathrm{R}}\right) \tag{4}$$

where

$$I_{\mathrm{R}} = \frac{k}{2}\int_{-L}^{L}\int_{-L}^{L}\left[k^2 J(z)\,J(z') - \nabla\cdot J(z)\,\nabla\cdot J(z')\right]\times\sin(kr)\;dzdz' \tag{5}$$

$$I_{\mathrm{e}} = \int_{-L}^{L}\int_{-L}^{L}\nabla\cdot J(z)\,\nabla\cdot J(z')\frac{\cos(kr)}{r}\,dzdz' \tag{6}$$

$$I_{\mathrm{m}} = k^2\int_{-L}^{L}\int_{-L}^{L}J(z)\,J(z')\frac{\cos(kr)}{r}dzdz' \tag{7}$$

where k is wavenumber, ω represents the angular frequency, and ε_0 stands for the free-space permittivity.

The distance r between interacting current elements is evaluated under the thin-wire approximation with a so-called reduced kernel [3]–[5] as

$$r = \sqrt{(z - z')^2 + a^2} \tag{8}$$

where a is the dipole radius. In this manner, the important "self-term" contributions occurring for $z = z'$ are easily resolved as $r_{\mathrm{self}} = a$.

The radiation Q-factor is readily calculated by definition [1]

$$Q = 2\omega\frac{\max\left(\widetilde{W}_{\mathrm{e}}, \widetilde{W}_{\mathrm{m}}\right)}{P_{\mathrm{r}}}. \tag{9}$$

The above-mentioned thin-wire formulation is well known from the literature dealing with the method of moments (MoM) [6]. It assumes that only z-oriented currents flow along a dipole. Moreover, the actual surface current is reduced to the filament located just in the dipole axis, and the actual antenna thickness is included by the approximation (8).

To validate our approach, Q results from (9) for a $2L = \lambda/2$ dipole with various radii a were compared to the FEKO [7] full-wave MoM simulator. The radiation Q-factor is estimated from

Manuscript received March 08, 2011; revised May 08, 2011; accepted May 11, 2011. Date of publication May 27, 2011; date of current version June 23, 2011. This work was supported by the projects MSM OC08018 and MSM 6840770014.

The authors are with the Department of Electromagnetic Field, Faculty of Electrical Engineering, Czech Technical University in Prague, 16627 Prague, Czech Republic (e-mail: hazdrap@fel.cvut.cz).

Color versions of one or more of the figures in this letter are available online at http://ieeexplore.ieee.org.

Digital Object Identifier 10.1109/LAWP.2011.2158050

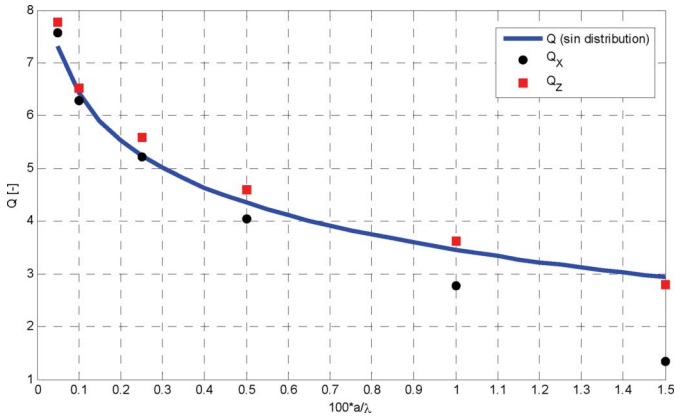

Fig. 1. Q, Q_X, and Q_Z as a function of dipole radius a.

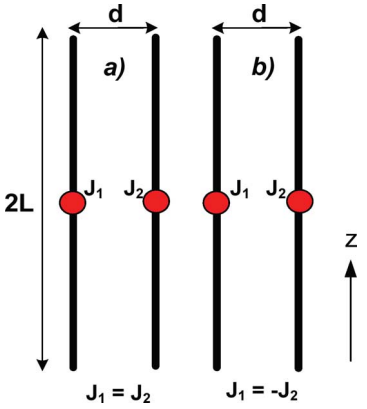

Fig. 2. Side-by-side coupled dipole antennas: *(left)* common mode and *(right)* difference mode. $2L = \lambda/2$.

the input impedance $Z = R + jX$ variation around the resonant frequency ω_0 [8]

$$Q_X = \omega_0 \frac{\frac{\mathrm{dX}(\omega)}{\mathrm{d}\omega}}{2R(\omega_0)} \tag{10}$$

$$Q_Z = \omega_0 \frac{\left|\frac{\mathrm{dZ}(\omega)}{\mathrm{d}\omega}\right|}{2R(\omega_0)}. \tag{11}$$

Relation (10) supposes that the dominant frequency change is due only to the reactance X, while (11) is more accurate (it is actually exact for a lossless RLC circuit; see details in [1] and [8]). However, the reason for evaluating (10) is that its definition is similar to the formulation of the modal radiation Q_n [6]. It is thus interesting to see the difference between Q_Z and Q_X.

It has to be noted that the dipole in FEKO was modeled as a real cylinder meshed with triangular surface mesh consisting of several hundred triangles (depending on radius). The dipole is fed by a voltage gap at the middle segment, and it is assumed that the resultant current distribution will contain mostly the dominant $\lambda/2$ mode. From Fig. 1, it can be seen that the thin-wire approximation is valid, say, up to $a/\lambda \approx 0.005$. As expected, Q_Z gives a better agreement even for thicker dipoles where the variation of their input resistance is not omitted as in (10).

For $a \to 0$, the self-term $\cos(ka)/a$ in (6) and (7) goes to infinity, producing infinite stored electric and magnetic energies, and consequently from (9), $Q \to \infty$.

III. Radiation Q of Mutually Coupled Dipoles

Let us now extend the presented formulation to study the radiation Q-factor of two side-by-side coupled dipoles of the same given radius $a/\lambda = 0.0025$ separated by the distance d (see Fig. 2). Two important feeding scenarios are discussed herein:

a) in-phase currents $J_1 = J_2$ (common, antenna mode);
b) out-of-phase currents $J_1 = -J_2$ (difference, transmission line mode).

These fundamental cases are equivalent to a single horizontal dipole lying $d/2$ above a perfect magnetic (a) and a perfect electric (b) infinite plane, respectively.

Integrals (2) and (5)–(7) are now expanded to include the interaction between these two dipole antennas of interest

$$P_{\mathrm{r}}{}' = \left(\frac{1}{8\pi\omega\varepsilon}\right)\int_{-L}^{L}\int_{-L}^{L}\left[k^2 J_1(z)\,J_2(z') - \nabla\cdot J_1(z)\,\nabla\cdot J_2(z')\right]\frac{\sin(kr_{12})}{r_{12}}dzdz' \tag{12}$$

$$I_{\mathrm{R}}{}' = \frac{k}{2}\int_{-L}^{L}\int_{-L}^{L}\left[k^2 J_1(z)\,J_2(z') - \nabla\cdot J_1(z)\,\nabla\cdot J_2(z')\right]\sin(kr_{12})\,dzdz' \tag{13}$$

$$I_{\mathrm{e}}{}' = \int_{-L}^{L}\int_{-L}^{L}\nabla\cdot J_1(z)\,\nabla\cdot J_2(z')\frac{\cos(kr_{12})}{r_{12}}\,dzdz' \tag{14}$$

$$I_{\mathrm{m}}{}' = k^2\int_{-L}^{L}\int_{-L}^{L}J_1(z)\,J_2(z')\frac{\cos(kr_{12})}{r_{12}}\,dzdz' \tag{15}$$

where the distance r_{12} is now

$$r_{12} = \sqrt{(z-z')^2 + a^2 + d^2}. \tag{16}$$

Because of symmetry, the radiated power of such an antenna arrangement P_{rsystem} may be expressed as

$$P_{\mathrm{rsystem}} = P_{\mathrm{r}} + P_{\mathrm{r}}{}'. \tag{17}$$

Similarly, stored energies are

$$\widetilde{W}_{\mathrm{e}}' = \frac{1}{16\pi\omega^2\varepsilon}\left(I_{\mathrm{e}}{}' - I_{\mathrm{R}}{}'\right) \tag{18}$$

$$\widetilde{W}_{\mathrm{m}}' = \frac{1}{16\pi\omega^2\varepsilon}\left(I_{\mathrm{m}}{}' - I_{\mathrm{R}}{}'\right) \tag{19}$$

and

$$\widetilde{W}_{\mathrm{esystem}} = W_{\mathrm{e}} + W_{\mathrm{e}}{}' \tag{20}$$

$$\widetilde{W}_{\mathrm{msystem}} = W_{\mathrm{m}} + W_{\mathrm{m}}{}'. \tag{21}$$

Primed quantities represent mutual radiated power and mutual energies that have similar meanings as mutual resistance and reactance.

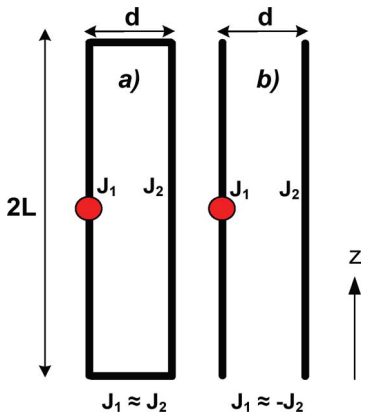

Fig. 3. *(left)* Folded dipole and *(right)* active and parasitic dipole. $2L = \lambda/2$.

Therefore, the radiation Q-factor is now evaluated as

$$Q = \frac{2\omega \max\left(\widetilde{W}_{\mathrm{e}}, \widetilde{W}_{\mathrm{m}}\right)}{P_{\mathrm{r}} + P'_{\mathrm{r}}} + \frac{2\omega \max\left(\widetilde{W}'_{\mathrm{e}}, \widetilde{W}'_{\mathrm{m}}\right)}{P_{\mathrm{r}} + P'_{\mathrm{r}}}. \tag{22}$$

For both in-phase and out-of-phase currents, a $2L = \lambda/2$ fundamental resonance is considered. The exact "sinusoidal" radiation Q-factor is compared to Q_Z and Q_X obtained from FEKO as a function of separation distance d/λ. Both dipoles in FEKO are active and simultaneously fed by a voltage gap.

However, in many cases there is only one active dipole as, for example, in a folded dipole [5] or in a system consisting of active and parasitic (shorted) dipole antenna. This forms the main building block for many antennas widely used in practice, like the Yagi–Uda [5]. These important scenarios have been also treated (see Fig. 3), yet some restrictions apply here and will be discussed later.

For a folded dipole with sufficient conductor coupling (i.e., for $d \ll 0.05\lambda$, [5]), the dipole mode currents are equal and in phase in the left and right conductors. Hence, we may use the situation in a) of Fig. 2. The later case is shown in b) of Fig. 3, i.e., it can be viewed as a "disconnected" folded antenna. When the parasitic dipole is very close to the active one, we may approximate its currents as out of phase [9], [10].

A. In-Phase Currents

The results for $J_1 = J_2$ are shown in Fig. 4.

It is interesting to note that Q is an oscillating function, but it has a clear absolute minimum for $d = 0.18\lambda$.

Results for a folded dipole (Q_Z from FEKO) are in very good agreement with the presented method for close separations ($d < 0.1\lambda$). Obviously, they start to deteriorate for bigger separations where the structure presents behavior more like a loop antenna.

B. Out-of-Phase Currents

When $J_1 = -J_2$, the radiated power P_{rsystem} [the denominator of (22)] goes to 0 for $d \to 0$ as expected (currents on both dipole antennas are canceling each other); this results in a high Q for very close separations (Fig. 5).

Again, Q reaches an absolute minimal value for a specific separation distance, in this case for $d = 0.72\lambda$. It is interesting to note that this value is equal to four times the "in-phase" minimum 0.18λ (Fig. 4).

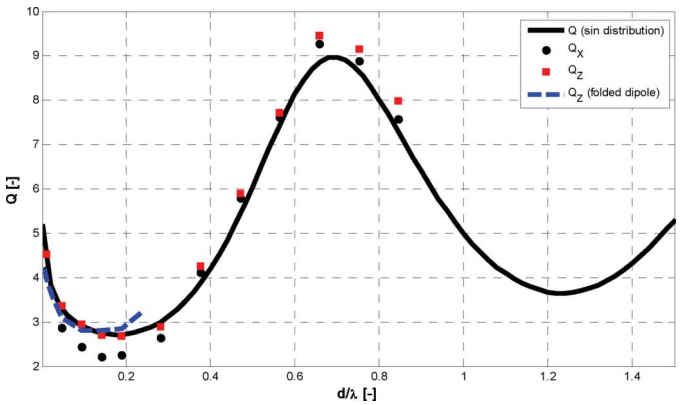

Fig. 4. Q, Q_X, and Q_Z for in-phase fed dipoles of distance d.

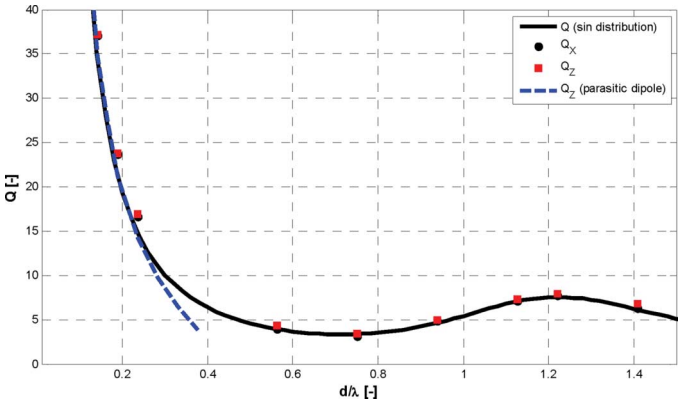

Fig. 5. Q, Q_X, and Q_Z for out-of-phase fed dipoles of distance d.

Among other authors, a similar dependence of the Q for dipoles with difference mode has already been evaluated (e.g., in [11]), but due to the graph's scale used, the discussed minimum remained unnoticed.

Following [10, Section 11-9a], it is found that for close distances, the out-of-phase mode is dominant. Assuming this, the system from b) in Fig. 3 can be treated as the original situation depicted in b) of Fig. 2. As the distance further increases ($d > 0.2\lambda$), the induced current on the second dipole tends to decrease (along with phase changes), and the results start to deteriorate (Fig. 5).

C. Input Impedance for Optimum Spacing

The input impedance for optimally spaced dipoles under simultaneous excitation (both the in- and out-of-phase configurations) is shown in Fig. 6. The impedance of a single dipole Z_{11} is shown for reference. For completeness, the input impedance Z_{in} at any port of the studied two-dipole system is given by [10, Section 11-2a]

$$Z_{\mathrm{in}} = Z_{11} \pm Z_{12} \tag{23}$$

where Z_{11} and Z_{12} are the self- and mutual impedances, respectively. The $+$ sign is for in-phase, while the $-$ sign is for out-of-phase excitation.

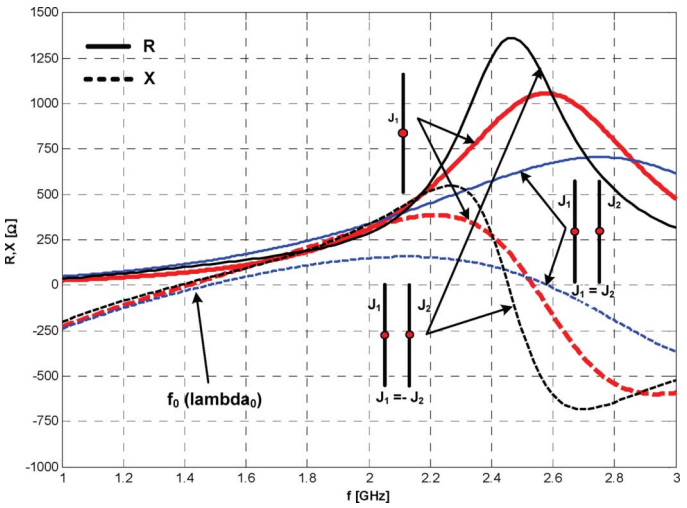

Fig. 6. Input impedance for reference dipole in free space and for two simultaneously fed dipoles with optimum spacing, calculated by FEKO.

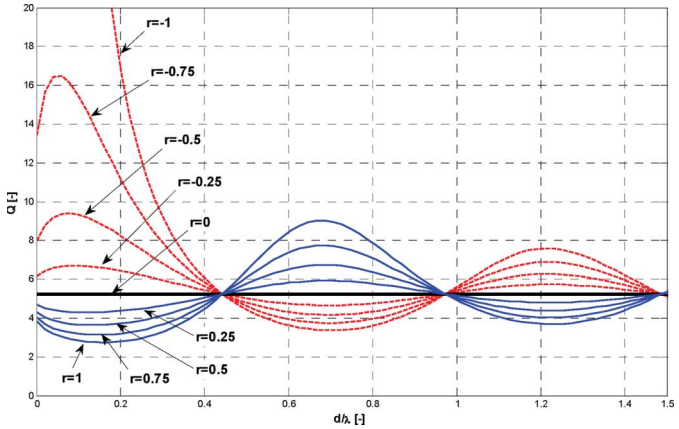

Fig. 7. Q as a function of d for different real currents on the second dipole.

It is seen that the impedance of the dual system has less steep behavior. Note that the resonant frequency changes slightly for different feeding cases due to mutual interaction.

D. Generalization for Arbitrary Real Currents

The presented method could be further generalized by taking into account an arbitrary real current on the second antenna (the procedure is not yet implemented for mutually complex distributions). Let us write

$$J_2 = r \cdot J_1 \tag{24}$$

where r gather values from interval $\langle -1, 1\rangle$. Particular quantities $r = -1$, $r = 0$, and $r = +1$ now represent a dipole $d/2$ above an infinite perfect electric ground, a dipole in free space, and a dipole $d/2$ above an infinite perfect magnetic ground, respectively (see Fig. 7.)

Detailed numerical analysis of (22) reveals that minimum of Q for the out-of-phase configuration is not very sensitive to actual current distribution and even to the length of dipoles or frequency. Moreover, the first part of (22) forms the dominant contribution to the overall out-of-phase Q. Therefore, an approximate analytical solution is available by considering elementary dipoles with constant currents (no integration is needed).

It is then found that the behavior of the out-of-phase Q in terms of separation distance $d \gg a$ is led by the function

$$f(d) \cong \frac{d}{kd - \sin(kd)}. \tag{25}$$

After deriving (25), the condition worked out is

$$\tan(kd) = kd. \tag{26}$$

The first nontrivial root of (26) could be approximated as [12]

$$\left(\frac{d}{\lambda}\right)_{\text{opt.}} \cong \frac{3}{4} - \frac{1}{3\pi^2} \cong 0.716. \tag{27}$$

This result is very close to the value 0.72 numerically obtained for sinusoidal currents.

Unfortunately, the in-phase situation is a much harder task to handle because the related minimum depends significantly on the dipole's length.

However, further attempts may be made to find specific separation values where the overall system Q is equal to the Q of a single dipole (denoted as a thick black horizontal line of value 5.2 in Fig. 7). It is interesting to note that these particular separations are the same regardless of current amplitudes.

Taking only the first (dominant) term of (22) for elementary out-of-phase currents, the condition is $P_{\text{r}}' = 0$, and hence from (12), we see for $d \gg a$ that

$$\sin(kd) = d \tag{28}$$

which has roots

$$\frac{d_n}{\lambda} = \frac{n}{2}, \qquad \text{n} = 1, 2, 3, \ldots. \tag{29}$$

For comparison, the first few values of d_n/λ for sinusoidal distributions are 0.44, 0.97, 1.49, see Fig. 7.

IV. Conclusion

Theoretical sinusoidal current distribution has been used to analyze the radiation Q-factors of a coupled dipole antenna system with different feeding configurations. Good agreement between the proposed "thin-wire" method based on rigorous Vandenbosch equations and FEKO full-wave simulation has been observed. The expressions are used for the first time in the case of a structure consisting of several (in this case, two) elements. Also, the simple Q_Z formula has been proven to produce satisfactory results, even for a mutually coupled system. Only real currents have been employed so far; mutually complex distributions will be addressed in future work.

It is interesting that all the excitation scenarios present minimum Q for a specific dipole separation distance. Since analytical derivation of the related distance d for sinusoidal currents would be quite tedious, only numerical results have been presented so far for this distribution. However, an approximate analytical solution has been found for elementary dipoles

with out-of-phase feeding. Because the main contribution to the overall Q for this case lies in canceling radiated power, the obtained distance d does not differ much from the original sinusoidal currents.

It can be concluded that the in-phase configuration (i.e., antenna mode) presents the lowest radiation Q from all the studied combinations of the two side-by-side coupled dipoles.

The presented formulation could also be easily extended to 2-D surfaces with prescribed current distributions. However, special care should be taken in evaluation of the self-term contribution. This work is currently in progress, and it seems that a rectangular microstrip patch antenna with the fundamental TM_{01} mode obeys similar behavior, i.e., a minimum of the radiation Q occurring for a height above infinite ground $H \approx d/2 = 0.36\lambda$

Further work is aimed at analyzing more complex 2-D geometries based on triangular Rao–Wilton–Glisson (RWG) mesh. This would allow us to optimize advanced wire and microstrip patch antennas (their shape, current mode, height above ground, etc.) for maximum bandwidth.

ACKNOWLEDGMENT

The authors would like to thank N. Bell and M. Vavrincova for their comments. P. Hazdra would like to thank Prof. G. Vandenbosch and Prof. C. Luxey for valuable discussions. The authors also thank the three anonymous reviewers who suggested some valuable improvements to the letter.

REFERENCES

[1] G. A. E. Vandenbosch, "Reactive energies, impedance, and Q factor of radiating structures," *IEEE Trans. Antennas Propag.*, vol. 58, no. 4, pp. 1112–1127, Apr. 2010.

[2] G. A. E. Vandenbosch and V. Volski, "Lower bounds for radiation Q of very small antennas of arbitrary topology," in *Proc. EUCAP*, Barcelona, Spain, 2010, pp. 1–4.

[3] R. F. Harrington, "Matrix methods for field problems," *Proc. IEEE*, vol. 55, no. 2, pp. 136–149, Feb. 1967.

[4] P. J. Papakanellos *et al.*, "On the oscillations appearing in numerical solutions of solvable and nonsolvable integral equations for thin-wire antennas," *IEEE Trans. Antennas Propag.*, vol. 58, no. 5, pp. 1635–1644, May 2010.

[5] C. A. Balanis, *Antenna Theory: Analysis and Design*, 3rd ed. New York: Wiley, 2005, sec. 8.3, 8.5.2.

[6] R. Harrington, *Field Calculation by the Method of Moments*. New York: IEEE Press, 1993.

[7] FEKO. ver. 5.4, EM Software & Systems-S.A. (Pty) Ltd., Stellenbosch, South Africa, Jun. 2011 [Online]. Available: http://www.feko.info

[8] A. D. Yaghjian and S. R. Best, "Impedance, bandwidth, and Q of antennas," *IEEE Trans. Antennas Propag.*, vol. 53, no. 4, pp. 1298–1324, Apr. 2005.

[9] D. Jefferies and K. McDonald, "Can an antenna be cut into pieces without affecting its radiation?," Nov. 2004 [Online]. Available: http://physics.princeton.edu/~mcdonald/examples/cutantenna.pdf

[10] J. D. Kraus, *Antennas*, 2nd ed. New York: McGraw-Hill, 1988.

[11] S. R. Best, "Improving the performance properties of a dipole element closely spaced to a PEC ground plane," *IEEE Antennas Wireless Propag. Lett.*, vol. 3, pp. 359–363, 2004.

[12] "Tanc function," Jun. 2011 [Online]. Available: http://mathworld.wolfram.com/TancFunction.html

XV

M. Capek, P. Hazdra, and M. Masek, "On some theoretical and numerical aspects of characteristic mode decomposition," 2015, submitted, arXiv: 1509.02825. [45∗]

On Some Theoretical and Numerical Aspects of Characteristic Mode Decomposition

Miloslav Capek, *Member, IEEE,* Pavel Hazdra, *Member, IEEE,* and Michal Masek, *Student Member, IEEE*

***Abstract*—Aspects of the theory of characteristic modes, based on its variational formulation, are presented and an explicit form of a related functional, involving only currents in a spatial domain, is derived. The new formulation leads to deeper insight into the modal behavior of radiating structures as demonstrated on a detailed analysis of few canonical structures: a dipole, an array of two dipoles and a loop. Important numerical aspects related to modal superposition and the residual ("evanescent") mode are also considered. It is shown that due to numerical issues, certain modes may actually exhibit incorrect (negative) radiated power, which, in turn, destabilize the solution of the generalized eigenvalue problem. A simple solution, based on splitting the superposition into two parts, is proposed.**

***Index Terms*—Antenna theory, eigenvalues and eigenfunctions, electromagnetic theory.**

I. Introduction

THE theory of characteristic modes (CMs), formally developed by Garbacz [1] and Harrington and Mautz [2], become very popular in recent years as this theory constitutes a general approach to characterizing the modal resonant behavior of arbitrarily shaped antennas and scaterrers. . In its original form, which is considered here, the CM assumes perfectly conducting electric conductors (PEC) in vacuum. Academic interest and professional publications dealing with the CM continue to grow. However, most journals focus only on the application character, such as [3]–[5]. Excluding the first attempt to summarize CMs in a book [6], there are also related chapters to be found in older books [7] and [8].

This paper briefly reviews characteristic mode decomposition and what constitutes the necessary theoretical background. An analytical form of the functional, composed from reactive and radiated power, is derived, based on previous research [9], [10]. This relation has to be satisfied for each mode but is not restricted to the characteristic basis. Hence, it is possible to specify arbitrary current distribution (the CM can be predicted, see [11]) and compare it with real characteristic modes. Based on this result, properties of canonical shapes are investigated, including inductive non-radiating modes. The second part of the paper focuses on modal superposition and, consequently, the so-called "evanescent mode", which emerges from subtracting the method of moments and modal current, is studied and eliminated indicating the cause is due to ill-conditioned generalized eigenvalue problem.

Manuscript received July 19, 2011; revised January 11, 2011. This work was supported by the project of the Czech Science Foundation, grant No. P102/12/2223 and by the TA04010457.

The authors are with the Department of Electromagnetic Field, Faculty of Electrical Engineering, Czech Technical University in Prague, Technicka 2, 16627, Prague, Czech Republic (e-mail: miloslav.capek@fel.cvut.cz).

II. Derivation of the functional

Based on previous work by Garbacz [1], Harrington [2] reduced the CM into the following generalized eigenvalue problem (GEP, [12])

$$\boldsymbol{X}\boldsymbol{J}_n = \lambda_n \boldsymbol{R}\boldsymbol{J}_n, \tag{1}$$

where $\boldsymbol{R}$ and $\boldsymbol{X}$ are real and symmetric operators forming the impedance operator $\boldsymbol{Z} = \boldsymbol{R} + j\boldsymbol{X}$. This continuous operator is usually discretized by the method of moments (MoM, [13]) to become an impedance matrix $\mathbf{Z}$.

The solution of the GEP produces the characteristic basis of eigencurrents $\{\boldsymbol{J}_n\}$ and associated eigenvalues λ_n and, due to the properties of the impedance matrix, all eigenvalues are real with all eigencurrents equiphasal (they can also be selected as real, [14]). Furthermore, the CMs (1) simultaneously maximise radiated power while minimising net reactive power. Note that the extremal value of radiated to stored power is considered for the basis as a whole. Despite (1) appearing quite simple, we show that there are many theoretical, as well as numerical issues that have to be considered.

It is known [6] that the GEP (1) minimizes an power functional[1]

$$\mathcal{F}\left(\boldsymbol{J}_n\right) = \frac{\langle \boldsymbol{J}_n, \boldsymbol{X}\boldsymbol{J}_n\rangle}{\langle \boldsymbol{J}_n, \boldsymbol{R}\boldsymbol{J}_n\rangle} = \frac{2\omega(W_{\mathrm{m}}^n - W_{\mathrm{e}}^n)}{P_{\mathrm{r}}^n} = \lambda_n, \tag{2}$$

where W_{m}^n and W_{e}^n are modal magnetic and electric energies, $2\omega(W_{\mathrm{m}}^n - W_{\mathrm{e}}^n)$ is reactive power of mode n and P_{r}^n is modal radiated power. A particular form of the above functional, defined directly for the sources (currents/charges) on the antenna, is derived using [9], [10]. Recalling expressions from [9] for radiated and reactive powers, obtained from electric field integral equation and complex power balance [15], which read

$$\mathcal{F}\left(\boldsymbol{J}_n\right) = \frac{\langle \boldsymbol{J}_n, \boldsymbol{X}\boldsymbol{J}_n\rangle}{\langle \boldsymbol{J}_n, \boldsymbol{R}\boldsymbol{J}_n\rangle} = -\frac{\Re\displaystyle\int_V (\boldsymbol{A}\cdot\boldsymbol{J}_n^* - \phi\rho_n^*)\,\mathrm{d}V}{\Im\displaystyle\int_V (\boldsymbol{A}\cdot\boldsymbol{J}_n^* - \phi\rho_n^*)\,\mathrm{d}V}, \tag{3}$$

where ρ and $\boldsymbol{J}$ are the charge and current densities and $\boldsymbol{A}$ and ϕ are magnetic and electric time-harmonic potentials respectively. Inserting the continuity equation [16], $\rho = -\nabla\cdot\boldsymbol{J}/\jmath\omega$, the functional has the following form which involve only currents

[1]Through this paper, the following notation is used $\langle \boldsymbol{f}, \boldsymbol{g}\rangle = \int_\Omega \boldsymbol{f}\cdot\boldsymbol{g}^*\mathrm{d}\Omega$ and $\langle \boldsymbol{f}, \boldsymbol{g}\rangle_{\mathrm{r}} = \int_\Omega \boldsymbol{f}\cdot\boldsymbol{g}\mathrm{d}\Omega$.

$$\mathcal{F}(\boldsymbol{J}_n) = \frac{\displaystyle\iint_{\Omega\,\Omega'} \mathcal{J}(\boldsymbol{J}_n)\frac{\cos(kR)}{R}\,\mathrm{d}\boldsymbol{r}'\,\mathrm{d}\boldsymbol{r}}{\displaystyle\iint_{\Omega\,\Omega'} \mathcal{J}(\boldsymbol{J}_n)\frac{\sin(kR)}{R}\,\mathrm{d}\boldsymbol{r}'\,\mathrm{d}\boldsymbol{r}}, \tag{4}$$

where $\mathcal{J}(\boldsymbol{J}_n) = \big(k^2\boldsymbol{J}_n(\boldsymbol{r})\cdot\boldsymbol{J}_n^*(\boldsymbol{r}') - \nabla\cdot\boldsymbol{J}_n(\boldsymbol{r})\nabla'\cdot\boldsymbol{J}_n^*(\boldsymbol{r}')\big)$, $R = |\boldsymbol{r}-\boldsymbol{r}'|$ is Euclidean distance, k is wavenumber and κ_n is Rayleigh quotient [17], which is equal to characteristic number λ_n if the true characteristic current $\boldsymbol{J}_n$ enters into (4)[2]. This functional is intimately connected with the characteristic modes, as they minimise its value. Thanks to the "source" formulation, arbitrary defined current distribution on defined geometry are studied and their properties with true CMs are compared. This formulation extends the understanding of the original definition in [2]. It is usual to normalize the radiated power for each mode so that $P_n^{\mathrm{r}} = 1$ W. From (4) we see, then, reactive power equals κ, being zero at resonance.

It is important to stress that the functional is minimised by characteristic currents, i.e. solutions of (1). Such a (eigen) basis maximises the radiated power and minimises the stored power, representing external resonances of the radiator. Hence, the extremum of (4) is given by characteristic basis $\{\boldsymbol{J}_n\}$ with associated eigenvalues λ_n.

As pointed out by Harrington [20], the frequency sensitivity

$$\frac{\omega}{\langle\boldsymbol{J},\boldsymbol{R}\boldsymbol{J}\rangle}\frac{\partial}{\partial\omega}\langle\boldsymbol{J},\boldsymbol{X}\boldsymbol{J}\rangle \tag{5}$$

is related to quality factor of the system if the input current is held constant. By performing the derivation in (5) analytically, we show in [10] that it is indeed true and the result is equal to the impedance quality factor Q_X [21]. For very special current distributions (modal currents in separable systems [22]), closed-form expressions for Q_X and Q_Z can be obtained, see [23].

An exact analytical solution for characteristic currents is exceedingly complicated. However, the expression (4) permits the definition of an arbitrary current distribution $\widetilde{\boldsymbol{J}}$ without the necessity of numerically computing the impedance matrix $\mathbf{Z}$ in (1). In addition, if we analytically try to test a basis $\widetilde{\boldsymbol{J}}$ that is similar to the true CM basis, we can exactly analyse its behaviour and estimate, how close the selected current distribution is to the optimal solution.

III. Elementary Radiators – Case Studies

This section demonstrates why the functional (4) is of interest. In certain (simple) cases the CM basis can be sufficiently approximated by analytical currents. We inspect three canonical examples:

- a thin-wire dipole,
- two parallel coupled dipoles, separated by distance h with in-phase and out-of-phase modes,
- a loop with static mode.

[2]In the nominator, the net reactive power may be further splitted into its "current" and "charge" parts to express the modified magnetic and electric energies separately. For more details see [18], [9], [19]

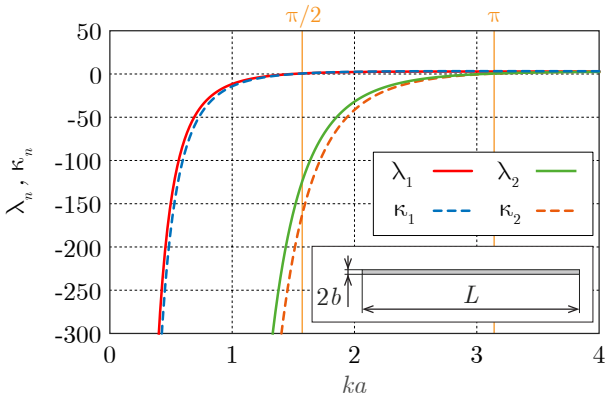

Fig. 1. The radiation quotients κ_n for the first two natural modes of a thin dipole ($L/b = 1\cdot 10^6$) compared to CM eigenvalues λ_n from FEKO. Resonance of mode 1 and mode 2 occur for $ka \cong \pi/2$ and $ka \cong \pi$ respectively.

These examples establish a direct way to understand the stationary inductive modes. It will be seen that those are fulfilling $\nabla\cdot\boldsymbol{J}(\boldsymbol{r}) = 0$, i.e. they have no charge.

A. Thin-wire dipole

Consider thin-wire dipole of length L and radius $b << L$. No inductive modes are possible since the dipole is thin and the current has to fulfill the Dirichlet boundary condition at its ends. It is significant that the choice of any mode from the basis predestinates the basis, as a whole, as the modes are orthogonal. We consider the natural one dimensional first-order current basis[3]

$$\widetilde{\boldsymbol{J}}_n(z) = \mathbf{z}_0 I_0\delta(x)\delta(y)\sin\left(\frac{\pi n z}{L}\right), \quad z\in(0,L), \tag{6}$$

where input current $I_0 = 1$A is assumed. The corresponding charge is

$$\frac{\mathrm{d}\widetilde{\boldsymbol{J}}_n(z)}{\mathrm{d}z} = \delta(x)\delta(y)\frac{I_0\pi n}{L}\cos\left(\frac{\pi n z}{L}\right). \tag{7}$$

Due to complexity, (6) and (7) were inserted in (4) and solved numerically in MATLAB. First two modes ($n = 1$ and $n = 2$) are considered. Fig. 1 shows the κ_n quotients, together with exact eigenvalues λ_n, obtained by solving (1) in FEKO software [24]. A good match is attained, even for such simple basis (6).

It can be seen from Fig. 2 that the agreement between CM current and its approximation is sufficient, especially for the dominant mode. The analytical current in (6) is, in fact, exact for non-radiating 1D resonator, while, in turn, the real CMs maximises radiation and, thus, the shape slightly deviates from the basis (6).

B. Two thin-wire dipoles

The next scenario involves two closely spaced collinear dipoles with length L, separation $h = L/50$ and radius of

[3]The tilde in $\widetilde{\boldsymbol{J}}_n(z)$ express that we insert approximate current, since exact form of the mode is not known.

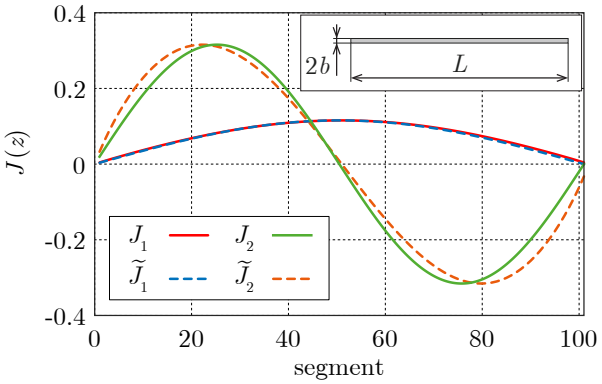

Fig. 2. Comparison of characteristic modes and analytical current distribution (6) for first two modes at resonance on a thin-wire dipole.

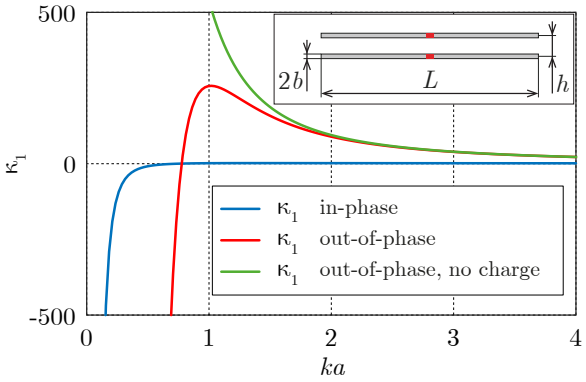

Fig. 3. The radiation quotients κ for in-phase, out-of-phase, and testing mode with no charge ($\nabla \cdot \mathbf{J} = 0$) of two closely spaced thin wire ($L/b = 500$) dipoles.

$b = L/500$. There are, depending on the actual orientation of currents, two possible basic modes: in-phase and out-of phase. Currents are considered in the form of fundamental distribution $\widetilde{\boldsymbol{J}}_1$ from (6).

For in-phase mode [25], the course of κ quotient (solid blue line at Fig. 3) is similar to that of the dominant mode on a single dipole. It radiates well and the two in-phase currents may be interpreted as one, flowing along thicker dipole in a manner similar to folded dipole.

This is not the case for the out-of-phase mode, where the radiated power is much lower. Consequently, the red line in Fig. 3 shows extremely steep resonance of this mode. Other properties, especially those regarding the radiated Q factors, have been discussed in [26] and analytically treated in [27].

Using (4), it is possible to investigate the hypothetical situation where the currents on the dipoles are out-of-phase but with the charge density eliminated ($\nabla \cdot \mathbf{J} = 0$). It strongly resembles the situation where the ends of the dipoles are connected and form a loop. The green line in Fig. 3 reveals that this mode does not resonate because the "charge" part in (4) is missing and the mode, thus, exhibits pure inductive character. In the next section we show that this behaviour is similar to the uniform zero-order mode on a loop.

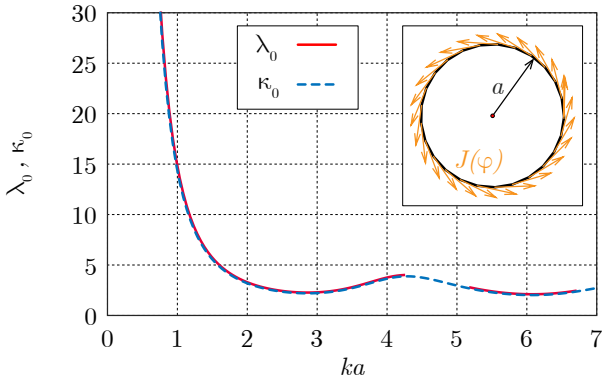

Fig. 4. The radiation quotient κ_0 for static mode of loop. Comparison with CM eigenvalue λ_0 from FEKO is also shown. Due to issues with sorting, some data from FEKO are missing.

C. A loop

A loop is an elementary radiator on which the uniform (also termed static or inductive) mode with $\nabla \cdot \widetilde{\boldsymbol{J}}_0 = 0$ exists and its behavior is similar to the modified out-of-phase mode previously analysed. Current distribution on a thin loop is expressed in cylindrical coordinates (r,φ,z) as

$$\widetilde{\boldsymbol{J}}_0(\varphi) = \boldsymbol{\varphi}_0 I_0 \delta(r)\delta(z), \tag{8}$$

which simplifies (4) to

$$\kappa_0(ka) = \frac{\displaystyle\int_0^{2\pi}\int_0^{2\pi} \cos(\varphi-\varphi') \frac{\cos\left(ka|\varphi-\varphi'|\right)}{a|\varphi-\varphi'|}\,\mathrm{d}\varphi\,\mathrm{d}\varphi'}{\displaystyle\int_0^{2\pi}\int_0^{2\pi} \cos(\varphi-\varphi') \frac{\sin\left(ka|\varphi-\varphi'|\right)}{a|\varphi-\varphi'|}\,\mathrm{d}\varphi\,\mathrm{d}\varphi'}. \tag{9}$$

The pure inductive character ($\kappa_0 > 0$) can be clearly seen in Fig. 4. The agreement between (9) and λ_0 obtained by FEKO is perfect as the current is uniquely defined and does not change with frequency.

Uniform modes does not contribute to farfield, but they are important when evaluation of near field, input impedance and stored energies. It can be also shown that these non-radiating modes are required to complete the orthogonal basis to fulfil boundary conditions and the equation of continuity.

IV. Modal Superposition

The second part of this paper addresses numerical issues related to the superposition of modes which occur when the excitation is connected. It is well known (see e.g. [2]) that the total current has the form of linear superposition

$$\mathbf{J}_{\mathrm{CM}} = \sum_n \gamma_n \mathbf{J}_n, \tag{10}$$

in which the expansion coefficients γ_n are

$$\gamma_n = \frac{\langle \mathbf{J}_n, \mathbf{E}^{\mathrm{i}} \rangle_{\mathrm{r}}}{1 + \jmath\lambda_n}, \tag{11}$$

where $\mathbf{E}^{\mathrm{i}}$ is incident electric field representing excitation of the structure in the form of plane wave or localized source. The product of (10) with $\mathbf{E}^{\mathrm{i}}$ is now taken in order to get complex power of total current expressed by its modal components. Interchanging the summation and integration after a little manipulation results in

$$P_{\mathrm{r}} + \jmath 2\omega(W_{\mathrm{m}} - W_{\mathrm{e}}) = \sum_n |\gamma_n|^2(1 + \jmath\lambda_n), \qquad (12)$$

in which the real and imaginary are

$$P_{\mathrm{r}} \quad = \sum_n |\gamma_n|^2 \quad = \sum_n P_{\mathrm{r}}^n, \qquad (13)$$

$$2\omega(W_{\mathrm{m}} - W_{\mathrm{e}}) \quad = \sum_n |\gamma_n|^2\lambda_n \quad = \sum_n 2\omega(W_{\mathrm{m}}^n - W_{\mathrm{e}}^n). \qquad (14)$$

The above relations can be used to calculate (modal) radiation Q and (modal) radiation efficiency [28]. For these purposes, the $\boldsymbol{\beta}$ matrix, connecting modes with excitation, has been derived in [26] as

$$\beta_{m,n} = \frac{\langle \mathbf{J}_m, \mathbf{E}^{\mathrm{i}} \rangle \langle \mathbf{J}_n, \mathbf{E}^{\mathrm{i}} \rangle (1 + \lambda_{\mathrm{m}}\lambda_n)}{(1 + \lambda_m^2)(1 + \lambda_n^2)}, \qquad (15)$$

where $m, n \in \{1, \ldots, N\}$. The coupling matrix (15) is real and symmetric. According to [2], it can be shown that the currents are orthogonal with respect to radiated P_{r}^n and net stored powers $2\omega(W_{\mathrm{m}}^n - W_{\mathrm{e}}^n)$. Hence, the total radiation power can be computed easily as the trace of the $\boldsymbol{\beta}$ matrix. On the other hand, the separate modified modal energies W_{m}^n, W_{e}^n of which the reactive power is formed, are not orthogonal. The same apply for their sum $W_{\mathrm{m}}^n + W_{\mathrm{e}}^n$, which arise as a dominant contribution from the evaluation of $\langle \mathbf{J}, \mathbf{X}'\mathbf{J} \rangle$ [10].

A. Residual Mode

It has been recognized in [29] that there are deeper aspects hidden in superposition (10), leading to slowly convergent solutions. If the impedance matrix is decomposed into n modes, excitation is applied and all the modes are summed using (10), the result is different compared to MoM solution. A residual current appears

$$\mathbf{J}_{\mathrm{res}} = \mathbf{J}_{\mathrm{MoM}} - \mathbf{J}_{\mathrm{CM}} = \mathbf{Z}^{-1}\mathbf{E}^{\mathrm{i}} - \sum_n \gamma_n \mathbf{J}_n, \qquad (16)$$

which has been linked in [29] to the evanescent, travelling wave mode of source. However, the nature of the residual current is different and is addressed to the ill-conditioned GEP decomposition, together with the limited numerical dynamic, as will be shown later in this section.

To demonstrate the problem clearly, a simple thin-wire Galerkin MoM, according to [13], was implemented for this purpose. This method generates perfectly symmetrical matrices $\mathbf{R}$ and $\mathbf{X}$. Consider thin-wire dipoles of length $\lambda/2$ and 5λ, discretized to $N = 101$ elements. An $(N \times N)$ impedance matrix is constructed and a voltage gap [15] with one volt across it, is connected to the dipoles.

The residual current arising from obtaining the difference between the MoM solution and the CM summation of all 101 characteristic modes is depicted in Fig. 5 and Fig. 6 for dipoles of length $\lambda/2$ and 5λ respectively. It will be later proved that the imaginary part of the residual current is dominant.

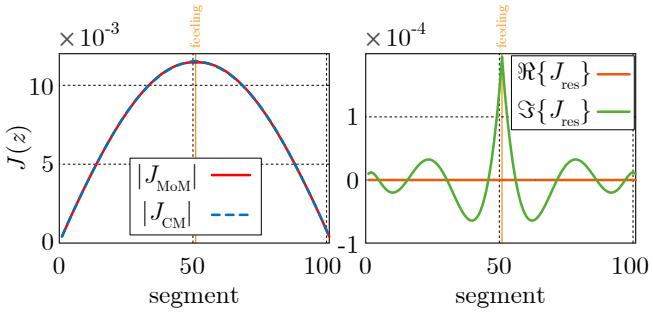

Fig. 5. Absolute values of $\mathbf{J}_{\mathrm{MoM}}$ and $\mathbf{J}_{\mathrm{CM}}$ for $\lambda/2$ dipole fed at middle (left) and real and imaginary parts of the residual current (right).

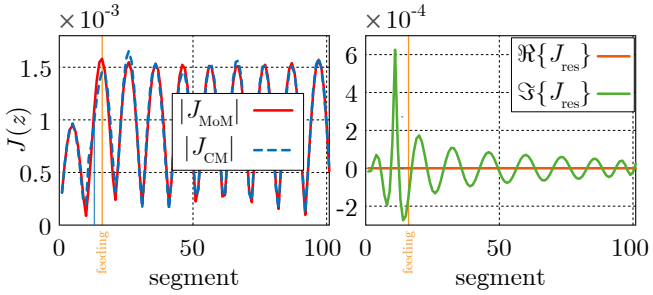

Fig. 6. Absolute values of $\mathbf{J}_{\mathrm{MoM}}$ and $\mathbf{J}_{\mathrm{CM}}$ for 5λ dipole fed $1/10$ of its length (left) and real and imaginary parts of the residual current (right).

B. On the indefiniteness of modal radiated power

For obvious reasons, radiated power is assumed to be non-negative. Hence $\mathbf{R}$ has to be a semi-definite operator. A the key question arises at this point: Does this presumption hold *for all modes* in discretized basis $\{\mathbf{J}_n\}$? It will be shown that – from the numerical point of view – the *answer is no*.

To support this statement, we calculate separately the $\langle \mathbf{J}_n, \mathbf{X}\mathbf{J}_n \rangle$ and $\langle \mathbf{J}_n, \mathbf{R}\mathbf{J}_n \rangle$ parts of (2) for the same $\lambda/2$ dipole as studied previously. The results are shown in Fig. 7. It is clearly observable that all modes $n > 6$ exhibit a small amount of negative power (depicted by the green line). In other words, the operator $\mathbf{R}$ is, in practice, indefinite for all modes $n > 6$. This problem was mentioned earlier in [14] but the summation (10) has not changed accordingly.

The residual mode issue may also be studied by a singular value decomposition (SVD, [30]) of the real part of the impedance matrix $\mathbf{Z}$

$$\mathbf{R} = \mathbf{U}\xi_n\mathbf{V}^{\mathrm{T}}. \qquad (17)$$

By definition, all singular values ξ_n are non-negative. If we suppose that $\mathbf{R}$ is real, symmetric and positive semi-definite, the unitary matrices $\mathbf{U}$ and $\mathbf{V}$ are equal and the singular values ξ are the exact (positive) eigenvalues of $\mathbf{R}$.

To confirm this premise, the SVD of both parts of the impedance matrix $\mathbf{X}$ and $\mathbf{R}$ has been performed. The singular values are depicted at Fig. 8 at the resonant frequency of the dominant mode. It is clear that the imaginary part $\mathbf{X}$ is numerically well-conditioned but real part $\mathbf{R}$ contains some strongly dominant solutions that radiates well while the others

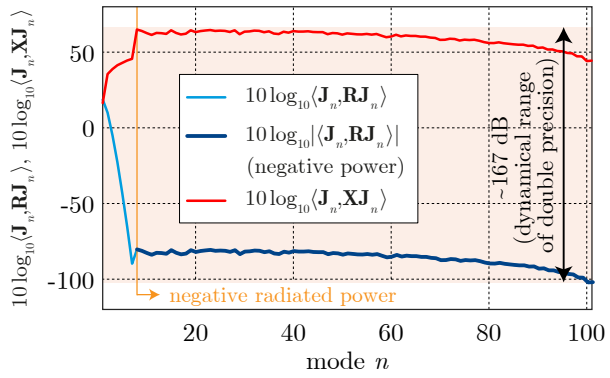

Fig. 7. Numerator and denominator of (2) for $\lambda/2$ dipole fed at middle. The radiated power $\langle \boldsymbol{J}_n, \boldsymbol{RJ}_n\rangle$ is positive only for first few modes.

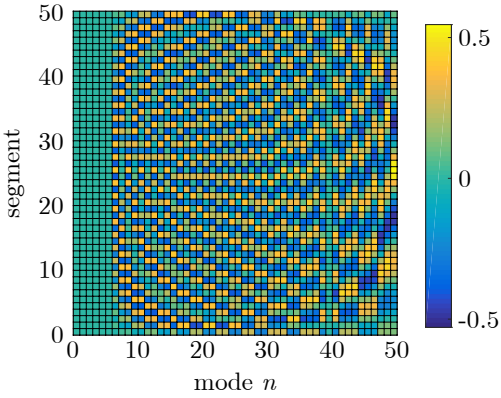

Fig. 9. The difference $\mathbf{D} = \mathbf{U} - \mathbf{V}$, based on (17) for $\lambda/2$ dipole at the resonant frequency of the dominant mode.

are ill-conditioned. This is an inherent property of the CM decomposition. As $\mathbf{R}$ serves as the weighting operator in the CM formulation (1), all difficulties mentioned are transferred to the GEP solution. These problems can be attributed to the scaling problems of the matrix pencil $(\mathbf{X} - \lambda\mathbf{R})$, as pointed out in [17].

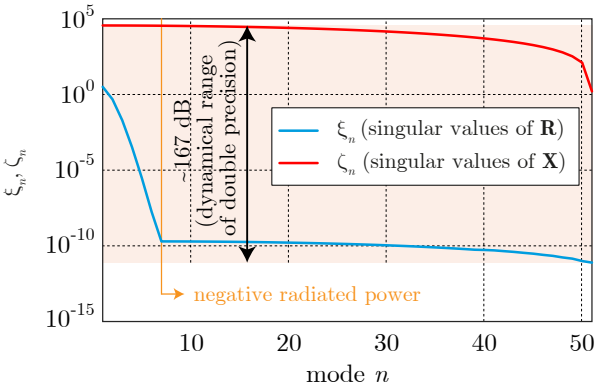

Fig. 8. The singular values of the real and the imaginary parts of the impedance matrix. Same example as in the previous figure.

Since the matrix $\mathbf{R}$ has to fulfill requirements on symmetry, we subtract the matrices as $\mathbf{D} = \mathbf{U} - \mathbf{V}$, see Fig. 9. While the first six columns are zero, as expected, the remainder of $\boldsymbol{D}$ contains exactly two times the remainder of the matrix $\mathbf{U}$ (i. e. $\mathbf{U} = -\mathbf{V}$). This means that positive semi-definite behaviour does not hold for all modes. Instead, most of them exhibit small amount of negative radiated power, no matter how they are normalized[4].

C. Numerical compensation of non-positive radiated power

To avoid issues with non-positive operator $\mathbf{R}$ leading to residual current, the following solution is suggested. The summation in (10) is split into two parts. The first part is the original total up to the mode M, for which $P_{\mathrm{r}}^n > 0$ ($M = 6$ for the above case). The second part is modified to obtain a negative eigenvalue λ_n as follows:

$$\mathbf{J} = \sum_{m=1}^{M} \frac{\langle \mathbf{J}_m, \mathbf{E}^{\mathrm{i}}\rangle_{\mathrm{r}}}{1 + \jmath\lambda_m}\mathbf{J}_m + \sum_{n=M+1}^{N} \frac{\langle \mathbf{J}_n, \mathbf{E}^{\mathrm{i}}\rangle_{\mathrm{r}}}{1 - \jmath|\lambda_n|}\mathbf{J}_n. \tag{18}$$

[4]Normalization of the radiated power is ex-post technique which does not preserve correct sign.

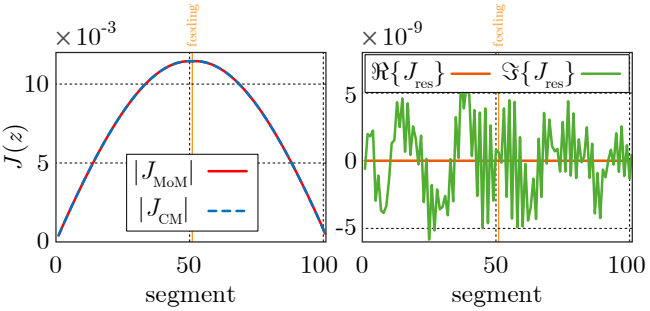

Fig. 10. The absolute value of $\mathbf{J}_{\mathrm{MoM}}$ and $\mathbf{J}$ (left) and the real and imaginary parts of compensated residual mode calculated as $\mathbf{J}_{\mathrm{MoM}} - \mathbf{J}_{\mathrm{CM}}$ (right), $\lambda/2$ dipole fed at the middle.

To verify the proposed approach, the currents at the $\lambda/2$ and 5λ dipoles were recalculated using (18), see Fig. 10 and Fig. 11, and compare with Fig. 5 and Fig. 6. The agreement between the corrected totals $\mathbf{J}$ and $\mathbf{J}_{\mathrm{MoM}}$ is excellent for both cases and the residual current is approximately six orders below the total current values.

Interestingly, the residual current can be isolated by subtracting the original term (10) from the corrected term (18):

$$\mathbf{J}_{\mathrm{res}} = \sum_{n=M+1}^{N} \langle \mathbf{J}_n, \mathbf{E}^{\mathrm{i}}\rangle_{\mathrm{r}} \left(\frac{1}{1 - \jmath|\lambda_n|} - \frac{1}{1 + \jmath\lambda_n} \right) \mathbf{J}_n. \tag{19}$$

Furthermore, the above current can be separated into particular modes, corresponding to the characteristic mode n:

$$\begin{aligned} \mathbf{J}_{\mathrm{res}_n} &= \langle \mathbf{J}_n, \mathbf{E}^{\mathrm{i}}\rangle_{\mathrm{r}} \left(\frac{1}{1 - \jmath|\lambda_n|} - \frac{1}{1 + \jmath\lambda_n} \right) \mathbf{J}_n \\ &= \langle \mathbf{J}_n, \mathbf{E}^{\mathrm{i}}\rangle_{\mathrm{r}} \frac{1 + \jmath\lambda_n - 1 + \jmath|\lambda_n|}{1 + \jmath\lambda_n - \jmath|\lambda_n| - \jmath^2|\lambda_n|\lambda_n} \mathbf{J}_n. \end{aligned} \tag{20}$$

Assume that all modes, for which this correction is applied, originally had positive eigenvalues. This simplifies the previ-

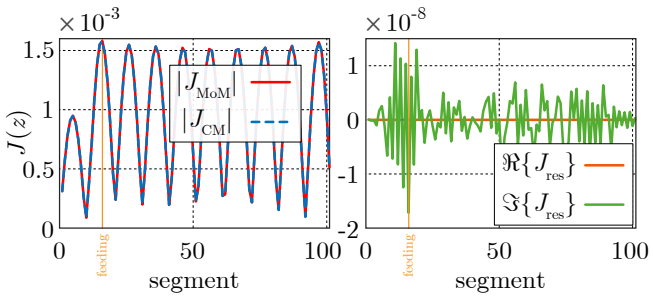

Fig. 11. The absolute value of $\mathbf{J}_{\mathrm{MoM}}$ and $\mathbf{J}$ (left) and the real and imaginary parts of compensated residual mode calculated as $\mathbf{J}_{\mathrm{MoM}} - \mathbf{J}_{\mathrm{CM}}$ (right), 5λ dipole fed at $1/10$ of its length.

ous equation to the form

$$\mathbf{J}_{\mathrm{res_n}} = \jmath \frac{|\lambda_n| + \lambda_n}{1 + \lambda_n^2} \langle \mathbf{J}_n, \mathbf{E}^{\mathrm{i}} \rangle_{\mathrm{r}} \mathbf{J}_n. \tag{21}$$

Expression (21) illuminates why the residual mode in Fig. 5 and Fig. 6 has purely imaginary character even for real feeding $\mathbf{E}^{\mathrm{i}}$. Notice that the residual mode (21) vanishes when associated value λ_n has the correct (negative) sign. The proposed correction also shows that only the badly radiating modes have to be treated by (18). These modes are all non-radiating (inductive) modes and all modes far from their own resonances. The residual current, hence, might become an issue when high number of modes is summed-up. On the other hand, FEKO uses iteratively restarted Arnoldi method [31] which generates only few strongly dominant solutions. In that case, the summation cannot, in principle, be done.

V. Conclusion

The paper discusses some advances of the theory of characteristic modes as introduced by Harrington and Mautz, but expressed here in terms of a particular functional, which is minimized by the eigencurrents. This novel formula provides a different perspective on the characteristic mode decomposition.

The usefulness and "strength" of the functional is illustrated by three canonical examples: a dipole, two closely spaced dipoles and a loop. It was shown that functional formulation is better suited to be analysed than the original formulation because there is no impedance matrix involved. A deeper investigation of the modes on a dipole reveals the limitations of the approximation of the zero-order current distribution expressed as a $\sin$ function.

The second problem treated in the paper is the modal superposition where, theoretically, the current obtained as the sum of a complete set of characteristic currents is exactly equal to the total current (as given e.g. by the method of moments). This statement is mathematically correct, however the results are usually computed numerically in practice. It was observed by several authors, that there is a substantial residual current after subtracting the sum of modal currents from the total current. This issue is investigated and challenged in this paper and it was found that the problem has to be addressed to a numerical scaling involved in the generalized eigenvalue problem. In order to correct the results a modification of numerical superposition formula was proposed. Using the new procedure, the residual current on a dipole in different frequency bands and for different feed positions was reduced to be six orders bellow the total current. Therefore, a near-perfect match between the moment method current and superposed modes is obtained numerically. As a result, adding more modes together may cause more numerical problems and more unstable solution.

Acknowledgement

The authors would like to thank L. Ryan and L. Jelinek for their comments.

References

[1] R. J. Garbacz, "A generalized expansion for radiated and scattered fields," Ph.D. dissertation, The Ohio State Univ., 1968.
[2] R. F. Harrington and J. R. Mautz, "Theory of characteristic modes for conducting bodies," *IEEE Trans. Antennas Propag.*, vol. 19, no. 5, pp. 622–628, Sept. 1971.
[3] E. Antonino-Daviu, M. Cabedo-Fabres, M. Gallo, M. F. Bataller, and M. Bozzetti, "Design of a multimode MIMO antenna using characteristic modes," in *Proceedings of the 3rd European Conference on Antennas and Propagation (EUCAP)*, Berlin, Germany, March 2009, pp. 1840–1844.
[4] K. A. Obeidat, "Design methodology for wideband electrically small antennas based on the theory of characteristic modes," Ph.D. dissertation, Univ. of Illinois, 2010.
[5] J. J. Adams, "Characteristic modes for impedance matching and broadbanding of electrically small antennas," Ph.D. dissertation, Univ. of Illinois, 2011.
[6] Y. Chen and C. Wang, *Characteristic Modes Theory and Application in Antenna Engineering*. Wiley, 2015.
[7] J. G. Van Bladel, *Electromagnetic Fields*, 2nd ed. John Wiley - IEEE Press, 2007.
[8] R. Mittra, Ed., *Numerical and Asymptotic Techniques in Electromagnetics*, ser. Topics in Applied Physics. Springer - Verlag, 1975, vol. 3.
[9] P. Hazdra, M. Capek, and J. Eichler, "Comments to 'Reactive Energies, Impedance, and Q Factor of Radiating Structures' by G. Vandenbosch," *IEEE Trans. Antennas Propag.*, vol. 61, no. 12, pp. 6266–6267, Dec. 2013.
[10] M. Capek, L. Jelinek, P. Hazdra, and J. Eichler, "The measurable Q factor and observable energies of radiating structures," *IEEE Trans. Antennas Propag.*, vol. 62, no. 1, pp. 311–318, Jan. 2014.
[11] Q. Wu and D. Su, "A broadband model of the characteristic currents for rectangular plates," *IEEE Trans. Electromagnetic Compatibility*, vol. 55, no. 4, pp. 725 – 732, 2013.
[12] H. Sagan, *Boundary and Eigenvalue Problems in Mathematical Physics*. Dover, 1989.
[13] R. F. Harrington, *Field Computation by Moment Methods*. John Wiley - IEEE Press, 1993.
[14] R. F. Harrington and J. R. Mautz, "Computation of characteristic modes for conducting bodies," *IEEE Trans. Antennas Propag.*, vol. 19, no. 5, pp. 629–639, Sept. 1971.
[15] C. A. Balanis, *Antenna Theory Analysis and Design*, 3rd ed. John Wiley, 2005.
[16] J. D. Jackson, *Classical Electrodynamics*, 3rd ed. John Wiley, 1998.
[17] G. W. Stewart and J. Sun, *Matrix Perturbation Theory*. Academic Press, 1990.
[18] G. A. E. Vandenbosch, "Reactive energies, impedance, and Q factor of radiating structures," *IEEE Trans. Antennas Propag.*, vol. 58, no. 4, pp. 1112–1127, Apr. 2010.
[19] M. Gustafsson and B. L. G. Jonsson, "Stored electromagnetic energy and antenna Q," *Prog. Electromagn. Res.*, vol. 150, pp. 13–27, 2014.
[20] R. F. Harrington and J. R. Mautz, "Control of radar scattering by reactive loading," *IEEE Trans. Antennas Propag.*, vol. 20, no. 4, pp. 446–454, July 1972.
[21] A. D. Yaghjian and S. R. Best, "Impedance, bandwidth and Q of antennas," *IEEE Trans. Antennas Propag.*, vol. 53, no. 4, pp. 1298–1324, April 2005.

[22] E. Antonino-Daviu, "Analysis and design of antennas for wireless communications using modal methods," Ph.D. dissertation, UPV, Feb. 2008.
[23] M. Capek, L. Jelinek, P. Hazdra, and J. Eichler, "An analytical evaluation of the quality factor Q_Z for dominant spherical modes," *IET Microw. Antennas Propag.*, vol. 9, no. 10, pp. 1096–1103, July 2015.
[24] EM Software & Systems-S.A. FEKO. [Online]. Available: www.feko.info
[25] P. Hazdra, M. Capek, and J. Eichler, "Radiation Q-factors of thin-wire dipole arrangements," *IEEE Antennas Wireless Propag. Lett.*, vol. 10, pp. 556–560, 2011.
[26] M. Capek, P. Hazdra, and J. Eichler, "A method for the evaluation of radiation Q based on modal approach," *IEEE Trans. Antennas Propag.*, vol. 60, no. 10, pp. 4556–4567, Oct. 2012.
[27] P. Hazdra, M. Capek, J. Eichler, and M. Mazanek, "The radiation Q-factor of a horizontal $\lambda/2$ dipole above ground plane," *IEEE Antennas Wireless Propag. Lett.*, vol. 13, pp. 1073–1075, 2014, submitted.
[28] M. Capek, J. Eichler, and P. Hazdra, "Evaluation of radiation efficiency from characteristic currents," *IET Microw. Antennas Propag.*, vol. 9, pp. 10–15, 2015, submitted.
[29] M. Cabedo-Fabres, "Systematic design of antennas using the theory of characteristic modes," Ph.D. dissertation, UPV, Feb. 2007.
[30] J. Kiusalaas, *Numerical Methods in Engineering with Matlab*. Cambridge University Press, 2005.
[31] D. J. Ludick, E. Lezar, and U. Jakobus, "Characteristic mode analysis of arbitrary electromagnetic structures using FEKO," in *ICEAA*, 2012, pp. 208–211.

Miloslav Capek (M'09) received the B.Sc., M.Sc., and Ph.D. degree in electrical engineering from the Czech Technical University (CTU), Prague, Czech Republic, in 2007, 2009, and 2014, respectively. He is currently research associate with the Department of electromagnetic field at the CTU in Prague. He authored or co-authored more than 20 conference and 10 journal papers. His current research interests are in the area of electromagnetic theory, electrically small antennas, numerical techniques, and optimization.

Dr. Capek is member of Radioengineering Society, regional delegate of EurAAP, and Associate Editor of Radioengineering.

Pavel Hazdra (M'03) received the M.Sc. and Ph.D. degree in electrical engineering from the Czech Technical University in Prague, Czech Republic, in 2003 and 2009, respectively. Since 2012 he is an associate professor with the Department of Electromagnetic Field at the CTU in Prague. He authored or co-authored more than 15 journal and 20 conference papers. His research interests are in the area of EM/antenna theory, electrically small antennas, reflector antennas and their feeds and antennas for radioamateur purposes.

Dr. Hazdra is member of the board of Radioengineering Society.

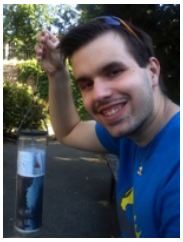

Michal Masek received the M.Sc. degree in electrical engineering from the Czech Technical University in Prague, Czech Republic, in 2015. He is now working towards his Ph.D. degree in the area of behavior of small antennas close to large objects.

I M. Capek, P. Hazdra, and J. Eichler, "A method for the evaluation of radiation Q based on modal approach" [1∗]

II M. Capek, L. Jelinek, P. Hazdra, and J. Eichler, "The measurable Q factor and observable energies of radiating structures" [2∗]

III M. Capek, J. Eichler, and P. Hazdra, "Evaluation of radiation efficiency from characteristic currents" [3∗]

IV M. Capek, L. Jelinek, and G. A. E. Vandenbosch, "Stored Electromagnetic Energy and Quality Factor of Radiating Structures" [47∗]

V M. Capek and L. Jelinek, "Various interpretations of the stored and the radiated energy density" [46∗]

VI M. Capek, L. Jelinek, and P. Hazdra, "On the functional relation between quality factor and fractional bandwidth" [40∗]

VII L. Jelinek, M. Capek, P. Hazdra, and J. Eichler, "An analytical evaluation of the quality factor Q_Z for dominant spherical modes" [31∗]

VIII M. Capek and L. Jelinek, "Comments on 'On Stored Energies and Radiation Q'" [41∗]

IX P. Hazdra, M. Capek, J. Eichler, and M. Mazanek, "The radiation Q-factor of a horizontal $\lambda/2$ dipole above ground plane" [43∗]

X J. Eichler, P. Hazdra, and M. Capek, "Aspects of mesh generation for characteristic mode analysis" [128∗]

XI P. Hazdra, M. Capek, and J. Eichler, "Comments to 'Reactive Energies, Impedance, and Q Factor of Radiating Structures' by G. Vandenbosch" [99∗]

XII J. Eichler, P. Hazdra, M. Capek, and M. Mazanek, "Modal resonant frequencies and radiation quality factors of microstrip antennas" [42∗]

XIII J. Eichler, P. Hazdra, M. Capek, T. Korinek, and P. Hamouz, "Design of a dual-band orthogonally polarized l-probe-fed fractal patch antenna using modal methods" [85∗]

XIV P. Hazdra, M. Capek, and J. Eichler, "Radiation Q-factors of thin-wire dipole arrangements" [44∗]

XV M. Capek, P. Hazdra, and M. Masek, "On some theoretical and numerical aspects of characteristic mode decomposition" [45∗]